LBL--22379

DE87 003622

WORKSHOP ON

NUCLEAR STRUCTURE AT MODERATE AND HIGH SPINS

Berkeley, California, October 13-16, 1986

Slide Report

Lawrence Berkeley Laboratory
University of California
Berkeley, California 94720

October 1986

Prepared bor the U.S. Department of Energy under
Contract DE-AC03-76SF00098.

FOREWORD

It has been a pleasure to host the first workshop on high-spin physics in the Western Hemisphere. We have observed for a number of years the stimulus provided by the Copenhagen workshops to the European community of high-spin physicists. This October seemed like a good time for such a workshop, coinciding with a number of large arrays of Compton-suppressed germanium detectors coming into operation and beginning to produce new and interesting physics. In our view the discussions and interactions provided by such workshops are important for the vitality of our field. We hope you have enjoyed this experience as much as we have.

M.A. Deleplanque   R.M. Diamond   F.S. Stephens

WORKSHOP ON
NUCLEAR STRUCTURE AT MODERATE AND HIGH SPIN

LAWRENCE BERKELEY LABORATORY
October 13-16, 1986

Day Time	MONDAY	TUESDAY	WEDNESDAY	THURSDAY
9.00 a.m.	Welcome *T.J.M. Symons* I. SUPERDEFORMATIONS *P. Twin* *M. de Voigt* *S. Aberg*	V. CONTINUUM PROPERTIES *I.Y. Lee* *F. Stephens* *G. Leander*	IX. HIGH TEMPERATURES *R. Janssens* *A. Goodman* *C. Gossett*	XIII. LIFETIMES *J. Bacelar* *N. Johnson* *Y. Chen*
10:30 a.m. BREAK 11:00 a.m.	II. HEAVY RARE EARTHS *H. Hubel* *R. Lieder* *E. Marshalek*	VI. CONTINUUM PROPERTIES *Th. Dossing* *R. Holzmann* *C. Baktash*	X. TRANSFER REACTIONS *D. Cline* *J. Gerl* *P. Ring*	XIV. MOMENTS *G. Hagemann* *M. Hass* *H. Emling*
12.30 p.m. LUNCH 2:00 p.m.	III. SINGLE-PARTICLE CONFIGURATIONS *M.A. Deleplanque* *M. Piiparinen* *K.H. Maier*	VII. LIGHT RARE EARTHS *P. Nolan* *D. Fossan* *E.M. Beck*	XI. TRANSITION REGION *L. Riedinger* *J. Wood* *M. Guidry*	
3:30 p.m. BREAK 4:00 p.m.	IV. BAND TERMINATION *M. Quader* *D. Headly* *I. Ragnarsson* RECEPTION	VIII. NEW TECHNIQUES *Th. Lindblad* *D. Ward* *J. Saladin* *Th. Byrski*	XII. SHAPES *T.L. Khoo* *N. Koller* *T. Czosnyka*	
5:30 p.m.				

MONDAY

I. SUPERDEFORMATIONS

P. Twin	Shape co-existence and shape changes in ^{152}Dy
M. de Voigt	γ-ray correlations and conversion electrons of superdeformed states in ^{152}Dy
S. Åberg	Feeding, spectroscopy and decay of superdeformed states

II. HEAVY RARE EARTHS

H. Hübel	High-spin structure of light Hf isotopes
R. Lieder	Study of high-spin isomers in ^{180}Os with OSIRIS
E. Marshalek	Mixed alignment in the Os region

III. SINGLE-PARTICLES CONFIGURATIONS

M.A. Deleplanque	Particle-hole states in ^{150}Dy
M. Piiparinen	Structure of ^{148}Gd
K.H. Maier	Spectroscopy and moments of Po isotopes with $114 \leq N \leq 126$

IV. BAND TERMINATION

M. Quader	High-spin states in ^{154}Dy
D. Headly	Comparison of experiment and theory for high spin states in ^{24}Mg and ^{25}Mg
I. Ragnarsson	Spectroscopic consequences of shape changes and shape co-existence at high angular momenta

TUESDAY

V. CONTINUUM PROPERTIES

I. Y. Lee	High-spin nuclear structure studies using the spin spectrometer
F. Stephens	Correlations in the γ-ray continuum
G. Leander	Rotational E2 strength function

VI. CONTINUUM PROPERTIES

Th. Dossing	Damping of rotational motion
R. Holzmann	Continuum lifetimes in ^{152}Dy
C. Baktash	Energetic M1 transitions: a probe of nuclear collectivity at high temperatures

VII. LIGHT RARE-EARTHS

P. Nolan	Study of nuclei near A = 130 at very high spin
D. Fossan	Band structure in A = 130 - 140 γ-soft nuclei
E.M. Beck	Spectroscopy of ^{135}Nd

VIII. NEW TECHNIQUES

Th. Lindblad	Analysis of multidimensional γ-ray coincidence spectra
D. Ward	The 8π spectrometer
J. Saladin	Results from the Pittsburgh multidetector array
Th. Byrski	γ-ray spectroscopic studies at the French crystal castle

WEDNESDAY

IX. HIGH TEMPERATURES

R. Janssens	Suppression of neutron emission in heavy-ion induced fusion reactions: entrance channel effect and/or superdeformed shapes
A. Goodman	Finite-temperature HFB calculations in rare-earth nuclei
C. Gossett	Nuclear structure of heated nuclei from the statistical decay of the giant dipole resonance

X. TRANSFER REACTIONS

D. Cline	Heavy-ion induced one and two neutron transfer reactions as a probe of high-spin collective states
J. Gerl	Nuclear reactions at the Coulomb barrier
P. Ring	Diabolic pair transfer and oscillating behavior of backbending in rotating nuclei

XI. TRANSITION REGION

L. Riedinger	The systematic occurrence of $i_{13/2}$ neutron and $h_{9/2}$ proton crossings in light Ir, Pt, Au nuclei
J. Wood	New results on shape coexistence in the light gold isotopes
M. Guidry	Microscopic calculations for high-spin properties using Fermion dynamical symmetries

XII. SHAPES

T.L. Khoo	Indications of octupole shapes around ^{144}Ba
N. Koller	Extension of transient field measurement of magnetic moments to higher spin states
T. Czosnyka	E2 properties of the nuclei studied via heavy-ion Coulomb excitation

THURSDAY

XIII. LIFETIMES

J. Bacelar	Collectivity at high spins
N. Johnson	Studies of collective behavior of nuclei at high spin from lifetime measurements
Y. Chen	E2 properties of high-spin states--multiband mixing model

XIV. MOMENTS

G. Hagemann	$\Delta I = 1$ transition rates
M. Hass	Nuclear polarization and the sign of nuclear deformation at high spin
H. Emling	High-spin g-factors and lifetimes in $N \sim 90$ rare earth isotopes

SUPERDEFORMATION IN ^{152}Dy

Peter Twin (Daresbury, U.K.)

Yrast superdeformed band

2% intensity of ^{152}Dy strength

Superdeformed pseudo-continuum

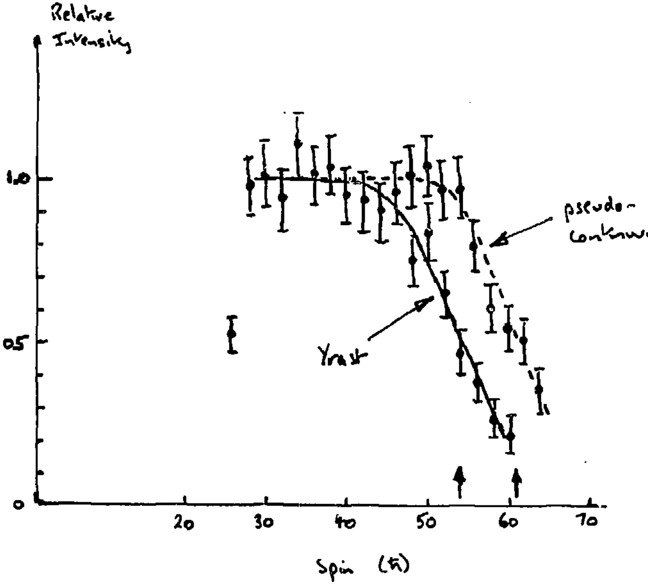

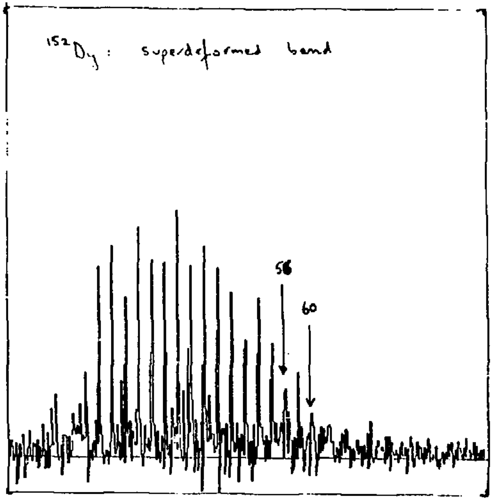

Isomer spectrum at 4keV /channel
corrected for response of Ge detectors

Additional intensity above 50ħ
- spread over 20-25 keV with periodicity close to superdeformed yrast separation
- Is it the superdeformed continuum above yrast ?

^{152}Dy : cuts across E_γ-E_γ matrix

ISOMER MATRIX

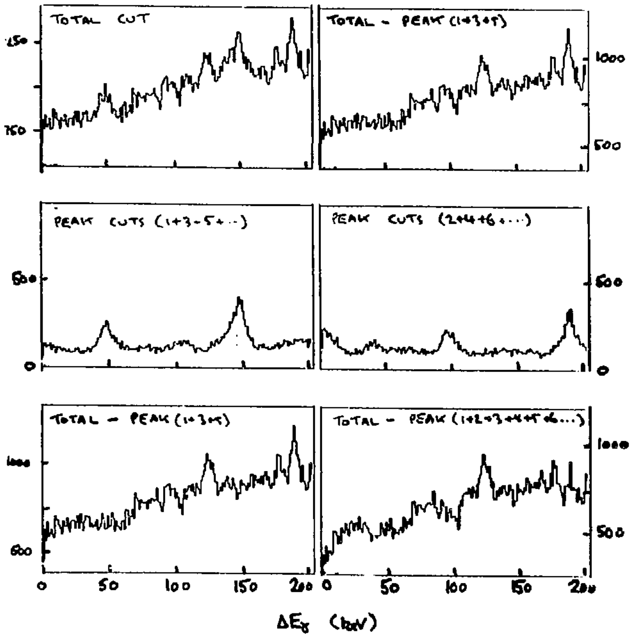

CUT ALONG THE FIRST RIDGE

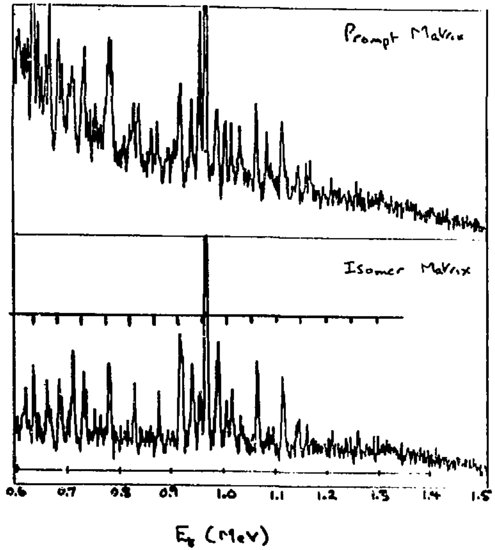

In isomer matrix the cuts across the matrix which involve only the known discrete lines account for all the observed ridge.

Therefore, there is no evidence for other super-deformed bands within the continuum.

$^{108}Pd\,(^{48}Ca, 4n)\,^{152}Dy$ at 205 MeV selected by isomer and by members of super-deformed band. – target 1.2 mg cm^{-2} backed by 15 mg cm^{-1} gold

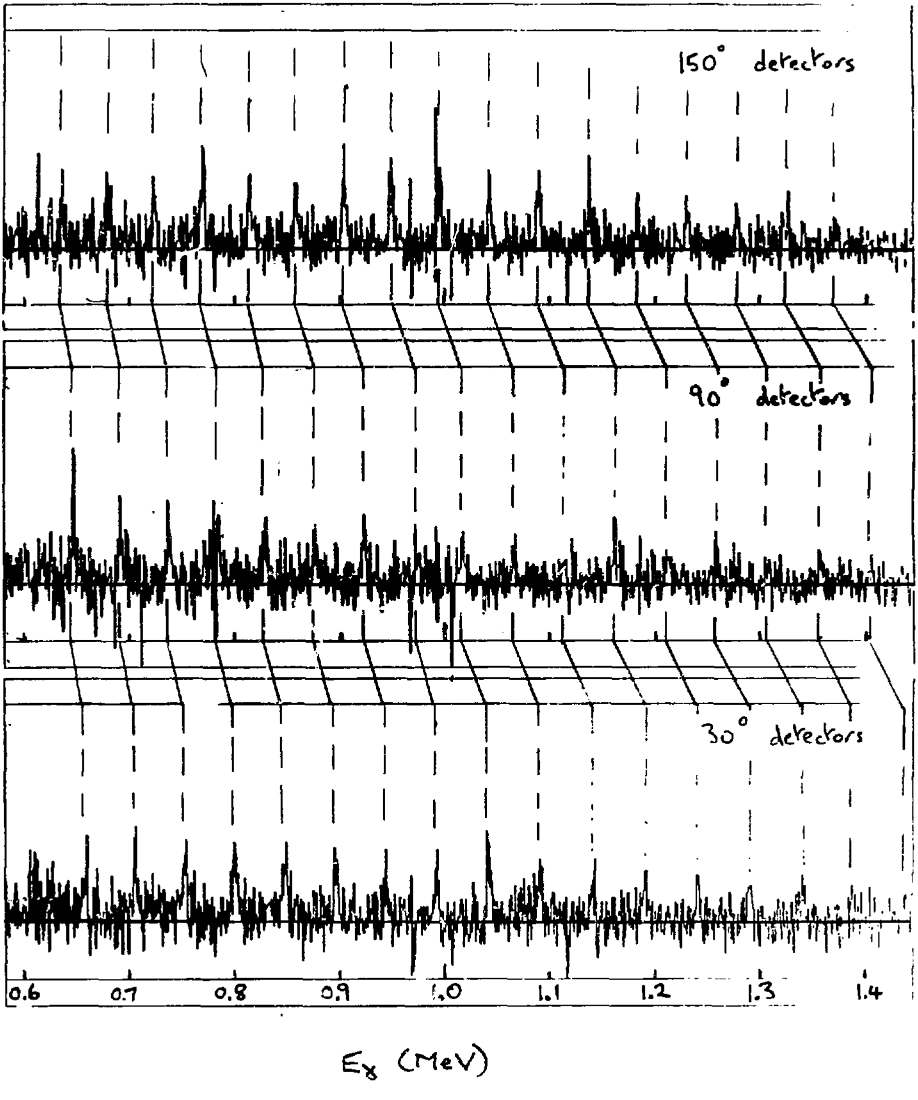

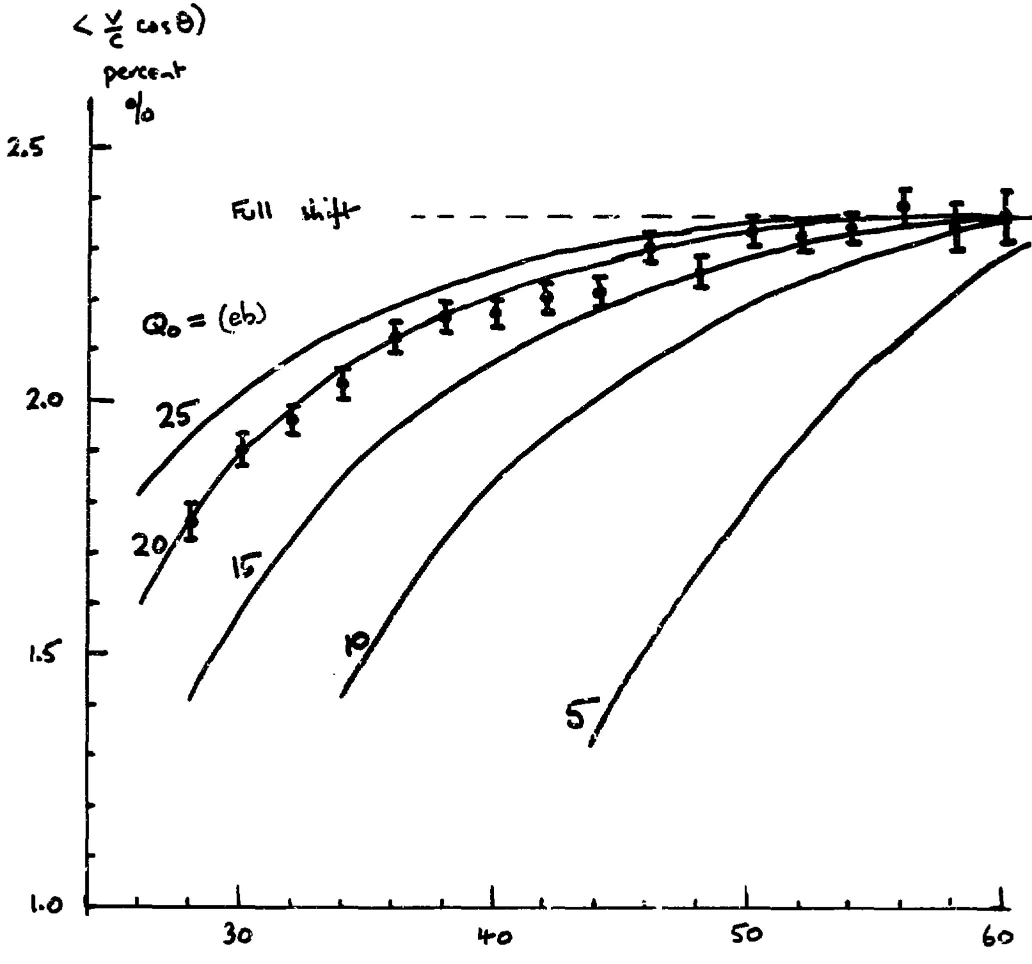

< v/c cos θ)
percent
%
2.5
2.0
1.5
1.0
Full shift
Q₀ = (eb)
25
20
15
10
5
30
40
50
60
Spin (ħ)

M. de Voigt γ-ray correlations and conversion electrons of superdeformed states in ^{152}Dy

180 MeV ^{40}Ar induced
HERA, Berkeley

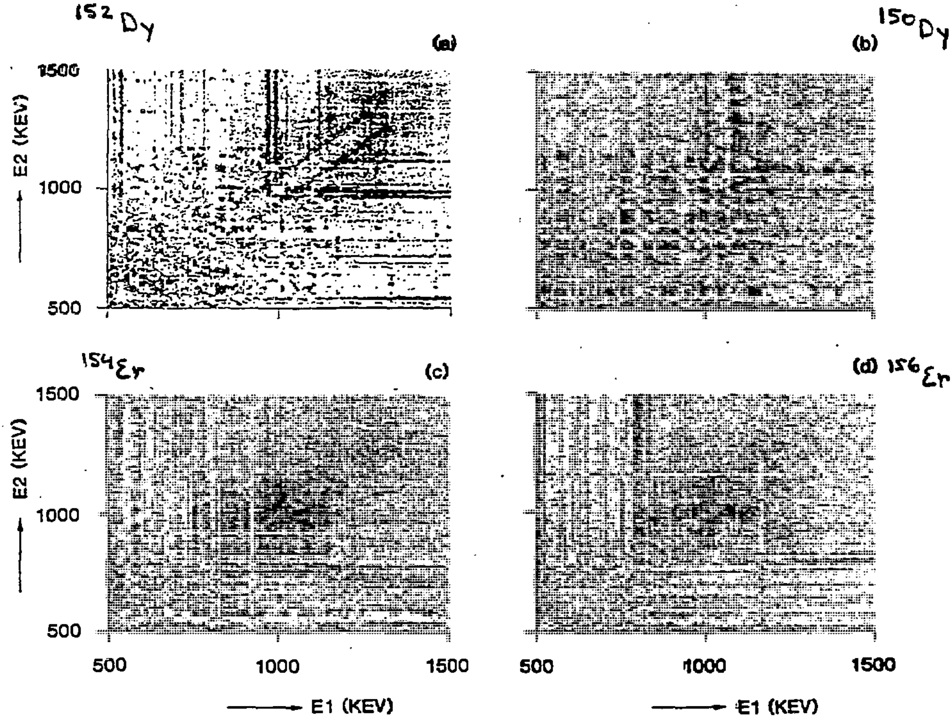

XBL 862-441

192 mill. events 73

64 76

^{152}Dy ~ 600 mill. doubles
~ 200 " triples, up

RAW DATA ONLY !

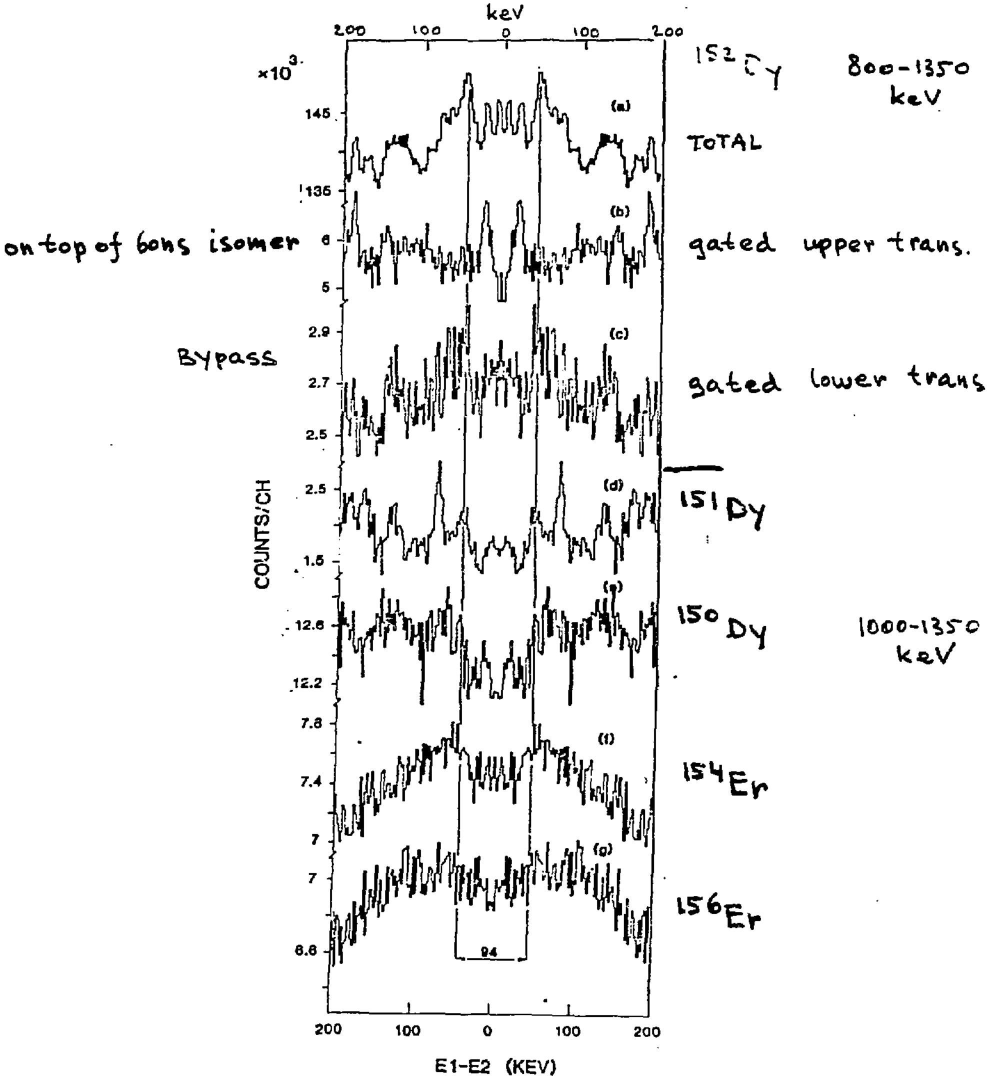

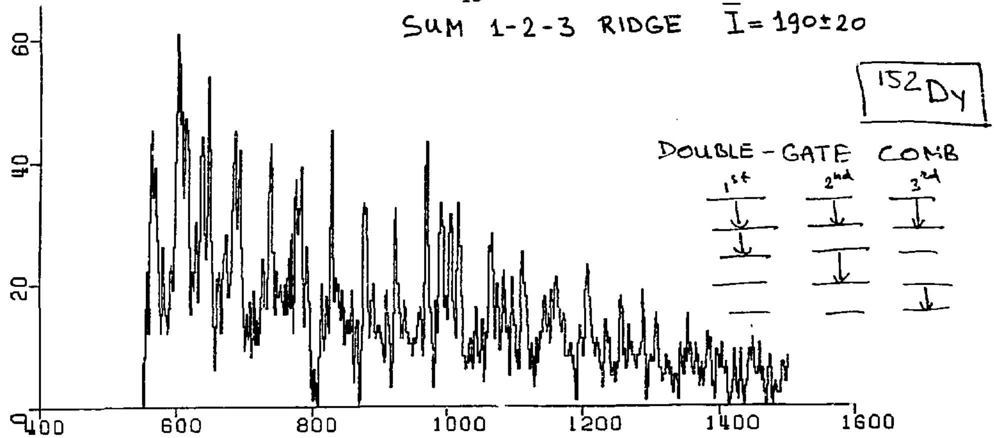
SUM 1-2-3 RIDGE $\bar{I}$ = 190±20
152Dy
DOUBLE-GATE COMB
1st
2nd
3rd
0
20
40
60
400
600
800
1000
1200
1400
1600

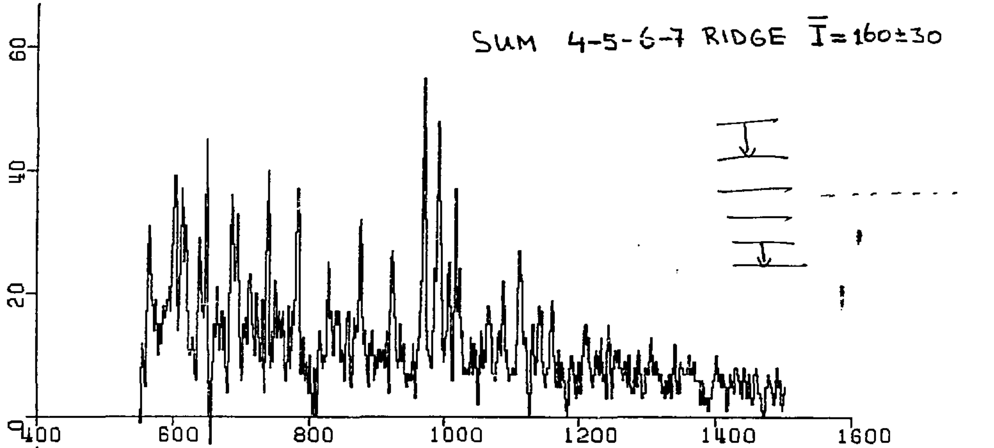
SUM 4-5-6-7 RIDGE $\bar{I}$ = 160±30
0
20
40
60
400
600
800
1000
1200
1400
1600

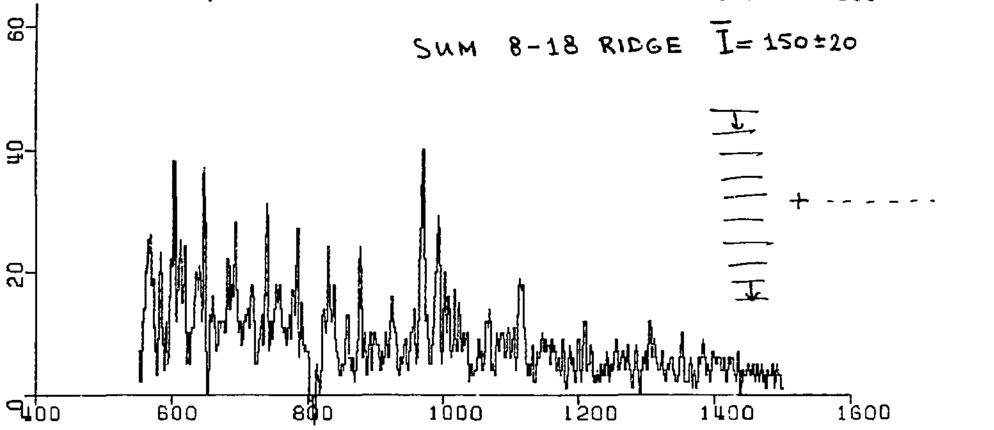
SUM 8-18 RIDGE $\bar{I}$ = 150±20
0
20
40
60
400
600
800
1000
1200
1400
1600

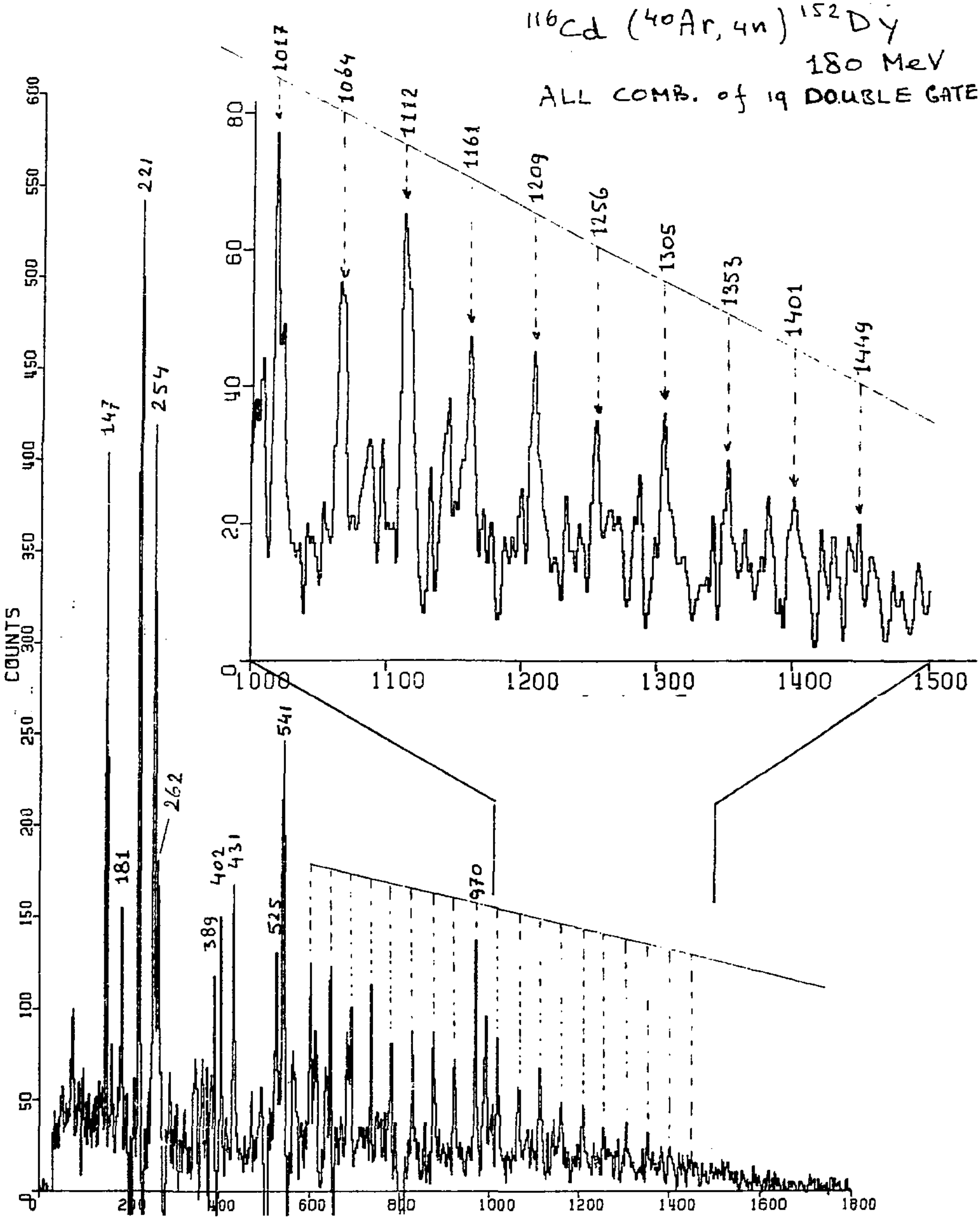

116Cd (40Ar, 4n) 152Dy
180 MeV
ALL COMB. of 19 DOUBLE GATE
COUNTS
1017
1064
1112
1161
1209
1256
1305
1353
1401
1449
147
181
221
254
262
389
402
431
525
541
970

15 On the Feeding Spectroscopy and Decay of Superdeformed States*)

Sven Åberg

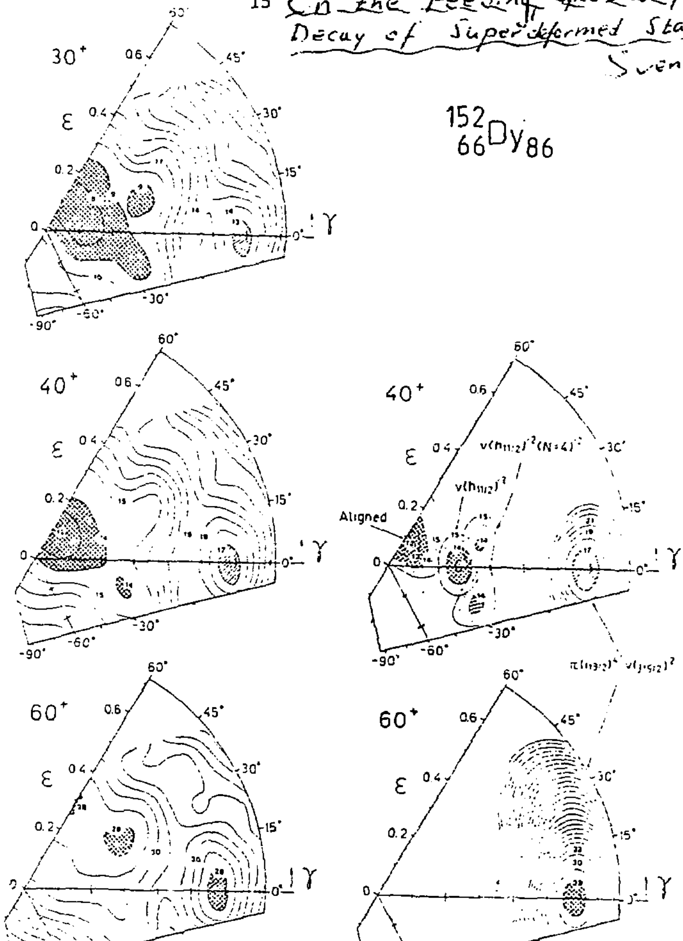

Fig.1 Calculated potential-energy surfaces at different spins for ^{152}Dy considering all $(\pi,\alpha) = (+,0)$ configurations (left) and some fixed configurations (right). The contour line separation is 1.0 MeV for full lines and 0.5 MeV for dashed lines.

*) Partly from I. Ragnarsson and S Åberg, Phys. Lett, to appear

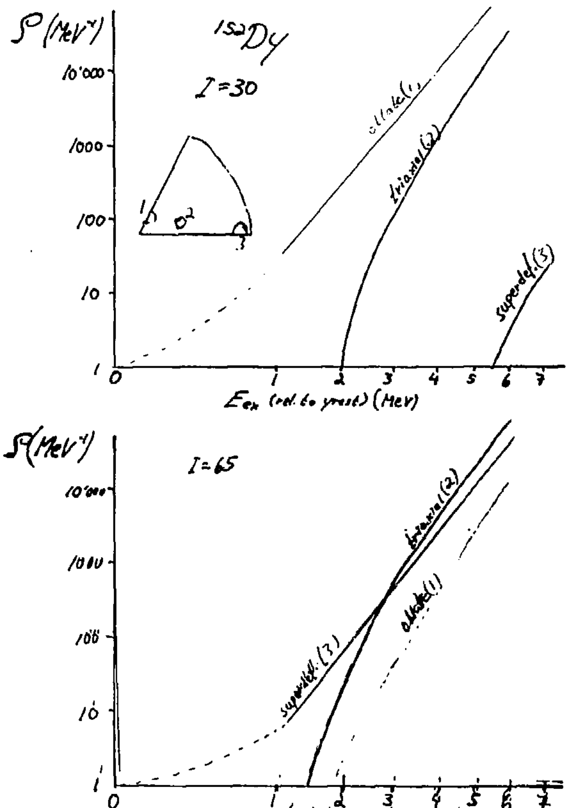

Level densities calculated in a microscopic model (cranked Nilsson) as many-particle many-hole excitations for three competing deformations, oblate (p-h-exc.), triaxial (or prolate) and superdeformed. At around spin 56 the three deformations come at approximately the same energy. Then we get for all reasonable excitation energies $\rho_o > \rho_t > \rho_s$. At spin 30 the oblate conf. come lowest and $\rho_o > \rho_t > \rho_s$. For very high E_{ex} ρ_s will however cross ρ_t. Similarly for I=65 when $E_s < E_t < E_o$ (I=?), then ρ_t is largest for small E_{ex} while ρ_s becomes larger for larger E_{ex}.

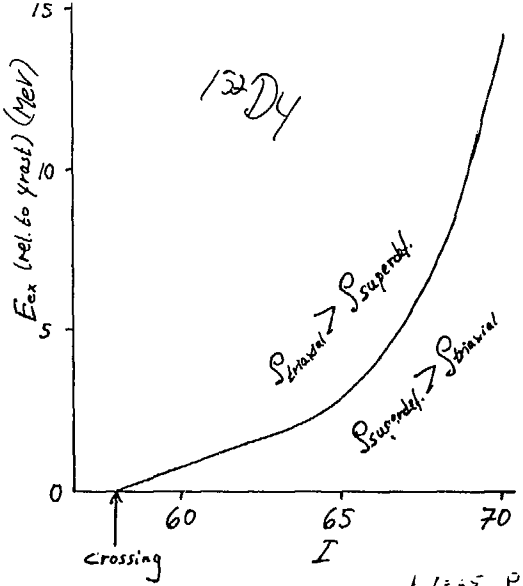

As was seen in the previous figure at I=65 ρ_s crosses ρ_t at around E_{ex} = 2.8 MeV. In this fig we see how this crossing point varies with spin. The way to populate superdeformed configurations is thus to have a low excitation energy and a high spin.

152Dy

$\varepsilon = 0.58$ $\Delta = 5$ keV

$50^+ \rightarrow 48^+ \rightarrow 46^+$

totally 500 states included

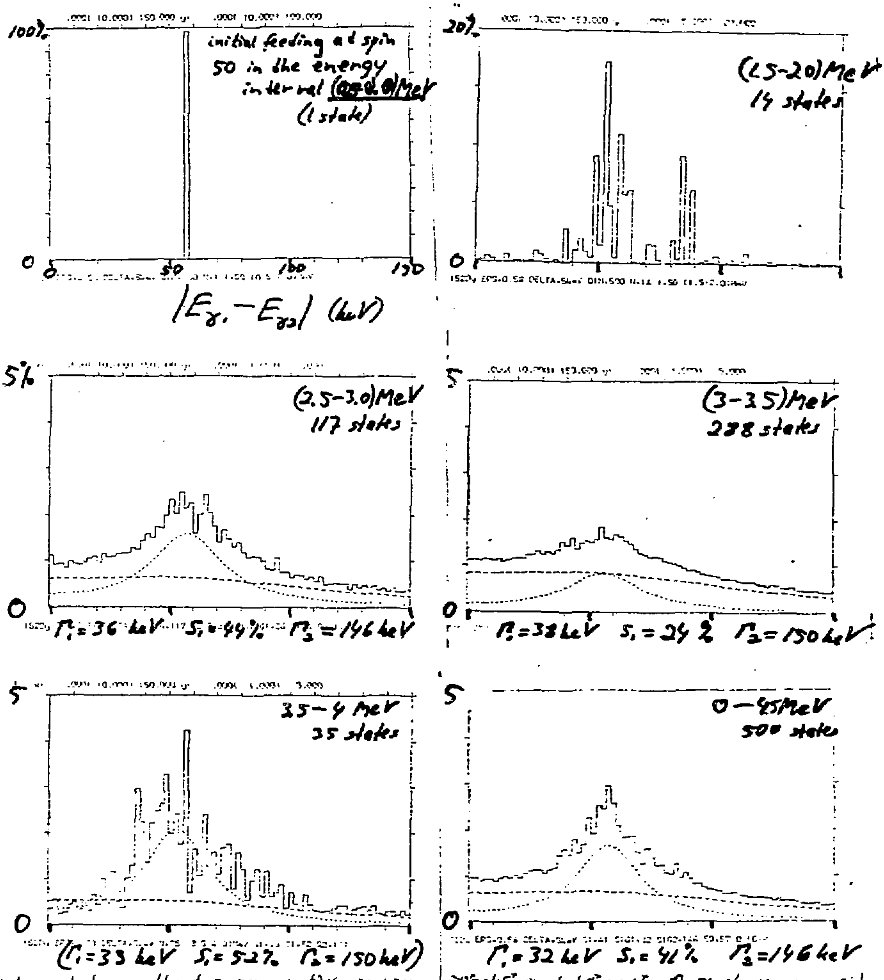

Correlations between the two consequtive γ-rays $50^+ \to 48^+$ and $48^+ \to 46^+$. A purely microscopic model is used to obtain the 500 lowest rotational bands at the 2:1 def in ^{152}Dy. Then a residual 2-body, 3-body and 4-body interaction is acting between the bands. This gives rise to some spreading in the B(E2)-strength, small for small excitation energies and larger for larger excitation energies. Different initial distributions are studied as is given in the six figures. Each state in the given energy interval is populated with the same probability at spin 50. The bargraphs gives the calculated result while the two dashed curves are two Breit-Wigner distributions fitted to the calculated curves. Note how the valley is filled in with increasing exc. energy. Above 3.5 MeV truncation effects become serious.

1. Rich structure at superdef with many exotic states occupied: $\pi i^{13/2\,4}\ \nu j^{15/2\,2}$ $\pi=+,\ \alpha=0$ (for ^{152}Dy)
   - Large $Q_0 = 1760\ efm^2 \triangleq$ 2400 W.u. $\Rightarrow \tau = 10$ fsec for $E_\gamma = 1$ MeV
   - Small variation in g-factor around $\frac{Z}{A}$
   - $\gamma^{(2)}$ decreases with ω in agreement with exp.
   - $\gamma^{(1)}$ larger than in exp (if $I_{max} \doteq 60$)
2. γ-γ measurements + int. in superdef. band in ^{152}Dy $\Rightarrow$ one band is presumably pushed down in energy due to big s.p. gaps at Z=66, N=86
3. Level densities strongly structure dep.:

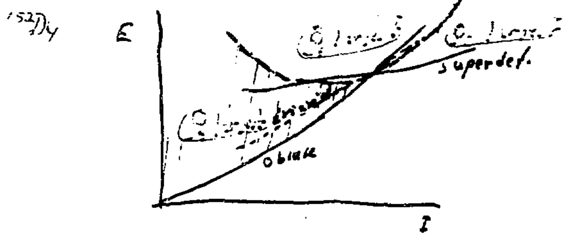

4. Damping mechanism for E2-trans. structure dep. quite different for ^{152}Dy (ε=0.58) than for ^{168}Yb (ε=0.25).
5. Ridge structure in γ-γ plots obtained in calc.:

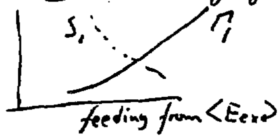

6. Slow cooling process in ^{152}Dy.
7. GQR(T=0), K=0 only 7.5 MeV above yrast. GDR 9 MeV

HIGH-SPIN STRUCTURE OF LIGHT Hf-ISOTOPES

H. HÜBEL, UNIVERSITY OF BONN

STUDIED $^{160-166}$Hf IN Sm + Ne AND Te + Ca REACTIONS

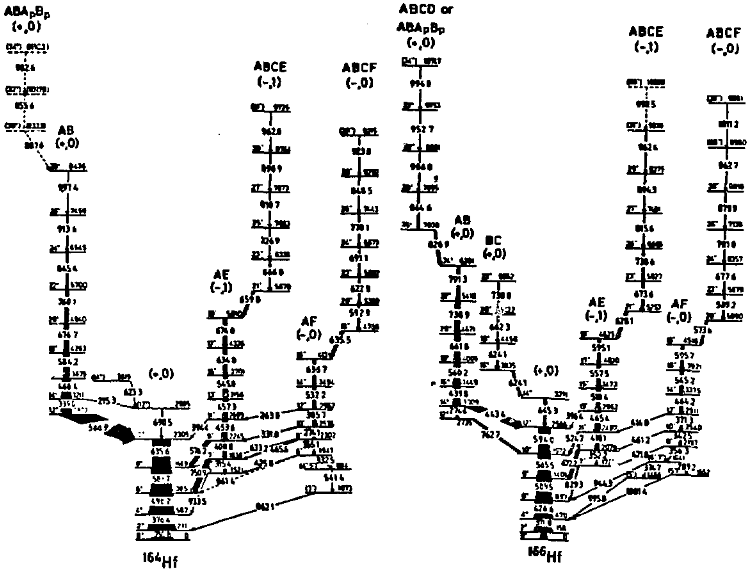

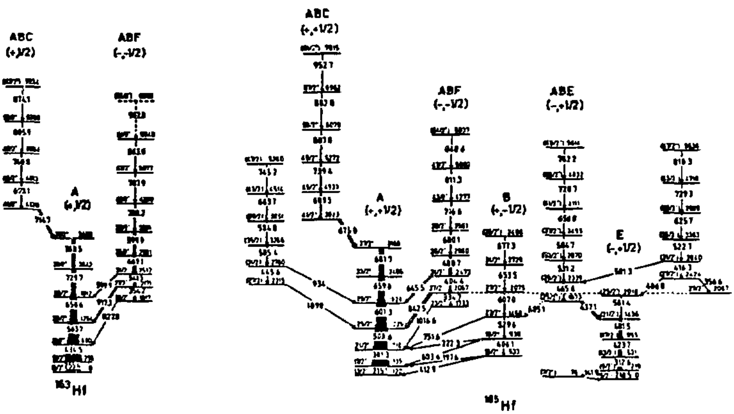

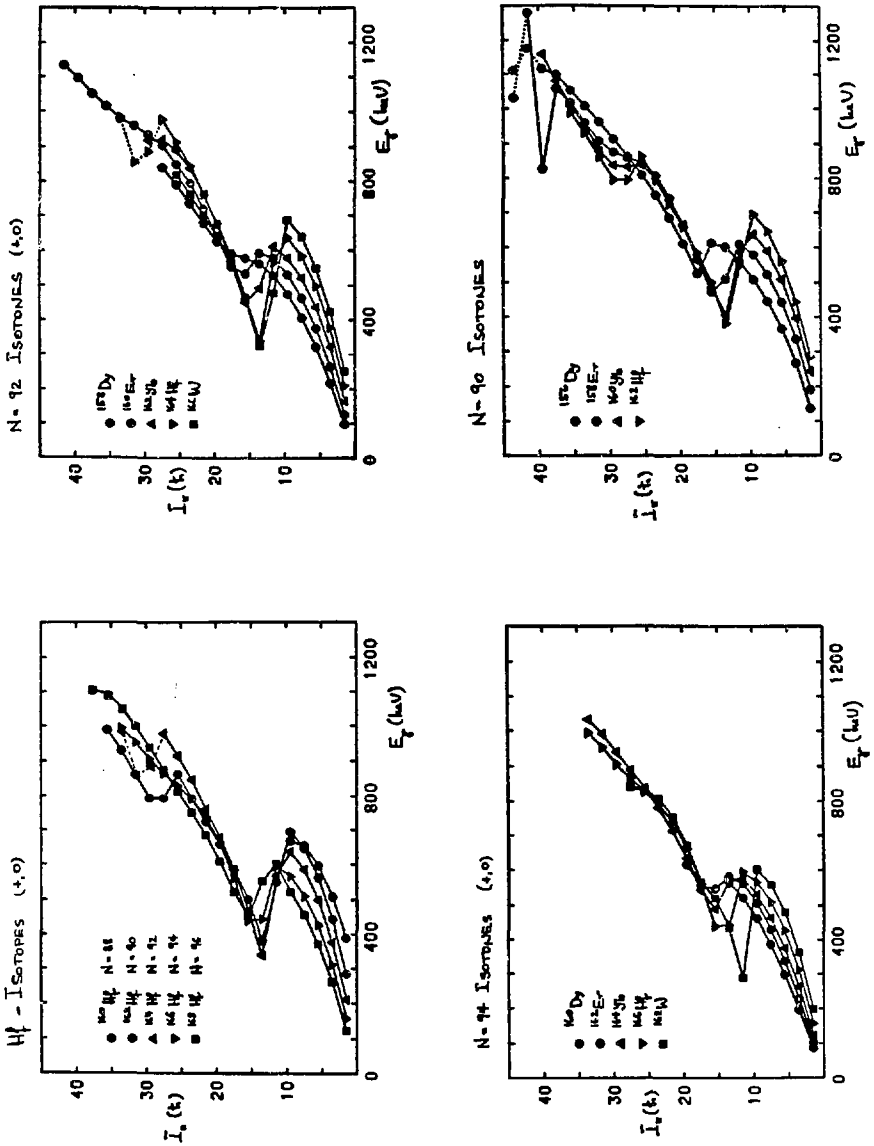

N=92 Isotones (+,0)
N=90 Isotones
Hf - Isotopes (+,0)
N=94 Isotones (+,0)
E_γ (keV)
I_x (ħ)
0
400
800
1200
10
20
30
40

Common Reference: Average S-Band $\mathcal{J}_0 = 22\ \hbar^2/\mathrm{MeV}$, $\mathcal{J}_1 = 63\ \hbar^4/\mathrm{MeV}^3$, $i = 9.9\ \hbar$

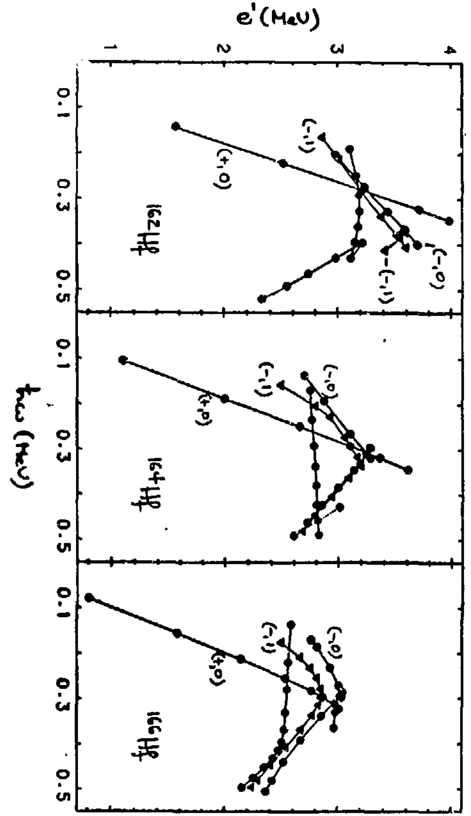

AB and BC Crossings

Nucleus	Config.	$\hbar\omega_c$ (MeV) Exp.	$\hbar\omega_c$ (MeV) Calc.	Δi ($\hbar$) Exp.	Δi ($\hbar$) Calc.
^{162}Hf	G → AB	0.28	0.25	10.8	10.8
	AE → ABCE	0.38	0.34	7.5	7.4
^{164}Hf	G → AB	0.26	0.25	10.3	10.7
	AE → ABCE	0.33	0.32	5.8	7.3
	AF → ABCF	0.31	0.32	6.1	7.3
^{166}Hf	G → AB	0.26	0.25	9.9	9.5
	G → BC	0.32	0.35	6.0	7.6
	AE → ABCE	0.31	0.31	6.2	7.3
	AF → ABCF	0.30	0.31	5.0	7.3
^{163}Hf	A → ABC	0.36	0.36	8.2	7.7
^{165}Hf	A → ABC	0.34	0.35	7.4	7.7
	E → ABE	0.23	0.22	6.6	10.0

What Is The Nature Of The Second Band Crossing ?

	^{162}Hf	^{164}Hf	^{166}Hf	^{168}Hf	
$\hbar\omega_{exp}$	0.42	0.44	0.42	≥0.5	(MeV)
Δi_{exp}	6	(6.7)	4.4	–	($\hbar$)
Calculation for Protons: A_pB_p					
$\hbar\omega_{CSM}$	0.41	0.44	0.46	0.46	(MeV)
Δi_{CSM}	7.1	7.1	6.4	6.0	($\hbar$)
Calculation for Neutrons: CD					
$\hbar\omega_{CSM}$	0.42	0.41	0.42	0.43	(MeV)
Δi_{CSM}	4.6	4.6	4.1	4.1	($\hbar$)

↑ For ^{166}Hf Better Agreement For CD Neutrons

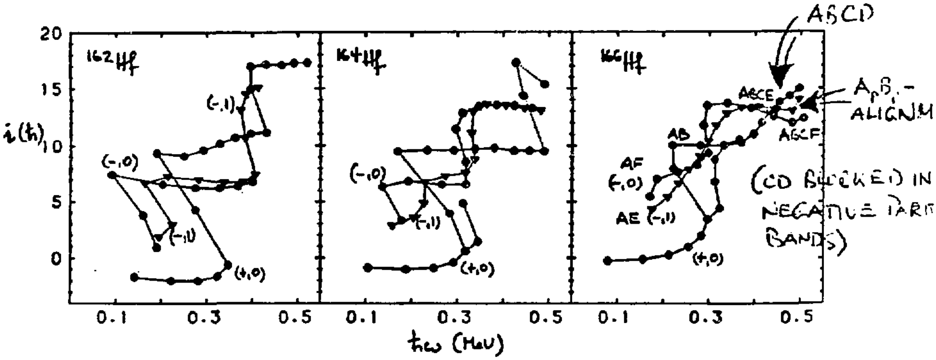

Conclusion: ^{162,164}Hf 2nd Band Crossing A_pB_p Alignment
^{166}Hf 2nd Band Crossing CD Alignment (Onset of A_pB_p Alignment Seen in Negative Parity Bands at $\hbar\omega \approx 0.5$ MeV)

R. Lieder Study of high-spin isomers in ^{180}Os with OSIRIS

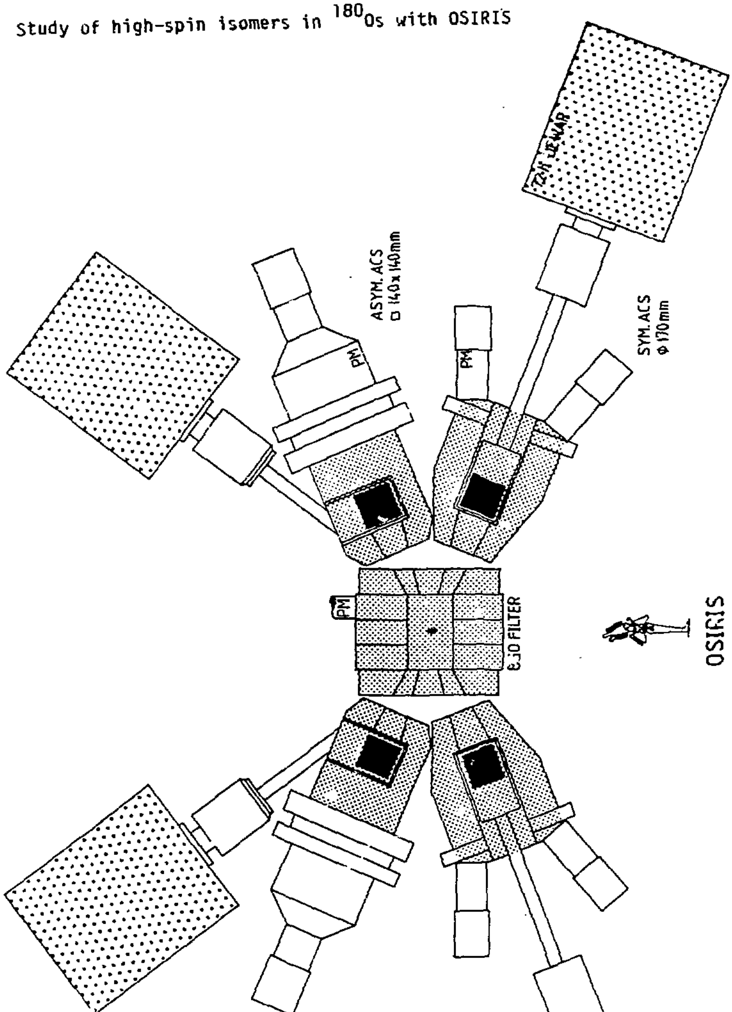

Side view of OSIRIS spectrometer consisting of 12 Compton-suppressed Ge detectors and a 50 element BGO ball.

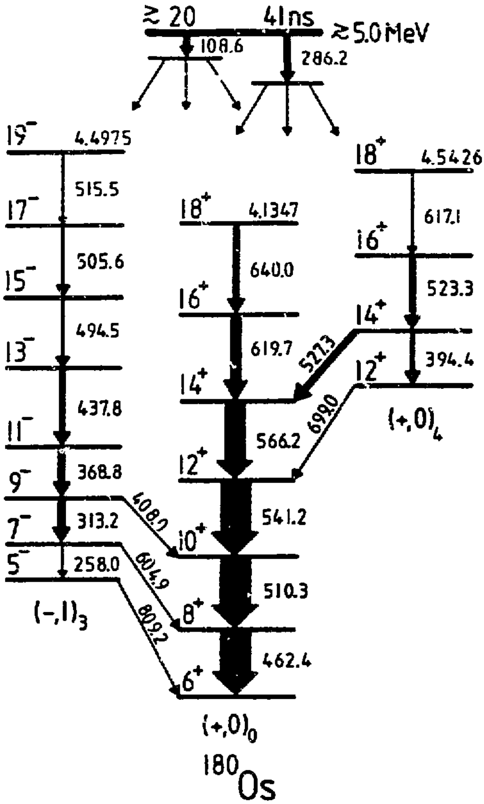

Partial level scheme of ^{180}Os as populated by the high-spin isomer.

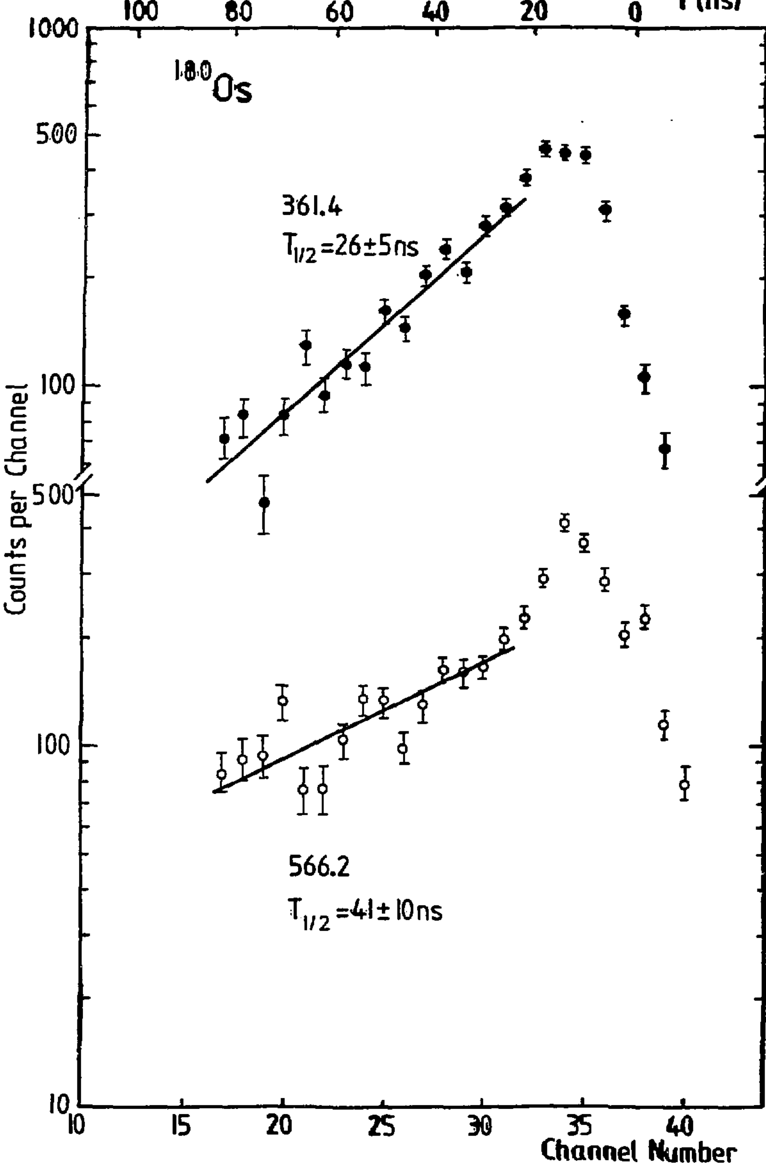

Time spectra with respect to the beam burst for the 361.4 and 566.2 keV transitions associated to the deexcitation of the low- and high-spin isomers, respectively, in ^{180}Os.

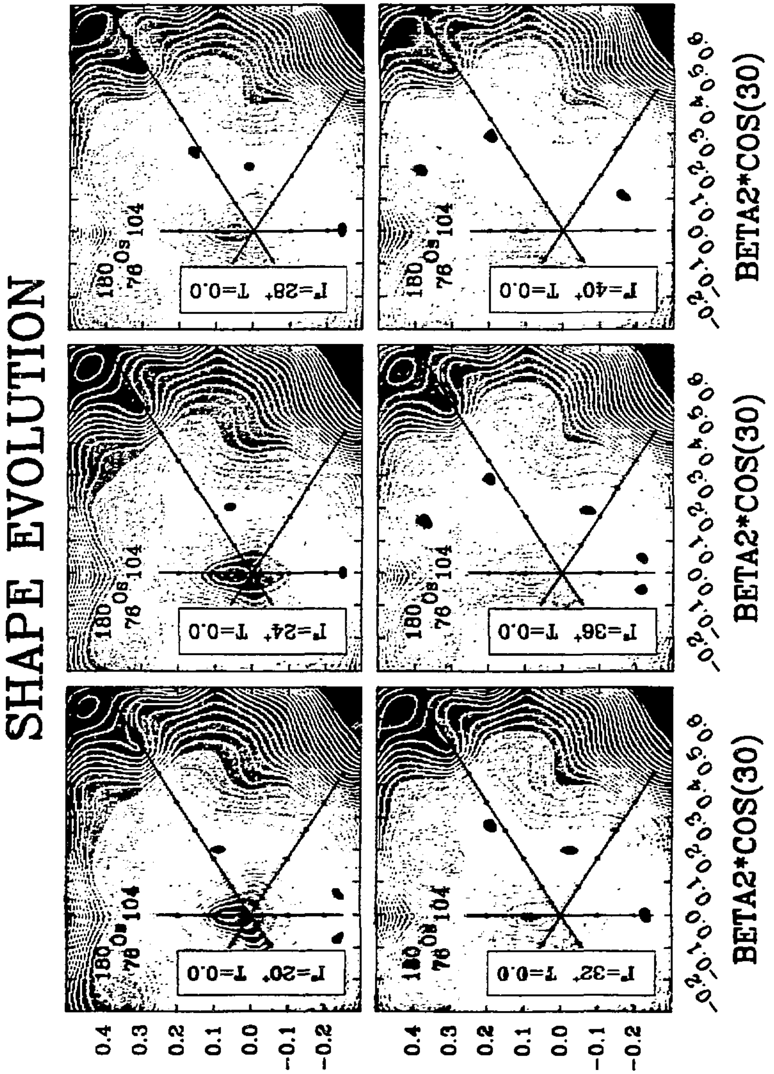

Results of total-energy calculations in the (β,γ) plane without pairing for (+,0) levels in ^{180}Os. The axes correspond to γ = 60°, 0°, -60° and -120° counted clockwise from the upper vertical axis. The individual plots are labelled by the spins I, parities π and temperatures T. Minima in the total-energy surfaces are indicated by dots. The minimum at γ ≈ -120° supports the interpretation of the high-spin isomer in ^{180}Os as K isomer.

Mixed Alignment in the Os-Ir Region

E.R. Marshalek
University of Notre Dame

Cranking Model:

$$H_\omega = H_{s.p.} + \sum_{\tau,k} \Delta_\tau (C^\dagger_{k,\tau} C^\dagger_{\bar{k},\tau} + H.c.) - \omega J_x$$

($H_{s.p.}$ ↑ Nilsson potential)

Calculations performed for ^{180}Os, ^{181}Ir using a large s.p. space (no core $\mathcal{J}$ needed). Defomation parameters ϵ_2, ϵ_4 were held constant. Calculations were performed for both fixed Δ_n, Δ_p and also for self-consistent gap parameters.

BCS vacuum state is

$$\Psi_0 = \prod_\mu (U_\mu + V_\mu a^\dagger_\mu a^\dagger_{\bar{\mu}}) |0\rangle$$

(↑ canonical basis)

$\hbar\omega = 0.41$ MeV, just beyond first BB.

Pair of protons with canonical wave fns.

$|+i\rangle = 0.8250|541\tfrac{1}{2}\rangle + 0.5093|532\tfrac{3}{2}\rangle + 0.1833|523\tfrac{5}{2}\rangle$ + small components. 97.5% $h_{9/2}$

$|-i\rangle = 0.2285|\overline{550\tfrac{1}{2}}\rangle - 0.3242|\overline{541\tfrac{1}{2}}\rangle + 0.4896|\overline{532\tfrac{3}{2}}\rangle - 0.6075|\overline{523\tfrac{5}{2}}\rangle + 0.4641|\overline{514\tfrac{9}{2}}\rangle - 0.1246|\overline{505\tfrac{11}{2}}\rangle$ + small components. 99.7% $h_{11/2}$

($\pm i$ denotes eigenvalue of $e^{i\pi j_x}$)

For this pair, $V_\mu^2 = 0.99993$,

$\Delta_{\mu\bar{\mu}} = 0.033$ MeV compared to $\bar{\Delta}_p = 0.768$ MeV

$\langle +i | j_x | +i \rangle = 4.127 \qquad \langle -i | j_x | -i \rangle = 4.487$

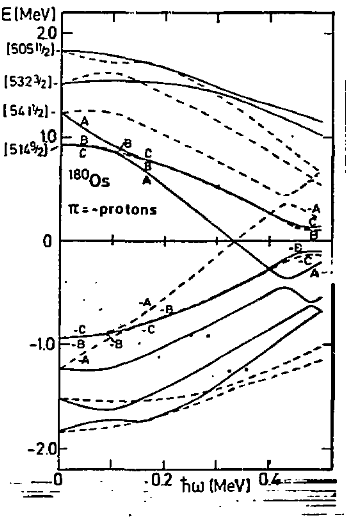

(a)

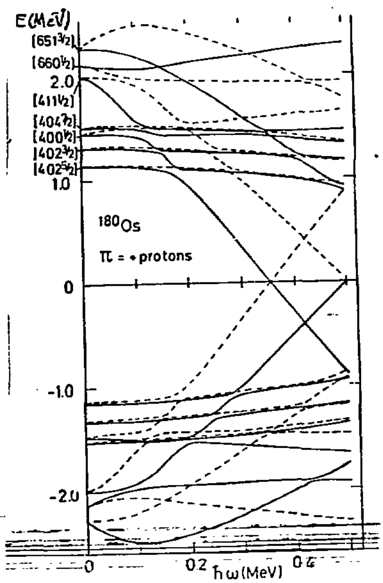

(b)

Plot of odd-parity (a) and even-parity (b) quasiparticle eigenvalues vs. ħω for ^{180}Os. Solid lines have $r = +i$, dotted lines $r = -i$. The crossing of the [541 1/2] and [514 9/2] levels at $\hbar\omega \approx 0.17$ MeV is responsible for the mixed alignment. On the other hand, the crossing of two $i_{13/2}$ protons in (b) is a normal alignment.

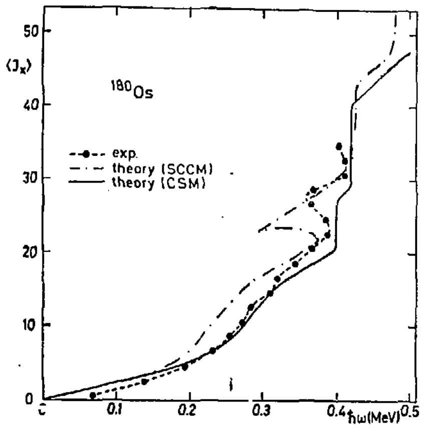

Plot of $\langle J_x \rangle = I + \frac{1}{2}$ vs $\hbar\omega$ for ^{180}Os

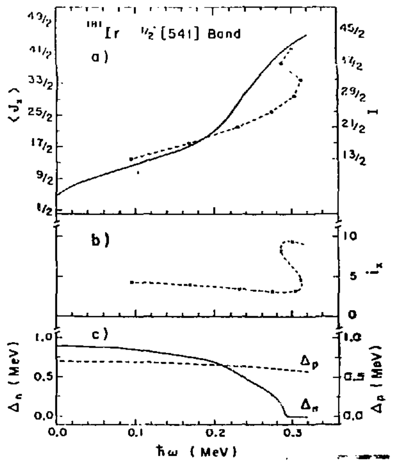

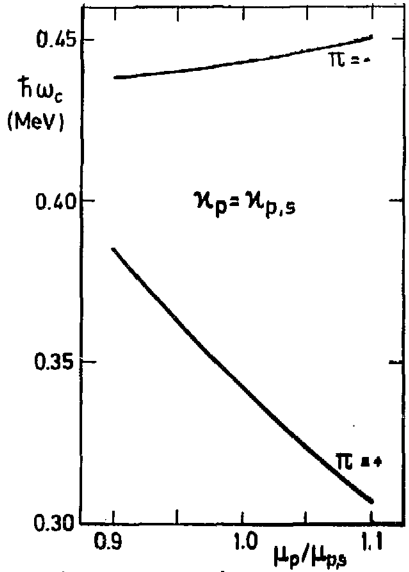

Crossing frequency $\hbar\omega_c$ for the mixed alignment (π_-) and the normal $i_{13/2}$ alignment (π_+) vs. the Nilsson parameter μ_p. Small variations of μ_p cannot change the ordering of the two alignments

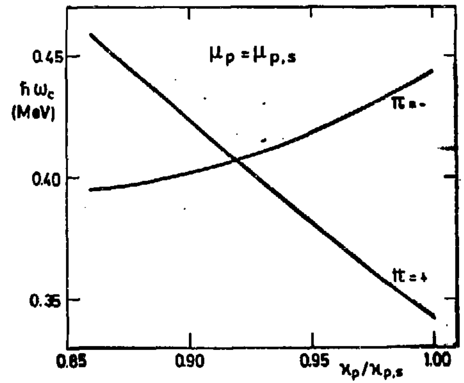

Crossing frequency $\hbar\omega_c$ vs the Nilsson parameter κ_p for the mixed $h_{11/2}$ - $h_{9/2}$ and the normal $i_{13/2}$ proton alignments. In units of the standard value $\kappa_p = \kappa_{p,s}$ for fixed $\mu_p = \mu_{p,s}$. Reducing κ_p by 10% gives correct sequence, in which the negative parity crossing comes below the positive parity one.

M.A. Deleplanque Particle-hole states in ^{150}Dy
L.B.L.

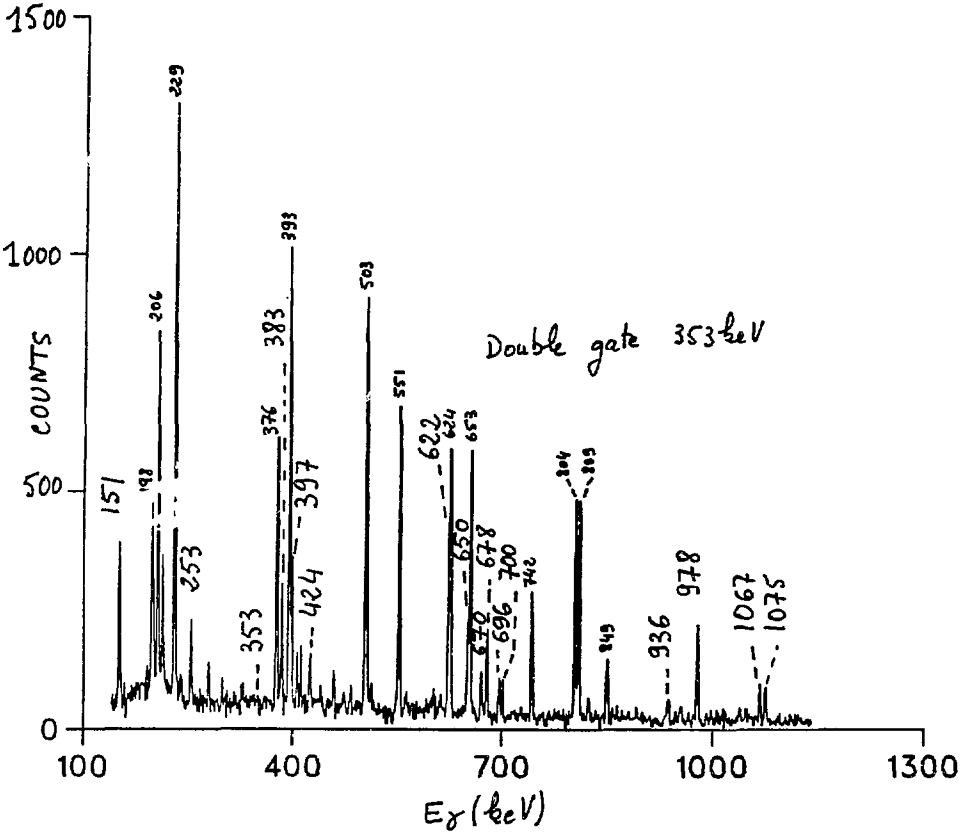

Figure 1.

The nucleus ^{150}Dy was produced by the reaction ^{114}Cd + ^{40}Ar at 175 MeV. In the spectrum shown, a [illegible] mg/cm^2 lead-backed target was used, producing 230 million events. The figure shows a triple coincidence spectrum with a double gate on the (new) 353 keV line (45%). The energies of the new lines are written in bigger characters. Thus, there were sufficient statistics to select and separate the many parallel decay pathways of this nucleus.

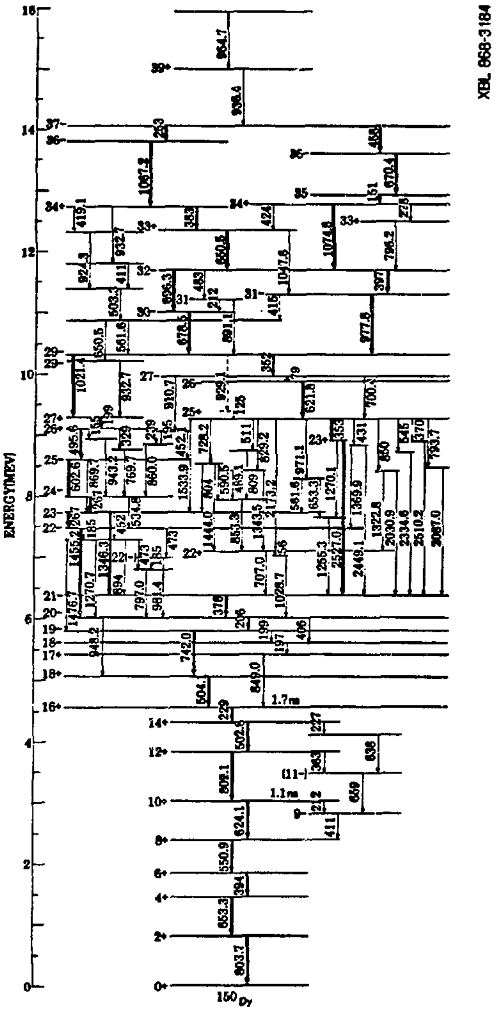

Figure 2.

Level scheme of ^{150}Dy. It can be interpreted with the Deformed Independent Particle Model (DIPM) of Døssing et al. which is successful in predicting the aligned states. There are three regions: up to spins 20–22, valence particle configurations; up to spin 32, one and two particle-hole (p-h) configurations; above, higher number of p-h configurations.

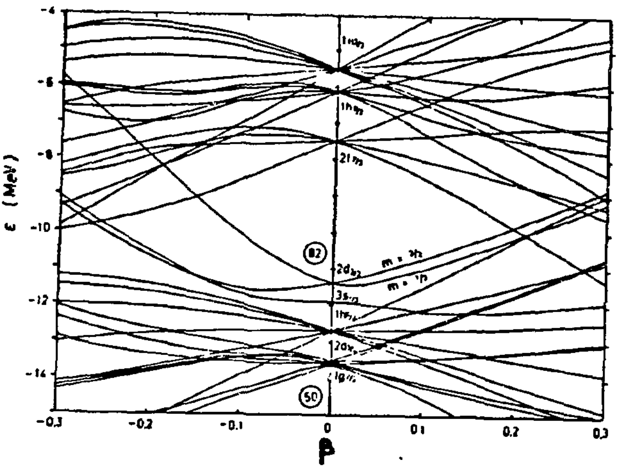

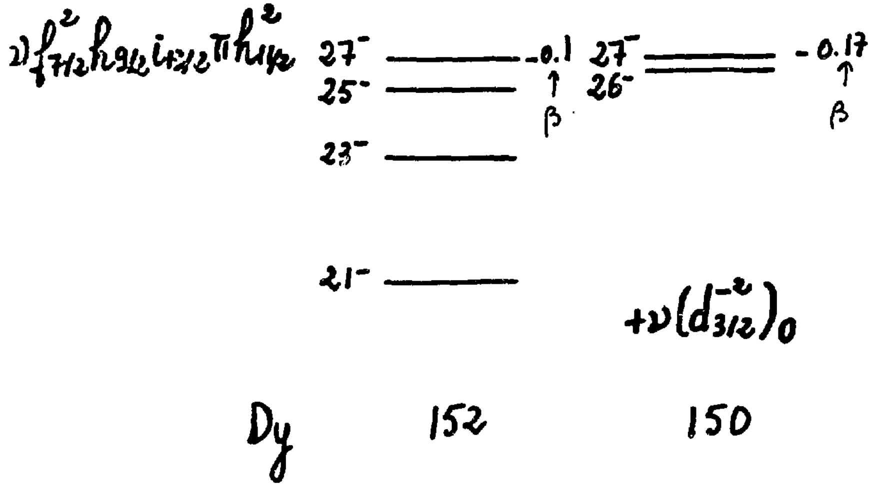

Figure 3.

The $s_{1/2}$, $d_{3/2}$ neutron hole orbitals drive the nucleus ^{150}Dy towards large oblate ($\beta\approx-0.2$) in the states which contain these holes. This nucleus is deformable because it has already four valence nucleons in the equatorial plane. ^{152}Dy, with identical particle configuration (no holes), is much less deformed and still shows a multiplet structure.

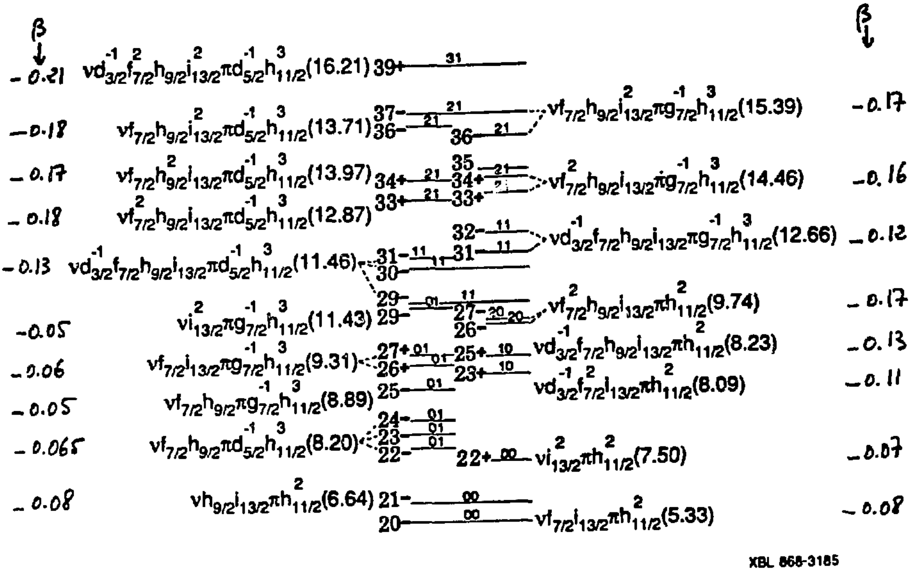

Figure 4.

Assigned configurations above spin 20. The numbers in parentheses are the calculated (DIPM) energy values for the aligned state of each configuration. The small numbers above each level are the number of neutron and proton particle-holes respectively. The most important feature in that nucleus is the breaking of the proton core (e.g. leftmost thick cascade in fig.2) and of the neutron core (e.g. rightmost thick cascade in fig.2) at the same energy and spin in parallel cascades. This is probably a result of both deformation effects and of the higher number of available high-spin neutron orbitals.

M. Piiparinen Structure of ^{148}Gd

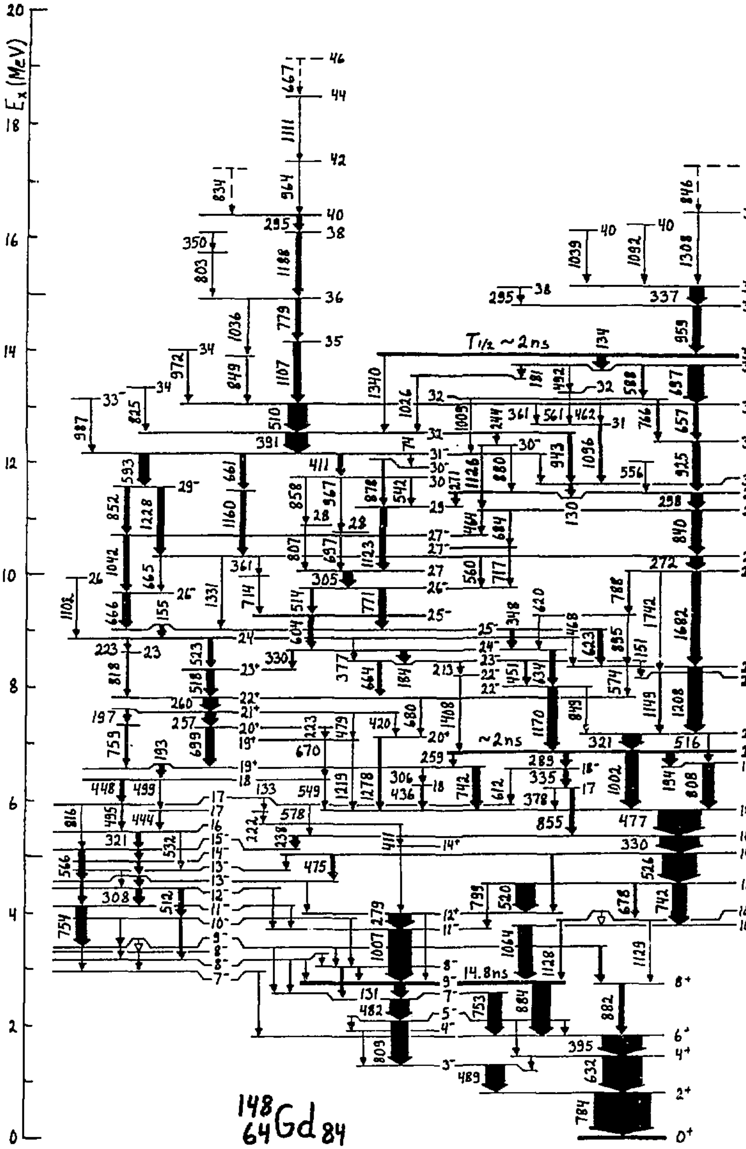

Calculations : R.R. Chasman

Rotationally invariant residual interactions
+ large valence space

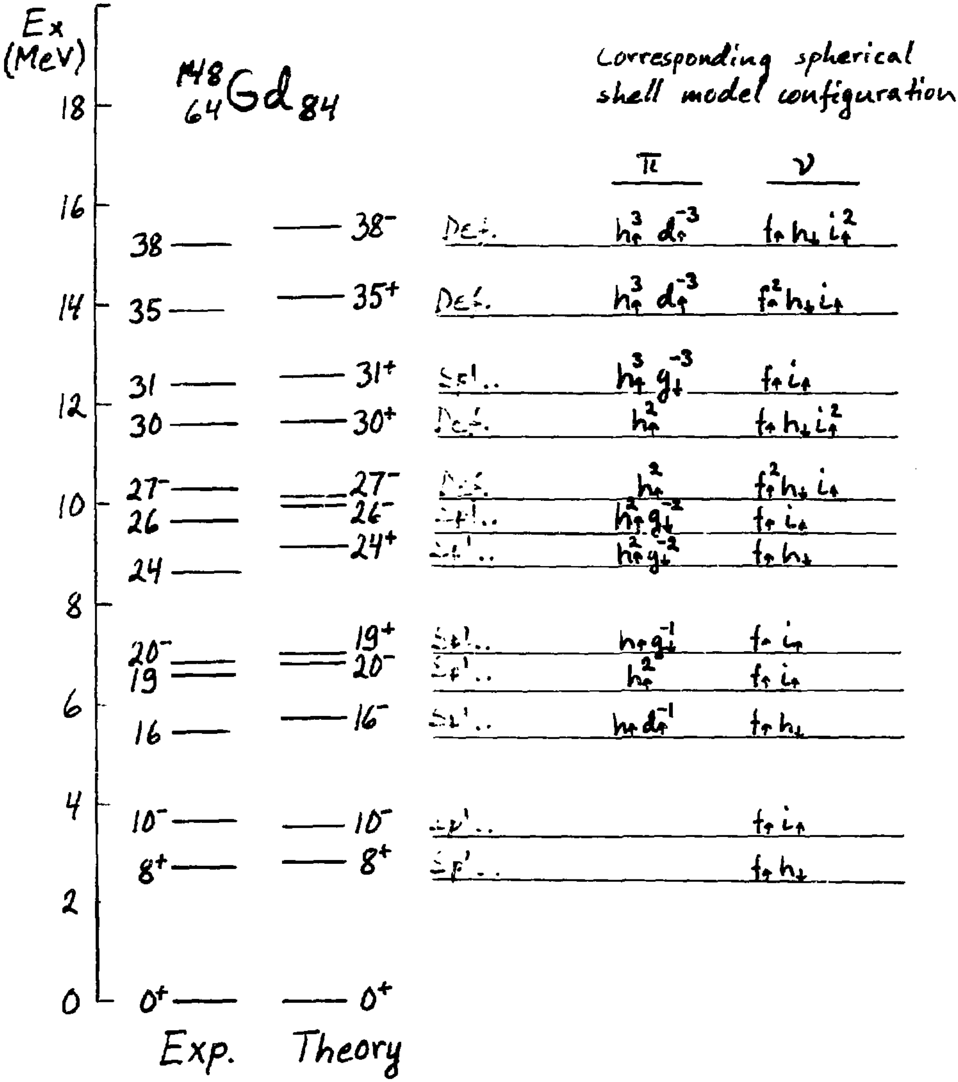

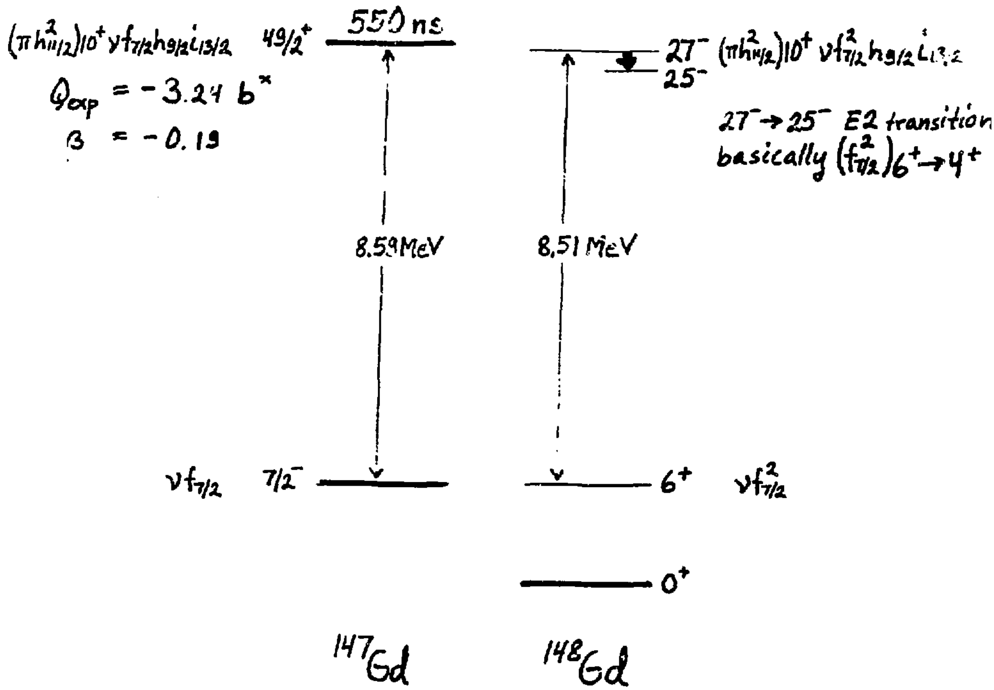

* Hausser et al.: Nucl. Phys. A379(82)287
Dafni et al.: Phys. Rev. Lett. 53(84)2473

Summary

- Complex level scheme of ^{148}Gd up to $I \sim 46$ at 19.1 MeV.
- Fast transitions above spin 38 : gradual change to collectivity ?
- A ns-isomer at $I = 35$, $E_x = 13.9$ MeV.
- Level interpretations : especially 27^- at 10.3 MeV $\longleftrightarrow$ $49/2^+$ 550 ns isomer in ^{147}Gd
- Classifications of types of configurations along the yrast line.
- Competition of deformed and spherical shapes influence to the yrast decay.

Participants :

Purdue Univ. : M. Piiparinen, P.J. Daly, Z. Grabowski, M.A. Quader, W. Trzaska

Notre Dame U. : M.W. Drigert, U. Garg

Argonne N.L. : R.V.F. Janssens, I. Ahmad, H. Emling, R. Holzmann, T.L. Khoo, W.C. Ma

Chalk River N.L. : D.C. Radford

Nils Bohr Inst. : J. Borggreen

Spectroscopy and moments of Po isotopes with 114 ≤ N ≤ 126

K. H. Maier, HMI Berlin and LLNL Livermore

Quadrupole moments have been measured by perturbed angular distribution in a Bi single crystal, following pulsed beam excitation, for the isomers in neutron magic 210Po: ($\pi h9/2^2$,8+), ($\pi h9/2$ i13/2 ,11-), (208Pb 5- $\pi h9/2^2$,13-) and (208Pb 5- $\pi h9/2$ i13/2,16+). We used the 209Bi(t,2n)210Po reaction with the LLNL spectroscopy setup at the LANL tandem except for the 11- level measured by 209Bi(15N,14C) at HMI. Q(8+)=-57.9(18) fm is derived from B(E2,8+→6+) and serves as calibration of the electric field gradient. The experimental results Q(11-)=-99(11) fm^2 , Q(13-)=-94(8) and Q(16+)=-136(5) allow to extract Q(π i13/2)=-56(12) fm^2 in agreement with theoretical predictions. Q(13-) - Q(8+) = Q(16+) - Q(11-) = Q(208Pb 5-) follows from the structure of these isomers and gives Q(5-)=-36(9) rsp. -37(13). This agrees with the main component of the 5- level, namely Q(ν g9/2 $p1/2^{-1}$)=Q(νg9/2)= -29(2) fm^2 from B(E2, 210Pb 8+→6+) but might indicate a small softening of the core due to the p1/2 hole.

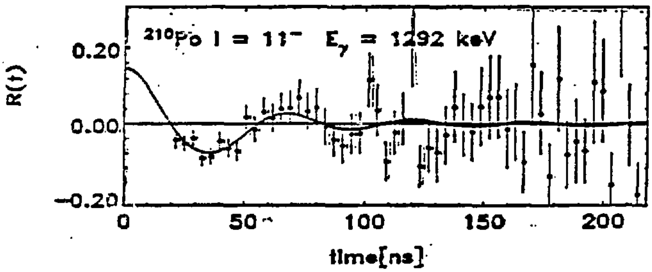

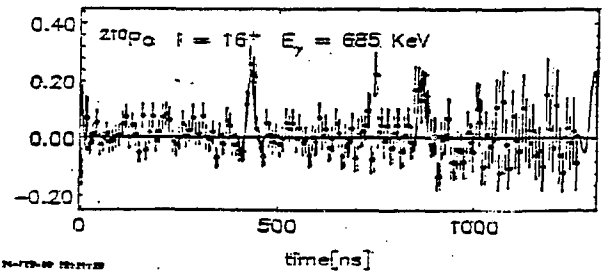

Measured and fitted theoretical quadrupole modulation patterns I(0 ,t)/I(90 ,t) in a Bi single crystal.

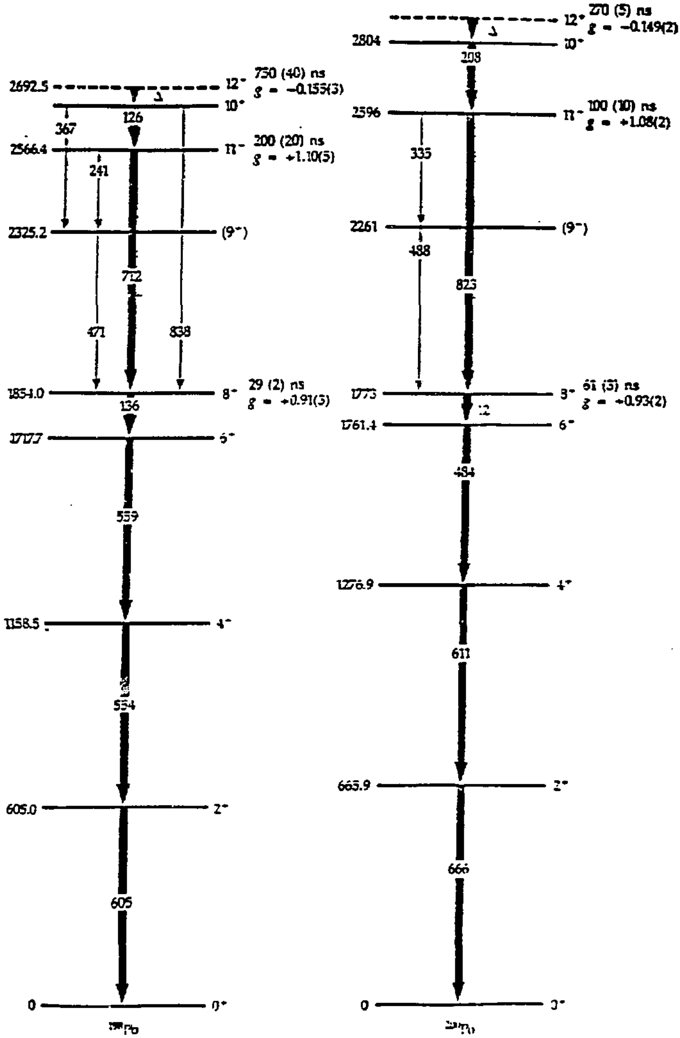

Partial level schemes of 198,200Po

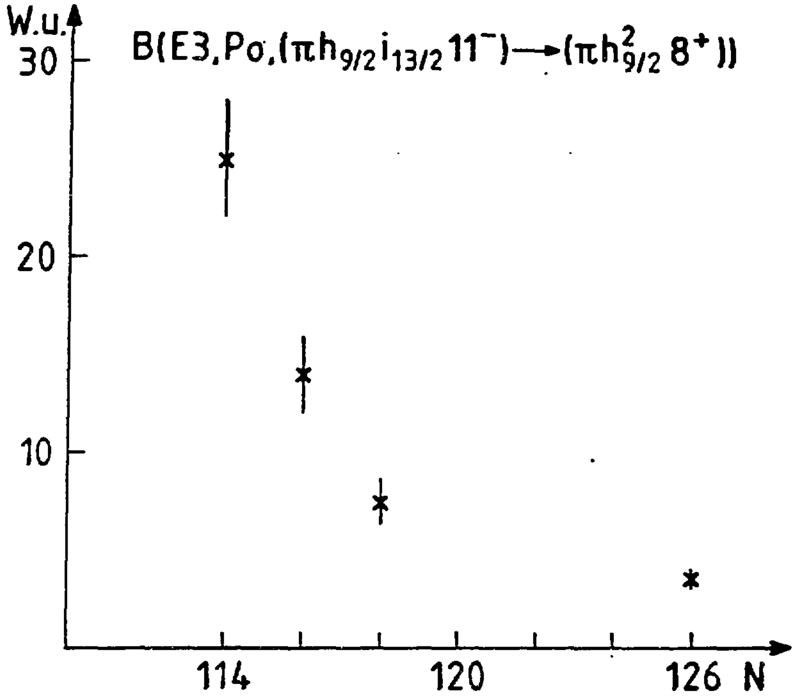

HMI-P-85-H-4549

Spectroscopy of 198,200Po with the 182,184W(20Ne,4n) reaction at Vicksi shows 8+ and 11- isomers with the same two proton structure as in 210Po, which is clear from their g factors. Also (νi13/2^{2} 12+) isomers are found that agree in excitation energy g factor and B(E2) value with the corresponding states in Pb isotones.
The B(E3, 11-→8+) values increase sharply with falling neutron number reaching a collective value of 25 Wu. in 198Po. This is surprisingly large, considering that the (i13/2→h9/2) spin flip transition is hindered by a factor 20.

HIGH SPIN STRUCTURE IN ^{154}Dy

W. C. Ma, I. Ahmed, B. Dichter, R. Holzmann, R.V.F. Janssens, T. L. Khoo – A.N.L.
P.J. DALY, Z. Grabowski, M. Piiparinen, W.H. Trzaska, M.A. Quader – Purdue Univ.
H. Emling – G.S.I.
M. W. Drigert, U. Garg – Notre Dame Univ.

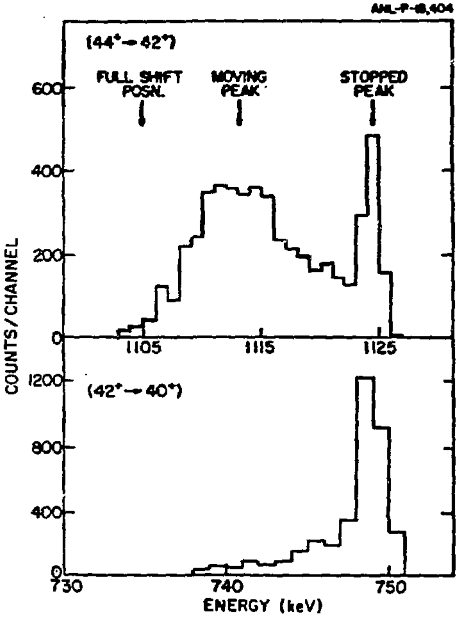

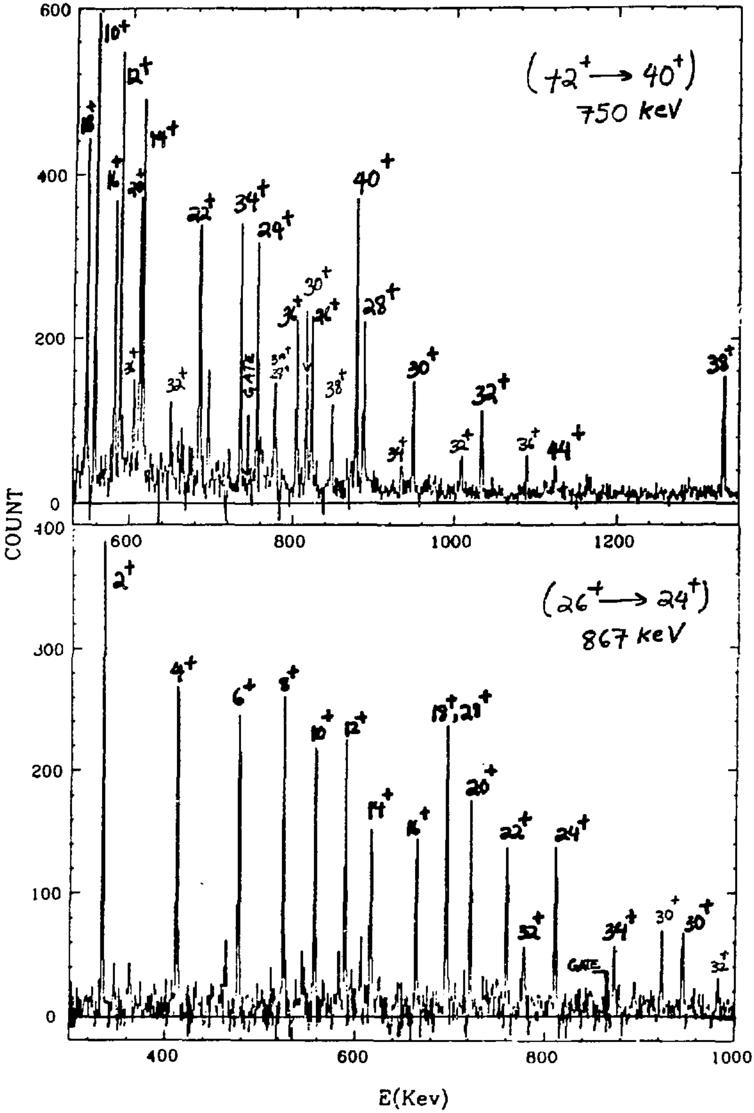
(42⁺ → 40⁺)
750 keV
(26⁺ → 24⁺)
867 keV
COUNT
E(Kev)
GATE

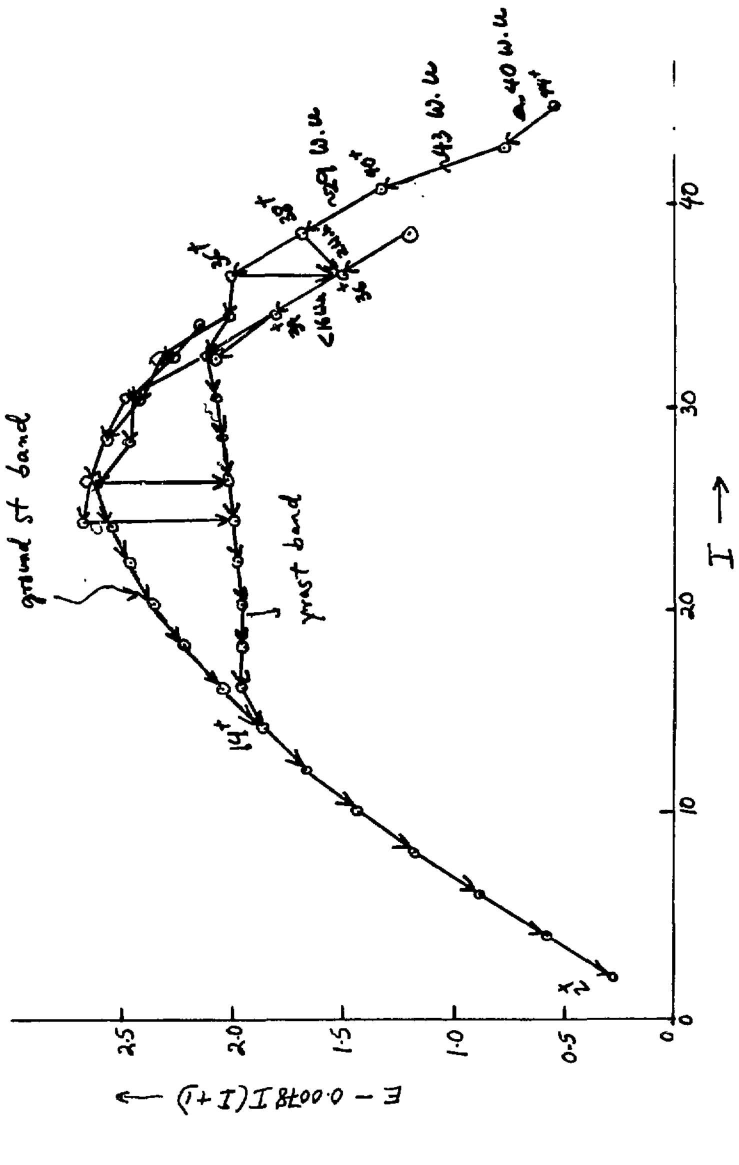
ground st band
yrast band
E − 0.0078 I(I+1)
I
0
10
20
30
40
0.5
1.0
1.5
2.0
2.5
2+
14+
36+
38+
40+
42+
43 W.u
40 W.u

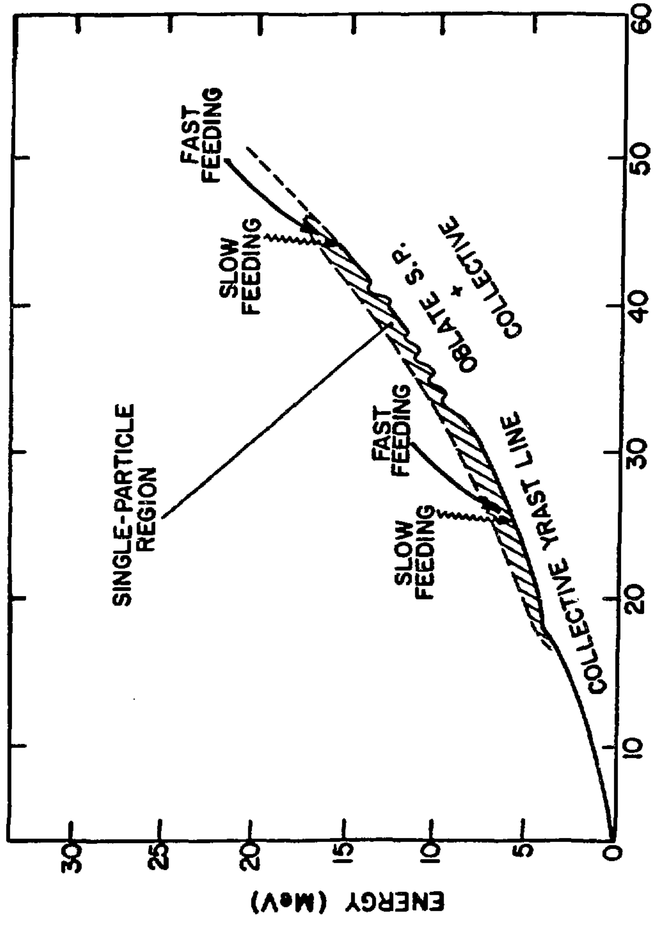
ENERGY (MeV)
I
0
5
10
15
20
25
30
10
20
30
40
50
60
SINGLE-PARTICLE REGION
SLOW FEEDING
FAST FEEDING
SLOW FEEDING
FAST FEEDING
OBLATE S.P. + COLLECTIVE
COLLECTIVE YRAST LINE

D. Headly — Comparison of experiment and theory for high spin states in ^{24}Mg and ^{25}Mg

SINGLE PARTICLE ROUTHIANS, NILSSON POTENTIAL, CRANKED AROUND SYMMETRY AXIS.

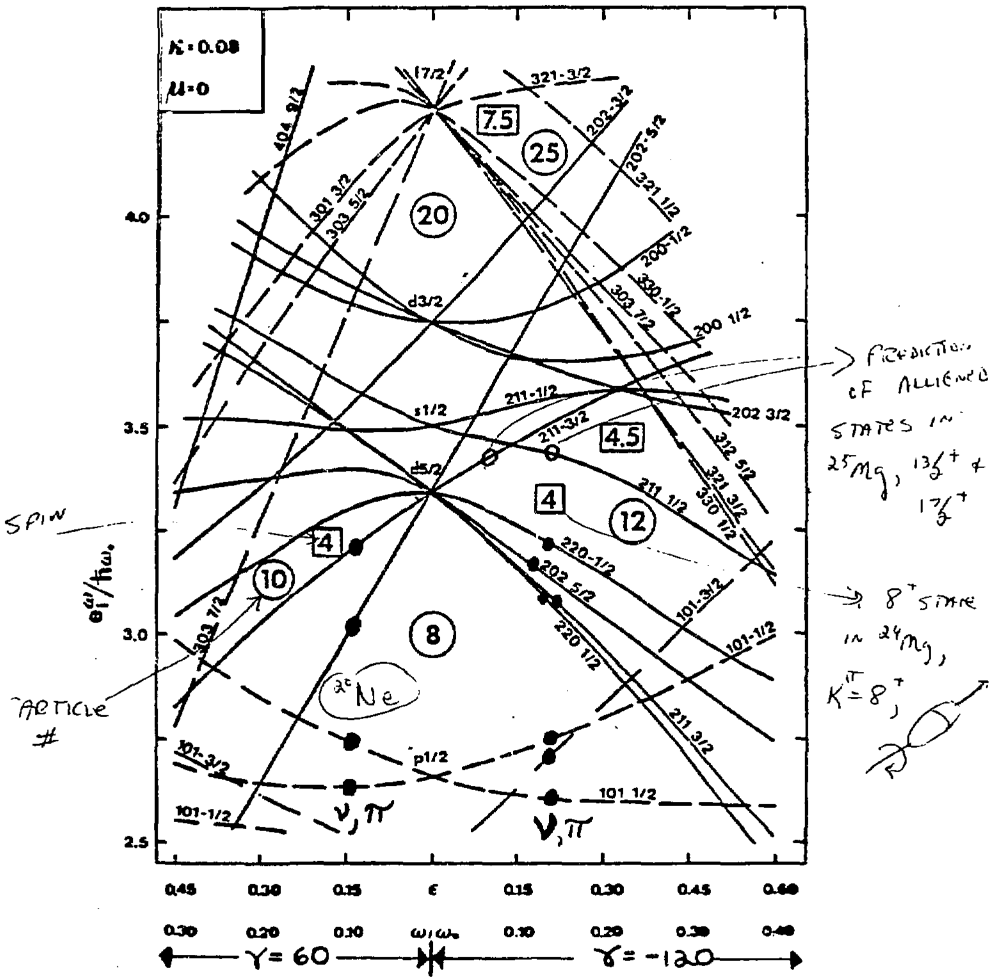

I. RAGNARSSON, T. BENGTSSON, S. ABERG, BORMIO WINTER MEETING, 1-81

^{25}Mg POTENTIAL ENERGY SURFACES

$[\varepsilon_2, \varepsilon_4, \gamma]$

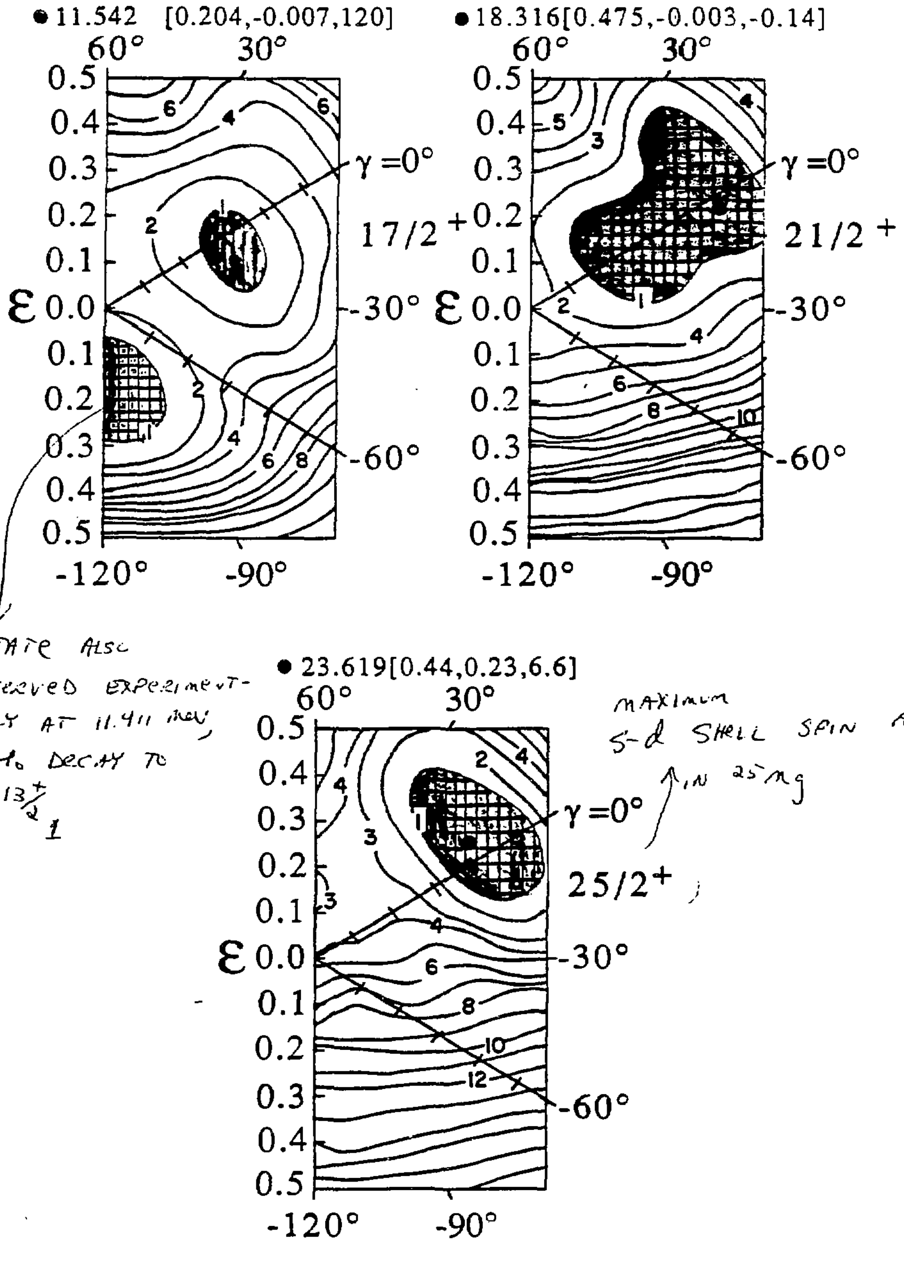

STATE ALSO OBSERVED EXPERIMENTALLY AT 11.411 MeV, 100% DECAY TO $13/2^+_1$

MAXIMUM s-d SHELL SPIN ALLOWED IN ^{25}Mg

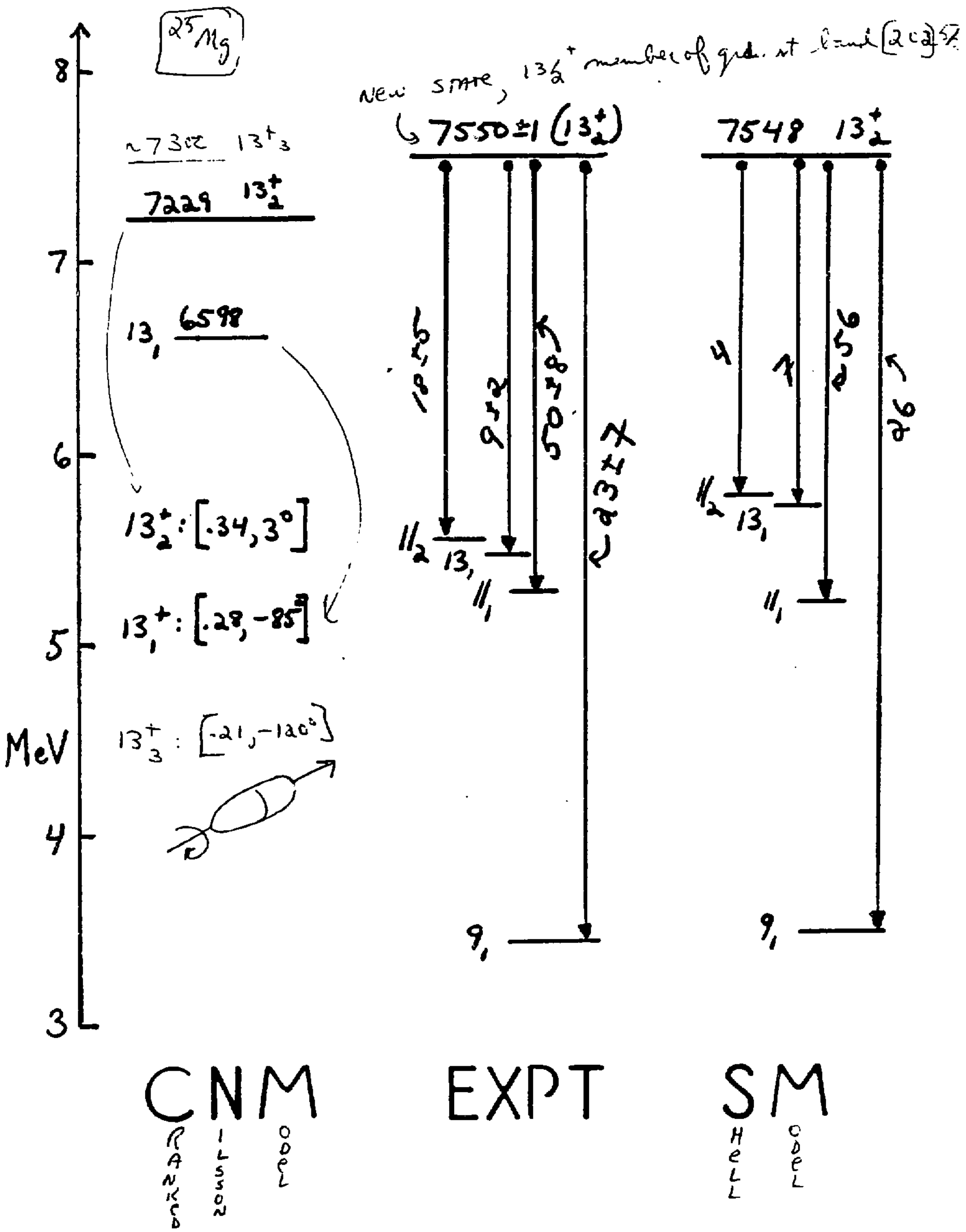
25Mg
New state, 13/2+ member of gnd. st. band
7550±1 (13/2+)
7548 13/2+
~7300 13/2+3
7229 13/2+
13/2 6598
13/2+: [.34, 3°]
13/1+: [.28, -85°]
13/3+: [.21, -120°]
MeV
8
7
6
5
4
3
18±5
9±2
50±8
23±7
4
7
56
26
11/2
13/1
11/1
9/1
CNM
RANKED NILSSON MODEL
EXPT
SM
SHELL MODEL

^{25}Mg POTENTIAL ENERGY SURFACES

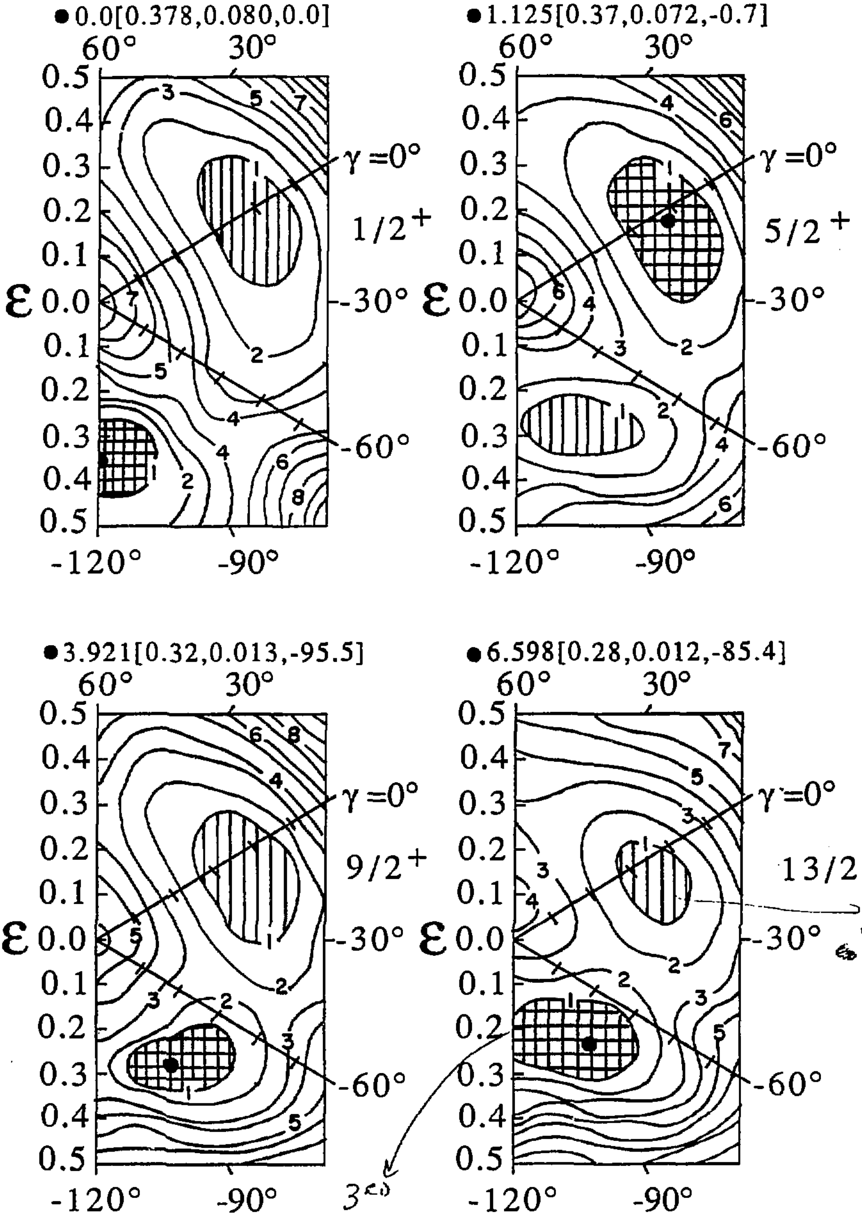

3rd minima, analogous to 8+ state in ^{24}Mg

SPIN ALIGNMENT AND BAND TERMINATIONS AT VERY HIGH ANGULAR MOMENTA.

Ingemar Ragnarsson

(based on work in cooperation with Tord Bengtsson)

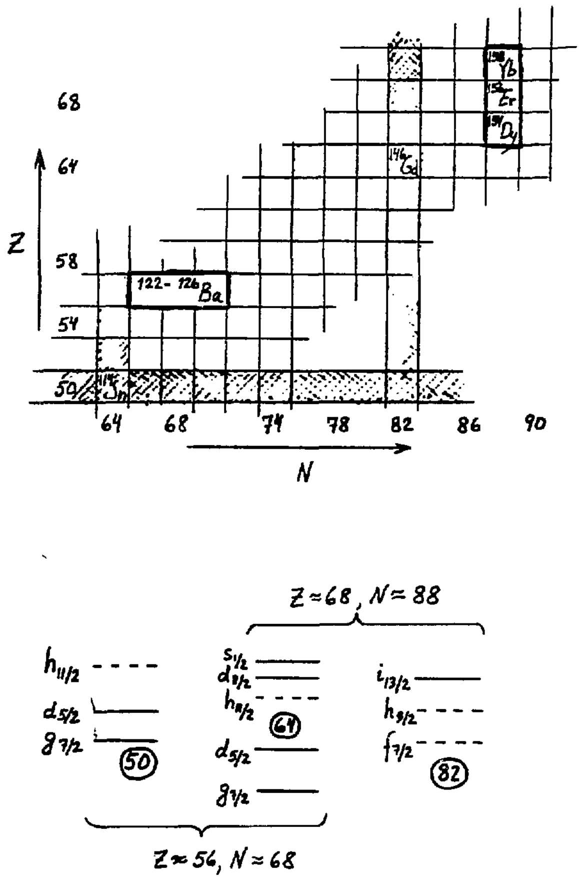

If neutrons and protons are exchanged and if the N=82 gap is exchanged by the Z=50 gap, the nuclei around ^{124}Ba can be characterized as having ~10 valence particles outside the ^{114}Sn core in the same way as the nuclei around ^{156}Er are characterized by having ~10 valence nucleons outside the ^{146}Gd core. This indicates the possibility of band terminations also in the former region. The lower part of the figure illustrates the high-j shells available for the valence nucleons in both cases.

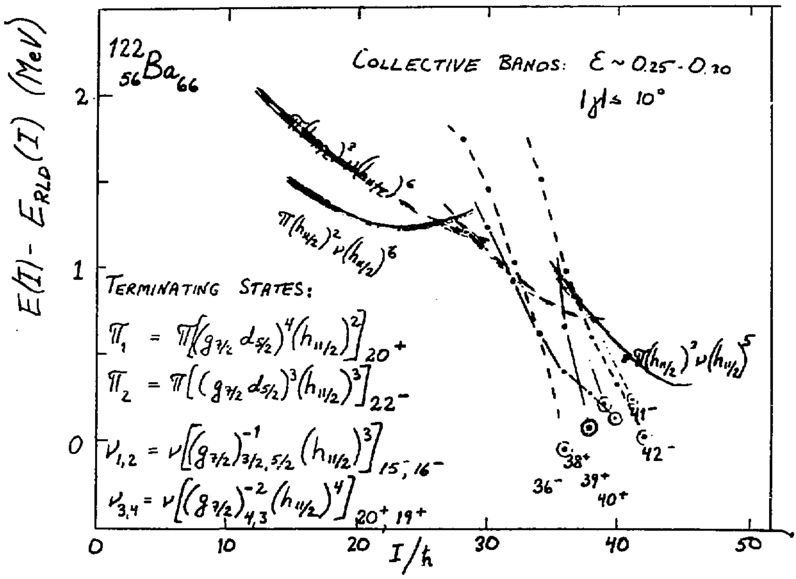

Calculated collective bands in ^{122}Ba having at least five neutrons in the $h_{11/2}$ shell (i.e. at least three holes in the N=64 core) and down-sloping terminating bands with three or four $h_{11/2}$ valence neutrons. The six encircled terminating states indicated have the proton configurations $\pi_{1,2}$ combined with the neutron configurations $\nu_{2,3,4}$.

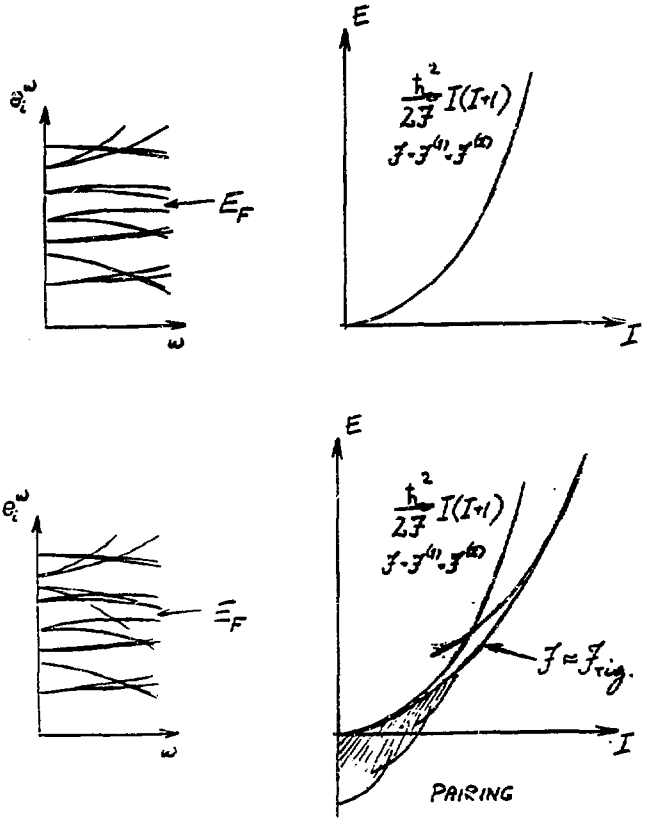

The upper part of the figure indicates that with the Fermi level in the middle of a shell, an approximate I(I+1) band is formed (no pairing). In the lower part, the band which results from a crossing single-particle orbital is added. It is also indicated that on the average, the energy increases by the rigid body moment of inertia i.e. with no band-crossings present, we will in many cases find $\mathcal{J}^{(1)} \approx \mathcal{J}^{(2)} \approx \mathcal{J}_{rig}$. Furthermore, at low spins, the pairing will change the band structure but as these band-crossings largely occur because of pairing, they are not relevant at higher spins where pairing is small or vanishing.

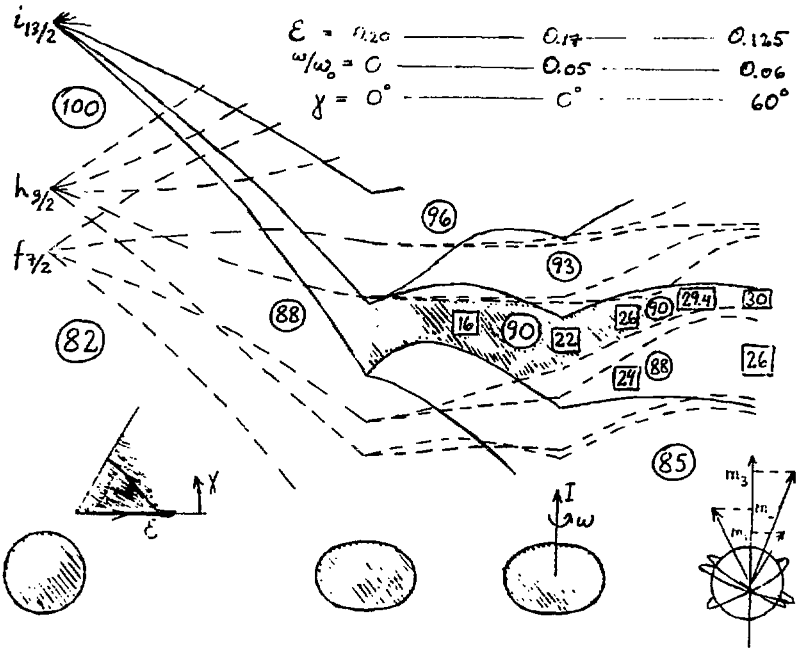

In the extreme case of band terminations, it is indicated how the nucleus finds its way through the deformation plane to avoid band crossings. Thus, the "N=90" gap is present from the collective rotation at low spins all the way to the aligned state when the 8 valence neutrons contribute with 30 spin units. Such shape changes is one important factor leading to large values of $\mathcal{J}^{(2)}$. Particle numbers are encircled while approximate spin contributions are given in squares.

I. Y. Lee High-spin nuclear structure studies using the spin spectrometer

ORNL— H. .RF LEE CESF.HIS CE130 K=15-24 G=970-1030KE

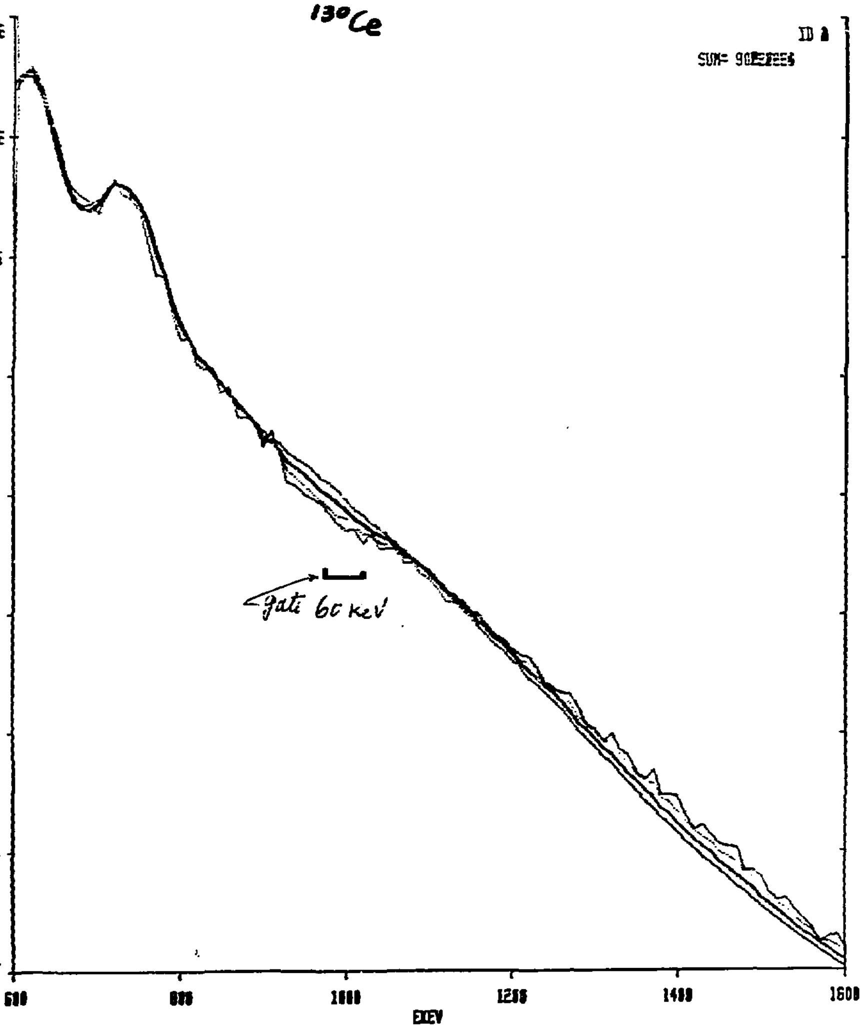

Simulation $2\mathcal{J}/\hbar^2 = 100\ \mathrm{MeV}^{-1}$

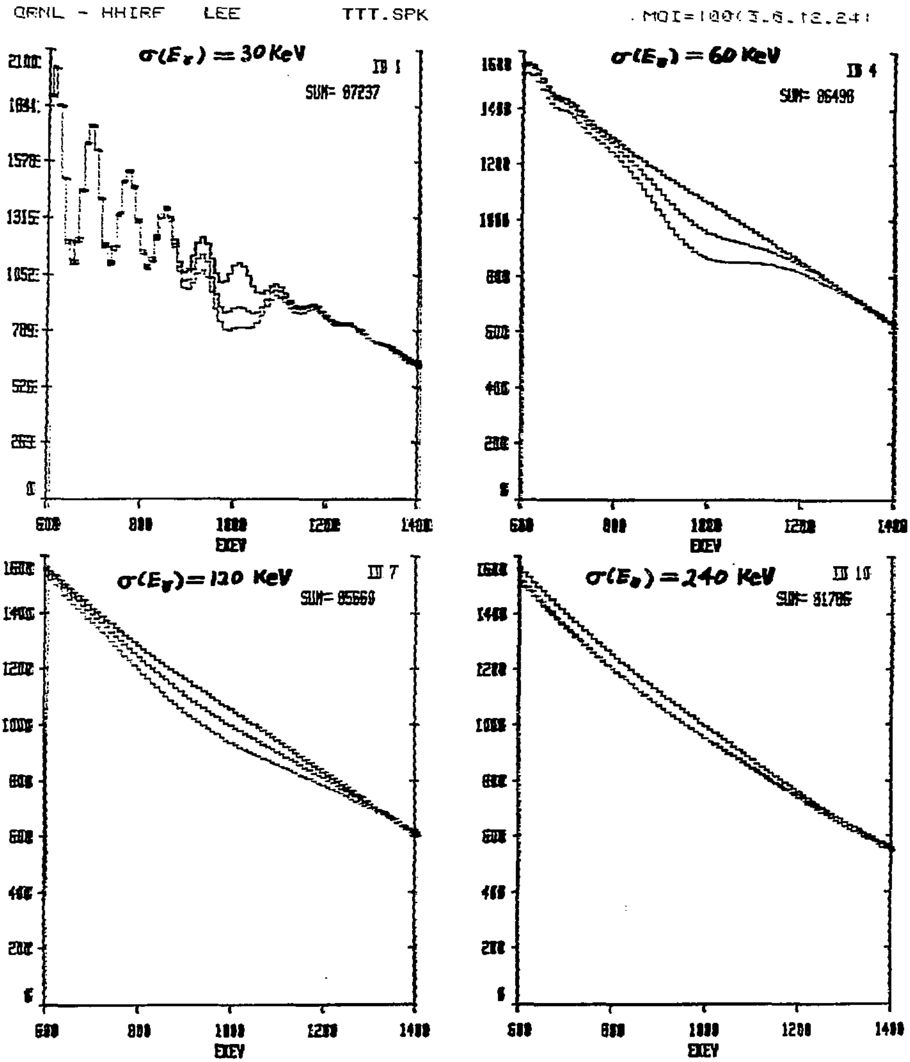

Table I. The γ-ray spreading width determined from double correlation spectra

	σ (Eγ)(KeV)					
	k = 15-17		k = 18-20		k = 21-24	
Eγ	H<15	H>15	H<18	H>18	H<21	H>21(MeV)
1.0	30(3)	33(4)	37(4)	30(4)	33(4)	34(6)
1.2	-	35(16)	49(11)	48(11)	43(11)	43(6)
1.4	-	-	49(20)		56(17)	

Table II. Ratio of the experimental valley depth to the calculated value

	δ					
	k = 15-17		k = 18-20		k = 21-24	
Eγ	H<15	H>15	H<18	H>18	H<21	H>21(MeV)
1.0	0.13(1)	0.16(1)	0.12(1)	0.15(2)	0.10(1)	0.11(2)
1.2	-	0.06(2)	0.06(1)	0.09(2)	0.06(2)	0.16(2)
1.4	-	-	0.04(1)		0.06(2)	

Conclusions

1) Gamma ray with narrow spreading width has intensity $<$ 15 %

2) The intensity is indepent of (H,k)

3) The double and triple correlation properties are similar

4) It is possible to study up to five fold correlation

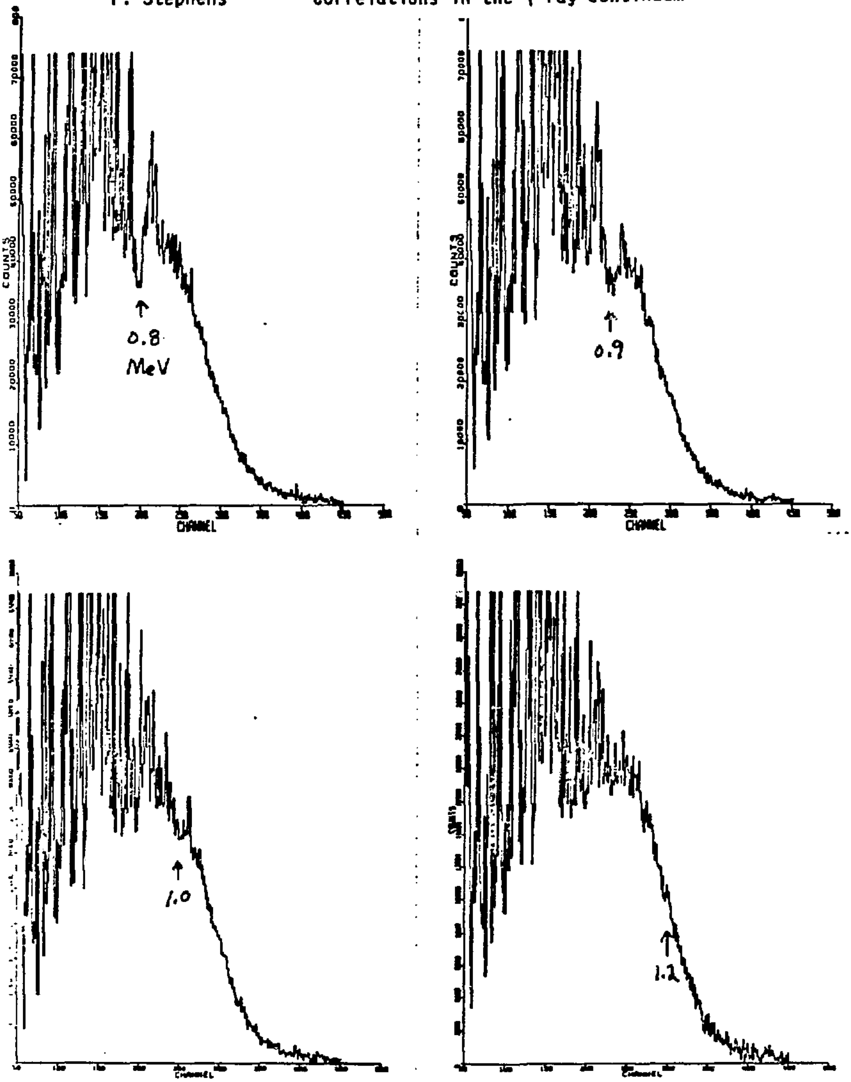

Fig. 1. Gated spectrum from the system; $^{48}Ti + ^{124}Sn \rightarrow ^{168}Hf^{*}$. The gate energies are indicated, and the dip areas run from about 30% of one transition at 0.8 MeV to no measurable dip at 1.2 MeV.

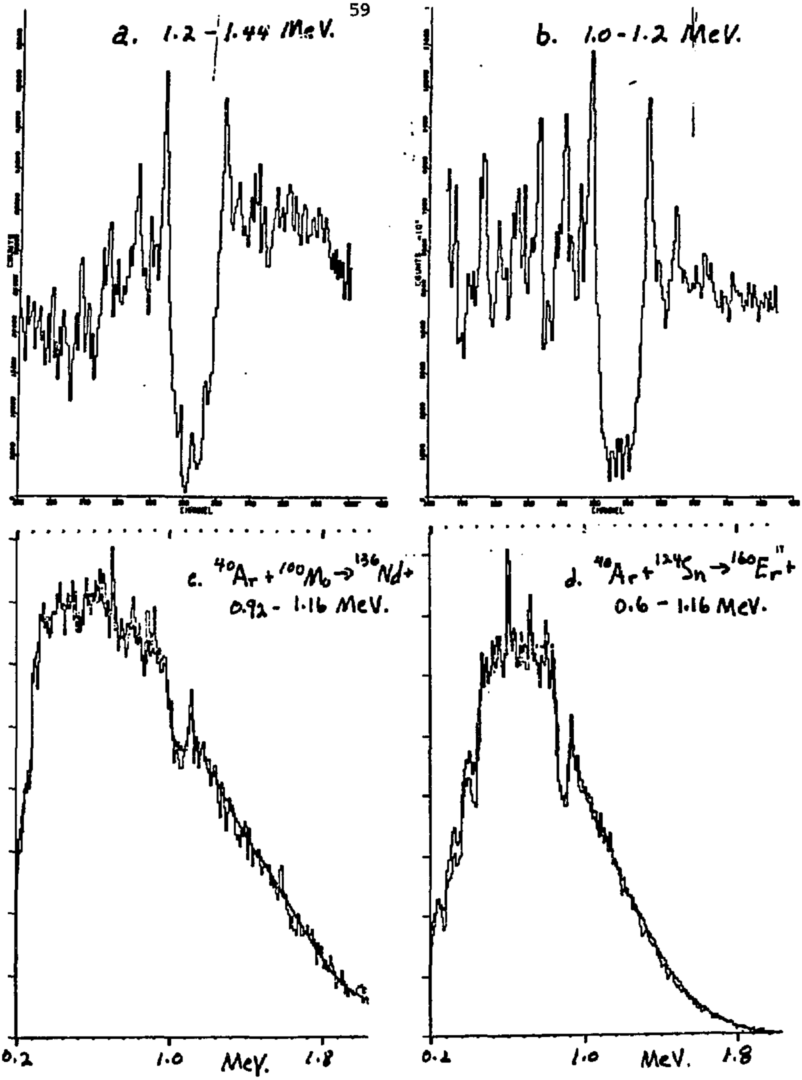

Fig. 2. a,b. Detailed dip shapes for the system: $^{40}Ar + ^{100}Mo \rightarrow ^{136}Nd +$. The channel widths and effective gate width are 4 keV, and individual gated spectra have been shifted and added over the indicated energy regions. For each gated spectrum a normaliz full-projection spectrum was subtracted to remove large scale variations. c,d. Single-gated (dark line) and double-gated (light line) spectra for the indicated systems. The effective gate width is 8 keV, and spectra have been shifted and added over the indicatec regions.

Observation	Conclusion
NARROW DIP	
1. Steep walls	little (no) smearing
2. Shape independent of E_γ	T ~ constant
3. Intensity falling with increasing E_γ	low-T effect
BROAD WIDTH	
1. Not easily visible	large smearing
2. Intensity increasing with increasing E_γ	high-T effect
3. Double gate similer to single gate	broad width $\gg$ 100 keV

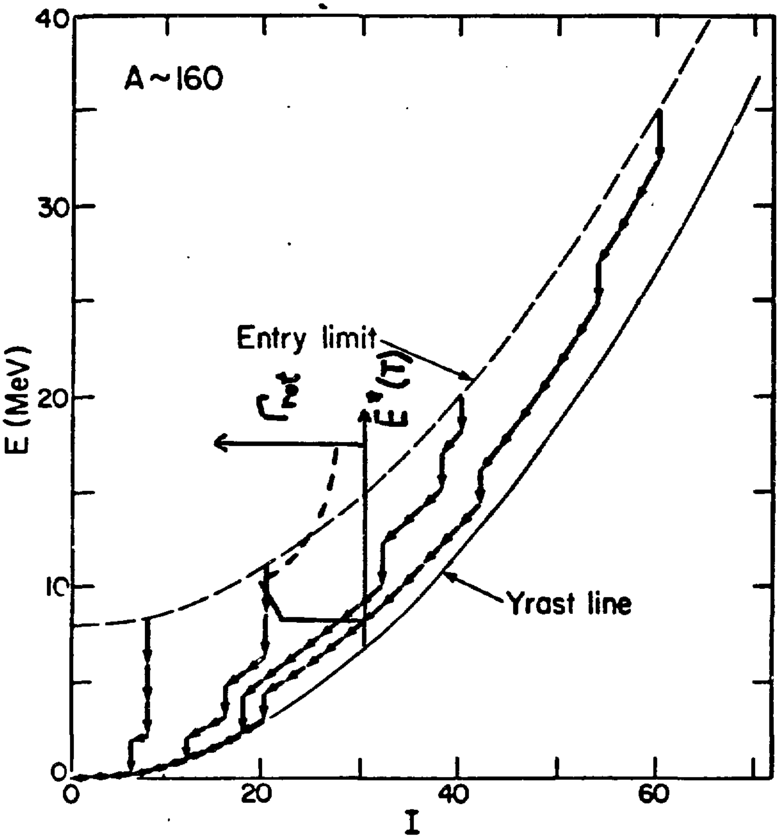

Fig. 4. Damping width, Γ_{rot}, calculated by Lauritzen, Døssing, and Broglia, superposed on some schematic cascades. Those cascades below the onset of the major damping give rise to the resolved lines and the narrow dip. The observed broad width corresponds to the large Γ_{rot} calculated above ~1 MeV excitation energy. The experimental values for the broad width, ~300 keV, seem larger than the calculated values, ~100-200 keV. Also there is no evidence for the narrow width (<100 keV) predicted at high excitation energies due to the motional narrowing. Such narrowing would produce dips at the highest γ-ray energies, which are not observed.

Does $B_{E2}(U_\gamma)$ have a tail ?

(Per Arve, Bent Lauritzen, G.A.L.)

Simplest model:

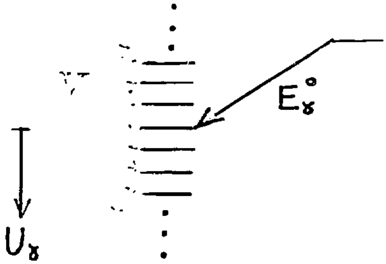

$$B_{E2}(U_\gamma) = \frac{\Gamma}{2\pi} \frac{1}{U_\gamma^2 + \left(\frac{\Gamma}{2}\right)^2} \; ; \qquad \Gamma = 2\pi \rho V^2$$

$$T_{E2}(U_\gamma) = \left(E_\gamma^\circ + U_\gamma\right)^5 \, B_{E2}(U_\gamma)$$

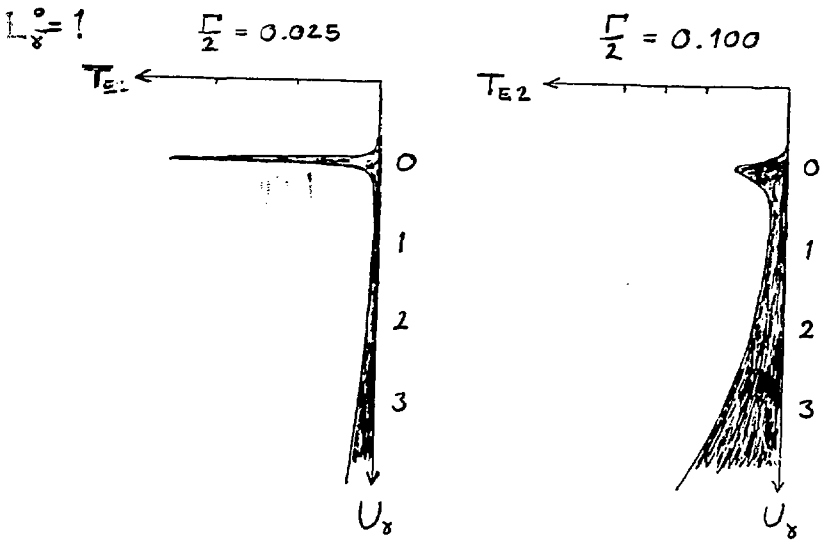

Numerical Study

$$H_I = \cos\omega_I \, H^A + \sin\omega_I \, H^B + H^C$$

where $$H^K = \sum_{\alpha\beta} f^K_{\alpha\beta} \, a^\dagger_\alpha a_\beta + \frac{1}{4}\sum_{\substack{\alpha\beta\\ \gamma\delta}} g^K_{\alpha\beta\gamma\delta} \, a^\dagger_\alpha a^\dagger_\beta a_\gamma a_\delta$$

$$f^K_{\alpha\alpha} = c^K_1 \, N(0,1)$$

$$f^K_{\alpha\beta} = c^K_2 \, N(0,1)$$

$$g^K_{\alpha\beta\gamma\delta} = c^K_3 \, N(0,1)$$

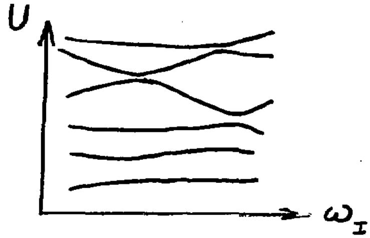

$50 \times$ (5 particles in 10 orbits, $N = \binom{10}{5} = 252$)

i) Weakly interacting but mixed bands
$c_1^A = c_1^B$, $(\omega_I - \omega_{I-2})\, c_1^{A,B} \gg c_3^C >$ level spacing

ii) Strongly interacting bands
$c_1^A = c_1^B \gtrsim c_3^C$, $(\omega_I - \omega_{I-2})\, c_1^{A,B} \ll c_3^C$

iii) H^A, H^B from GOE.

Plot $U_\gamma^2 \, B_{E2}(U_\gamma)$:

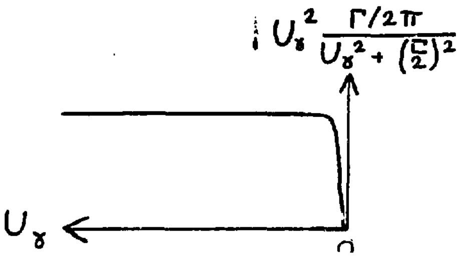

Weakly interacting but mixed bands

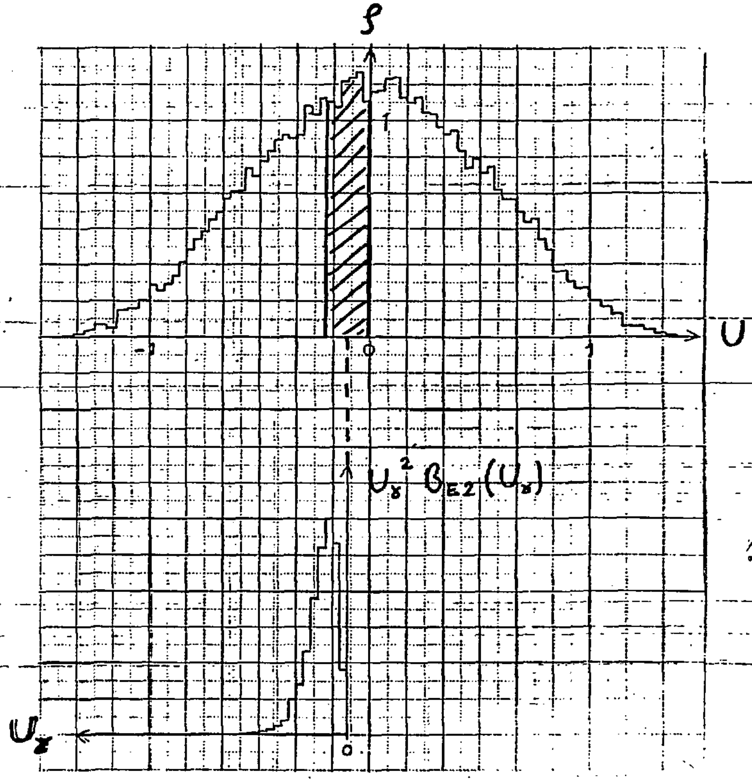

$B_{E2}(U_\gamma)$ is rapidly (exponentially) decreasing!

Strongly interacting bands

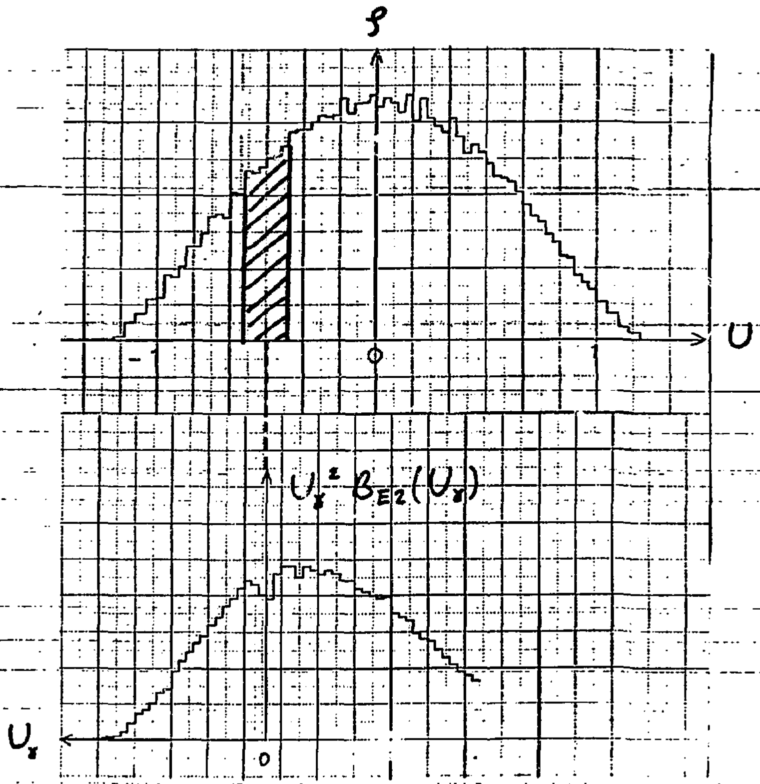

$B^{\downarrow}_{E2}(U_\gamma)$ = Breit-Wigner × level density ← decreasing

⇒ strength function similar to that for statisticals

$B^{\uparrow}_{E2}(U_\gamma)$ < B.-W. × level density ← increasing due to selection rules (c.f. GOE) ⇒ <u>some</u> E2 strength may be lost into a tail at large U.

MODEL FOR MIXING OF ROTATIONAL BANDS

(DAMPING OF ROTATIONAL MOTION)

Nucl. Phys. A457(1986)61

B. Lauritzen
R. A. Broglia
T. Døssing

(B. Mottelson)

Basic assumption: Quadrupole decay operator is diagonal in basis of eigenstates of the rotating mean field. (cranking ansatz)

$|\mu(I)\rangle \equiv$ many - particle - many - hole state at angular momentum I

$$\langle \mu'(I-2) \| \mathcal{M}(E2) \| \mu(I) \rangle = \mathcal{M}_{E2}(\mu)\, \delta_{\mu'\mu}$$

Corrections to the cranking ansatz are expected to show up as non - diagonal matrix elements of smaller order of $\mathcal{M}_{E2}$, related to wobbling motion. More important corrections may occur as corrections of three - body and higher order to the residual interaction mixing these bands. We do not know at present how to estimate such corrections.

1'st step: mixing of bands while neglecting dispersion in frequency

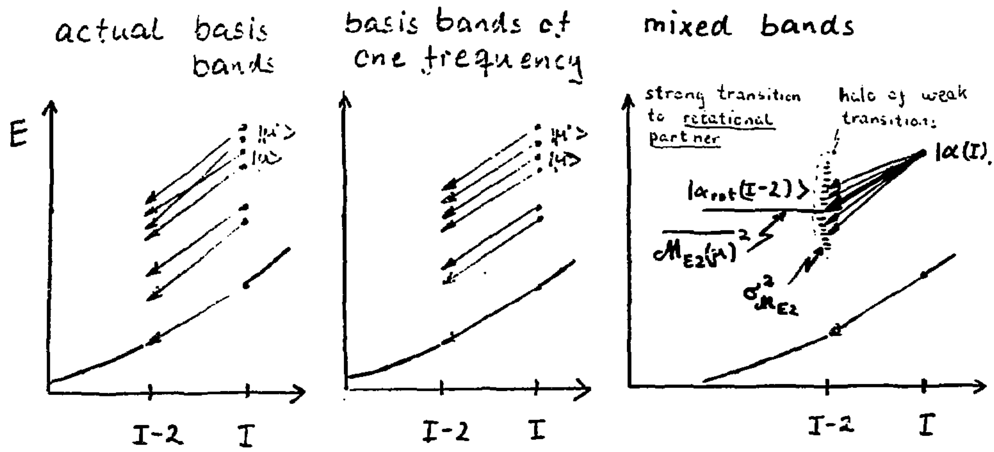

$\Gamma_\mu^\downarrow$ = spreading width of many-particle - many-hole state

$$\Gamma_\mu^\downarrow = \frac{2\pi}{d} |\langle\mu| V_{residual} |\mu'\rangle|^2 \propto d_2^{-1} \propto E^{*\,3/2}$$

Input: spreading width of single particle state

$$\Gamma^\downarrow_{s.p} \underset{\sim}{\propto} E^{*\,2}_{s.p.} \qquad \left(\Gamma^\downarrow_{sp} = \frac{E^{*\,2}_{s.p}}{15} MeV \right)$$

determines size of residual two-body interaction matrix elements $\langle\mu| V_{residual} |\mu'\rangle$

2nd step: include variation in frequency and change in $V_{residual}$

$$\Delta H(I-2) = \sum_{\mu} |\mu\rangle\, 2(\omega_\mu - \omega_0)\langle\mu| + \sum_{\mu\mu'} |\mu\rangle\langle\mu|\Delta V_{residual}|\mu'\rangle\langle\mu'|$$

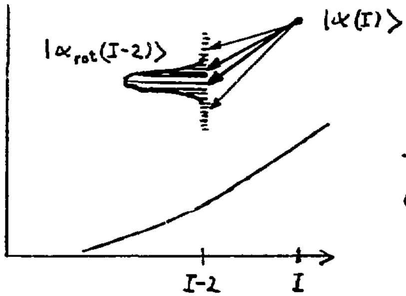

strength function of $|\alpha_{rot}(I-2)\rangle$

Resulting width $\Gamma^{\downarrow}_{rot}$ of strength function

(4.) $$\Gamma^{\downarrow}_{rot} = \frac{2\pi}{d_2}\langle \Delta V^2_{\mu\mu'}\rangle$$

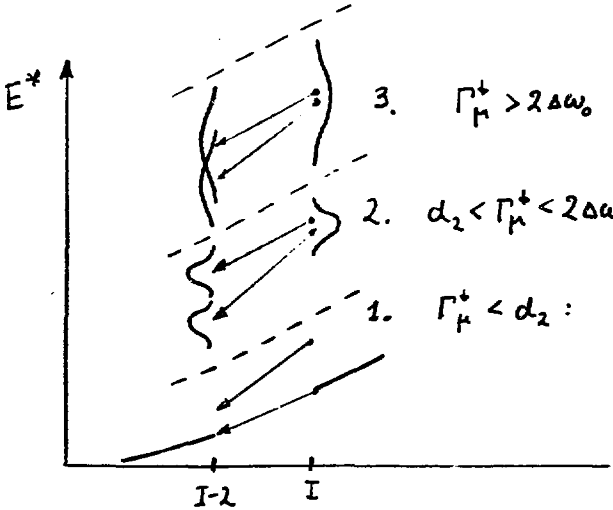

3. $\Gamma^{\downarrow}_{\mu} > 2\Delta\omega_0$: $\Gamma^{\downarrow}_{rot} = 2\,\frac{(2\Delta\omega_0)^2}{\Gamma^{\downarrow}_{\mu}}$

2. $d_2 < \Gamma^{\downarrow}_{\mu} < 2\Delta\omega_0$: $\Gamma^{\downarrow}_{rot} = 2(2\Delta\omega_0)$

1. $\Gamma^{\downarrow}_{\mu} < d_2$: $\Gamma^{\downarrow}_{rot} = 0$

Input: spread in cranked harmonic oscillator alignments

$$(2\Delta\omega_0)^2 \approx \left(\frac{2}{3}\right)^2\langle(\Delta i_\mu)^2\rangle \approx \left(\frac{2}{3}\right)^2 v\,\langle i^2_{v=1}\rangle\ , \quad \langle i^2_{v=1}\rangle = \frac{1}{6}(N+1)^2\left(\frac{2\hbar\omega}{\hbar\omega_0\delta}\right)^2$$

Dynamical model of band mixing, (due to Per Arve)
formulated by the analogy to the width of the nuclear magnetic resonance in condensed matter.

NMR:	Rotational Damping:
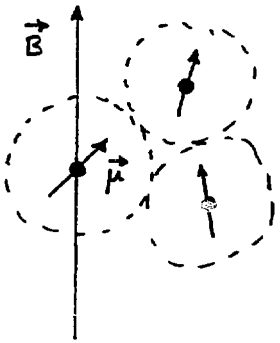	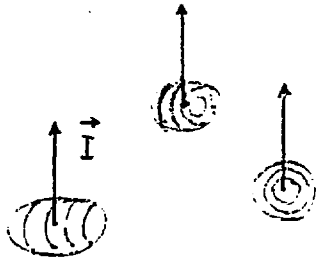
direction of transverse magnetic field	direction of transverse quadrupole field
spread in frequency at sites $\Delta\omega = g\Delta B$	spread in frequency of rotational bands $\Delta\omega_0$
hopping time between sites τ	hopping time between bands $\tau = \hbar / \Gamma_\mu^+$

Two regimes:

a) $\tau\Delta\omega > 1$: loss of directional correlation before hopping: $\Gamma = \hbar\Delta\omega$

b) $\tau\Delta\omega < 1$: relaxation of directional correlation occurs as a random walk

$$\frac{T_{relax}}{\tau} \cdot (\tau\Delta\omega)^2 \approx 1; \qquad \Gamma = \frac{\hbar}{T_{relax}} = \frac{\hbar^2\Delta\omega^2}{\Gamma_\mu^+}$$

Investigation of Continuum Properties in ^{152}Dy

R. Holzmann et al. (ANL, Notre Dame, Purdue

Total γ-ray spectra tagged on the 60ns isomer have been measured with Compton-suppressed Ge detectors of the ANL 360 facility

After background subtraction and unfolding the spectra could be decomposed into their various parts: trees and grass (i.e. discrete lines), dipole and quadrupole soil (i.e. continuum), and finally statisticals.

From the measured multiplicities, multipolarities, energies and Doppler-shifts the average γ-decay path from the entry states into the yrast line could be reconstructed accurately.

A simple model taking into account the competition between collective E2 decay and statistical E1 decay at high temperature could be adjusted to the data with a consistent set of parameters: Q_0, $\mathcal{J}_{eff}$ and level density parameter a.

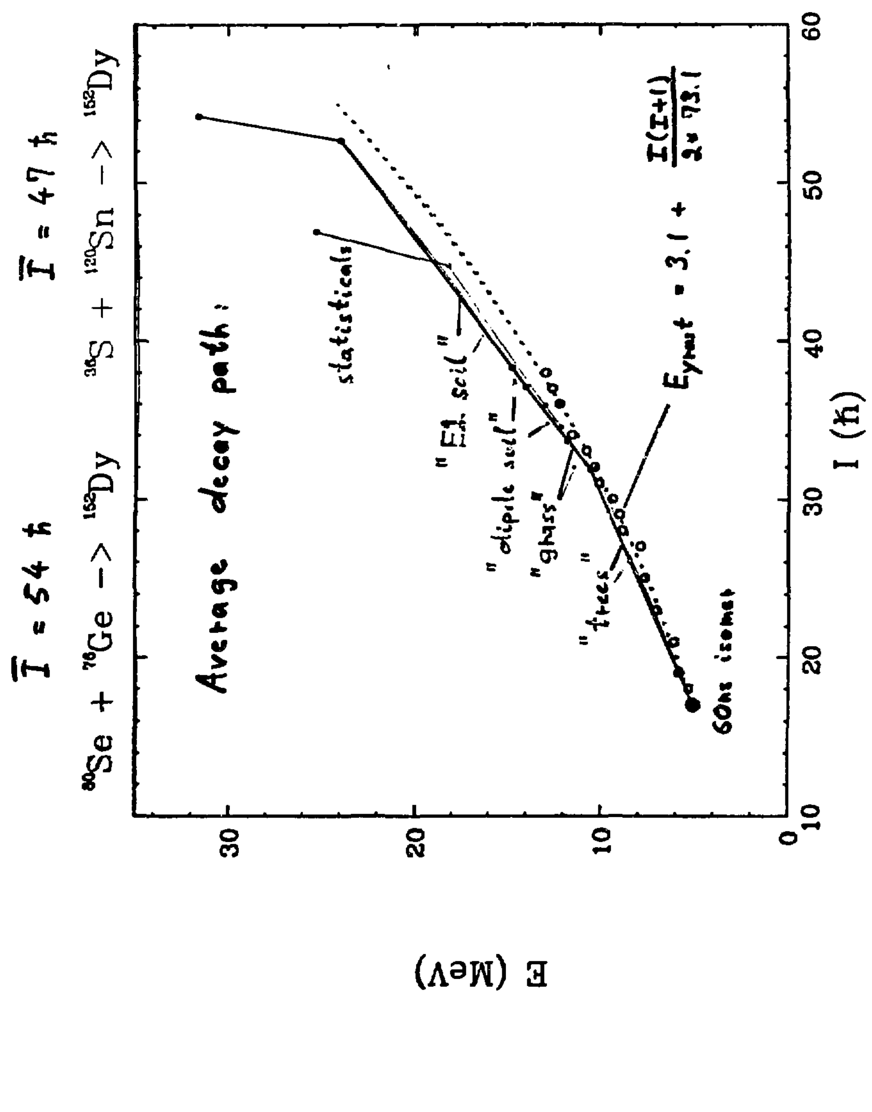

Ī = 54 ħ
80Se + 76Ge -> 152Dy
Ī = 47 ħ
32S + 120Sn -> 152Dy
Average decay path:
statisticals
"E1 scil"
"dipole scil"
"glass"
"trees"
60ns isomer
E_yrast = 3.1 + I(I+1)/(2* 73.1)
I (ħ)
E (MeV)

Calculate competition between collective and statistical decay:

Input:

- quadrupole moment Q_0
- effective moment of inertia $\tilde{\mathcal{I}}_{eff}$
- level density parameter a

} fitted to da

- cut-off of collectivity U_0 ← measured directly

Output:

- multiplicities M_{E2}, M_{stat}
- energy spectra E2 bump, statisticals

} given by the competiti

$$\frac{B(E2)_{col}}{B(E1)_{stat}}$$

- Doppler shifts τ_{col}, τ_{stat} } given by Q_0 & a

Comparison between model and data:

$^{80}Se + ^{76}Ge \rightarrow ^{152}Dy$

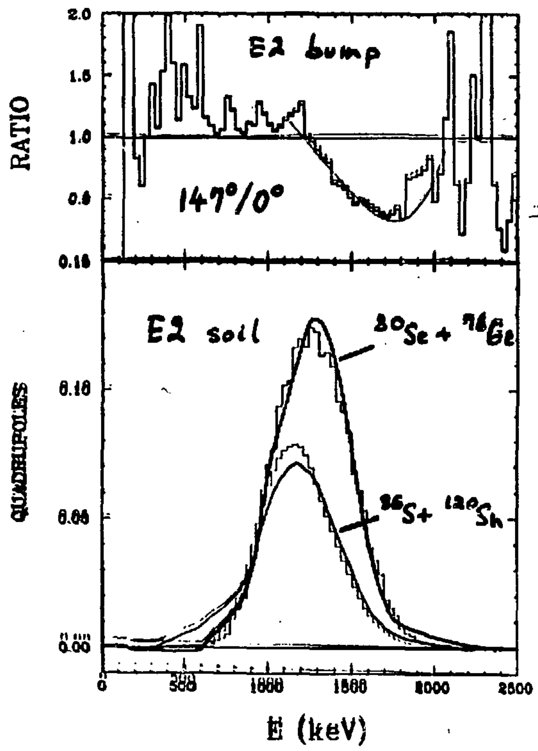

Best fit:

$a = \frac{A}{7}$

$\bar{\mathcal{J}}_{eff} = 76$

$\bar{\bar{Q}}_0 \approx 700 \ fm^2$

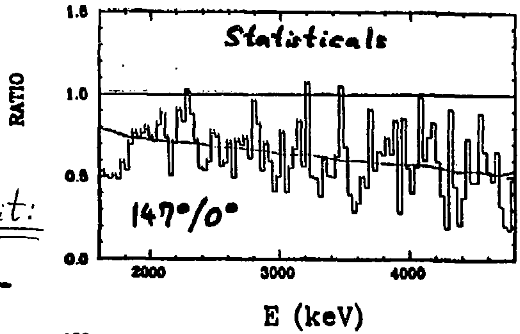

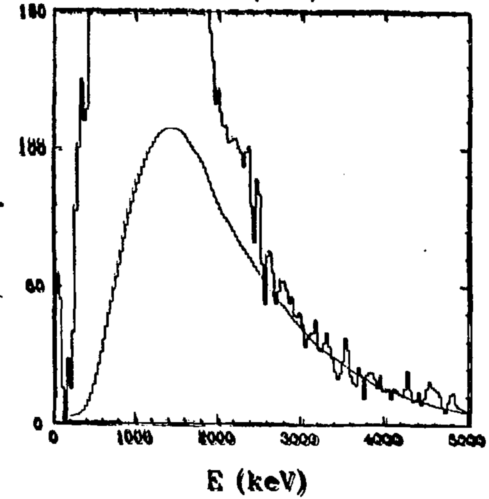

Energetic M1 Transitions: Probe of Nuclear Collectivity at High Temperatures

CYRUS BAKTASH (ORNL)

- Used Spin Spectrometer to study differential effects of spin and temperature.
- Reaction: 285 MeV $^{64}Ni + ^{98}Mo$
- The following figure shows the effect of multiplicity (M=21, 25, 29) at 3 different excitation energies.

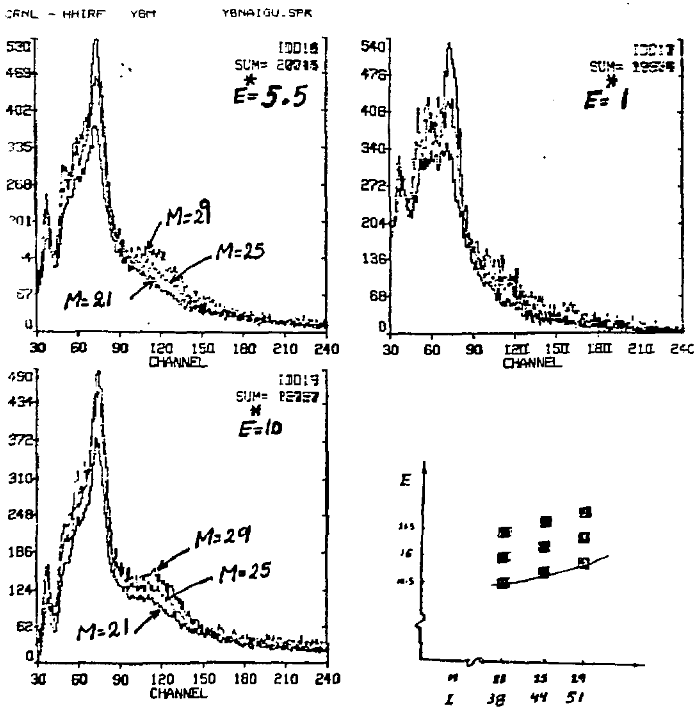

Note the growth of E2 collective bump at high spins and high temperature. It is Absent near the yrast line at all multiplicities.

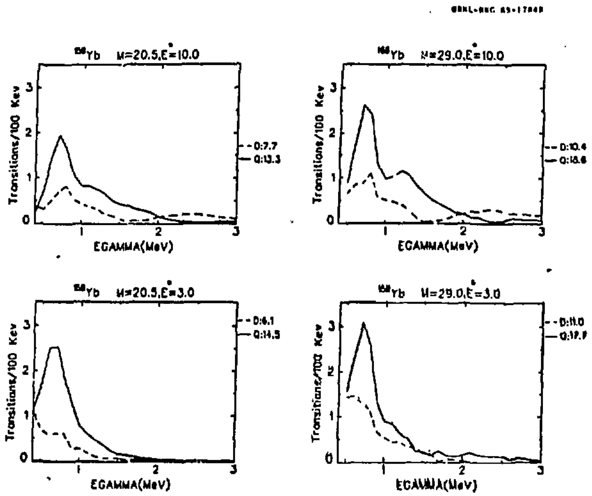

- Unfolded and decomposed spectra At two multiplicities (M=20.5, 29) and excitation energies (E* = 3 and 10 MeV).
- Solid curves show the Quadrupole transitions. Broken lines indicate the dipole transitions.
- Note the growth of an E2 (Collective) bump at 1.2 MeV with spin and Temperature (It is absent near the yrast line).
- The low-energy dipole increases with M but <u>decreases</u> with E*. It is anticorrelated with the E2 bump.
- The high-energy dipole bump (centered at 2.5 MeV) increases with temperature and correlates with the E2 bump. Angular distribution shows a large mixing ratio ($\delta \simeq 1$) and, hence, indicates M1/E2 character for this bump.

76 Chen & Leander

Chen & Leander have pointed out for large deformations and high excitation energies, M1 transitions can compete effectively with E2 transitions.

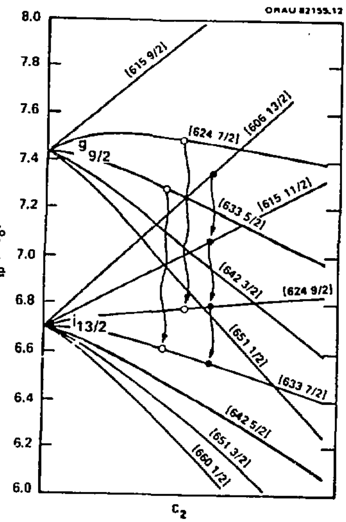

- Centroid of the M1 bump increases with increasing ε;
- The intensity of the M1 bump increases with excitation energy.

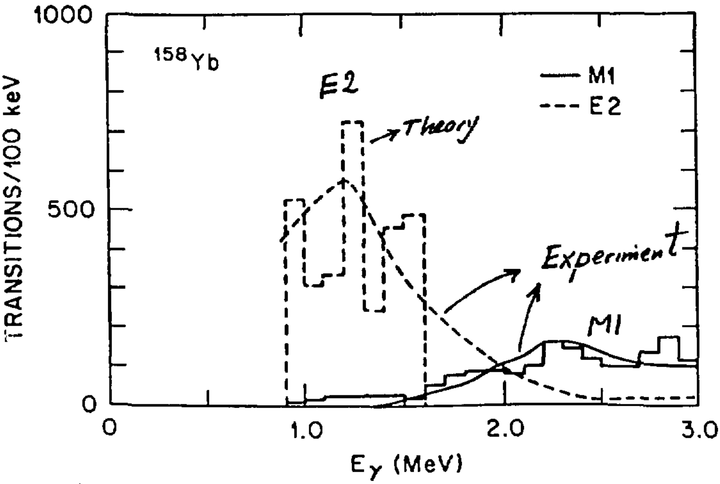

A calculation by Y.C. Chen reproduces the experimental trend of the M1 bump. Its centroid is reproduced if a deformation of $\varepsilon \simeq 0.35$ is assumed. This sensitivity could be utilized to infer deformation of the collective structures at high E^*.

Summary

We have studied the differential effects of spin and temperature on nuclear shapes and collectivity in the light rare-earth region. The results indicate:

(1) At low excitation energies, collective structures give way to non-collective states with increasing spin. This is referred to as "Band Termination" and is a consequence of finite angular momentum of the valence shell

(2) At high spins:
Non-collective structures give way to collective states with increasing Temperature.

(3) Shell effects survive and dominate the nuclear structure at least up to one neutron binding energy in this region.

(4) Energetic M1 transitions can compete effectively with collective E2 at high E and T. These transitions can be used as a probe of nuclear collectivity at high temperatures (e.g. superdeformed states). Their contribution to Non-statistical cooling should be taken into account.

LIFETIME MEASUREMENTS IN ^{132}Ce FROM I = 10 → 50

P J NOLAN et al.

LIVERPOOL UNIVERSITY/
DARESBURY LABORATORY

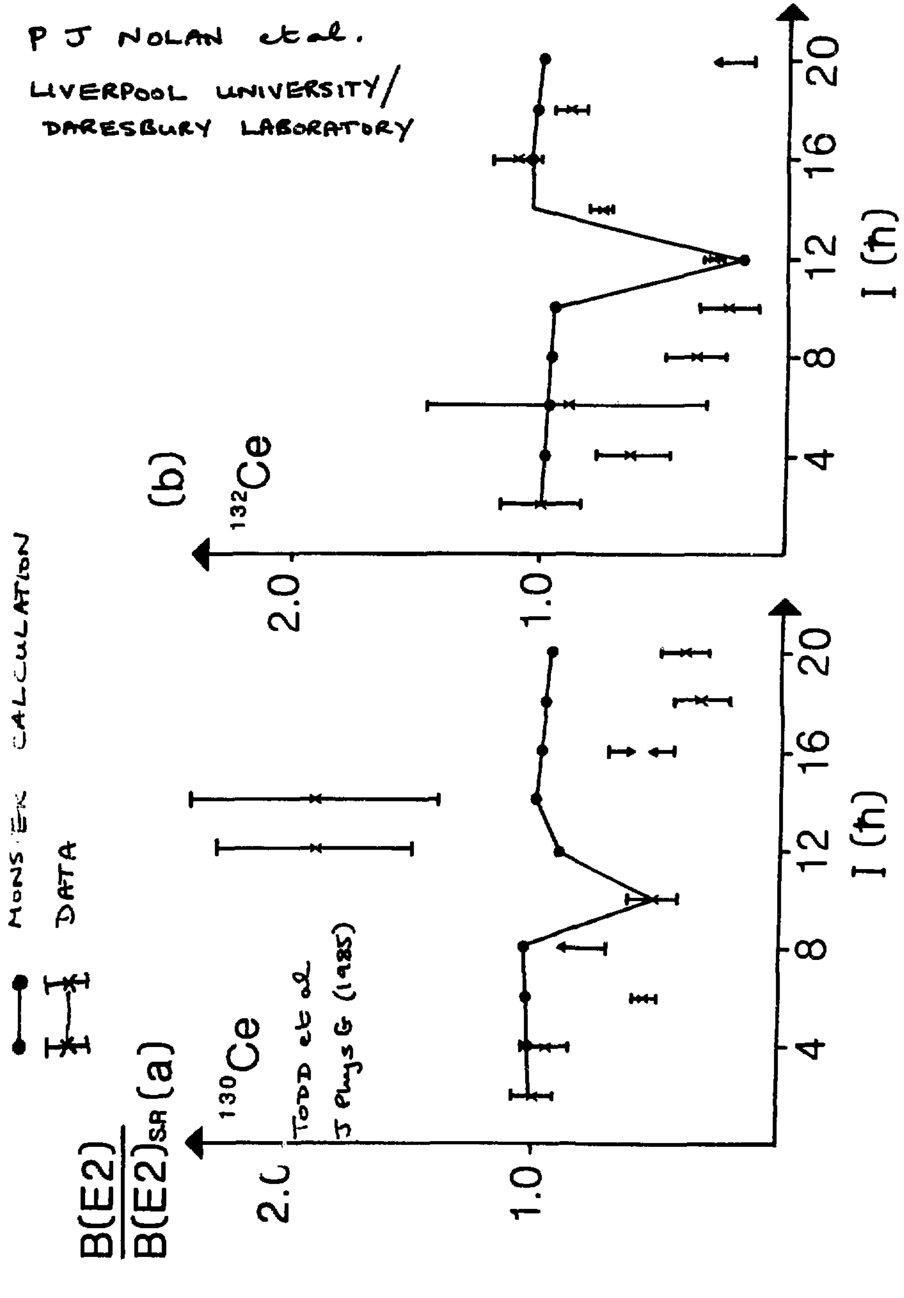

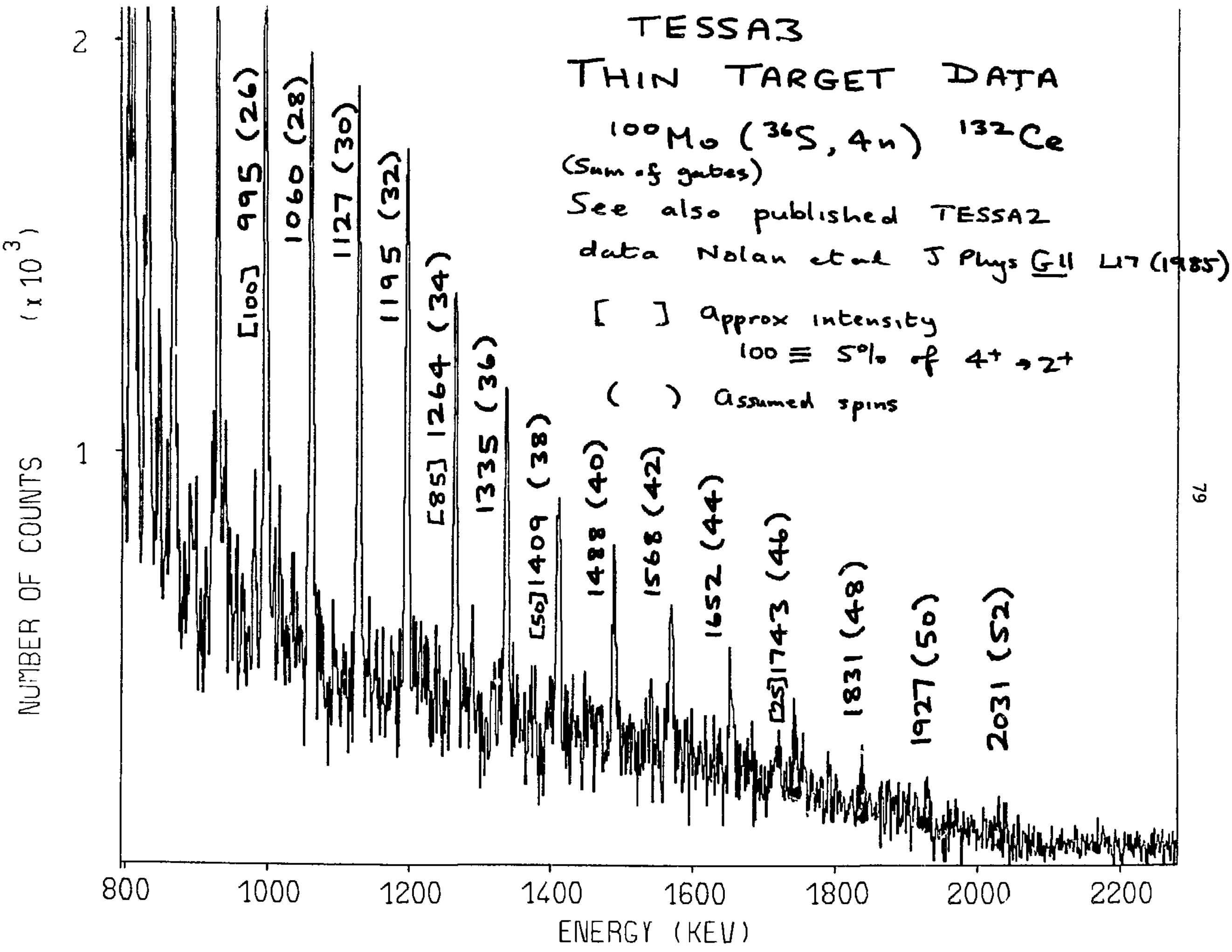
TESSA3
THIN TARGET DATA
$^{100}Mo(^{36}S, 4n)^{132}Ce$
(Sum of gates)
See also published TESSA2
data Nolan et al J Phys G11 L17 (1985)
[ ] approx intensity
100 ≡ 5% of 4+ → 2+
( ) assumed spins
[100] 995 (26)
1060 (28)
1127 (30)
1195 (32)
[85] 1264 (34)
1335 (36)
[50] 1409 (38)
1488 (40)
1568 (42)
1652 (44)
[25] 1743 (46)
1831 (48)
1927 (50)
2031 (52)
NUMBER OF COUNTS
(x 10^3)
2
1
800
1000
1200
1400
1600
1800
2000
2200
ENERGY (KEV)

BAND MOMENT OF INERTIA

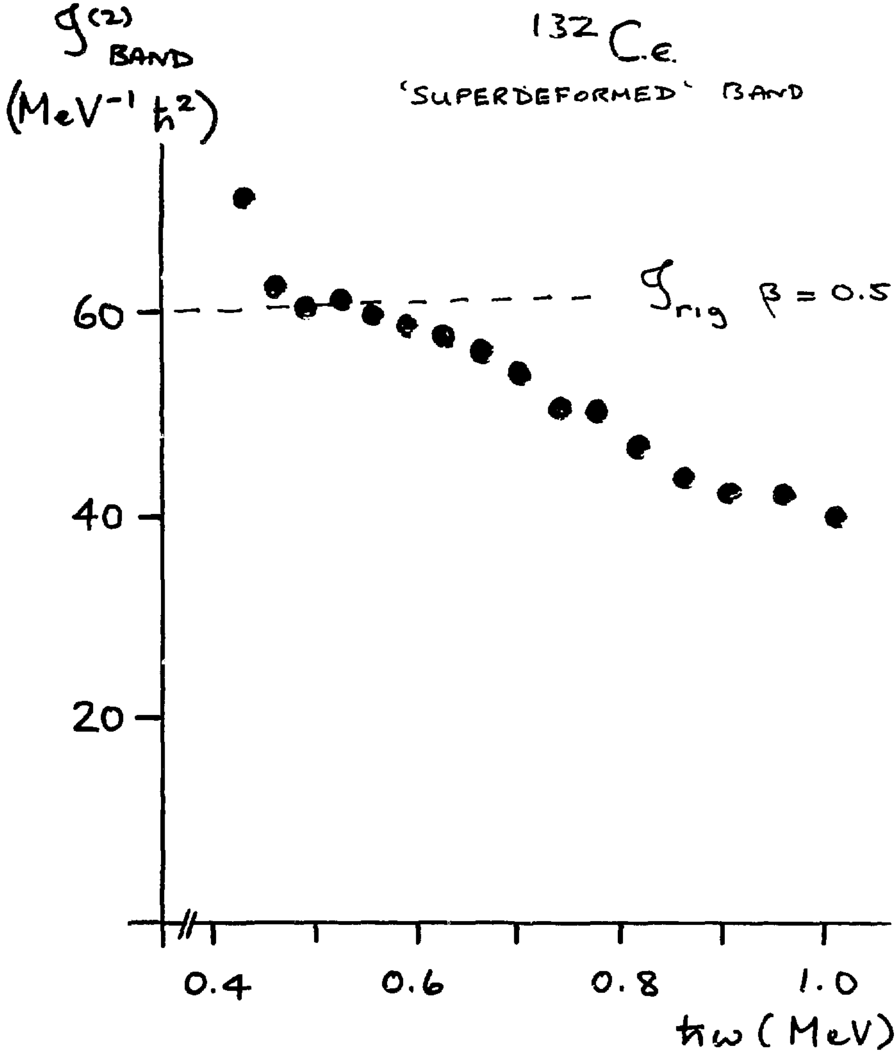

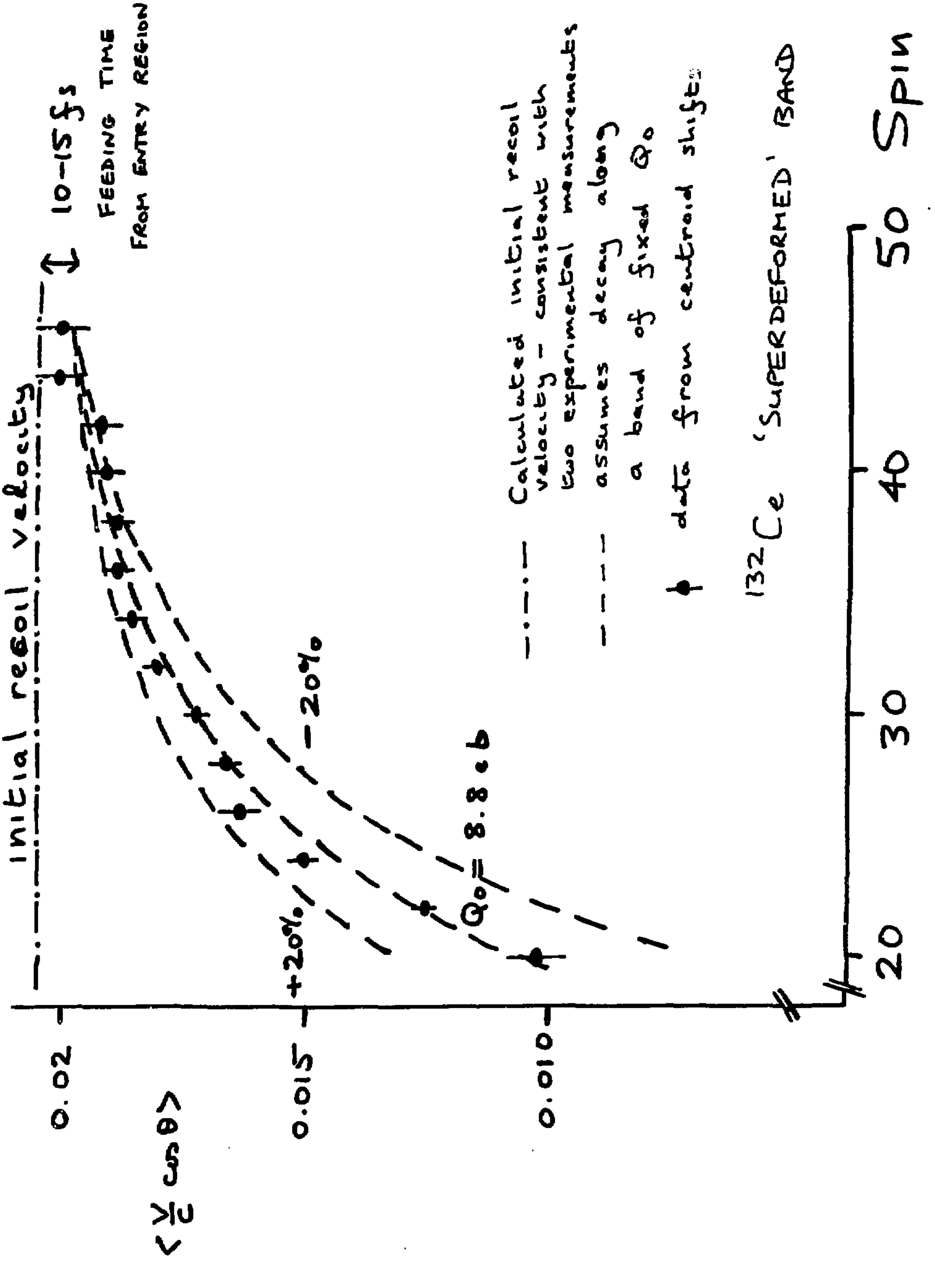

initial recoil velocity
10–15 fs
FEEDING TIME
FROM ENTRY REGION ?
Calculated initial recoil velocity – consistent with two experimental measurements
assumes decay along a band of fixed Q_0
data from centroid shifts
^{132}Ce 'SUPERDEFORMED' BAND
+20%
−20%
Q_0 = 8.8 eb
$\langle \frac{v}{c} \cos\theta \rangle$
0.02
0.015
0.010
20
30
40
50
Spin

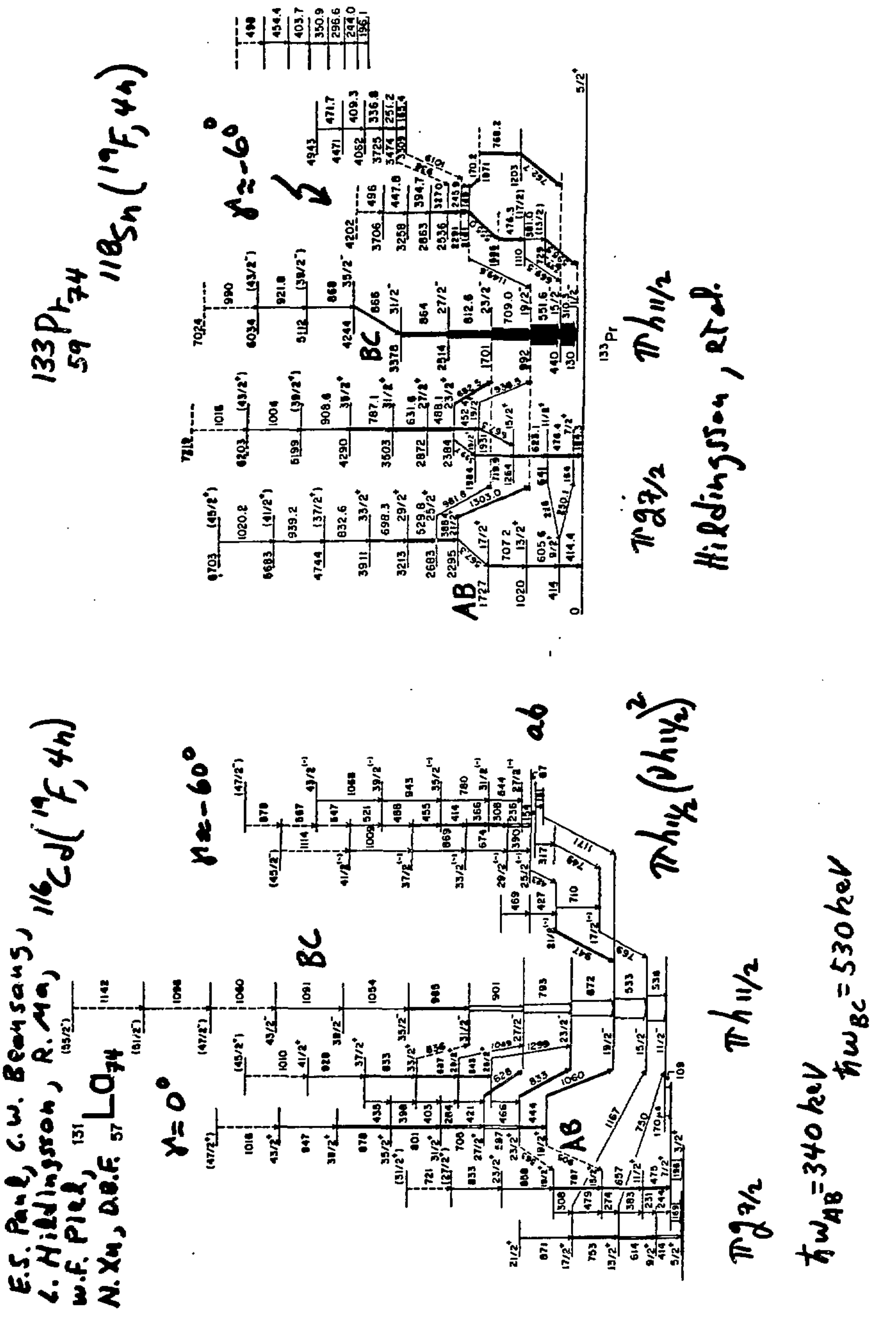

Z = 61

ALIGNED ANGULAR MOMENTUM FOR
PM139 137 135 133

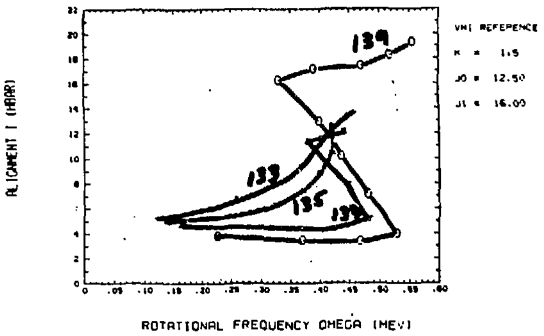

— ^{133}Pm (DARESBURY) N = 72
— ^{135}Pm 74
— ^{137}Pm 76
— ^{139}Pm 78

C.W. Beausang et al.

N = 74

ALIGNED ANGULAR MOMENTUM FOR
PM135

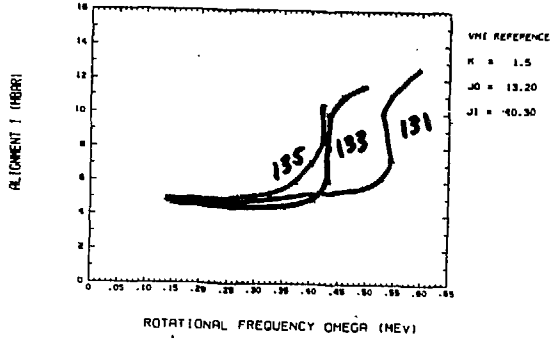

— ^{131}La Z = 57
— ^{133}Pr 59
— ^{135}Pm 61

C.W. Beausang, R. Ma, E.S. Paul,
W.F. Piel, Jr., P.K. Weng, N. Xu, D.B.F.

$^{114}Cd(^{27}Al, p4n)$

$^{116}Cd(^{24}Mg, 4n)^{136}Nd$
106/111 MeV

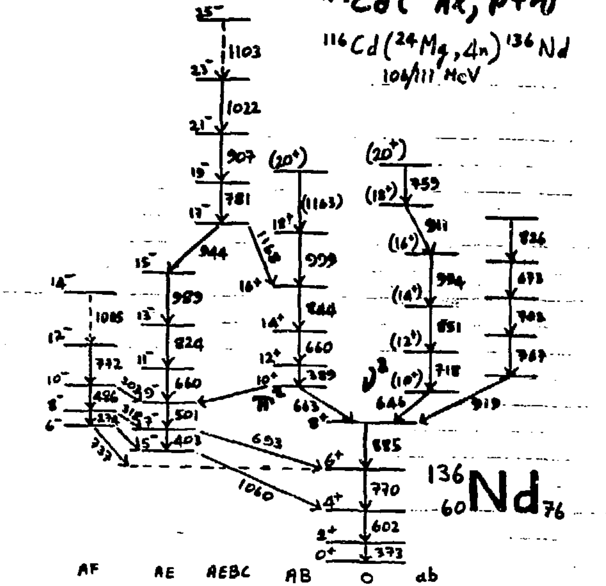

$^{136}_{60}Nd_{76}$

γ sensitive to particle configuration
(high j orbitals)

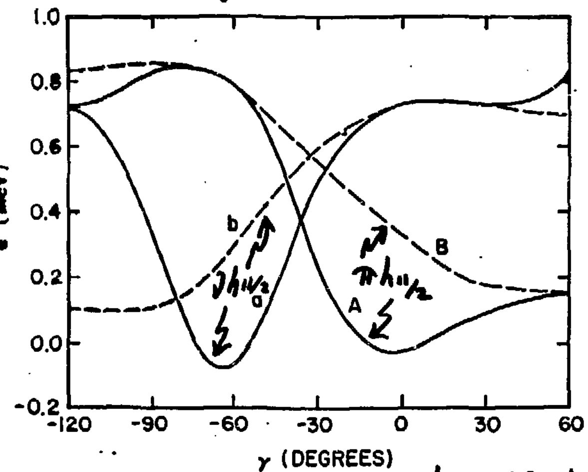

ħω = 250 keV

W.F. Piel, Jr., C.W. Beausang, L. Hildingsson, E.S. Paul, D.B.F.

$\hbar\omega_{AB}(a) = 336$ keV
$\hbar\omega_{AB}(b) = 317$ keV

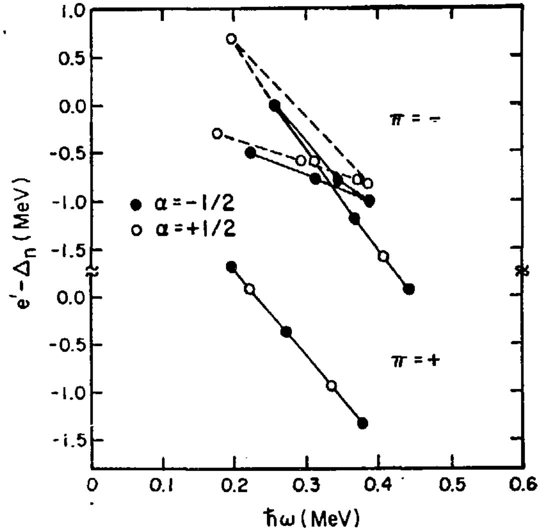

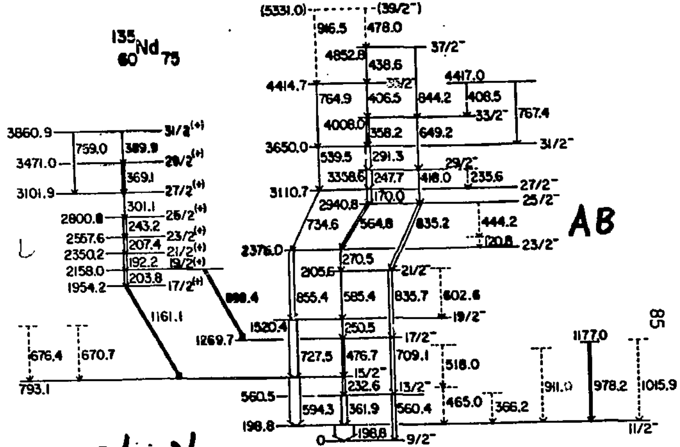

$\pi g_{7/2}\, \pi h_{11/2}\, \nu h_{11/2}$

$\nu h_{11/2} \rightarrow \nu h_{11/2} (\pi h_{11/2})^2$

$\hbar\omega_{AB}(a) = 336$ keV
$\hbar\omega_{AB}(b) = 317$ keV

$^{112}Cd(^{27}Al, p3n)$
$^{116}Sn(^{24}Mg, 2p3n)$

Stony Brook

Spectroscopy of ^{135}Nd

E.M. Beck, J.C. Bacelar, M.A. Deleplanque, R.M. Diamond, R.J. McDonald
F.S. Stephens - Lawrence Berkeley Laboratory
J.E. Draper, C. Duyar - U.C. Davis

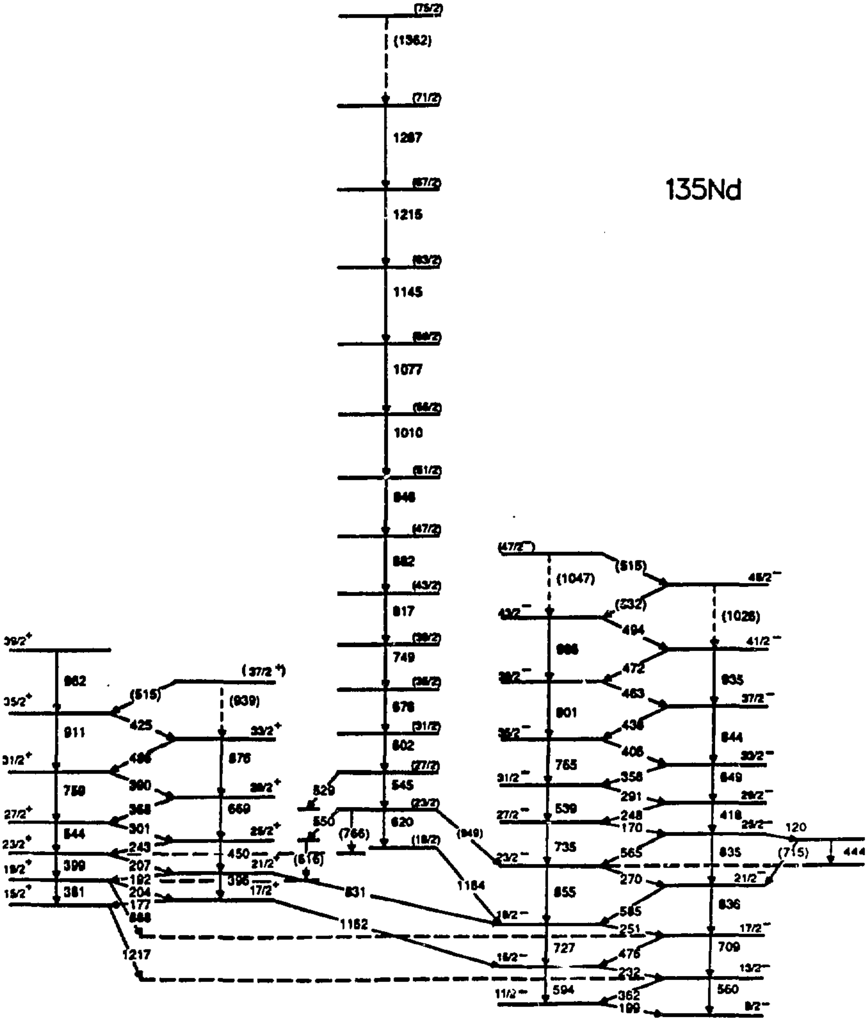

135Nd Strongly deformed band

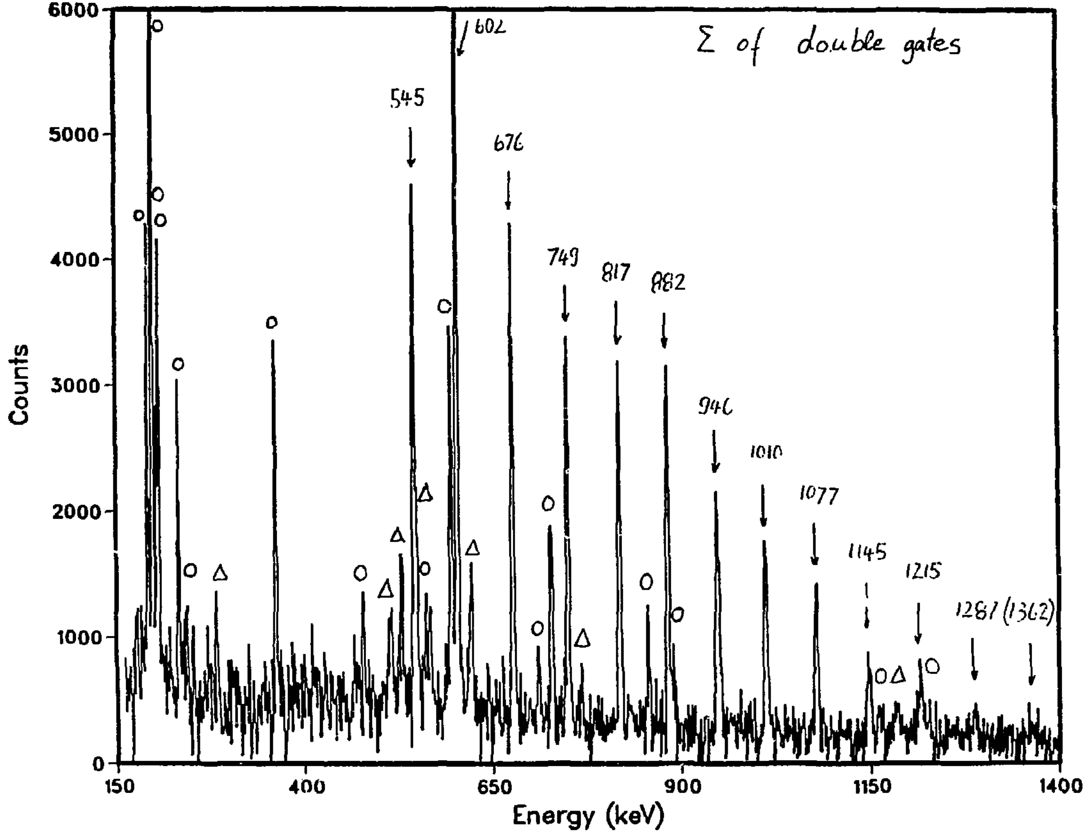

o known lines in ^{135}Nd

↓ strongly def. band

Δ (possible) linking trans.

reaction:

173, 177 MeV

$^{40}Ar + ^{100}Mo$ (thin)

≈ $570 \cdot 10^6$ events

135Nd   135Nd strongly deformed band

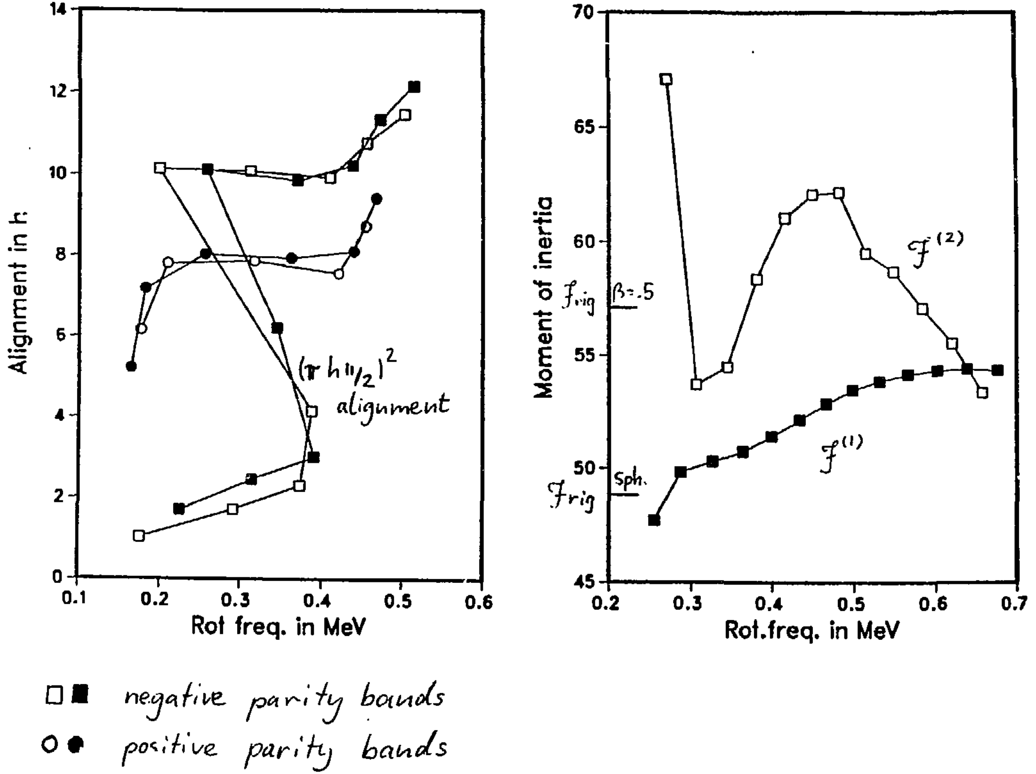

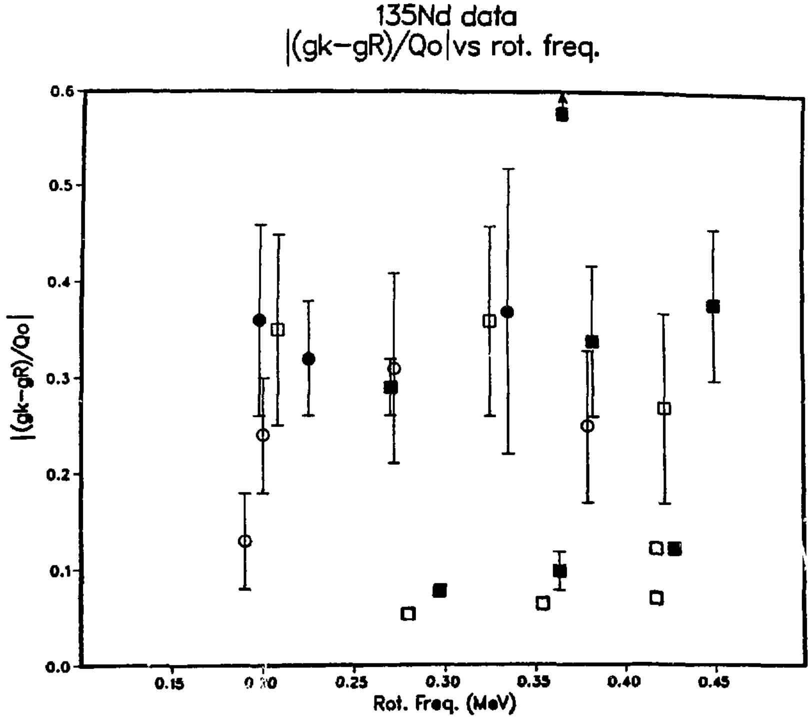

□ ■ neg. parity bands
○ ● pos. parity bands
$K = 9/2$ assumed

$$\lambda = \frac{T_\gamma (I \to I-2)}{T_\gamma (I \to I-1)}$$

$$\left| \frac{g_K - g_R}{Q_0} \right| = \frac{E_\gamma (I \to I-1)_{MeV}}{1.07 \sqrt{(I+1)(I-1)}} \left[\left(\frac{E_\gamma (I \to I-2)}{E_\gamma (I \to I-1)} \right)^5 \frac{1}{\lambda} * F(K,I) - 1 \right]^{1/2}$$

$$F(K,I) = \frac{1}{K^2} \frac{(I-1+K)(I-1-K)(I+1)}{2(2I-1)}$$

"LOOKING AT TRIPLES"

Th. Lindblad, D. Jerrestam, L. Hildingsson, W. Klamra, G. Szekely

First method uses the full 3D matrix displayed using an image processor. The six fold symmetry and the "tunnel of no events" along the $E_{\gamma_1} = E_{\gamma_2} = E_{\gamma_3}$ diagonal are clearly visable. The "balls" closest to this tunnel are tripple events involving transitions which are adjacent. Next "layer" shows events with one transition "missing", etc.

Second method uses the reduction from 3D → 2D in order to measure the rotational parameter $A = \hbar^2/2\mathcal{I}$ for ^{122}Ba (Experimental data from A. Johnson et al taken at Daresbury). This exploratory method shows that one can obtain values for the moment of inertia at ≈ 1/10 of the statistics needed for a conventional correlation matrix.

Exploratory studies of other methods are also carried out. These involves Fourier-tranforms, "sliding gates", etc

PERSPECTIVE IMAGE OF A COINCIDENCE MATRIX *)

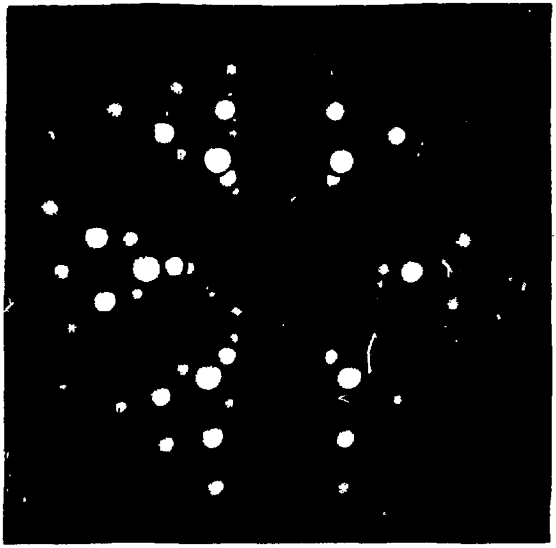

*) simulated data

BOTH VIEWS ARE ALONG THE X = Y = Z DIAGONAL, BUT WITH A HIGHER THRESHOLD FOR THE UPPER FIGURE. NOTE THE SIX-FOLD SYMMETRY. THE MATRIX IS BASED ON ROTATIONAL SPECTRA, WHICH YIELDS A "TUNNEL" OF NO EVENTS ALONG THE X = Y = Z DIAGONAL

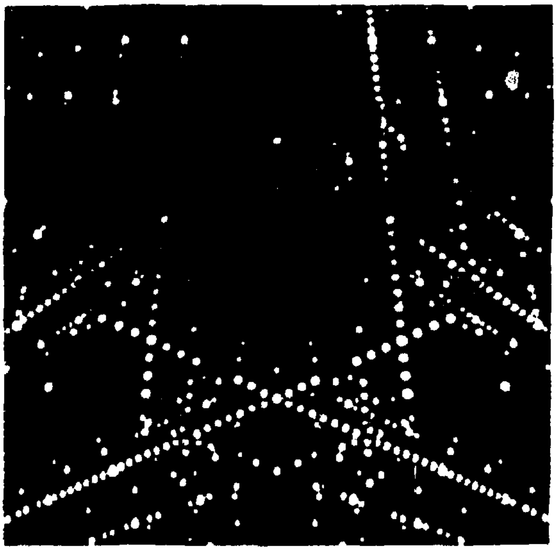

EXAMPLE OF REDUCTION METHOD:

$$E_{tot} = A * [(I-j)*(I-j+1)] + C$$

$$\Delta E = E_{tot}(I+2) - E_{tot}(I) =$$

$$= 4A \cdot I - \underbrace{4A\left[j - \tfrac{3}{2}\right]}_{\text{constant}} = E_{\gamma}(I)$$

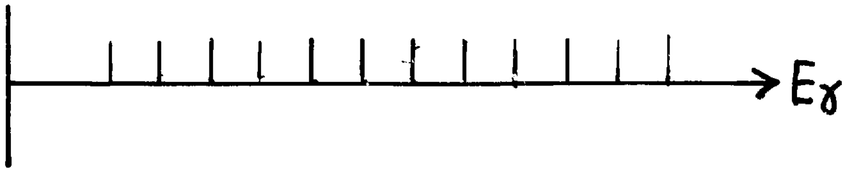

<u>REDUCTION</u>:

$$E_{\gamma_3} > E_{\gamma_2} > E_{\gamma_1}$$

$$\begin{cases} E_x = E_{\gamma_2} - E_{\gamma_1} & — \\ E_y = E_{\gamma_3} - E_{\gamma_2} & — \end{cases}$$

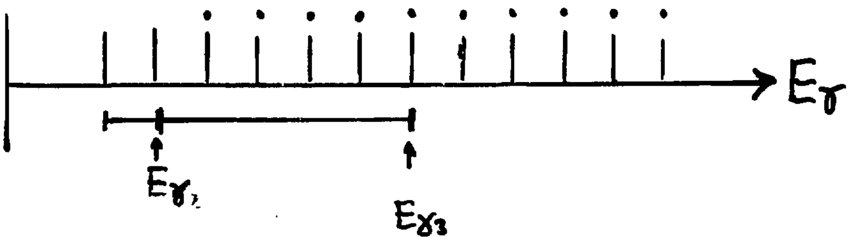

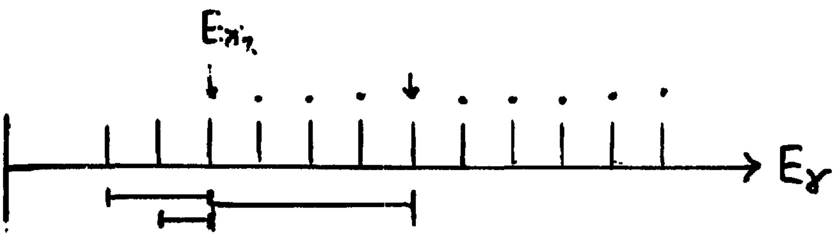

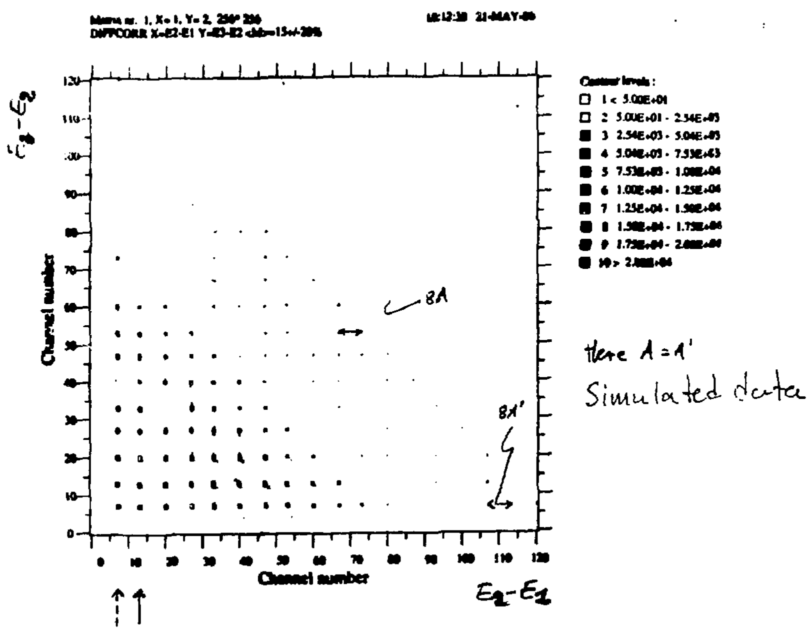

CUT IN MATRIX OF REAL DATA

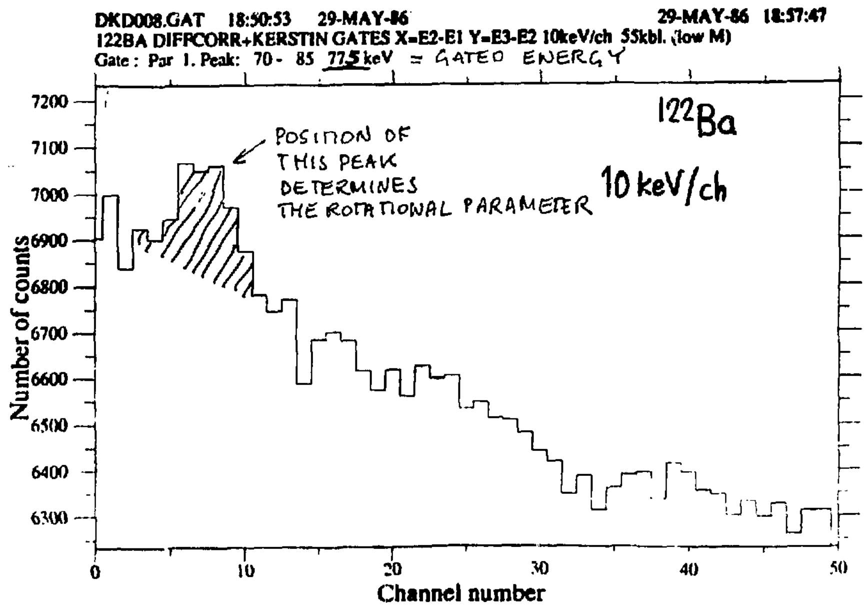

Proposal for a National Facility

THE 8π SPECTROMETER

P. TARAS
Université de Montréal

J.C. WADDINGTON
McMaster University

H.R. ANDREWS and D. WARD
Chalk River Nuclear Laboratories

October 1983

CANADIAN 8π SPECTROMETER

INNER BALL	72 BGO Detectors (60 Hexagonal, 12 Pentagonal) equal solid angles covering 95% of 4π forms a spherical shell 6.7 cm thickness of BGO. Inner cavity takes a 22 cm diameter chamber.
OUTER ARRAY	20 HPGe Detectors (24% efficiency) suppressed by axial BGO Detector Systems. Total collimated solid angle is 5%. Front face to target is 22.5 cm.
MECHANICAL	Weight of Detectors supported is 1720 lbs. HPGe Detectors view the target through 20 holes in the inner ball. The instrument is spherically symmetric eg. Phototubes emanate radially from ball detectors.
CONSTRUCTION	Funded at K$ 4995 on 1984 July 01. Scheduled completion 1986 Oct. 31. Shared funding between Canadian Universities and Atomic Energy of Canada (Chalk River).

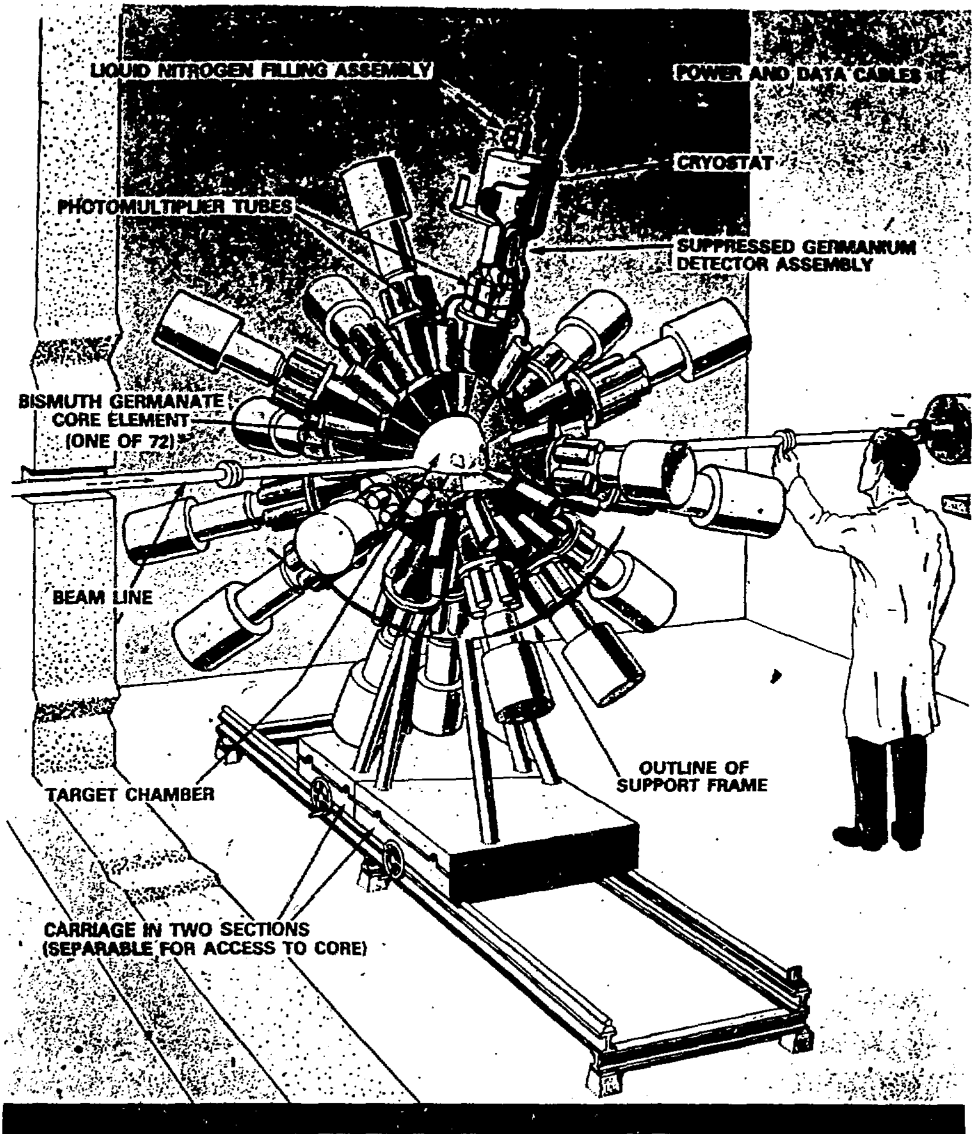

THE 8π SPECTROMETER

J. Saladin Results from the Pittsburgh multidetector array

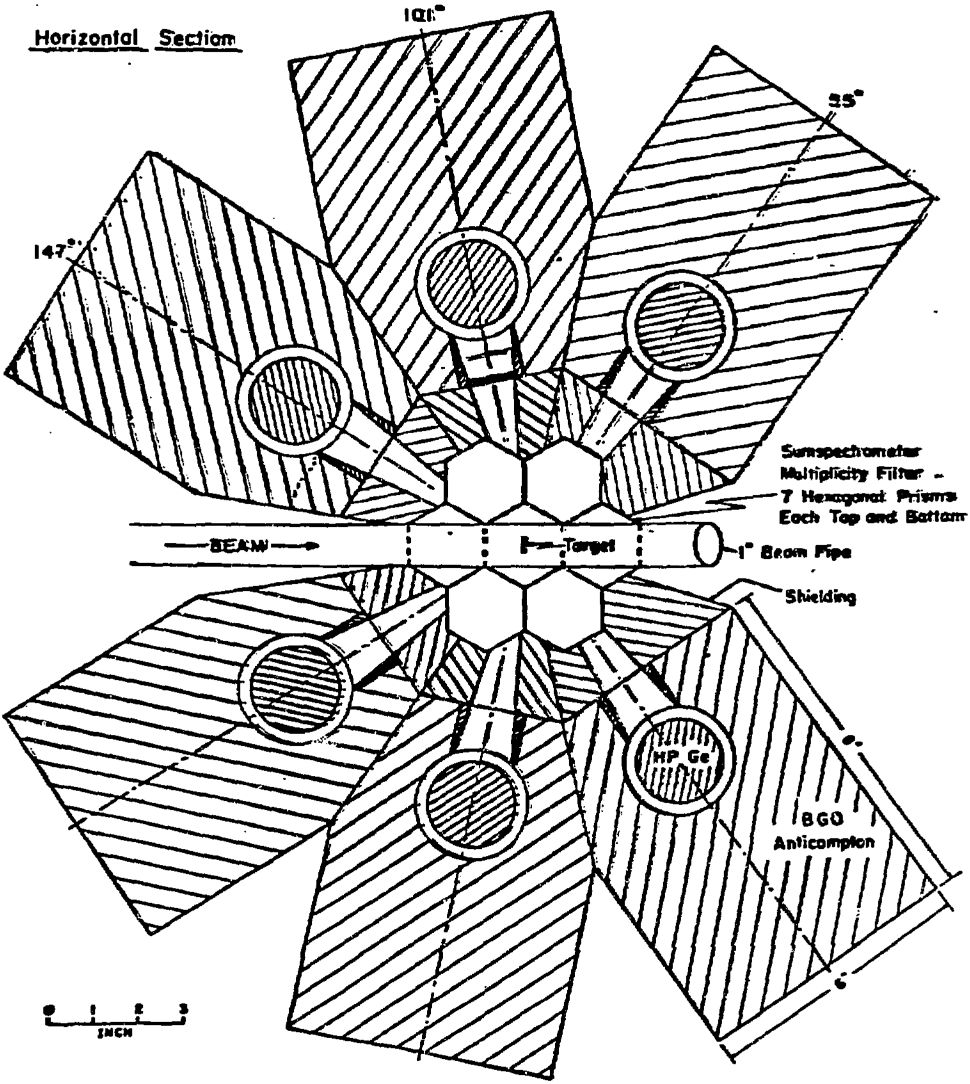

Fig. II-la. Horizontal section of detector assembly.

Multidetector array Pittsburgh

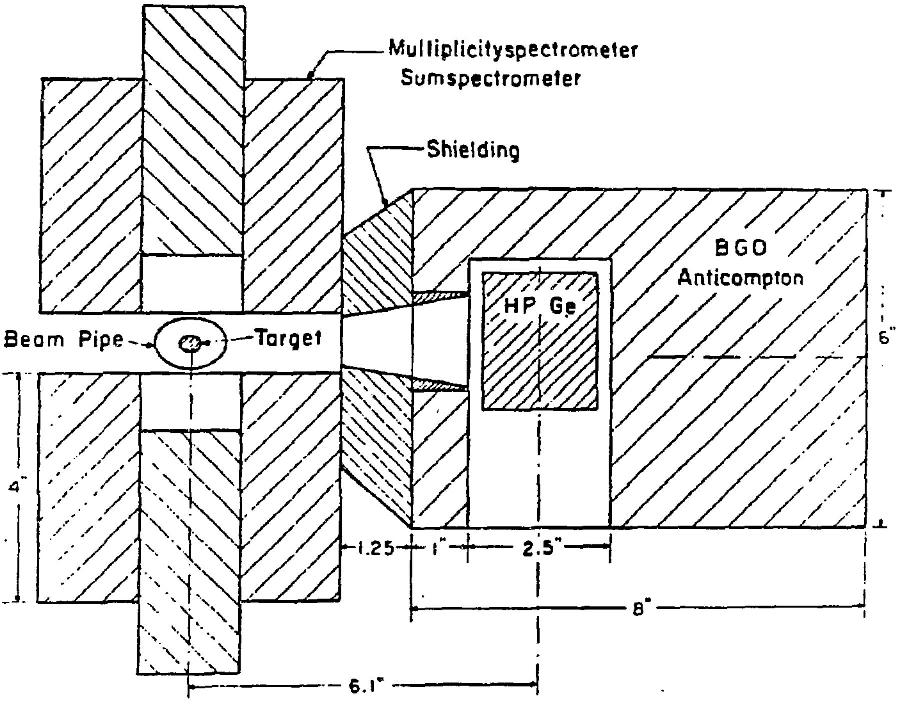

Vertical cross section through detector assembly.

220 MeV ^{22}Ne + ^{170}Er

γ-ray lines in coincidence with ^{18}O particles

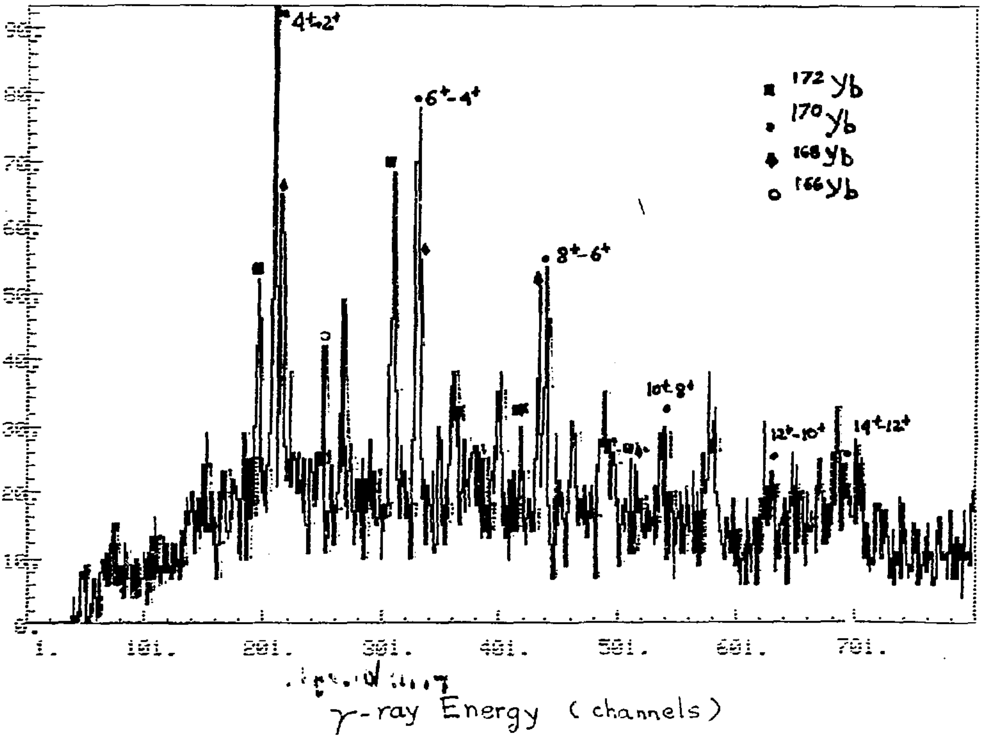

220 MeV ^{22}Ne + ^{170}Er

SMS TOTAL ENERGY VS. FOLD

gate on Nitrogen isotopes

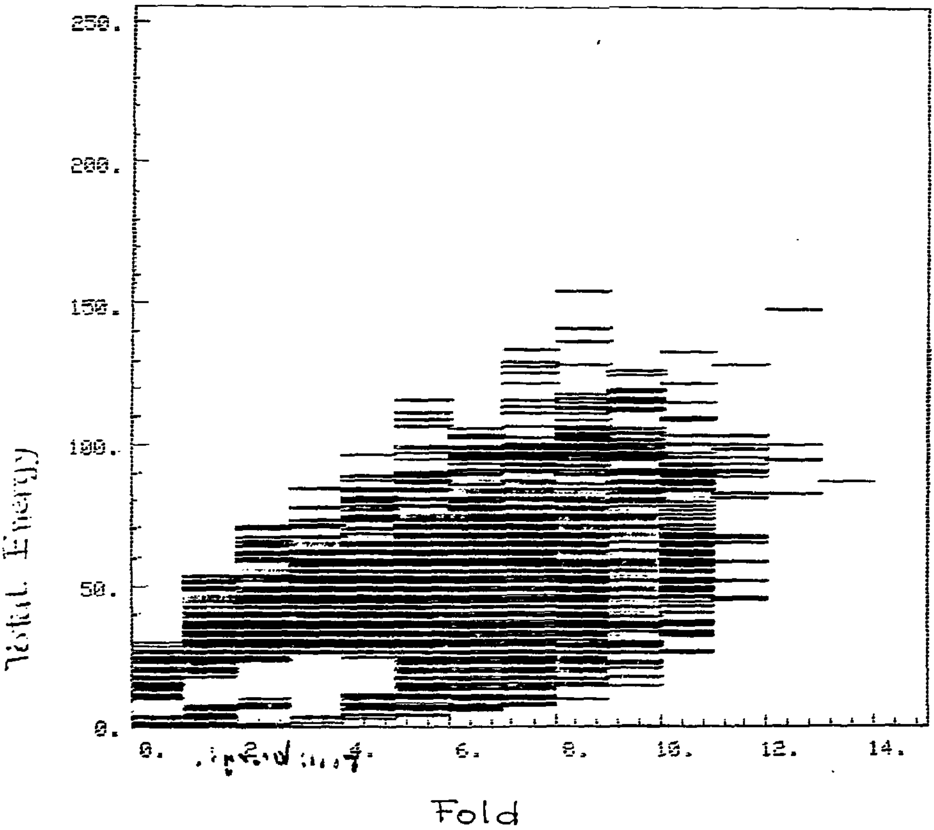

γ-ray spectroscopic studies at the French crystal castle

Th. BYRSKI

The french 4π-γ Chateau de cristal has been built in a collaboration between 6 laboratories, namely: Bordeaux, Grenoble, Lyon, Orsay IPN and Orsay CSNSM and Strasbourg. This device is a modularized BaF_2 detector allowing a great versatility in its use; two main geometries has been decided, one with 74 counters, the second with 38 counters surrounded by 12 Compton-suppressed Ge detectors.

The Château de Cristal has been used, these last months, in the second geometry, for several experiments dealing mainly with discrete γ-ray spectroscopy. They concern the studies of Hg, Xe and Ba isotopes, the search of shape transitions and shape coexistence in ^{155}Er, lifetimes measurement in ^{152}Dy related to superdeformed and low deformation bands...

The properties of individual BaF_2 counters are summarize below:

- hexagonal type with diameter = 10 cm and length = 14 cm
- good energy resolution: 10,5% for ^{137}Cs 662 keV γray
- high time resolution: 700 ps for ^{60}Co γrays
  - this allow high counting rates
  - good neutron-γ discrimination
- good γray detection efficiency (20%) due to a high density (4.
- low sensitivity to capture of neutrons
- very stable and non hygroscopic

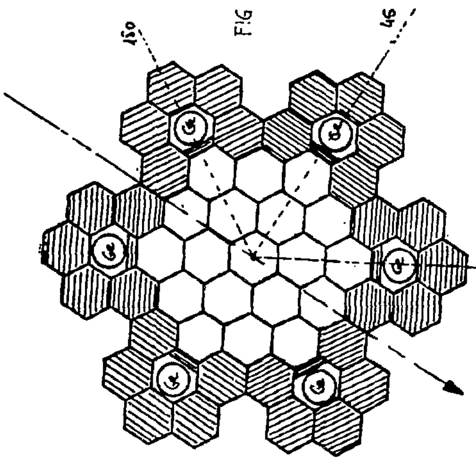

FIG 2a

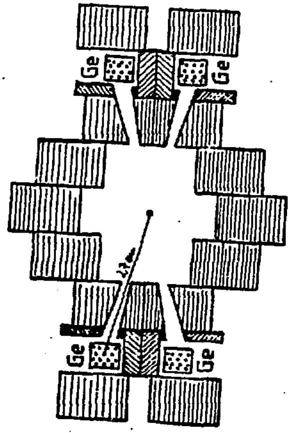

FIG 2b

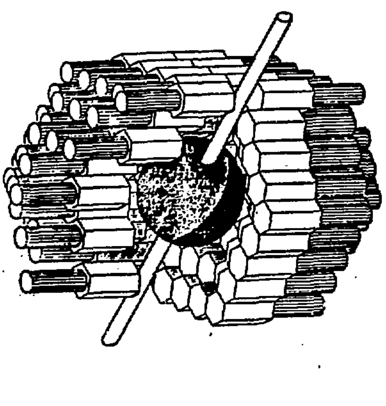

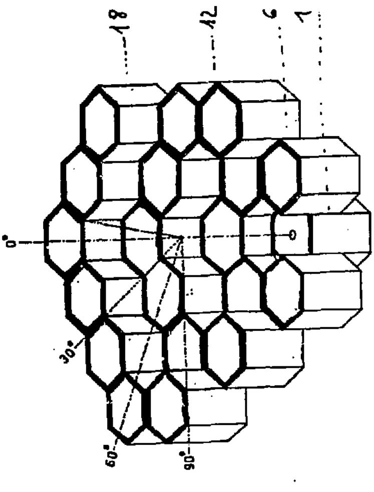

FIG 1

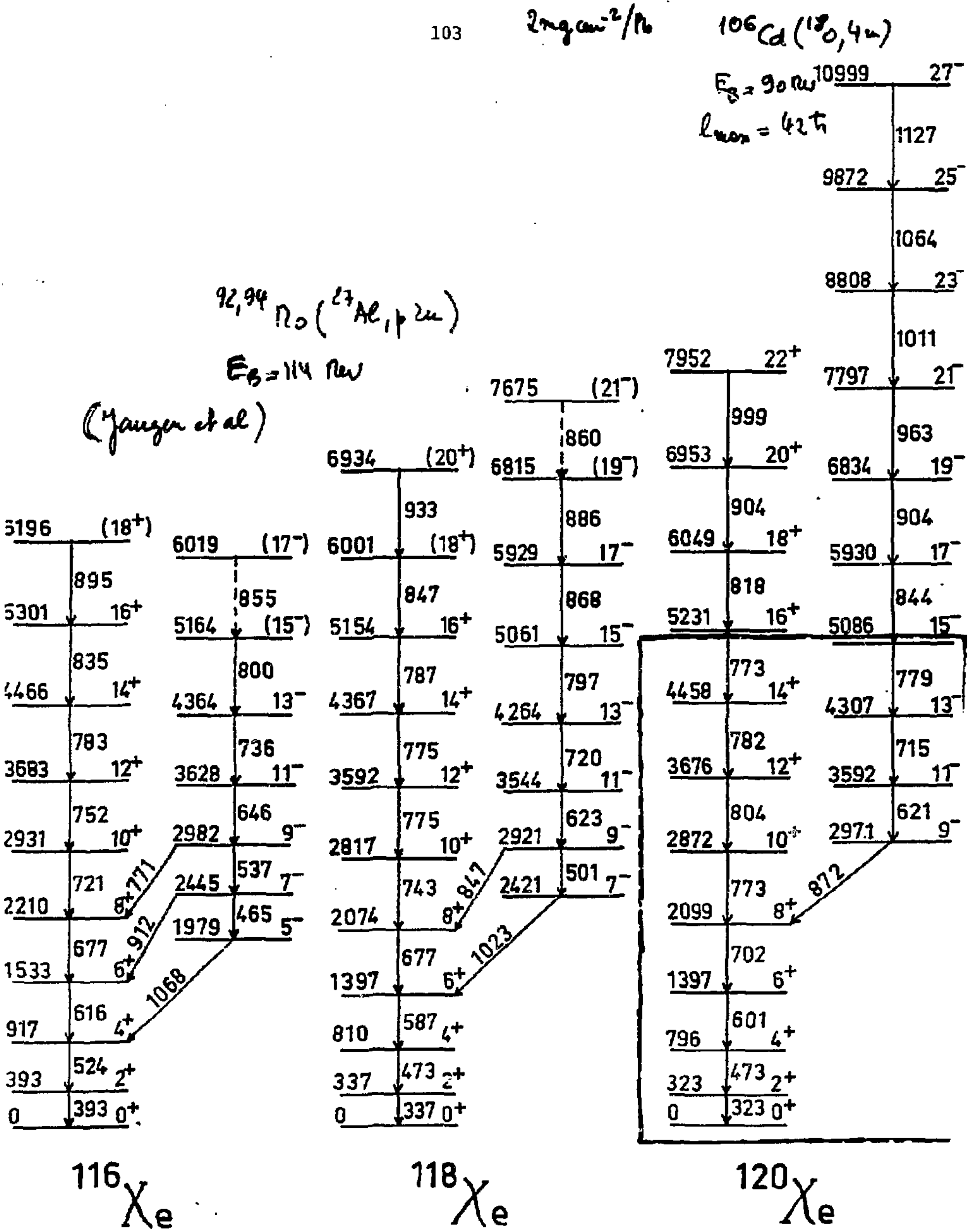
2mg cm⁻²/Ni
106Cd(18O,4n)
EB = 90 MeV
lmax = 42ħ
92,94Mo(27Al,p2n)
EB = 114 MeV
(Jaugen et al)
5196 (18+)
5301 16+
4466 14+
3683 12+
2931 10+
2210 8+
1533 6+
917 4+
393 2+
0 0+
895
835
783
752
721
677
616
524
393
6019 (17−)
5164 (15−)
4364 13−
3628 11−
2982 9−
2445 7−
1979 5−
855
800
736
646
537
465
771
912
1068
6934 (20+)
6001 (18+)
5154 16+
4367 14+
3592 12+
2817 10+
2074 8+
1397 6+
810 4+
337 2+
0 0+
933
847
787
775
775
743
677
587
473
337
7675 (21−)
6815 (19−)
5929 17−
5061 15−
4264 13−
3544 11−
2921 9−
2421 7−
860
886
868
797
720
623
501
847
1023
7952 22+
6953 20+
6049 18+
5231 16+
4458 14+
3676 12+
2872 10+
2099 8+
1397 6+
796 4+
323 2+
0 0+
999
904
818
773
782
804
773
702
601
473
323
10999 27−
9872 25−
8808 23−
7797 21−
6834 19−
5930 17−
5086 15−
4307 13−
3592 11−
2971 9−
1127
1064
1011
963
904
844
779
715
621
872
116Xe
118Xe
120Xe

FIG 10

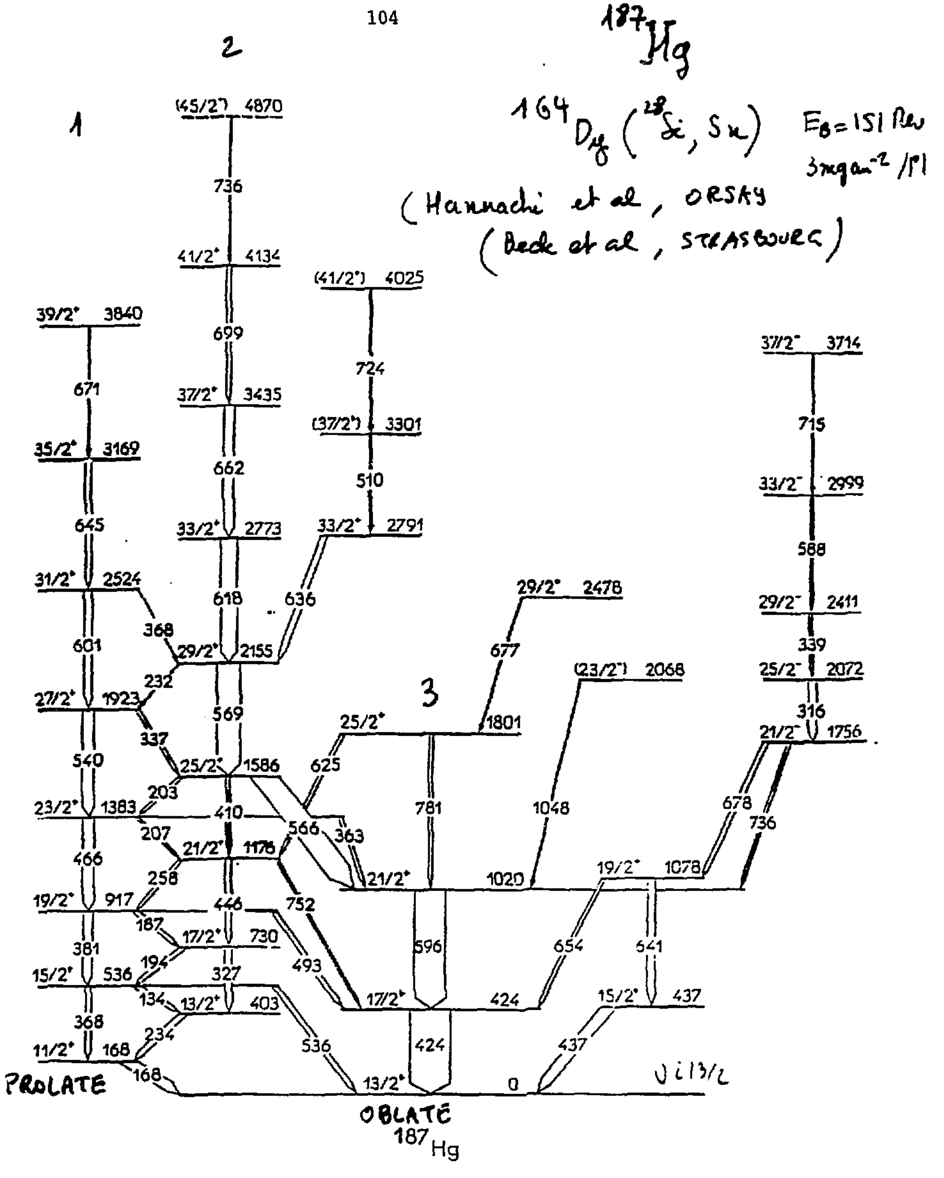

187 Hg
164 Dy (28 Si, 5n) E_B=151 MeV
(Hannachi et al, ORSAY
(Beck et al, STRASBOURG)
1
2
3
PROLATE
OBLATE
187 Hg
νi13/2

FIG 13

R. Janssens Suppression of neutron emission in heavy-ion induced fusion reactions: entrance channel effect and/or superdeformed shapes

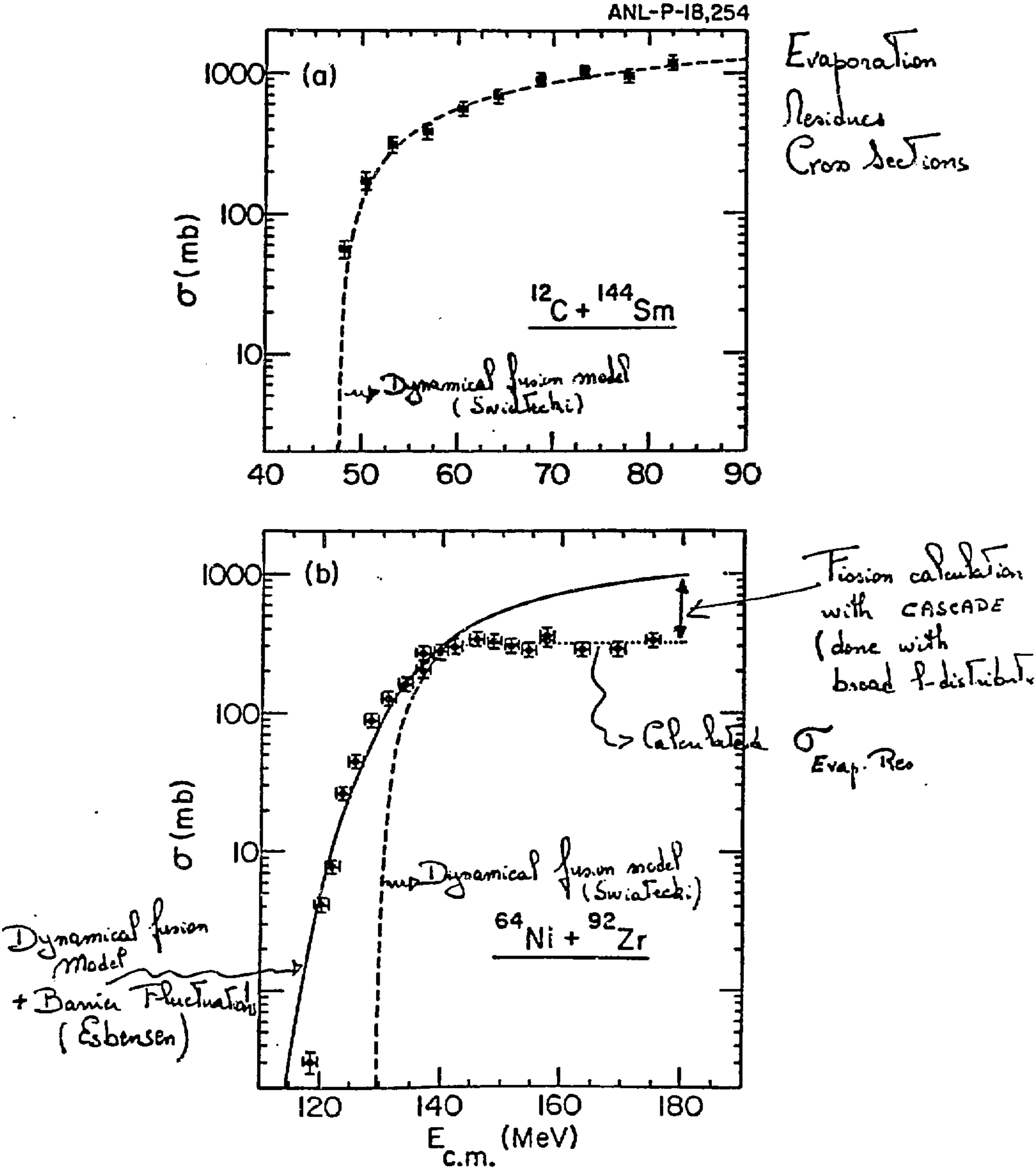

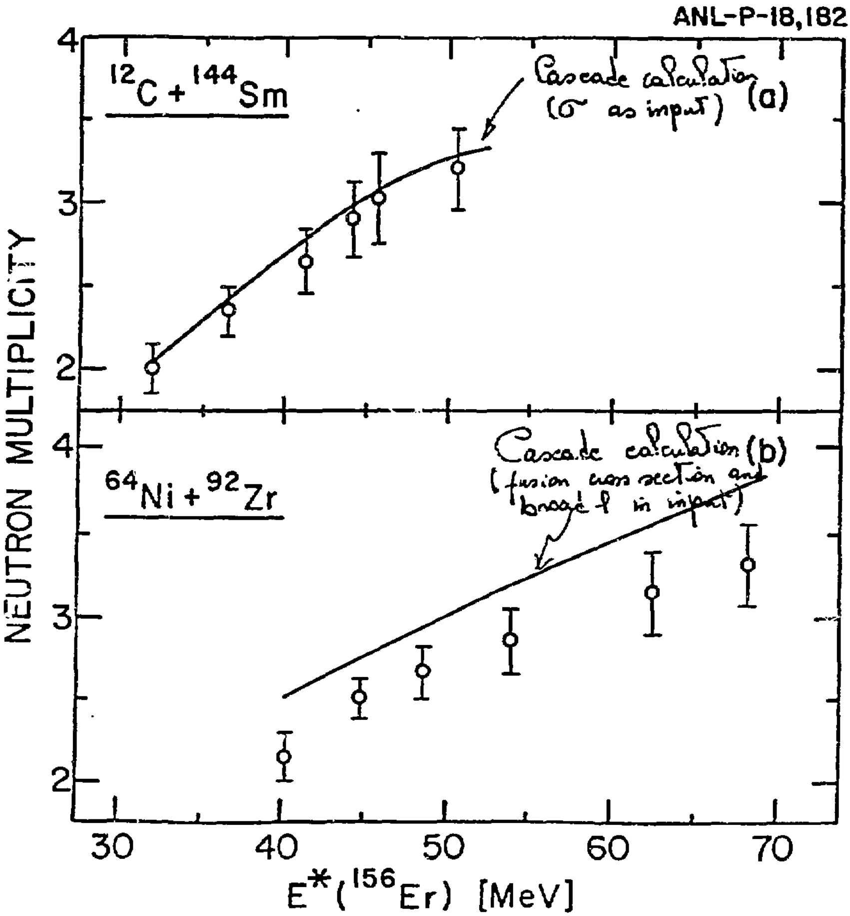

Fig. 2

⇒ ~ 0.35 n missing!

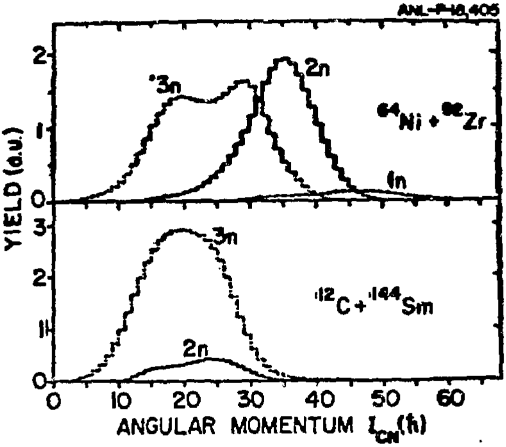

$E^*(^{156}Er) \simeq 47$ MeV for **both** reactions

l-distributions from crystal ball data

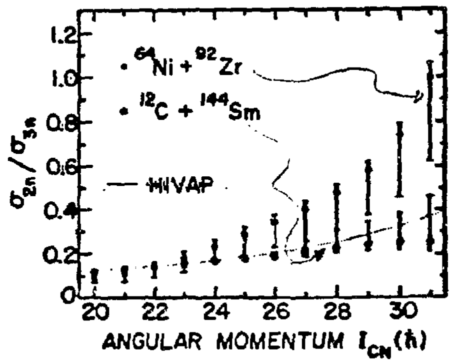

$\frac{\sigma_{2n}}{\sigma_{3n}}$ different in both reactions

i.e. breakdown of compound nucleus hypothesis

$^{64}Ni + ^{92}Zr$

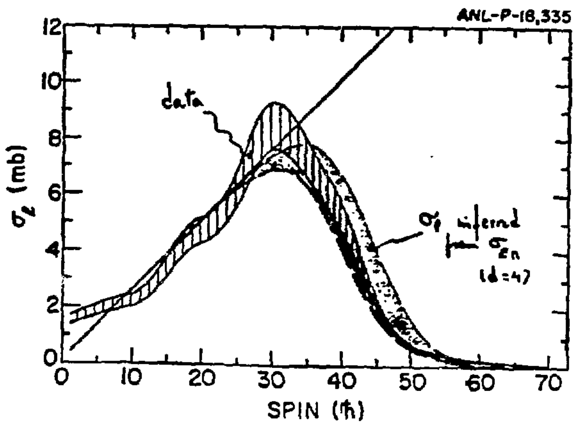

- Evidence for broad l-distribution (large fluctuations)
- Agreement between σ_{ER} measurements and σ_l from ball data

Compound Nucleus Spin Distribution

Conclusions

- All the available data in $^{12}C + ^{144}Sm$ can be explained with existing models.

- $^{64}Ni + ^{92}Zr$

  Cross section data → broad ℓ-distribution
  → competition fission-particle emission

  Crystal ball data → broad ℓ-distribution
  → agreement with σ_{ER}

  But neutron multiplicities smaller than expected even when all data are taken into account i.e.;
  - known yrast line
  - level density – constrained by Hauser spectra
  - γ-strength function
    - en. dep. GDR
    - strength EWSR
  - broad ℓ dist.

⇒ For ℓ ≥ 88

CN. decay cannot be accounted for in $^{64}Ni + ^{92}Zr$

Memory of entrance channel in decay !

Possible clue:

Initial deformation is larger in $^{64}Ni + ^{92}Zr$ than in $^{12}C + ^{144}Sm$

⟶ Kinetic Energy could be tied up in deformation energy instead of being converted into heat for n-emission; i.e. delay in shape relaxation by 3 orders of magnitude in time.

Collaborators:

1. σ_{ER} and Excit function

A. Holzmann, W. Henning, T.L. Khoo, K. Lesko, G.S. Stephans, D.C. Radford, A.M. Van Berg, R.J. (ANL), W. Kühn (Giessen), R.M. Ronningen (MSU).

2. Crystal Ball Exp

W. Kühn, V. Metag, A. Ruckelshausen (Giessen), D. Habs, H. Gross, R. Repnow, D. Schwalm, T.L. Khoo (Heidelberg), S. Hlavac, R.S. Simon (GSI), G. Duchêne, F.A. Beck, B. Haas, F. [illegible] (Strasbourg), R. [illegible] (ANL)

Finite-Temperature HFB Calculations in Rare Earth Nuclei

Alan L. Goodman

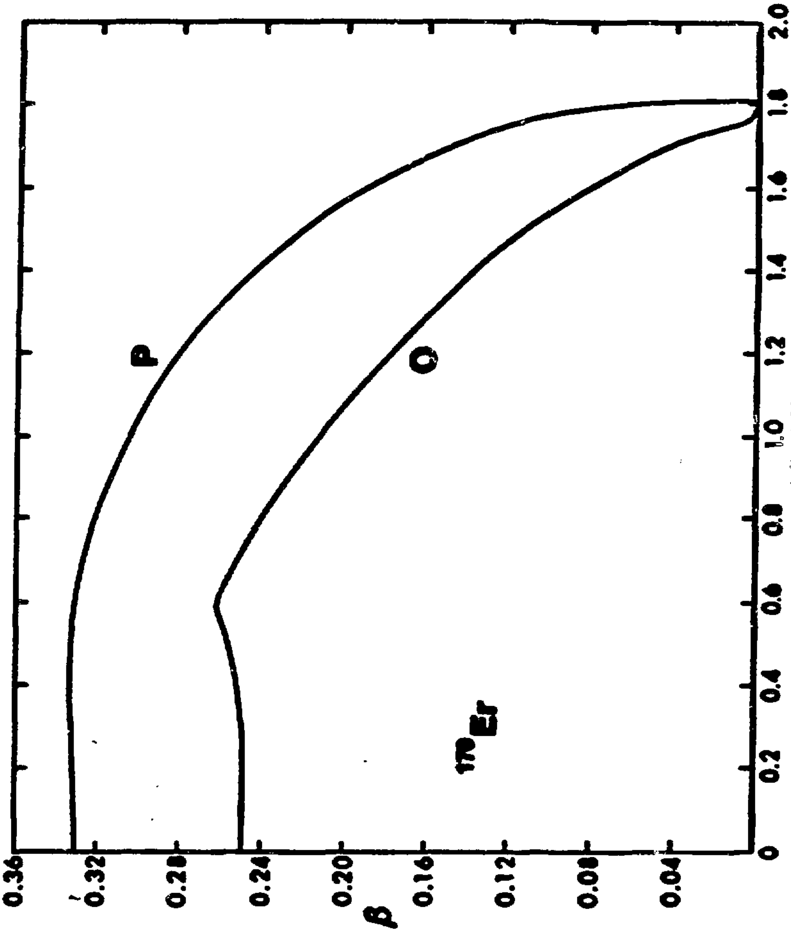

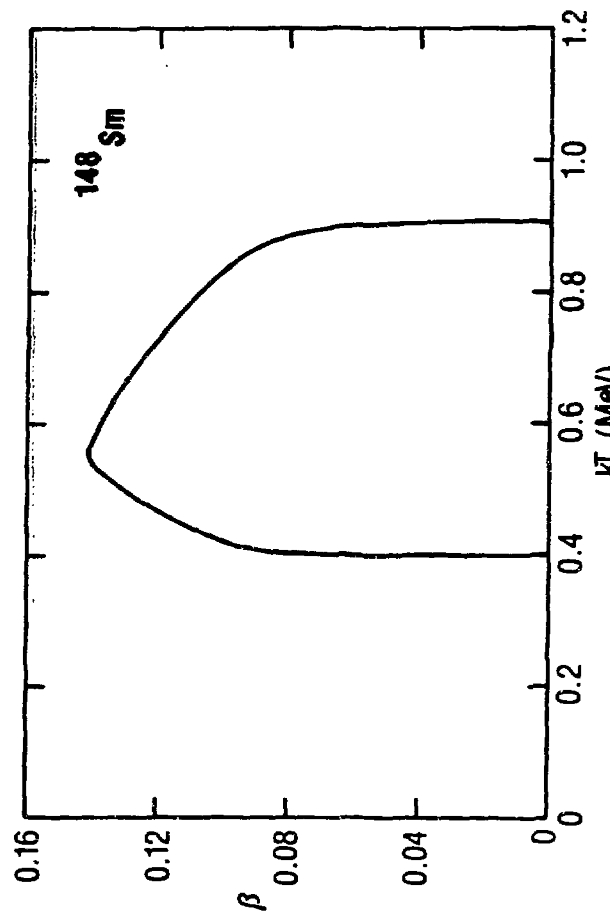

^{148}Sm
β
kT (MeV)
0
0.04
0.08
0.12
0.16
0
0.2
0.4
0.6
0.8
1.0
1.2

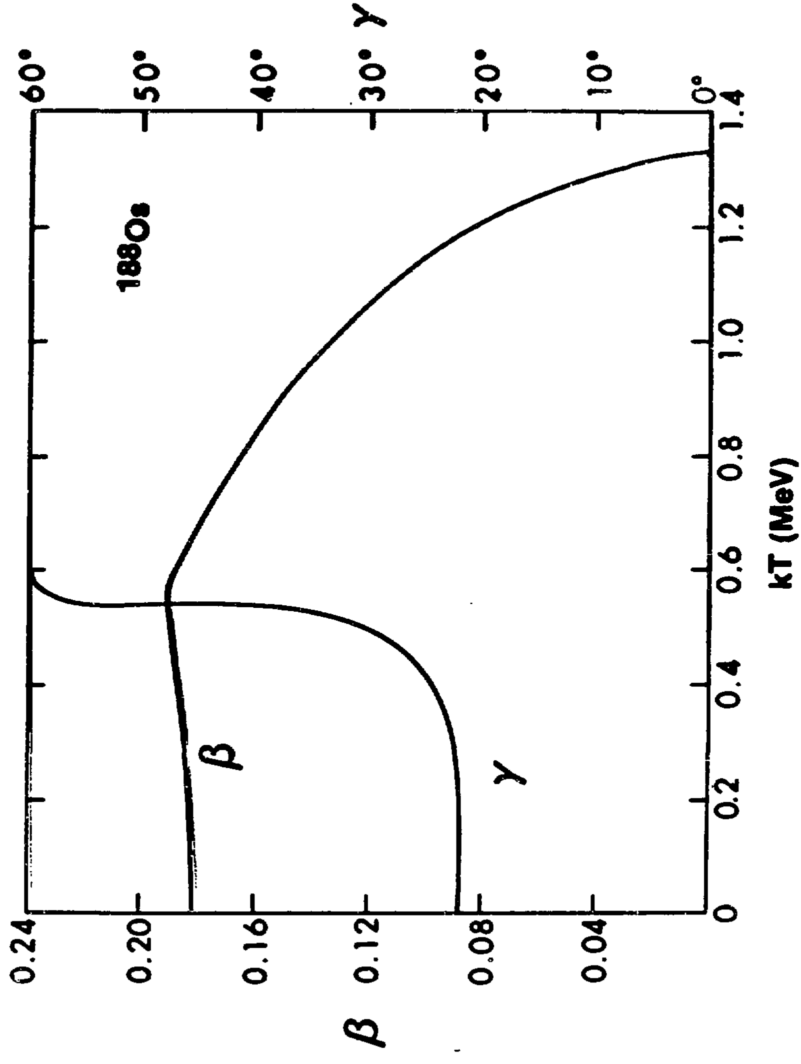

188Os
β
γ
kT (MeV)
0
0.2
0.4
0.6
0.8
1.0
1.2
1.4
0.24
0.20
0.16
0.12
0.08
0.04
60°
50°
40°
30°
20°
10°
0°

Conclusions

In the mean field approximation, raising the temperature induces a variety of phase transitions.

Pair correlations: superfluid → normal

Shape:

(1) Rotational nuclei
^{170}Er, prolate → spherical

(2) Transitional nuclei
^{188}Os, triaxial → oblate → spherical
^{148}Sm, spherical → prolate → spherical

Conditions:

(1) Pairing interaction is slightly more effective than Q·Q interaction in ground state.

(2) Critical temperature for pairing collapse is lower than critical temperature for deformation collapse

Statistical fluctuations will smooth out sharp phase transitions.

CA Gossett et al PRL 54 1486 (1985)

$E(^{12}C) = 61.5$ MeV

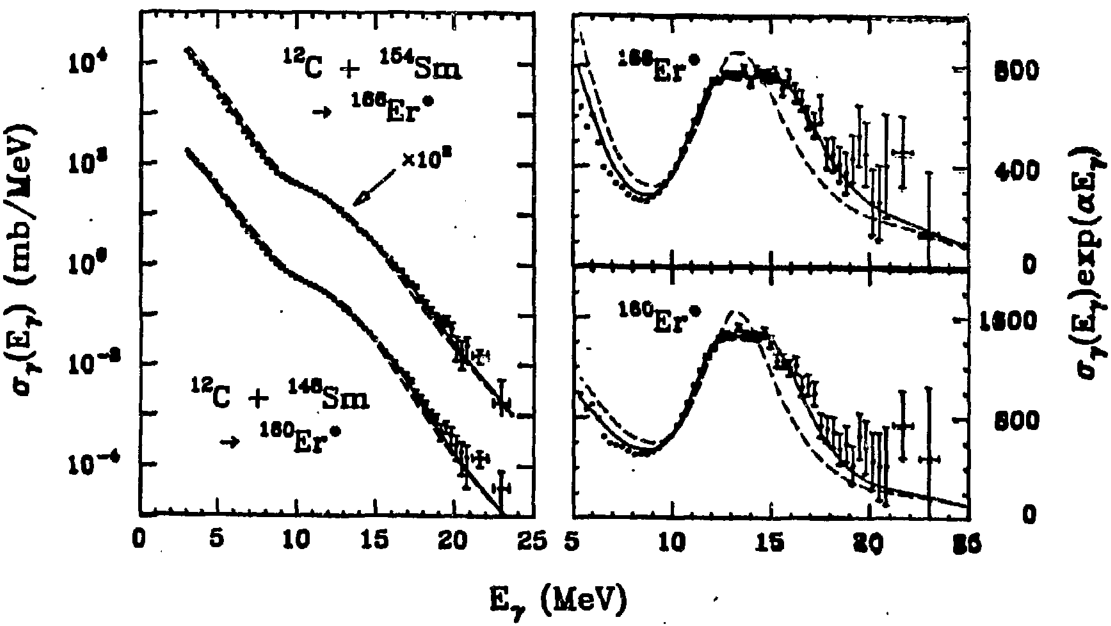

Figure 1. Left: γ decay spectral shapes from decays of $^{166}Er^*$, $^{160}Er^*$ along with statistical model fits in which either a two-component Lorentzian (solid curve) or one component Lorentzian (dashed curve) was used for the shape of the GDR built on excited states. Right: Data and fits from left rescaled by $e^{\alpha E_\gamma}$ for better visual comparison. GDR parameters from best fit (solid curve) indicate the same prolate deformation for these nuclei at T~1.2 MeV as in the ground state.

C A Gossett et al, in preparation

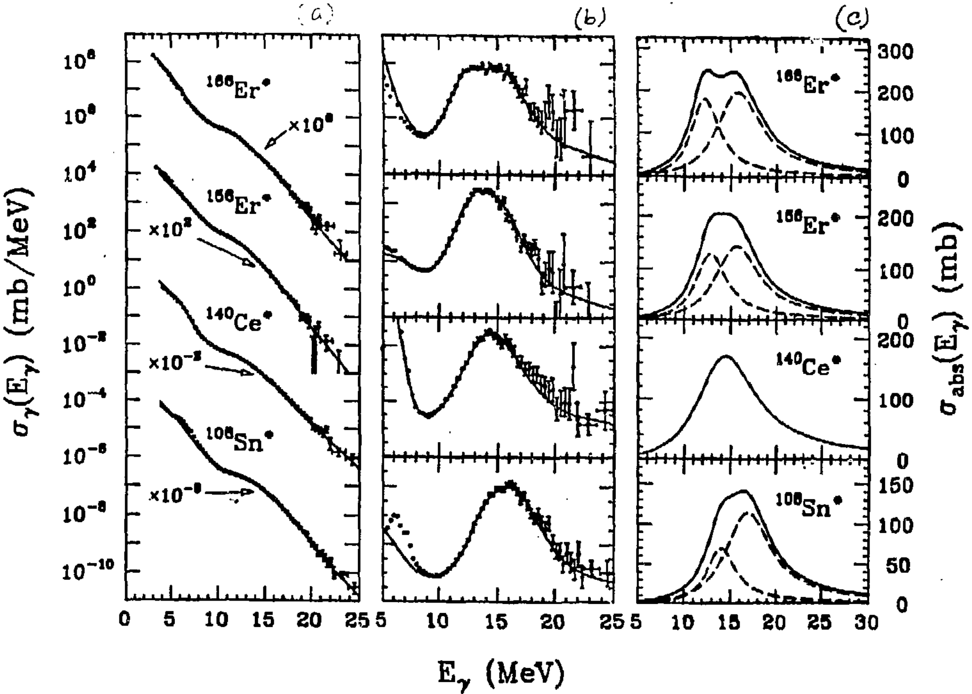

Figure 2. (a+b) Measured continuum spectra and best fits from decays of $^{166}Er^*$, $^{156}Er^*$, $^{140}Ce^*$, $^{108}Sn^*$.
(C) Inferred shape of photoabsorption cross section at elevated temperature from best fits in (a). $^{166}Er^*$ is case of a nucleus which has the same large prolate deformation at $T \sim 1$ MeV as in the ground state. The observation of a single component GDR shape for $N=82$ $^{140}Ce^*$ (also seen in ^{90}Zr) much broader than the ground state indicates thermal averaging roughly symmetrically over prolate and oblate shapes while the broadenings in $^{156}Er^*$ and $^{108}Sn^*$ favor prolate deformations at high T.

CA Gossett et al in preparation

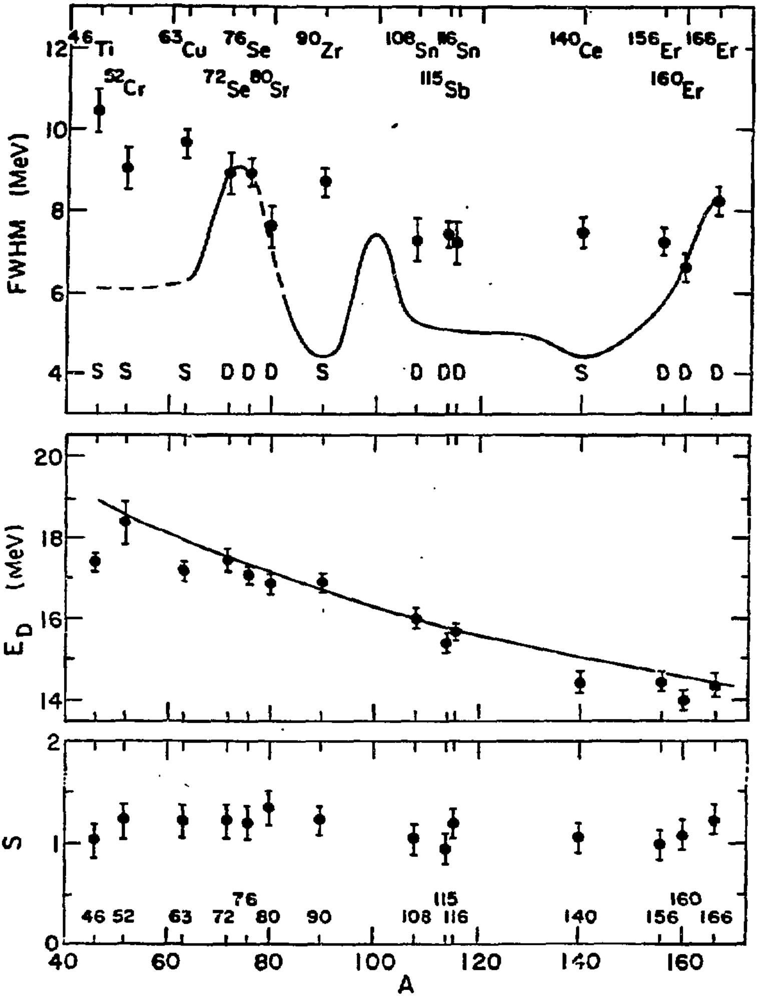

Figure 3. Total strength, S, mean resonance energy, E_D and full width at half maximum, FWHM of the GDR built on excited states at temperatures $T \sim 1$-2 MeV and $I \sim 10$-$20\ \hbar$ as function of mass. Curves show ground state photoabsorption results. In top figure S and D represent analyses of γ-ray spectral shapes in which either single or double component Lorentzian was used for the GDR shape.

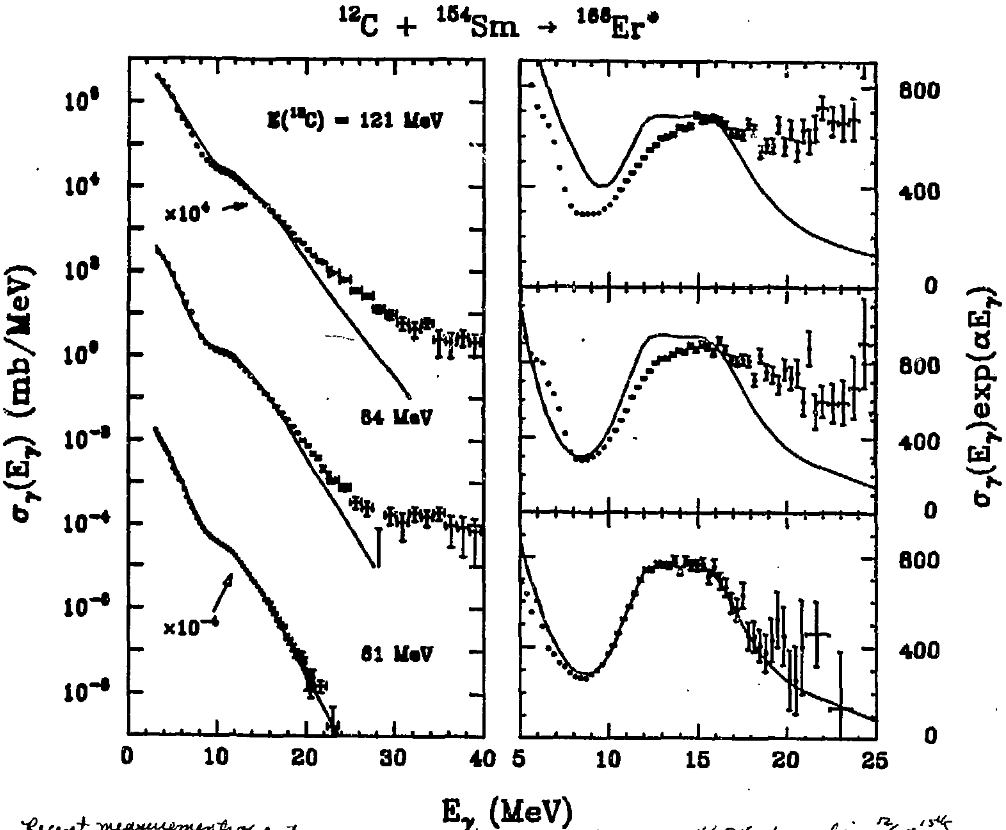

Figure 4. Recent measurements of continuum γ-ray spectra from decays of $^{166}Er^*$ formed in $^{12}C + ^{154}Sm$ reaction for $E(^{12}C) = 61, 84, 121$ MeV. Solid curves are calculations using fixed GDR parameters from best fit to spectrum at $E(^{12}C) = 61$ MeV. Data at 84 MeV and 121 MeV suggest strength moved to higher energy but more likely explanation is that of evidence of both change in shape, prolate to oblate, and change in slope of the level density, $a = A/8 \rightarrow a = A/9$ MeV^{-1}. These results are very preliminary and much further work on the interpretation is required. The spectra at 84 MeV, 121 MeV exhibit the onset of nonstatistical processes.

Heavy-ion Induced One and Two Neutron Transfer Reactions as a Probe of High-Spin Collective States

DOUGLAS CLINE

Nuclear Structure Research Laboratory*
University of Rochester

Strong collective excitation inherent to heavy-ion reactions implies that one and two nucleon transfer can be induced between states carrying many quanta of collective excitation. This opens the possibility of probing the dependence of single-particle and pairing degrees of freedom on collective excitation. One and two-neutron transfer reactions have been studied at the Holifield Heavy Ion Research Facility using 5MeV/nucleon ^{58}Ni and ^{116}Sn projectiles and ^{161,162,163,164}Dy targets[1,2]. In addition one-neutron transfer has been studied[3] for 325MeV ^{58}Ni on a ^{235}U target. The target-like and projectile-like fragments were observed in kinematic coincidence using position-sensitive parallel plate avalanche detectors in coincidence with the deexcitation gamma rays observed using the Spin Spectrometer which comprised up to 14 Compton-suppressed Ge detectors and ≈60 NaI detectors. The Spin Spectrometer was used to measure the total energy and the multiplicity of the deexcitation gamma rays from the reaction products.

At the grazing angle the coincident gamma-ray spectra are dominated by the inelastic, one and two-neutron reaction channels. For these channels the reaction selectively excites states adjacent to the yrast sequence, such as, rotationally-aligned two quasi-particle states, up to spin 30 with large cross sections which is consistent with a direct process for the transfer. That is, this reaction populates a distinctly different region of spin and excitation energy compared with other reactions. Moreover the deexcitation spectra are clean even for transfer on ^{235}U opening the prospect of studying high spin states to spin 40 in the actinide nuclei unimpeded by the fission channel. It is shown that the exponential radial dependence of the two-particle transfer form factors at large separation distances for very heavy ion collisions is anomalous leading to large cross sections for distant collisions. It is demonstrated that this effect depends on the angular momentum of the states excited and is not due to intrinsic excitation of reaction fragments.

The results of this work and related studies were reviewed and the implications of using such reactions as a spectroscopic probe of selected states near the yrast sequence was discussed.

* Supported by the National Science Foundation.

[1] M.W. Guidry, S. Juutinen, X.T. Liu, C.R. Bingham, A.J. Larabee, L.L. Riedinger, C. Baktash, I.Y. Lee, M.L. Halbert, D. Cline, B. Kotlinski, W.J. Kernan, T.M, Semkow, D.G. Sarantites, K. Honkanen, M. Rajagopalan, Phys. Letts. 163B (1985) 79.
[2] S. Juutinen et al, To be published 1986
[3] C.Y. Wu et al, To be published 1986

EXPERIMENTAL SETUP

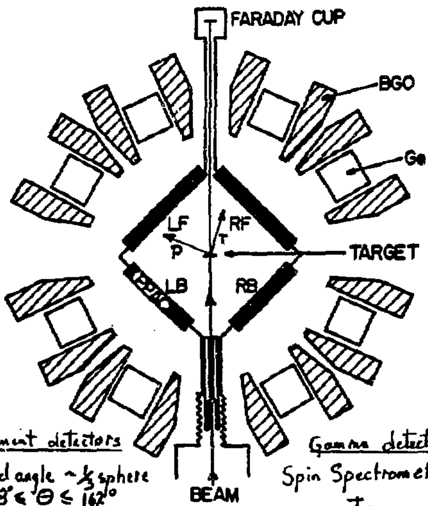

Fragment detectors
Solid angle ~ 1/3 sphere
8° ≤ Θ ≤ 162°
ΔΘ ~ 0.8°
Δt ~ 0.6 nanoseconds

Gamma detectors
Spin Spectrometer
+
≤14 Compton suppressed Ge detectors

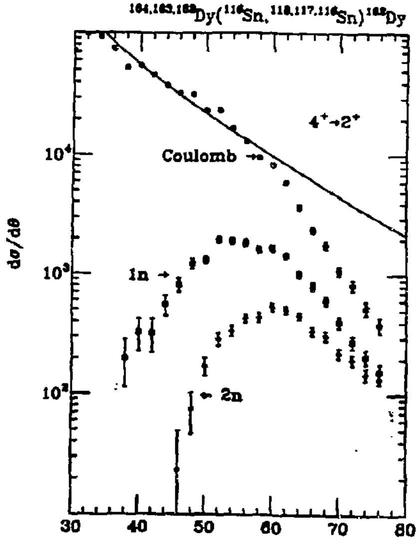

Differential cross sections for inelastic, 1n and 2n transfer to ^{162}Dy

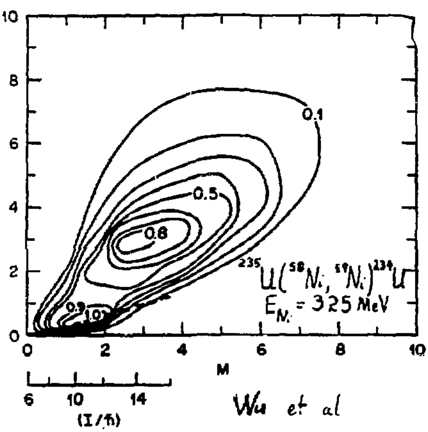

Wu et al

Total energy versus multiplicity

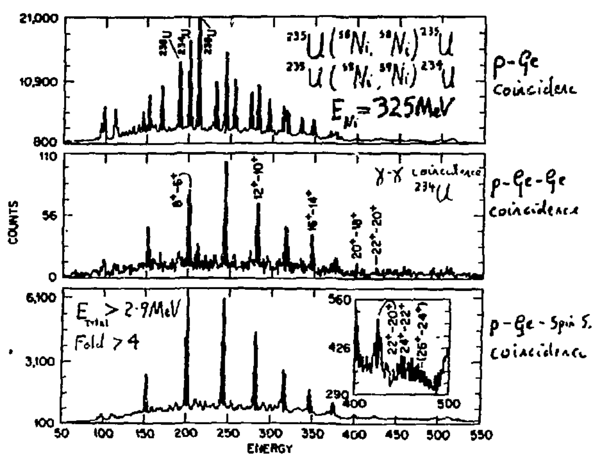

Typical gamma spectra for grazing angle collisions

GENERAL FEATURES OF REACTION

1) Selectively populates cold states to ≳30 ħ
2) Distinctly different population region from other reactions
3) Cross sections large
4) Gamma-ray spectra are clean
5) Ideal method for populating high-spin states
   a) Direct population
   b) Excite cold states - actinide nuclei
   c) Large recoil velocities

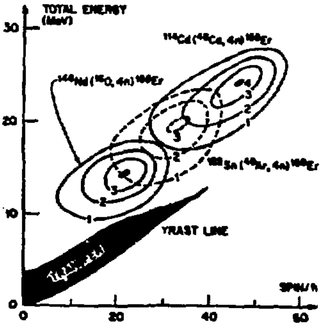

Feasibility for quantitative spectroscopy of 1neutron transfer

Experiment

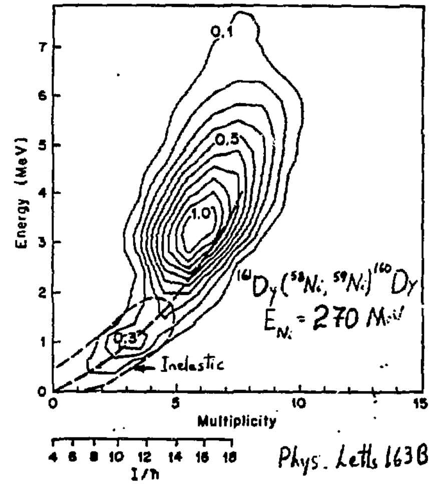

Phys. Letts 163B(85)79

Theory

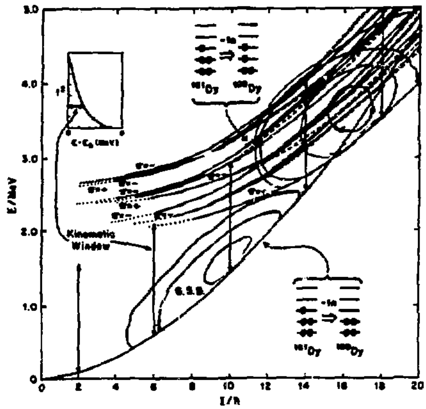

Bengtsson & Frauendorf Nucl. Phys. A327(79)139

1n transfer favours high-spin, cold, rotationally-aligned states

Transfer consistent with direct population of ground and 2 quasi-particle collective bands

Two neutron transfer

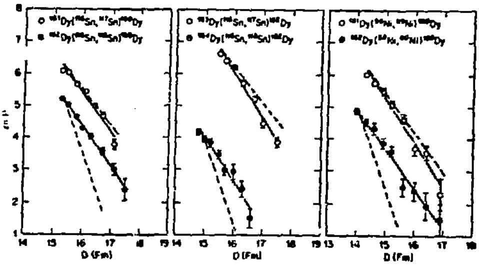

Transfer probability vs distance of closest approach. Dotted and dashed lines calculated from average ground state separation energies. Solid lines are least-squares fit to data. Note anomalous slopes for 2-n transfer.

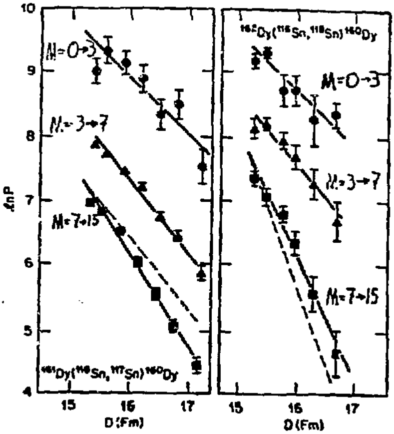

As opposite but with total energy-fold gates set

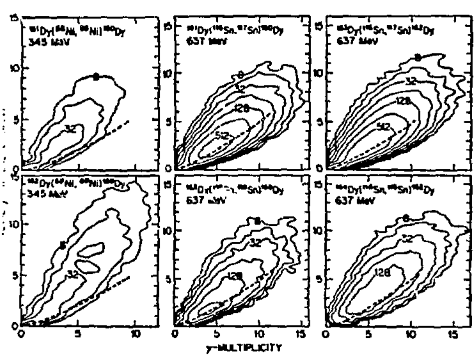

Total energy versus multiplicity shows that 2n transfer leads to cold final states.

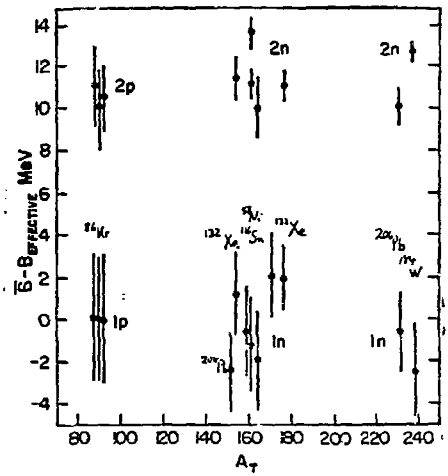

Effective excitation energies required to reproduce anomalous slopes for 2 nucleon pickup compared with one nucleon values. Note that the population of cold final states implies that the 11 MeV excitation for 2 nucleon transfer is a virtual effect

J. Gerl

Nuclear reactions at the Coulomb barrier

$^{90}Zr \rightarrow {}^{232}Th$ [1.4 mg/cm² Target]

a.) Coulex: $E_L = 396$ MeV ; b.) Transfer: $E_L = 497, 520, 560$ MeV

Set up: Heidelberg Crystal ball, 6 Ge-counters, PPC's ($92° \leq \theta_L \leq$ [illegible]

Coulex: Candidate for 2 phonon band found (Fig. 1)

Backbending of γ-band at $I^{\pi} = 16^{+}$ ($\hbar\omega \approx .16$ MeV, $i_x \approx 4\hbar$)

Transfer: Unexpected strong 2n pickup, rather weak 1n pickup (Fig. 2)

High spin states populated ($I \leq 22\hbar$ in ^{230}Th)

Transfer goes to states slightly above yrast line

^{230}Th from ^{231}Th after neutron emission (only a part)

^{228}Th mainly populated by neutron evaporation.

No fission component in neutron transfer channels.

No "cold" transfer (^{232}Th yrast $\rightarrow$ ^{230}Th yrast) observed.

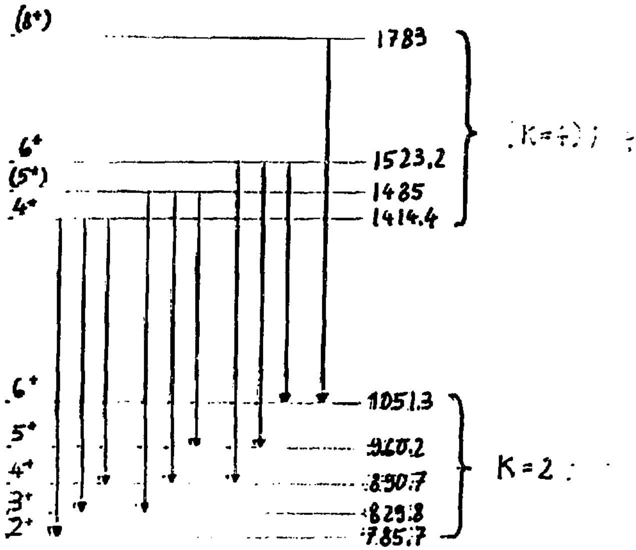

	Alaga K=2	Alaga K=3	Alaga K=4
$\frac{B(E2;\,4_?^+ \to 3_\gamma^+)}{B(E2;\,4_?^+ \to 2_\gamma^+)} = 0.68\,(8)$	2.2	0.14	0.56

$$\frac{B(E2;\,4_?^+ \to 2_\gamma^+)}{B(E2;\,4_?^+ \to 2^+)} > 7.0 \cdot 10^2$$

$$\frac{B(E2;\,4_?^+ \to 2_\gamma^+)}{B(E2;\,4_?^+ \to 4^+)} > 5.6 \cdot 10^2$$

No direct transition to the ground state band

$$\frac{B(E2;\,4_?^+ \to 2_\gamma^+)}{B(E2;\,4_\gamma^+ \to 2^+)} \gtrsim 1$$

High collectivity

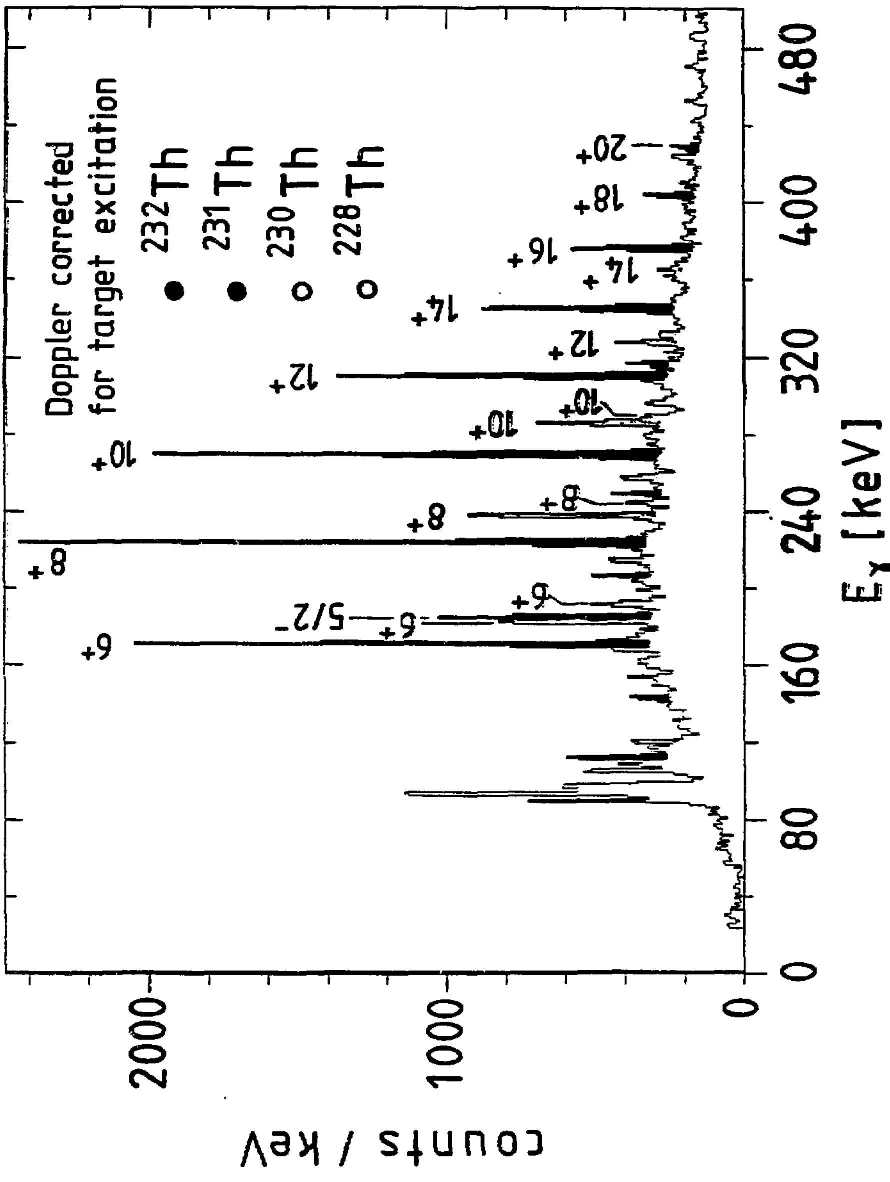
Doppler corrected
for target excitation
● 232Th
● 231Th
o 230Th
o 228Th
Eγ [keV]
counts / keV
0
80
160
240
320
400
480
0
1000
2000
6+
8+
10+
12+
14+
16+
18+
20+
5/2-

Gate on Ge-detector

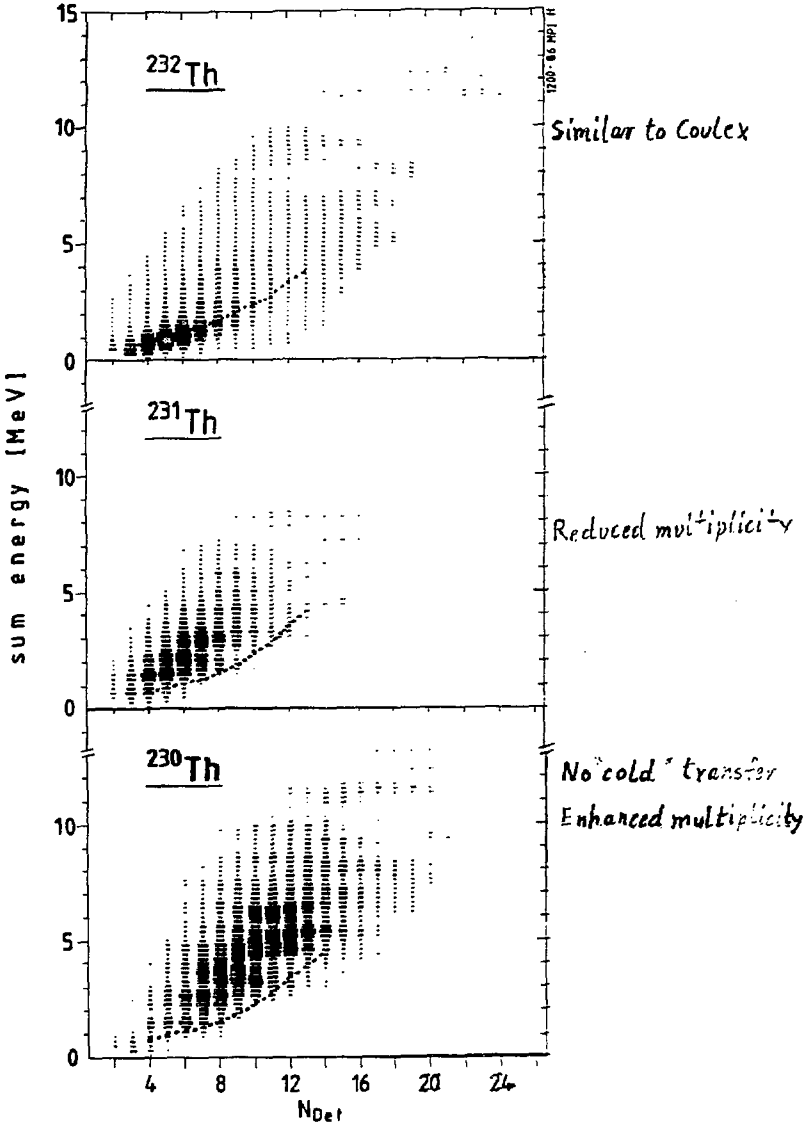

Diabolic Pair Transfer and Oscillating Behavior of Backbending

P. Ring and R.S. Nikam
Physik-Department, Technisch Universitat München
and L.T. Canto
Instituto de Fisica, Univ. Federal do Rio de Janeiro

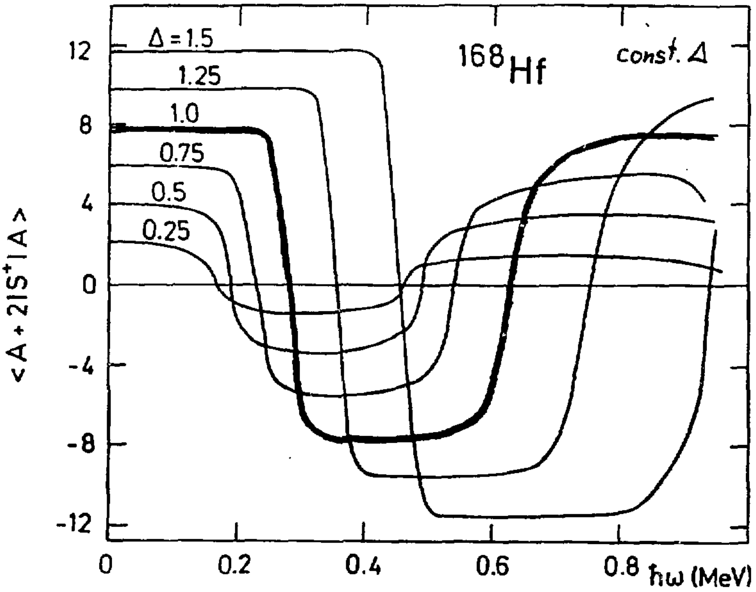

Fig. 1 Pair transfer matrix elements $\langle A+2,I|S^{+}|A,I\rangle$ as a function of the angular velocity for various pairing parameter Δ in the nucleus ^{168}Hf. An oscillating behavior is found, which is in close analogy to the DC-Josephson effect in solid superconductors in a magnetic field, where the amplitude of the current oscillates with the strength of the flux going through the junction. We call the regions, where the matrix elements vanish, regions of "Diabolic Pair Transfer".

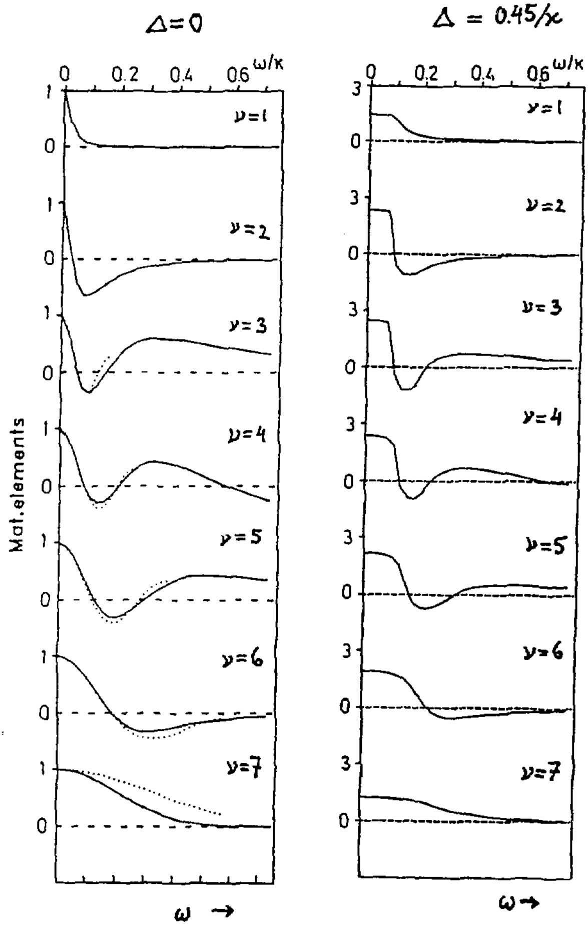

Fig 2. The same oscillations occur in a deformed single j=13/2 shell. The number of oscillations depends on the orbits ($\bar{\nu},\nu$) to which the pair is transfered. ν = 1,2... are ordered with respect to the energy, i.e. for small ω-values ν = 1,2,... corresponds to K = 1/2, 3/2, 5/2,... The qualitative pattern depends little on the gap parameter Δ.

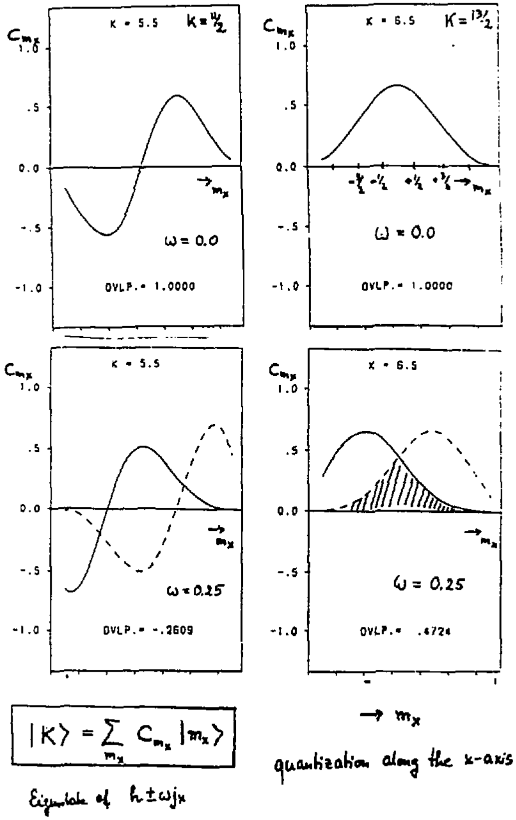

Fig. 3 The oscillations can be understood easily for $\Delta = 0$, where the transfer matrix element is just the spatial overlap $\langle\nu|T|\bar{\nu}\rangle$ of the two singleparticle wavefunctions obtained from the diagonalization of $h \pm \omega j_x$. For the large K-values K = 13/2, 11/2, ... these wavefunctions are represented in a basis quantized along the x-axis. In this basis they behave like wavefunctions of an harmonic oscillator shifted in momentum space. For K = 13/2 the overlap is decreasing with ω, but it stays always positive. For K = 11/2 it has one node, for K = 9/2 it has two nodes etc. For the small K-values early alignment gives vanishing overlaps and reduces the number of nodes.

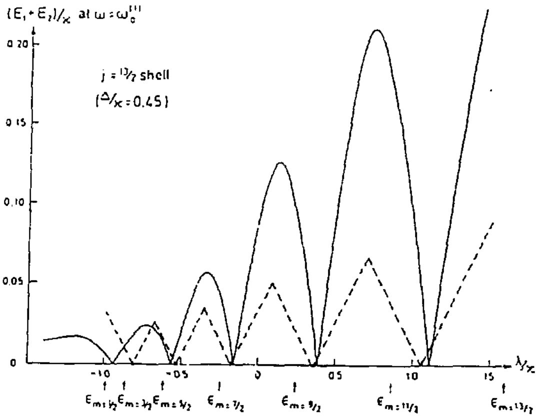

Fig. 4 The oscillating behavior of the interaction matrix element between the gs band and the s-band as a function of the chemical potential. The full lines are the exact results obtained by Hamamoto et. al. The dashed lines correspond to the approximation where the off diagonal matrix elements of the pairing tensor in the rotating frame are neglected. The critical "diabolical" points, where this matrix element vanishes are in this approximation identical to the points, where the pair transfer matrix-element $\langle \nu | \tau | \bar{\nu} \rangle$ vanishes, i.e. to the regions of "diabolic" pair transfer

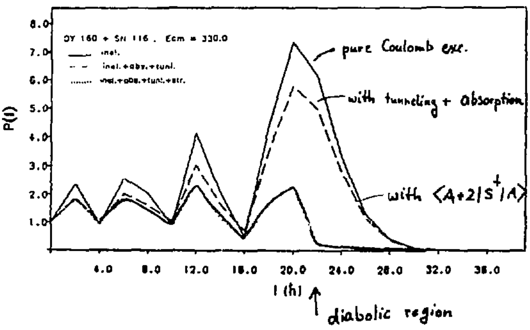

Fig. 5 The probability to excite a deformed target nucleus ^{160}Dy by coulomb excitation up to spin I with simultaneous transfer of a Cooper pair in sudden approximation at 180°.

COLLEAGUES - STUDIES OF HIGH-SPIN STATES IN Pt-Au-Ir NUCLEI

UNIV. TENNESSEE	McMASTER UNIV.	OAK RIDGE NAT. LAB
W. P. CARPENTER	J.C. WADDINGTON	C. BAKTASH
V. P. JANZEN	D. POPESCU	M.L. HALBERT
W. SCHMITZ	J. JOHANSSON	N.R. JOHNSON
A.J. LARABEE	G. KAJRYS	I.Y. LEE
C.R. BINGHAM		M.N. RAO
L.L. RIEDINGER		

UNIV. OF MONTREAL	RESEARCH INST. OF PHYSICS - STOCKHOLM
S. MONARO	J. NYBERG
S. PILOTTE	A. JOHNSON
J. DUBUC	

THEORETICAL COLLABORATORS

J.Y. ZHANG - INST. MODERN PHYSICS, LANZHOU
R. BENGTSSON - LUND UNIV.
W. NAZAREWICZ - WARSAW
G. LEANDER - UNISOR
T. BENGTSSON - LUND UNIV.

} JIHIR* VISITORS

* JOINT INSTITUTE FOR HEAVY ION RESEARCH

Z \ N	104		106		108		110
82			^{188}Pb		^{190}Pb		^{192}Pb
81			^{187}Tl		^{189}Tl		^{191}Tl
80	^{184}Hg		^{186}Hg		^{188}Hg		^{190}Hg
79	^{183}Au		^{185}Au	^{186}Au	^{187}Au	^{188}Au	
78	^{182}Pt	^{183}Pt	^{184}Pt	^{185}Pt	^{186}Pt	^{187}Pt	^{188}Pt
77	^{181}Ir		^{183}Ir		^{185}Ir		

· McMASTER EXPTS: $^{182-188}Pt$, $^{185-188}Au$, ^{183}Ir
HOWFIELD EXPTS: ^{183}Au, $^{183,184}Pt$

HIGH-j ORBITALS:

PROTON:

$h_{9/2}$, $f_{7/2}$, $i_{13/2}$ — PARTICLE STATES ABOVE Z=82 AT $\varepsilon_2 = 0$

$h_{11/2}$ ↓ FILLED FOR Z=76 AT $\varepsilon_2 = 0$

NEUTRON:

$i_{13/2}$ ↑ ~½ FILLED FOR N=106 AT $\varepsilon_2 = 0$

$h_{9/2}$ ↑ FILLED

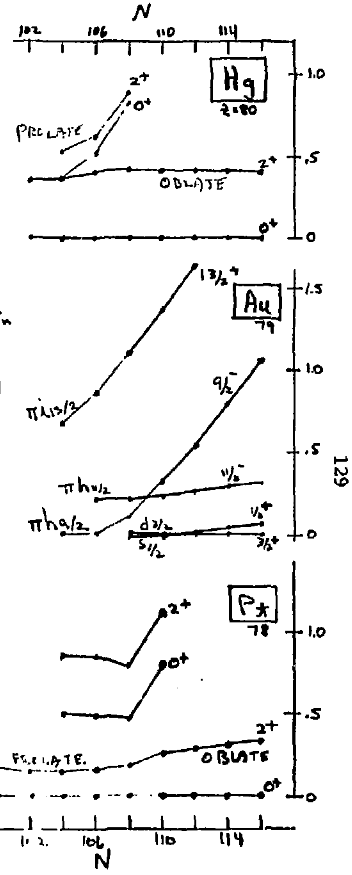

LEE RIEDINGER
UNIV. OF TENNESSEE

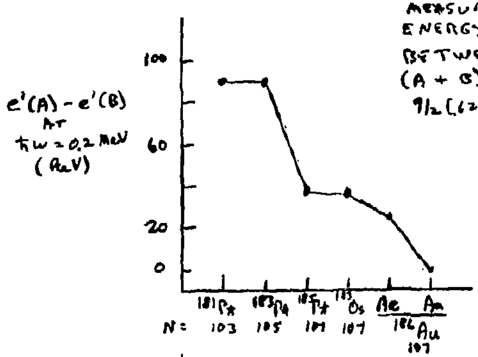

MEASURED ENERGY SPLITTING BETWEEN SIGNATURES (A + B) OF $\nu i_{13/2}$ BAND, 9/2[624], AT ħω = 0.2 MeV.

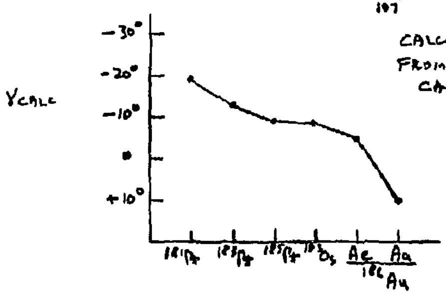

CALCULATED γ VALUE FROM S.C. PES CALCULATION.

9/2 [624] : $\nu i_{13/2}$: A, B
1/2 [541] : $\pi h_{9/2}$: e
1/2 [660] : $\pi i_{13/2}$: a

MIXING OF CLOSE-LYING 13⁻ STATES IN ^{184}Pt

EXPT:

$$\frac{B(E2;\,15^- \to 13^{-\prime})}{B(E2;\,15^- \to 13^-)} = 0.518 \pm .052$$

$$\frac{B(E2;\,15^{-\prime} \to 13^-)}{B(E2;\,15^{-\prime} \to 13^{-\prime})} = 0.536 \pm .066$$

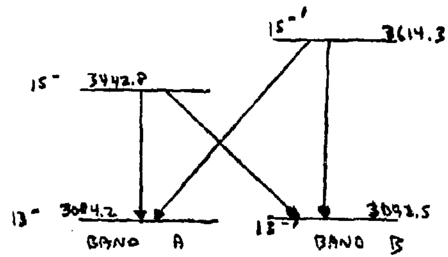

TWO-LEVEL MIXING OF 13⁻ STATES: (NAZAREWICZ)

$|13\rangle = a|A\rangle + b|B\rangle$

$|13'\rangle = -a|B\rangle + b|A\rangle$

$|V|$ = INTERACTION MATRIX ELEMENT

$$= \frac{E_{13'} - E_{13}}{2[\rho^2+1]^{1/2}} \quad \text{WHERE} \quad \rho = \left[\frac{1}{4a^2(1-a^2)} - 1\right]^{1/2}$$

DATA: $a = .81 \qquad b = .59$

$E_{13'} - E_{13} = 8.3$ keV

$|V| = 4$ keV

$e_{13'} - e_{13} = 2.6$ keV

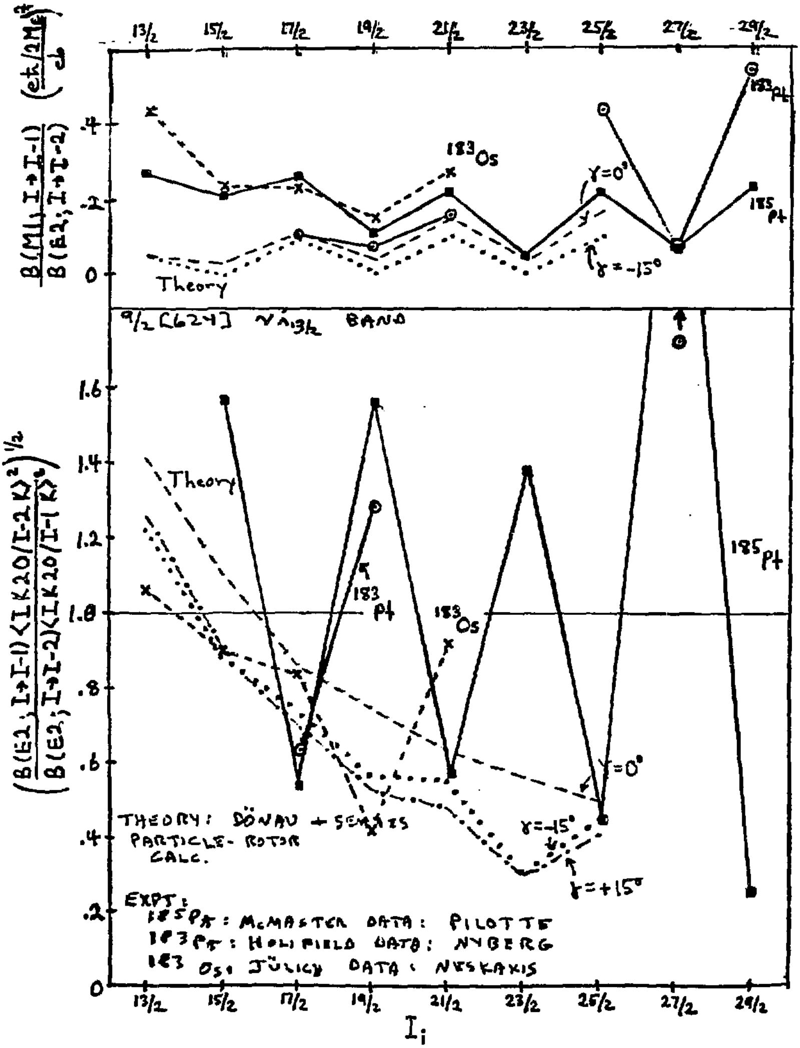
13/2
15/2
17/2
19/2
21/2
23/2
25/2
27/2
29/2
183Os
183Pt
185Pt
Theory
9/2 [624] ν i13/2 BAND
1.6
1.4
1.2
1.0
.8
.6
.4
.2
0
THEORY: DÖNAU + SEMMES PARTICLE-ROTOR CALC.
EXPT:
185Pt: McMASTER DATA: PILOTTE
183Pt: HOLIFIELD DATA: NYBERG
183 Os: JÜLICH DATA: NESKAKIS
I_i

SHAPE VARIATIONS IN ^{184}Pt

β_2, γ FOR PES MINIMA FOR VARIOUS CONFIGURATIONS

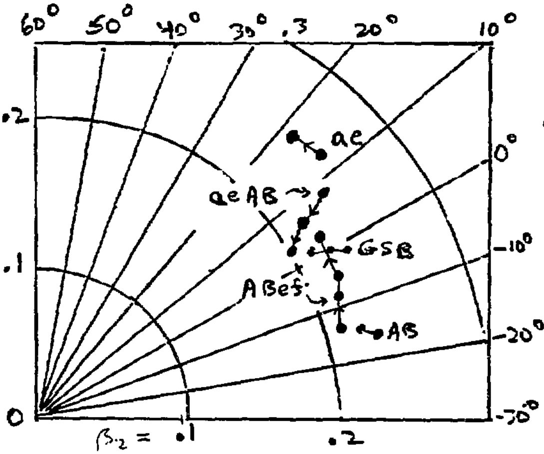

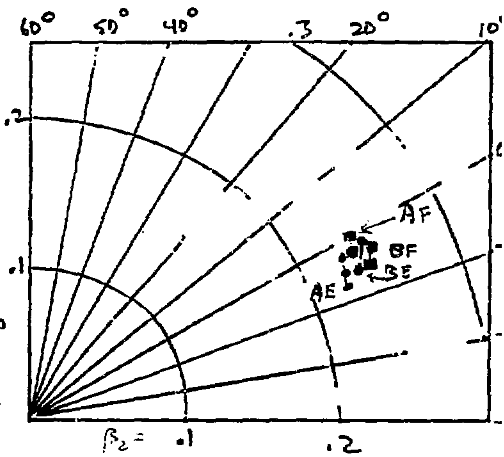

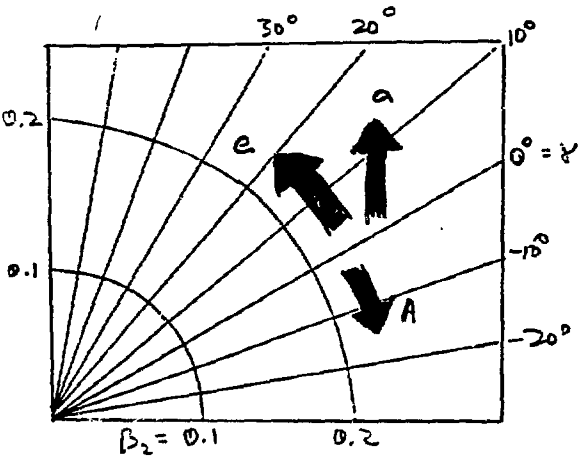

QUASINEUTRON ORBITALS:

$\nu i_{13/2}$: 9/2 [624] AT $\omega = 0$: A, B

$\nu f_{7/2}$: 7/2 [514] : E, F

QUASIPROTON ORBITALS:

$\pi i_{13/2}$: 1/2 [660] : a, b

$\pi h_{9/2}$: 1/2 [541] : e, f

Comment from M. de Voigt

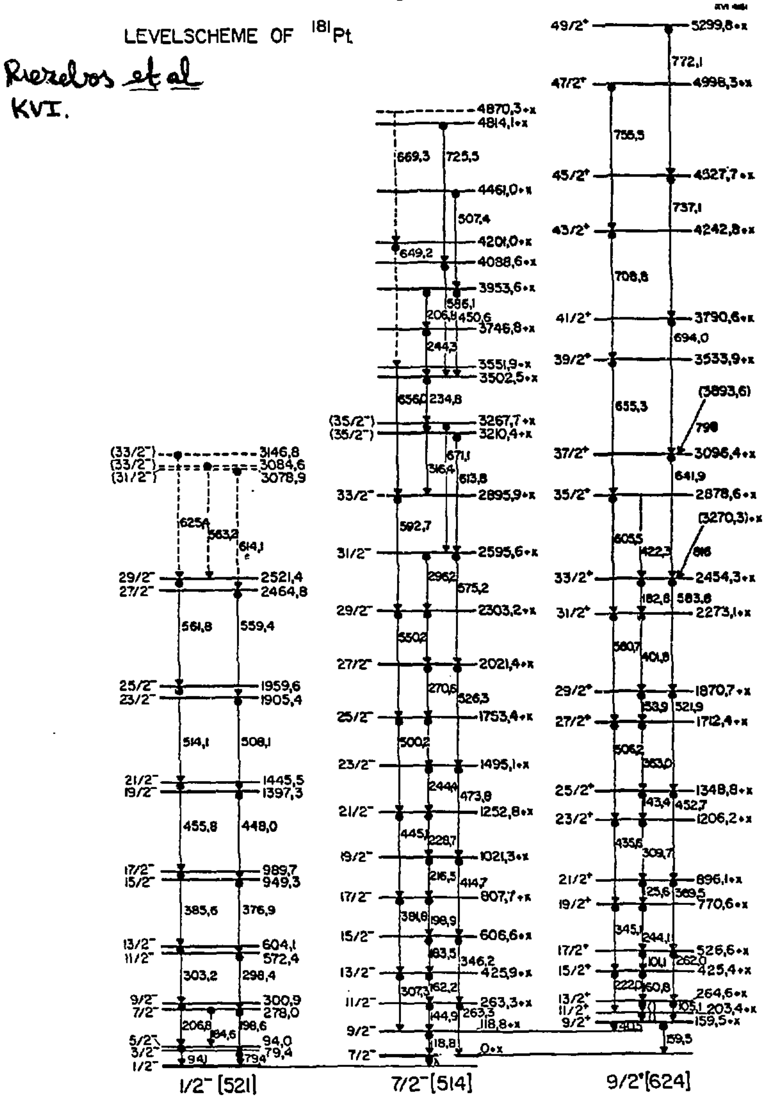

J. Wood New results on shape coexistence in the light gold isotopes

J.L. WOOD - 1

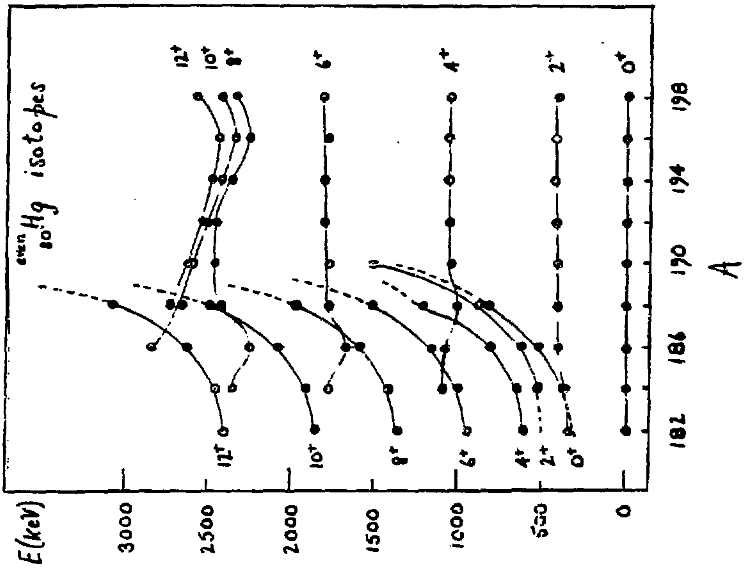

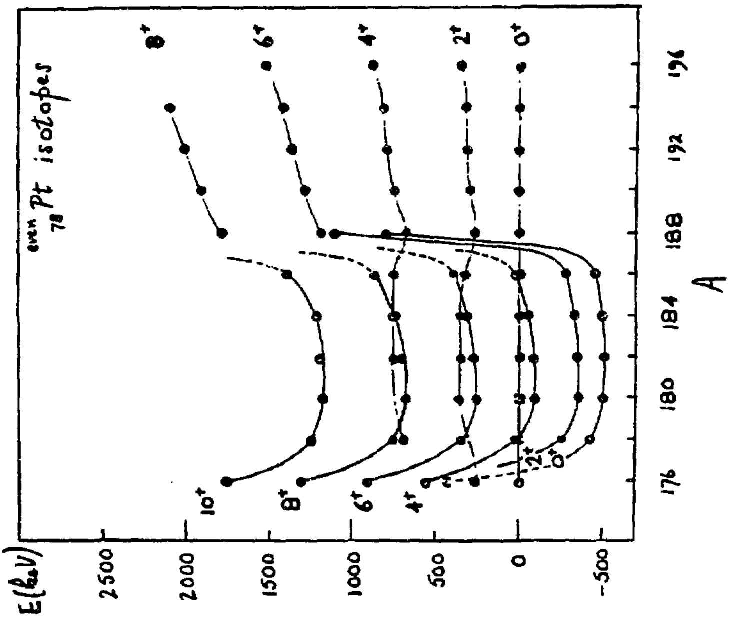

J.L. Wood - 2

Negative parity states in the odd-Au isotopes

$\pi h_{11/2}^{-1}\ \pi h_{9/2}^{+1}$

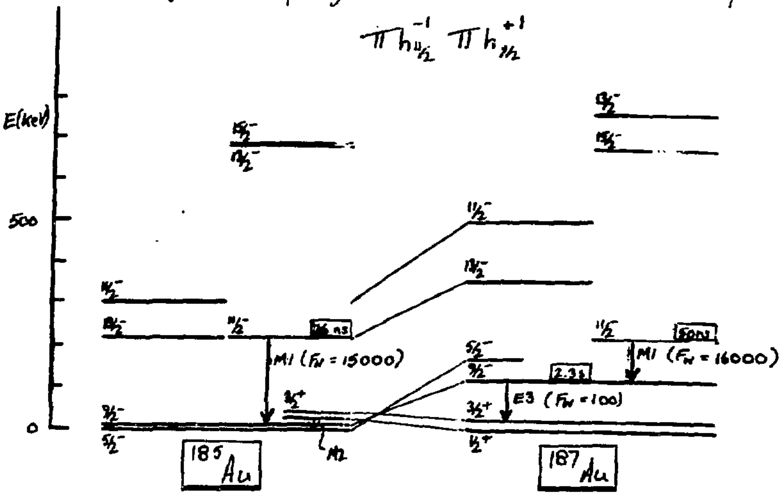

$Hg^{m,g}$ decay: $J^{\pi} = 13/2^{+}, 1/2^{-}$ $J^{\pi} = 13/2^{+}, 3/2^{-}$

UNISOR and ISOCELE (Orsay)

Particle-core coupling in ^{185}Au:

$\pi h_{11/2}^{-1}\ \pi h_{9/2}^{+1}$

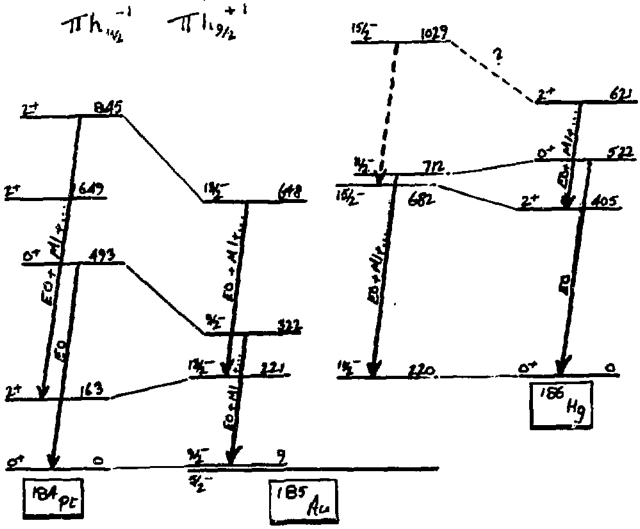

$Hg^{m,g}$: UNISOR (C.D. Papanicolopulos, JW -- Ga. Tech.
M. Kortelahti, E.F. Zganjar -- LSU)

J. L. WOOD - 3

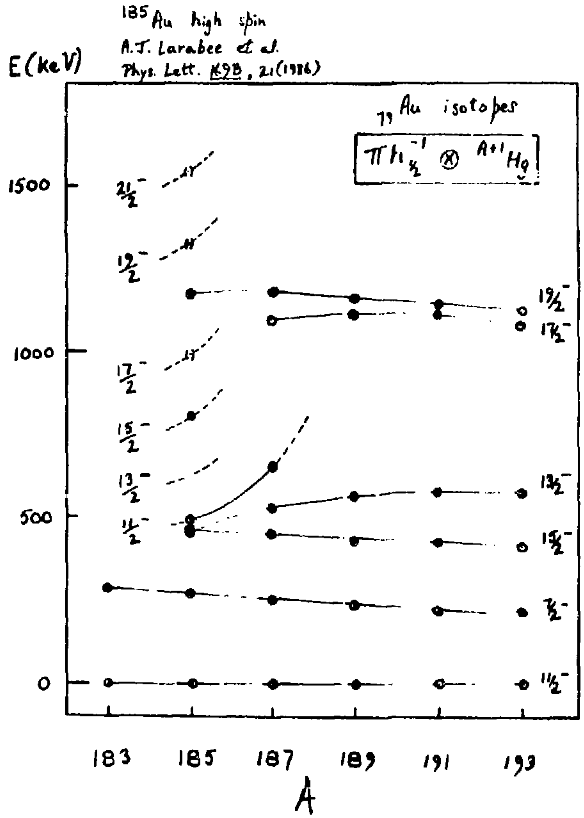
185Au high spin
A.T. Larabee et al.
Phys. Lett. K9B, 21(1986)
E(keV)
$_{79}$Au isotopes
$\pi h_{11/2}^{-1} \otimes {}^{A+1}Hg$
1500
1000
500
0
21/2$^-$
19/2$^-$
17/2$^-$
15/2$^-$
13/2$^-$
11/2$^-$
19/2$^-$
17/2$^-$
13/2$^-$
15/2$^-$
7/2$^-$
11/2$^-$
183
185
187
189
191
193
A

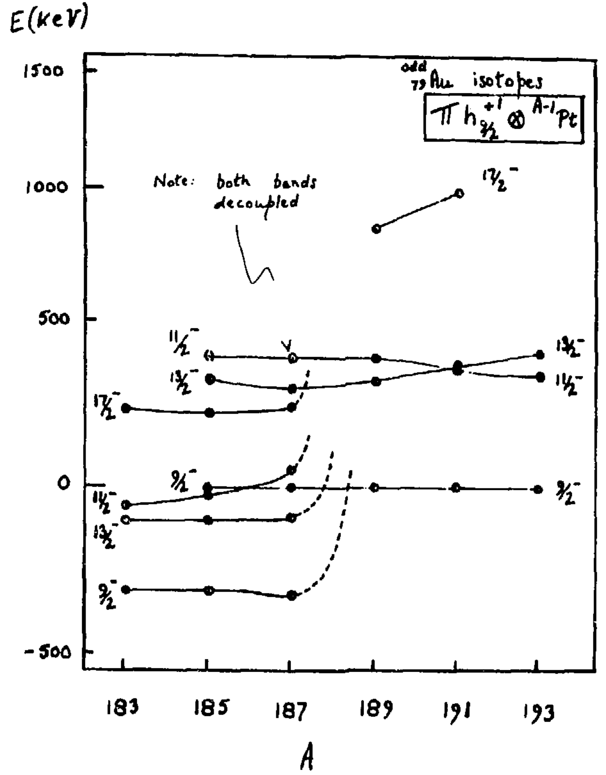
E(keV)
odd $_{79}$Au isotopes
$\pi h_{9/2}^{+1} \otimes {}^{A-1}Pt$
1500
1000
500
0
-500
Note: both bands decoupled
17/2$^-$
11/2$^-$
13/2$^-$
17/2$^-$
9/2$^-$
11/2$^-$
13/2$^-$
9/2$^-$
13/2$^-$
11/2$^-$
9/2$^-$
183
185
187
189
191
193
A

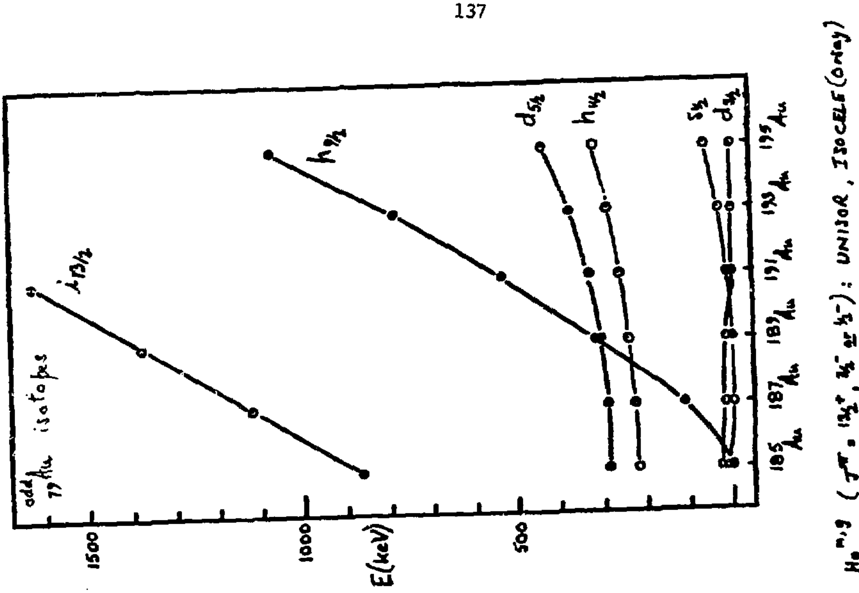

Hg^{m,g} (J^π = 13/2+, 3/2− or 1/2−): UNISOR, ISOCELE (Orsay)

Isotope shifts in the Hg and Au nuclei

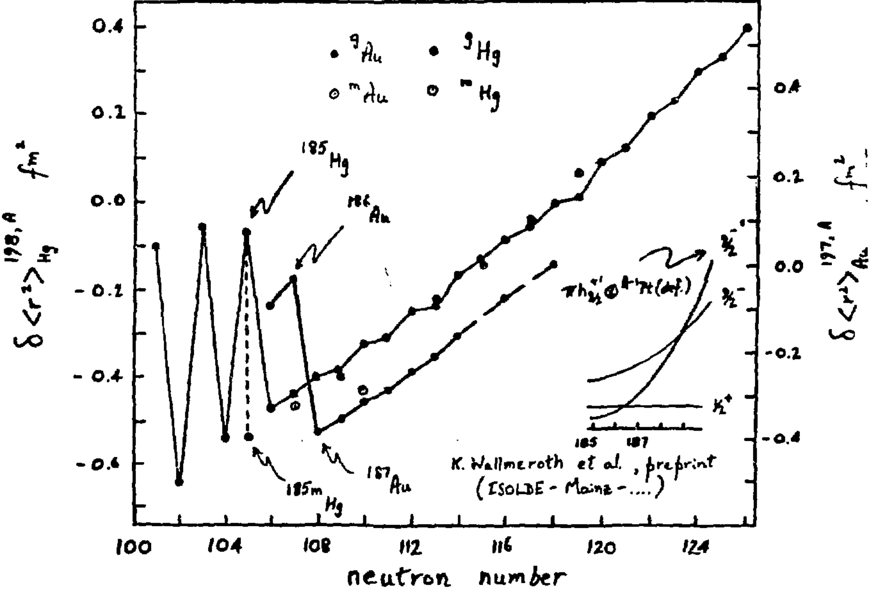

TL WED-4

The Fermion Dynamical Symmetry Model

M.W. Guidry (Tenn.)
C.L. Wu (Tenn.)
D.H. Feng (Drexel)
J.Q. Chen (Nanjing)
X.G. Chen (Drexel)
Z.P. Li (Tenn.)
H. Wu (Drexel)

THE PROCEDURE

1) Recouple the angular momenta

$$\vec{j} = \vec{k} + \vec{i}$$

{ k = pseudorbital
{ i = pseudospin

2) Truncate the Spherical Shell Model

{ k = 1 or i = 3/2 (Normal parity orbitals)
{ k = 0 (unique parity orbitals)

{ $J = |\vec{j}_1 + \vec{j}_2| = 0, 2$
(Coherent SD fermion Subspace)

{ u ≡ 'heritage'
≈ # particles not coherently paired to S or D fermion pairs

{ S + D fermion "core"
+ unpaired particles }

Not a Mapping

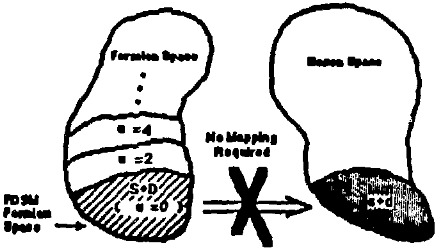

Fig. 9-2 Schematic illustrations of the shell-model truncation implicit in the FDSM. For no broken pairs (u=0), the coherent (S,D,S) subspace is decoupled from the remainder of the shell-model space. By breaking pairs (u≠0), a richer basis of shell-model states may be constructed. Since the FDSM is formulated entirely in the fermion space, it requires no fermion → boson mapping procedure.

3) Exploit the group structure:

The Fermion Dynamical Symmetry Model (FDSM):

A solution of the spherical shell model by radical symmetry-dictated truncation in the fermion space.

High - Spin Limit for SU_3

$$Sp_6 \otimes SU_2 \supset SU_3 \otimes SU_2$$

u_1 $\quad$ v_0 $\quad$ $(\lambda\mu)$

$u \equiv u_1 + v_0 \equiv$ "heritage"

Simple Spectrum :

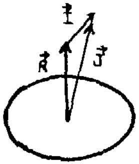

{Coriolis is attenuated

$$E \sim \Delta + \alpha J^2 + \frac{\alpha}{2}(1-\epsilon)\vec{J}\cdot\vec{I} + \beta I^2$$

$$\Delta = \Delta_{Sp_6} + \Delta_{SU_2} + \Delta_{SU_3}$$

$= f($ degeneracies, # broken pairs, part. #$)$

{ R - total pseudo-orbital
I - total pseudo spin }

Corresponding E2 Matrix elements

$$\langle J+2 \| M(E2) \| J \rangle \cong Q_F \left[\frac{3(R+1)(R+2)\ (2N_1+R+3)(2J+5)}{4(2R+3)\ (2R+5)} (2N_1 - R) \right]^{\frac{1}{2}}$$

$$+ \langle J+2 \| M(E2) \| J \rangle_{S.P.}$$

{ N_1 = # pairs in Normal-parity orbitals }

^{232}Th

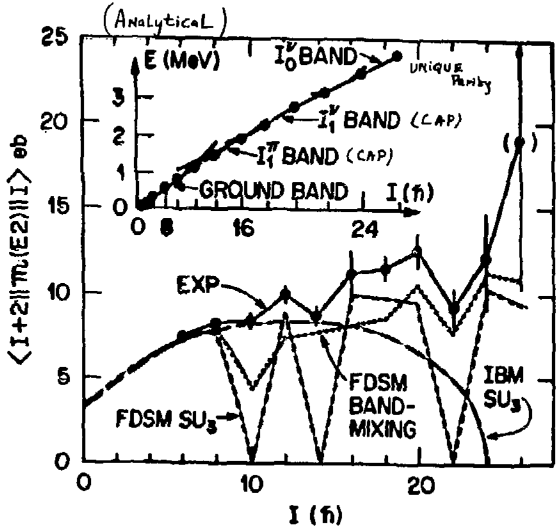

{Emling, et al. (GSI) data

Fig. 1

(Almost Analytical)

$(E_I - E_{13/2})/(\hbar^2/2\mathcal{J})$: $\hbar^2/2\mathcal{J} = \alpha = 0.0167$ MeV, $\chi = 53\,\varepsilon_2$ — FDSM

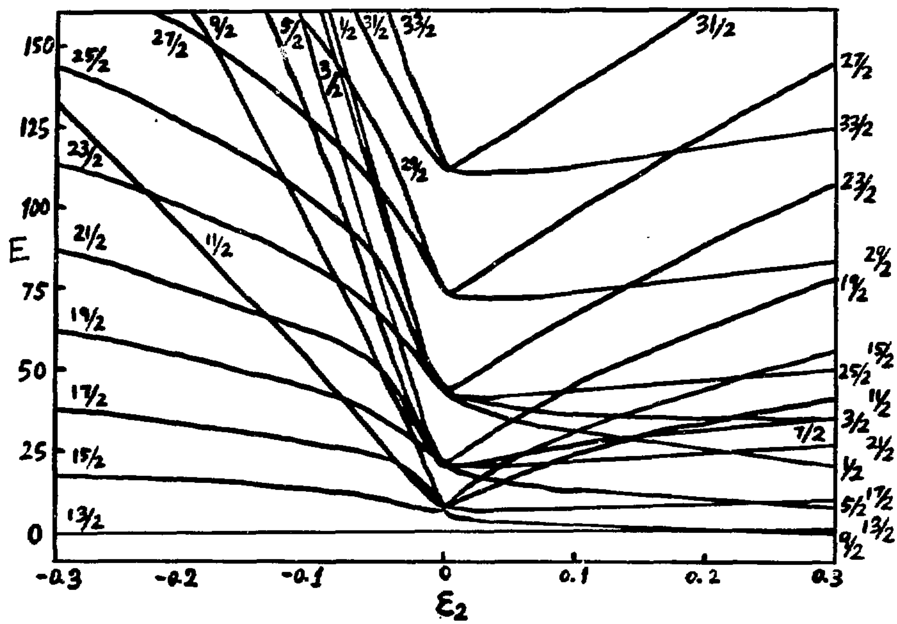

— P.R.M

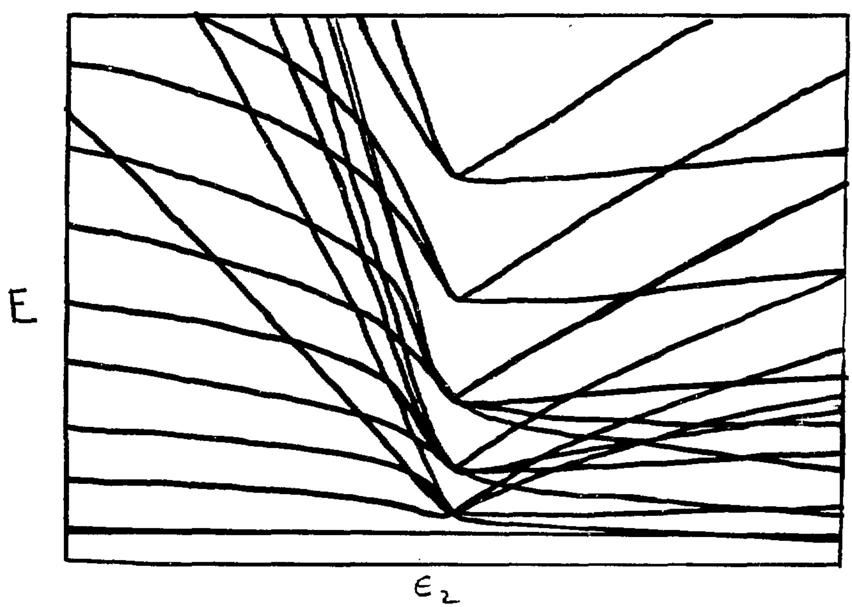

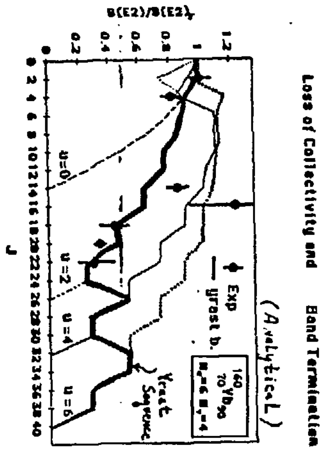

Data from
- LBL
- ORNL
- UT
- Stony Brook

(Analytical)

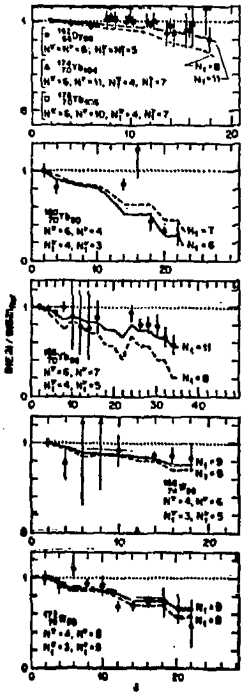

Conclusions

1) Microscopic Spherical Shell Model Description of High-Spin Physics.

2) In some physically-interesting cases the solutions are analytical.

3) A natural description of loss of E2 strength and band termination w/o phenomenological deformation parameters.

4) A natural description of high-spin bands directly in the laboratory reference frame.
   - a) No 'reference bands' (CAP calculated microscopically).
   - b) No phenomenological deformation parameters.

5) Same theory can describe rotations, vibrations, transitional (Rot/vib) + broken particles (strong, weak, and R. Aligned Coupling) in
   - a) even-even
   - b) odd mass
   - c) odd-odd

Theories fall into two categories:

1) Testable
2) Detestable (diabolical?)

** FDSM is fully microscopic, And hence is fully testable **

Indications of octupole deformations in Ba isotopes

W.R. Phillips, I. Ahmad, M. Prigent, H. Emling, R. Holzmann
R.V.F. Janssens, T.L. Khoo

Theory: W. Nazarewicz, G. Leander, J. Dudek

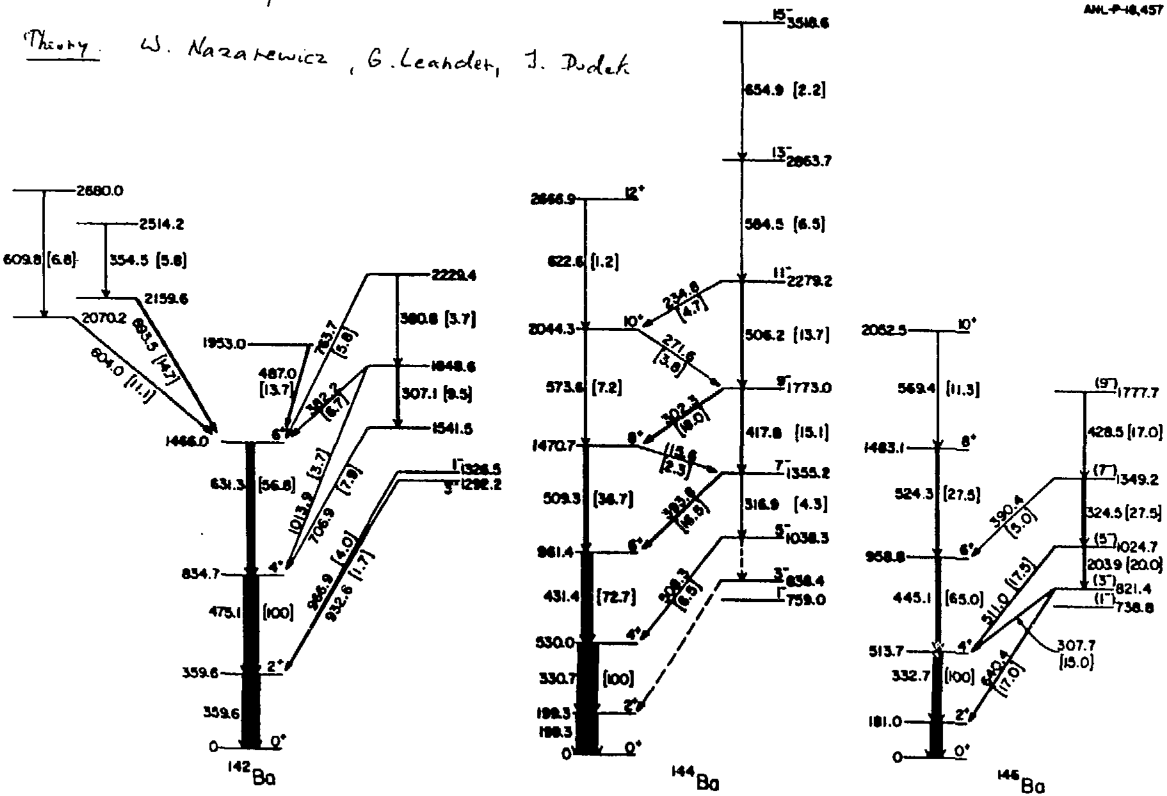

Level schemes inferred from spectroscopy of fission fragments of ^{252}Cf

TABLE 1. Electric dipole transition strengths in ^{144}Ba and ^{146}Ba.

N.B. $\frac{B(E1)}{B(E2)}$ larger for $\pi^+ \to \pi^-$ than for $\pi^- \to \pi^+$

E_γ keV	$I_i\pi \to I_f\pi_f$	I_γ	$B(E1)/B(E2)$ a) 10^{-6} fm^{-2}	$B(E1)/B(E1)_W$ b)
^{144}Ba				
317	$7^- \to 5^-$	4.3(0.9)	0.16(3)	$0.33(6)\times10^{-3}$
394	$7^- \to 6^+$	16.5(1.5)		
509	$8^+ \to 6^+$	36.7(2.9)	1.06(34)	$2.3(7)\times10^{-3}$
116	$8^+ \to 7^-$	2.3(0.6)		
418	$9^- \to 7^-$	15.1(1.4)	0.43(6)	$0.93(12)\times10^{-3}$
302	$9^- \to 8^+$	18.0(1.5)		
574	$10^+ \to 8^+$	7.2(1.1)	1.27(36)	$2.8(8)\times10^{-3}$
272	$10^+ \to 9^-$	3.8(0.9)		
506	$11^- \to 9^-$	13.7(2.2)	0.68(18)	$1.5(4)\times10^{-3}$
235	$11^- \to 10^+$	4.7(1.1)		
^{146}Ba				
204	$5^- \to 3^-$	20.0(2.8)	0.0018(3)	$4.5(8)\times10^{-6}$
511	$5^- \to 4^+$	4^+	17.5(2.8)	
325	$7^- \to 5^-$	27.5(3.8)	0.0088(21)	$2.4(6)\times10^{-5}$
390	$7^- \to 6^+$	5.0(1.3)		

a) $B(E2;2_1^+\to0_1^+)$ for ^{144}Ba = 0.23 e^2b^2 for ^{146}Ba = 0.29 e^2b^2.

b) $B(E1)_W$ for ^{144}Ba = 0.0173 e^2b, for ^{146}Ba = 0.0174 e^2b.

A constant quadrupole moment was assumed for each nucleus, although an increase with spin is possible.

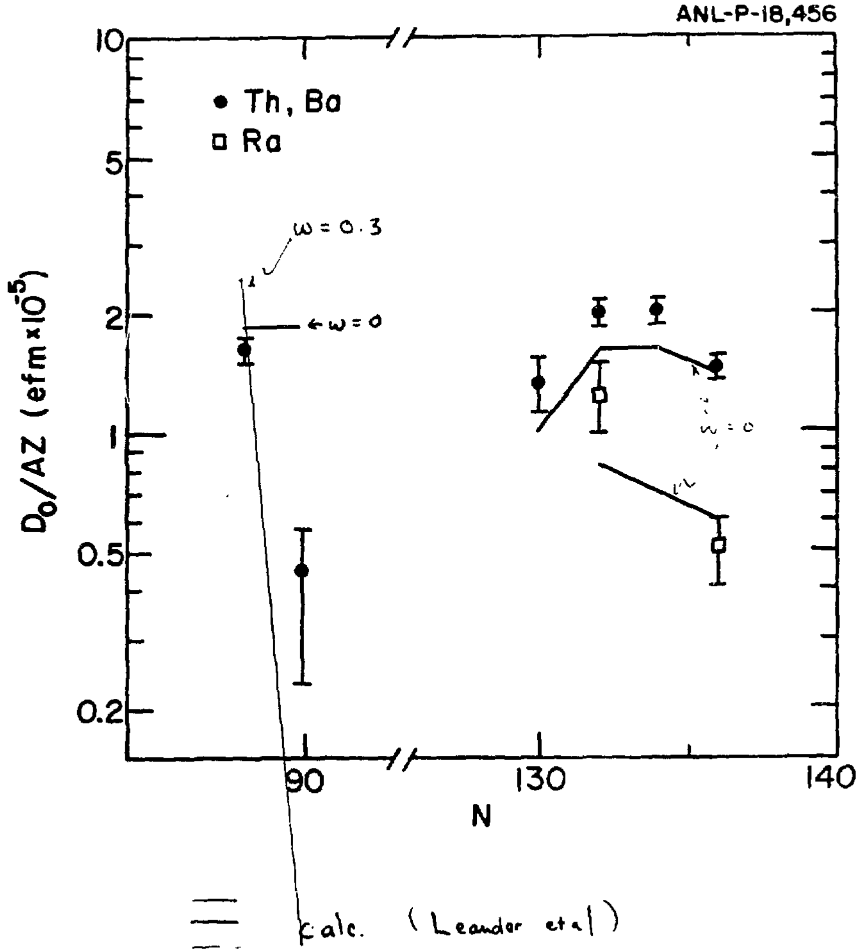
ANL-P-18,456
Th, Ba
Ra
ω = 0.3
ω = 0
D_0/AZ (efm × 10^{-5})
N
10
5
2
1
0.5
0.2
90
130
140
calc. (Leander et al)

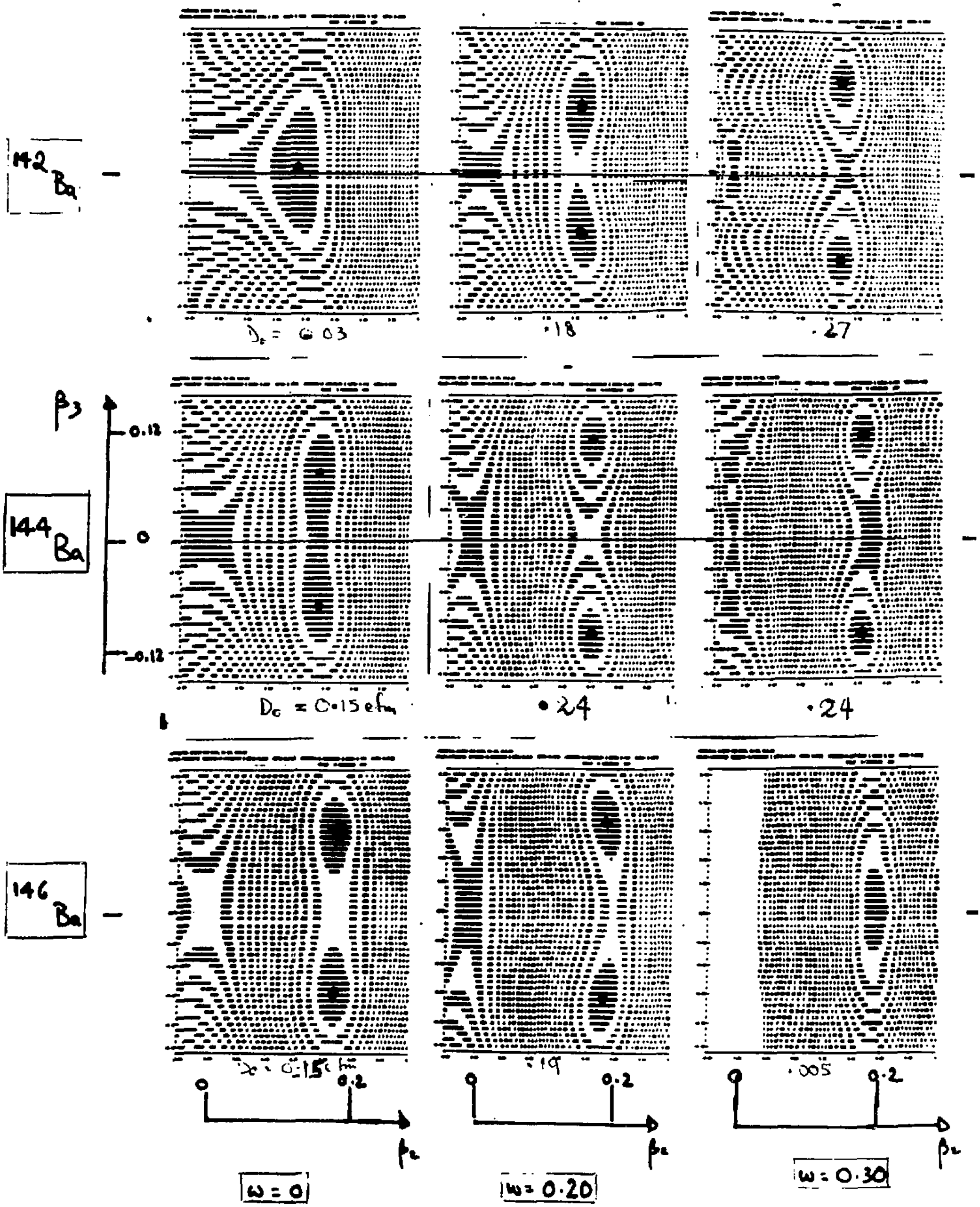
^{142}Ba
D_0 = 0.03
·18
·27
β_3
0.12
0
-0.12
^{144}Ba
D_0 = 0.15 efm
·24
·24
^{146}Ba
D_0 = 0.15 efm
·19
·005
0
0.2
β_2
ω = 0
ω = 0.20
ω = 0.30

N. Koller — Extension of transient field measurement of magnetic moments to higher spin states

VIBRATIONAL NUCLEI

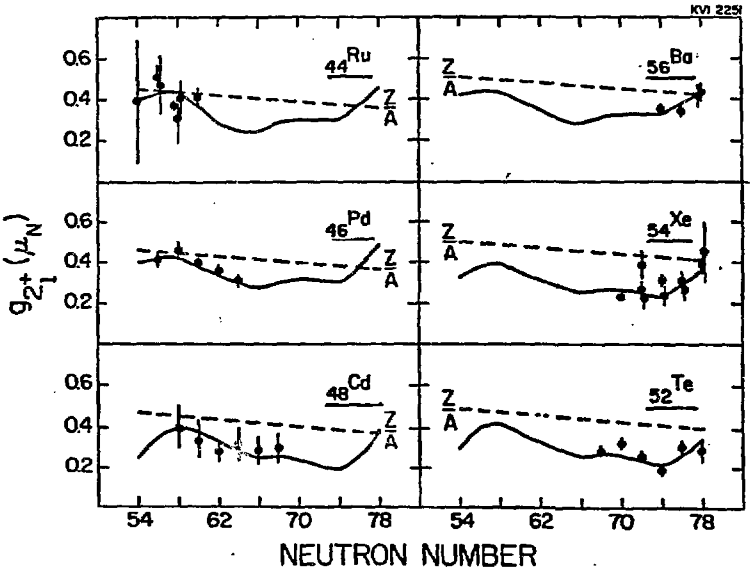

— IMPAC

— Transient field measurements.

— IBA

Comparison of IBA predictions with the magnetic moments of 2_1^+ states of vibrational nuclei.

$$g_{calculated} = g_\pi \frac{N_\pi}{N_\pi + N_\nu} + g_\nu \frac{N_\nu}{N_\pi + N_\nu}$$

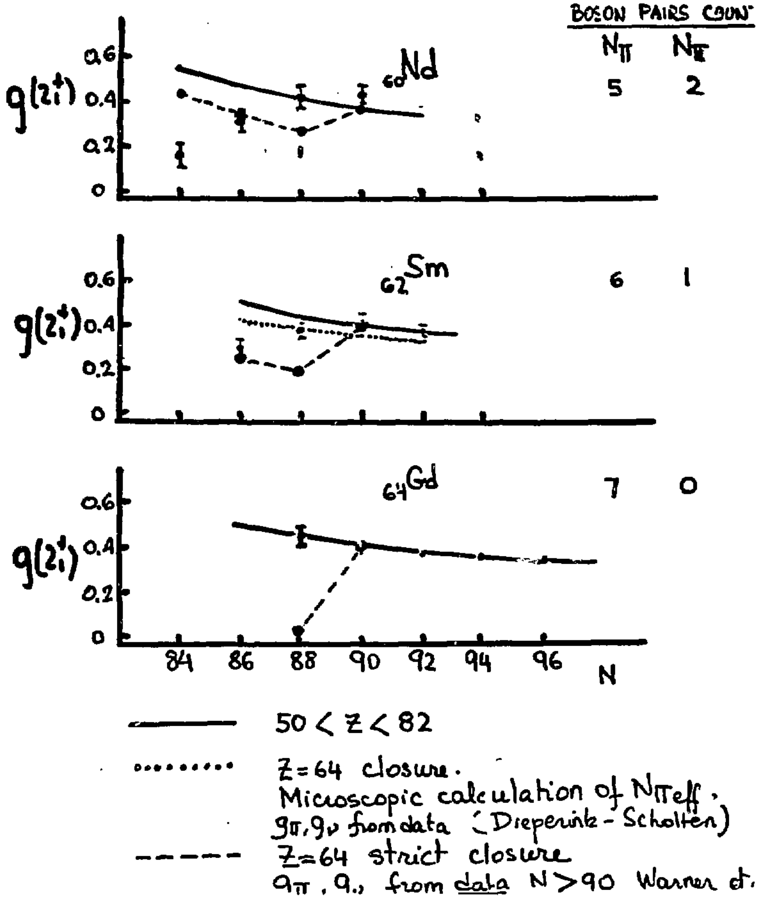

Magnetic moments of 2_1^+ states in Nd, Sm and Gd isotopes showing that for $N<88$, $Z=64$ acts as a closed shell while for $N \geq 88$ the gap is washed out as protons are pulled into the $h_{11/2}$ orbital.

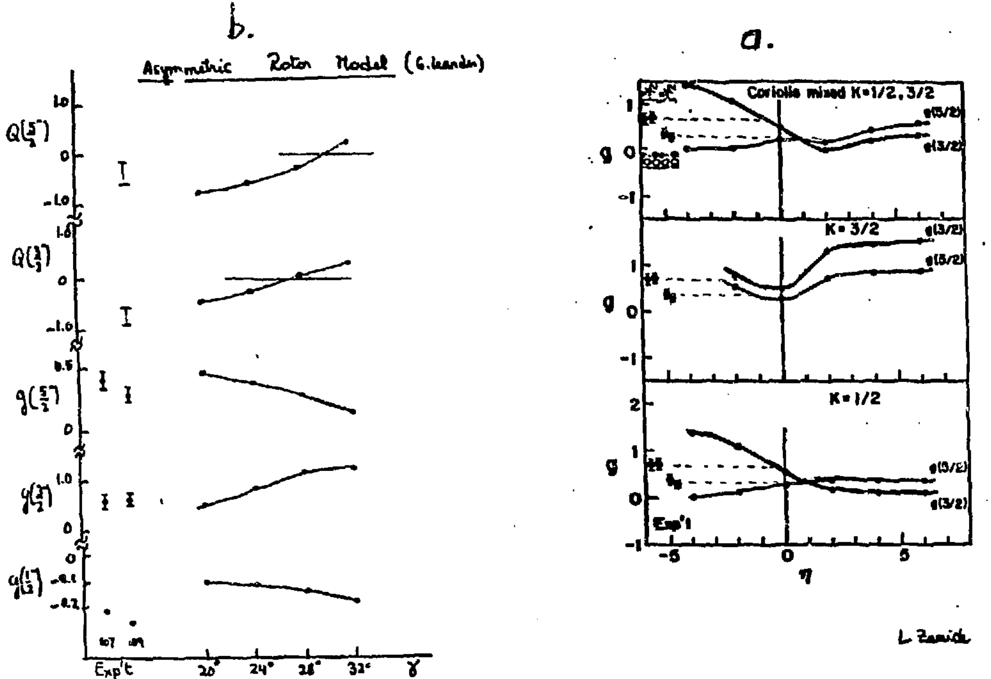

Magnetic moment measurements of 3/2⁻ and 5/2⁻ states in ^{107}Ag and ^{109}Ag and comparison with the predictions of the:

a. Axial Nilsson model

b. Asymmetric rotor model

^{166}Er

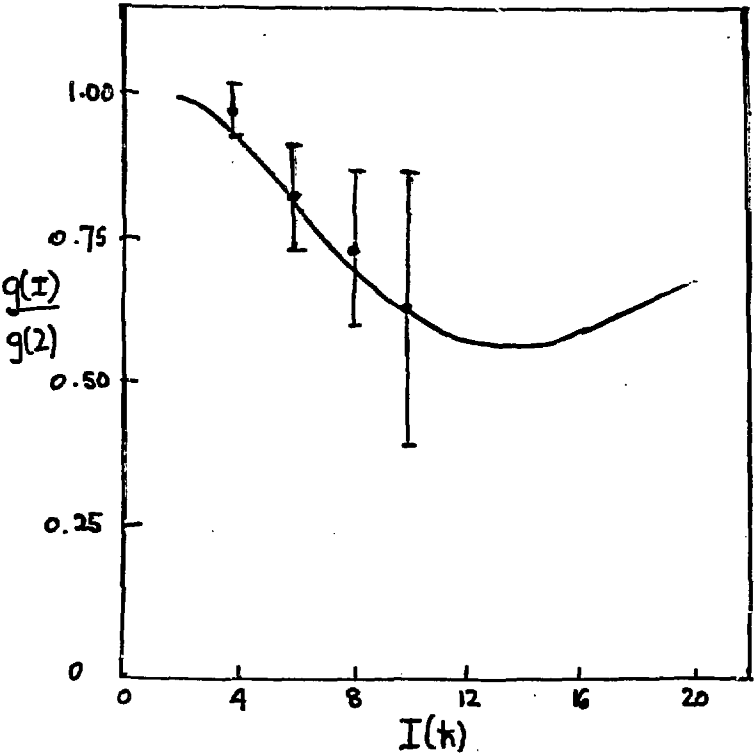

Ratio $g(I)/g(2_1^+)$ of moments of the low-lying levels of ^{166}Er compared to predictions of Cranked Hartree-Fock calculation.

Th.

Ansari, Wüst - Mükhans NP A415, 215 (1984) Cranked Hartree-Fock-Bogoliubov

Exp.

Doran, Bolotin, Stuchbery & Byrne Transient fields

E2 PROPERTIES OF THE NUCLEI STUDIED VIA HEAVY-ION COULOMB EXCITATION

T.Czosnyka, NSRL,* The University of Rochester, Rochester, NY 14627

A major progress, stimulated by the availability of the heavy-ion beams, has occured over the last few years in the field of heavy-ion Coulomb excitation. Recently developped experimental techniques - such as the position-sensitive particle detectors and the Compton-suppressed γ-detectors - made possible to perform the multiple Coulomb excitation experiments yielding a large amoumt of high quality data which can be acquired during a relatively short accelerator run. The data collected using these techniques uniquely determine the full sets of the E2 matrix elements coupling the accesible levels, thus providing the complete description of the dominating electromagnetic properties of the nuclei. The availability of the extensive experimental data has, in turn, prompted the developpment of the sophististicated computer software, capable of handling the whole information resulting from a given experimental program to model-independently determine the electromagnetic properties of an investigated nucleus. The sample results shown were obtained using the Coulomb excitation data analysis code GOSIA, developped at the Nuclear Structure Research Laboratory of The University of Rochester as the result of the Rochester-Uppsala-Warsaw collaboration. The experimental work has been carried out at NSRL, LBL, BNL and TLU (Uppsala).

* Supported by the National Science Foundation.

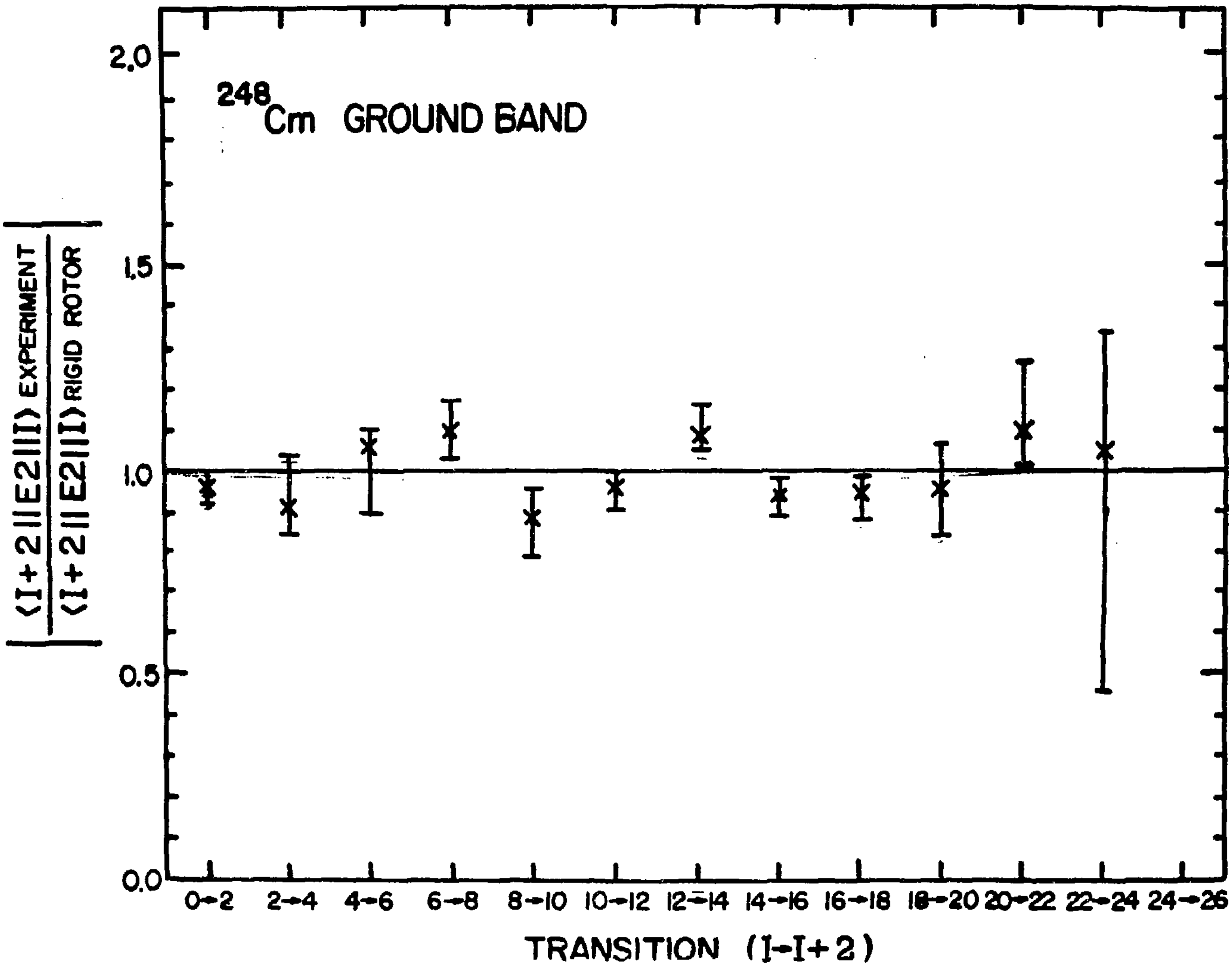

248Cm GROUND BAND
|⟨I+2||E2||I⟩ EXPERIMENT / ⟨I+2||E2||I⟩ RIGID ROTOR|
2.0
1.5
1.0
0.5
0.0
0→2
2→4
4→6
6→8
8→10
10→12
12→14
14→16
16→18
18→20
20→22
22→24
24→26
TRANSITION (I→I+2)

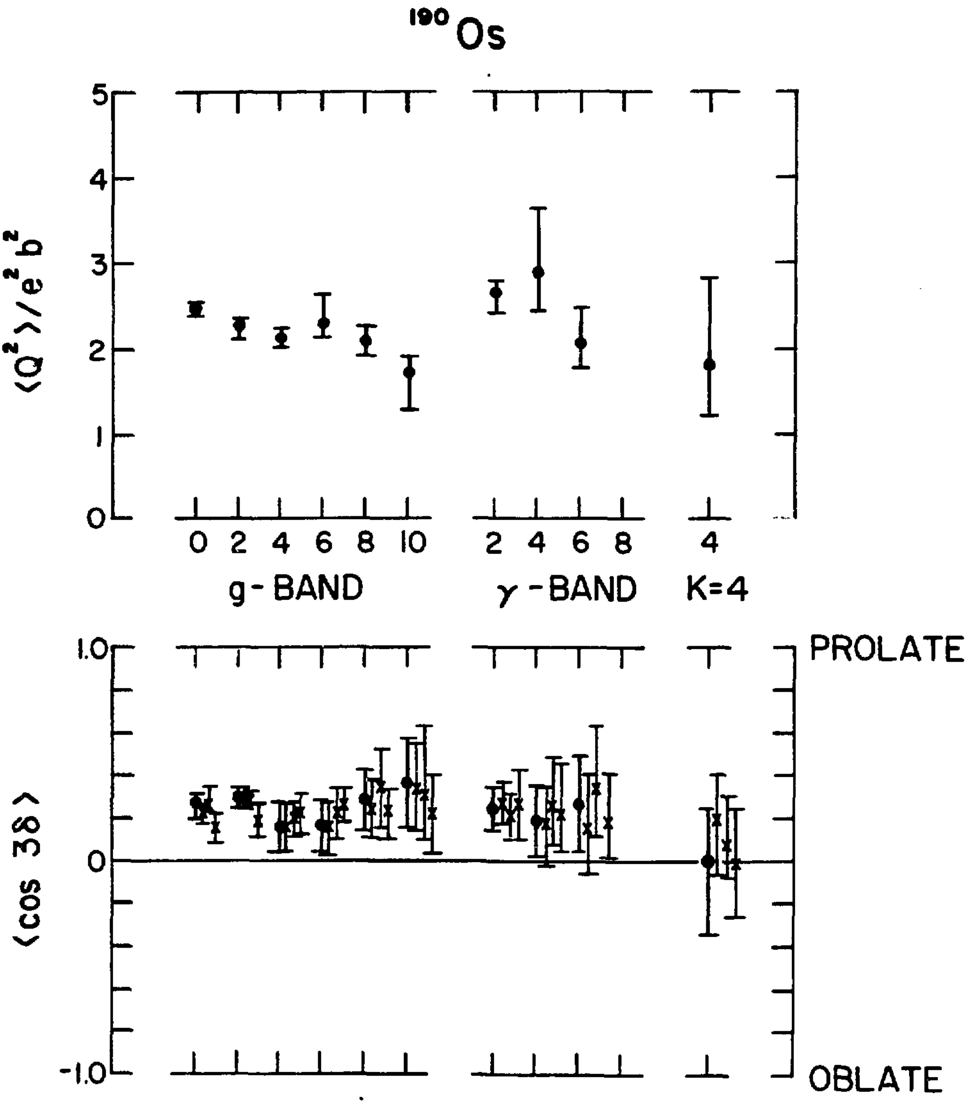
190 Os
5
4
3
2
1
0
⟨Q²⟩/e²b²
0 2 4 6 8 10
2 4 6 8
4
g - BAND
γ - BAND
K=4
1.0
0
-1.0
⟨cos 3δ⟩
PROLATE
OBLATE

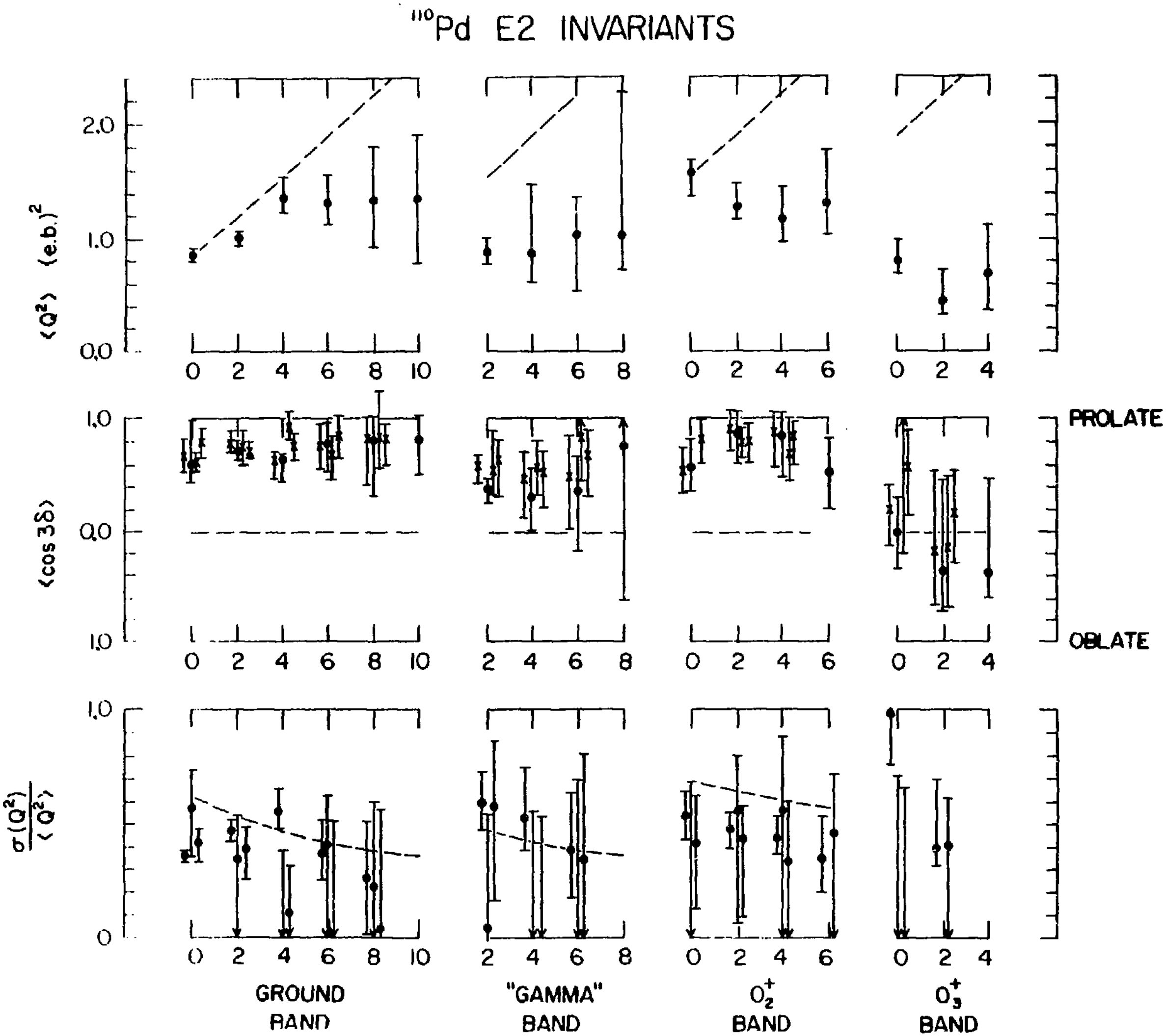
110Pd E2 INVARIANTS
⟨Q²⟩ (e.b.)²
⟨cos 3δ⟩
σ(Q²)/⟨Q²⟩
PROLATE
OBLATE
GROUND BAND
"GAMMA" BAND
0₂⁺ BAND
0₃⁺ BAND

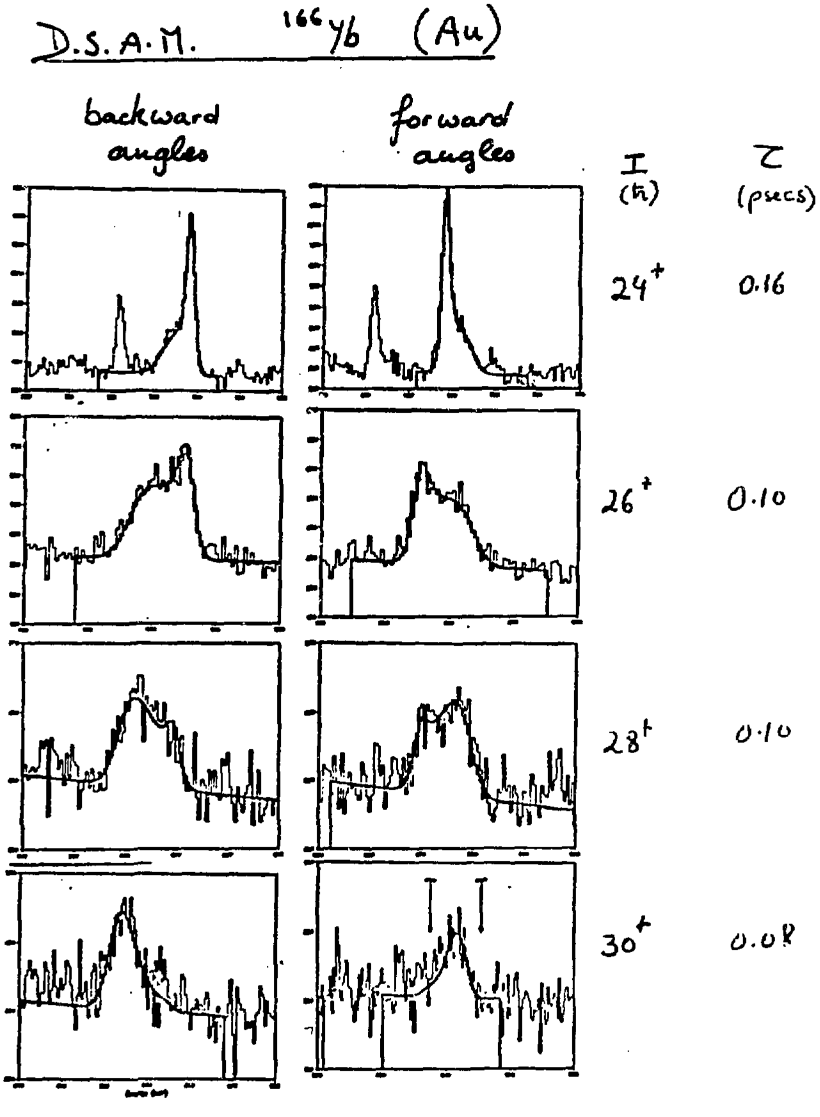
D.S.A.M. 166Yb (Au)
backward angles
forward angles
I (ħ)
τ (psecs)
24+
0.16
26+
0.10
28+
0.10
30+
0.08

D.S.A.M. ^{166}Yb backward angles

Au Backing | Pb backing

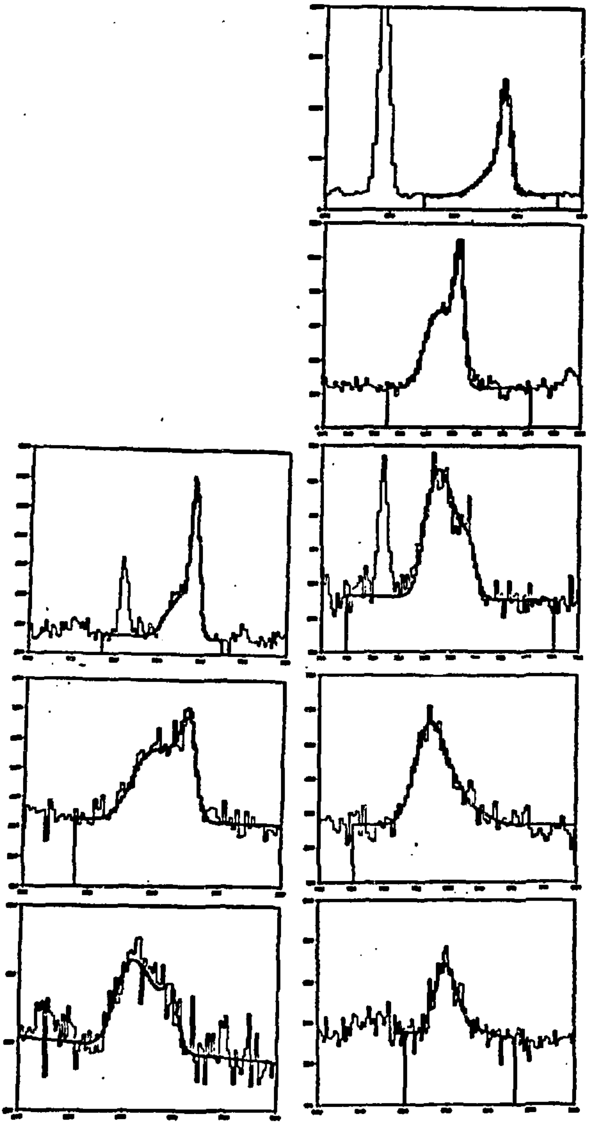

I (ħ)	τ (psecs)
20^+	0.57
22^+	0.26
24^+	0.17
26^+	0.11
28^+	0.10

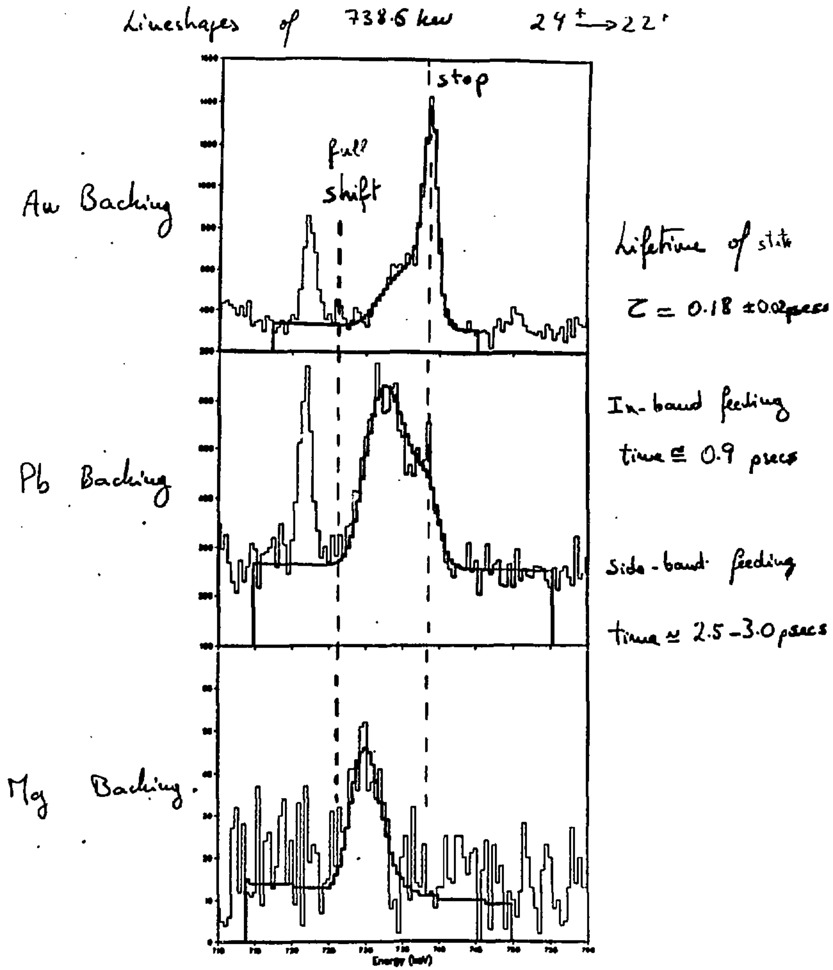
Lineshapes of 738.6 kev 24+ → 22+
stop
full shift
Au Backing
Lifetime of state
τ = 0.18 ±0.02psecs
Pb Backing
In-band feeding
time ≅ 0.9 psecs
Side-band feeding
time ≃ 2.5-3.0psecs
Mg Backing.
Energy (keV)

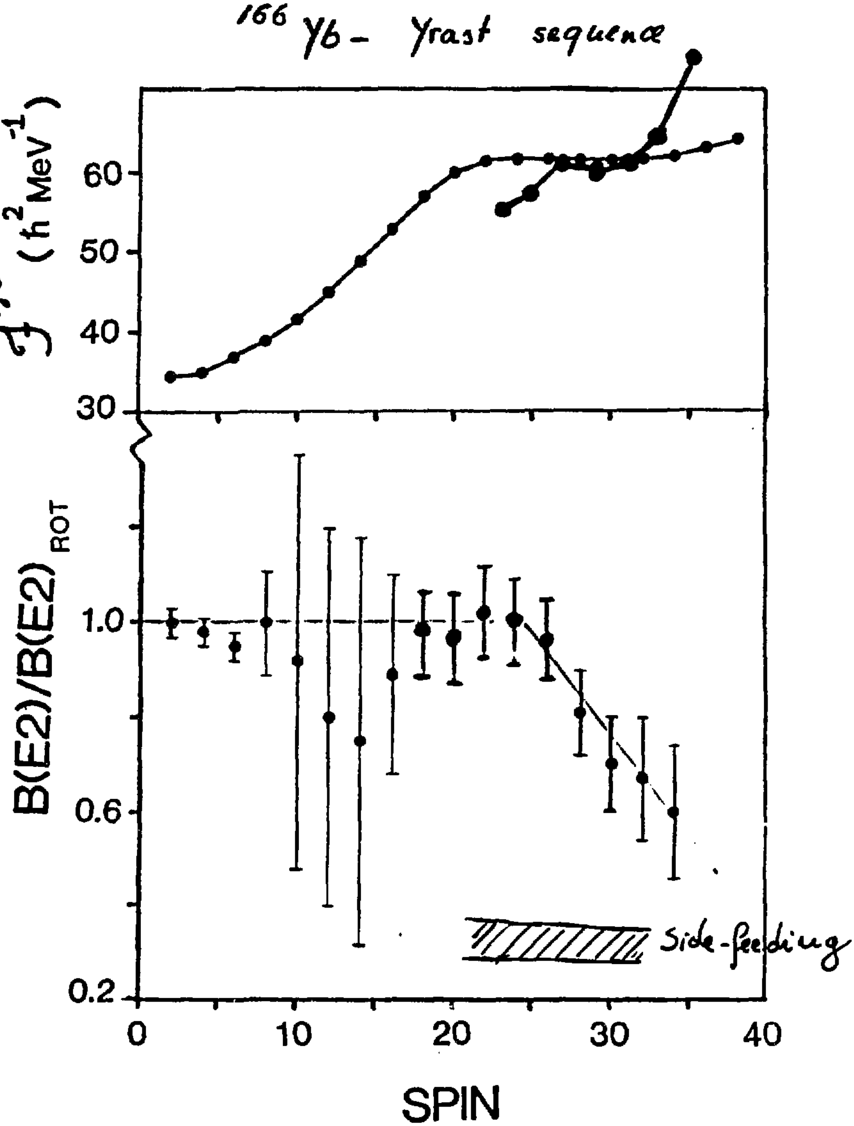

166 Yb - Yrast sequence
$\mathcal{J}^{(2)}$ ($\hbar^2$ MeV^{-1})
30
40
50
60
B(E2)/B(E2)$_{ROT}$
0.2
0.6
1.0
Side-feeding
0
10
20
30
40
SPIN

XBL 862-556

N. Johnson — Studies of collective behavior of nuclei at high spin from lifetime measurements

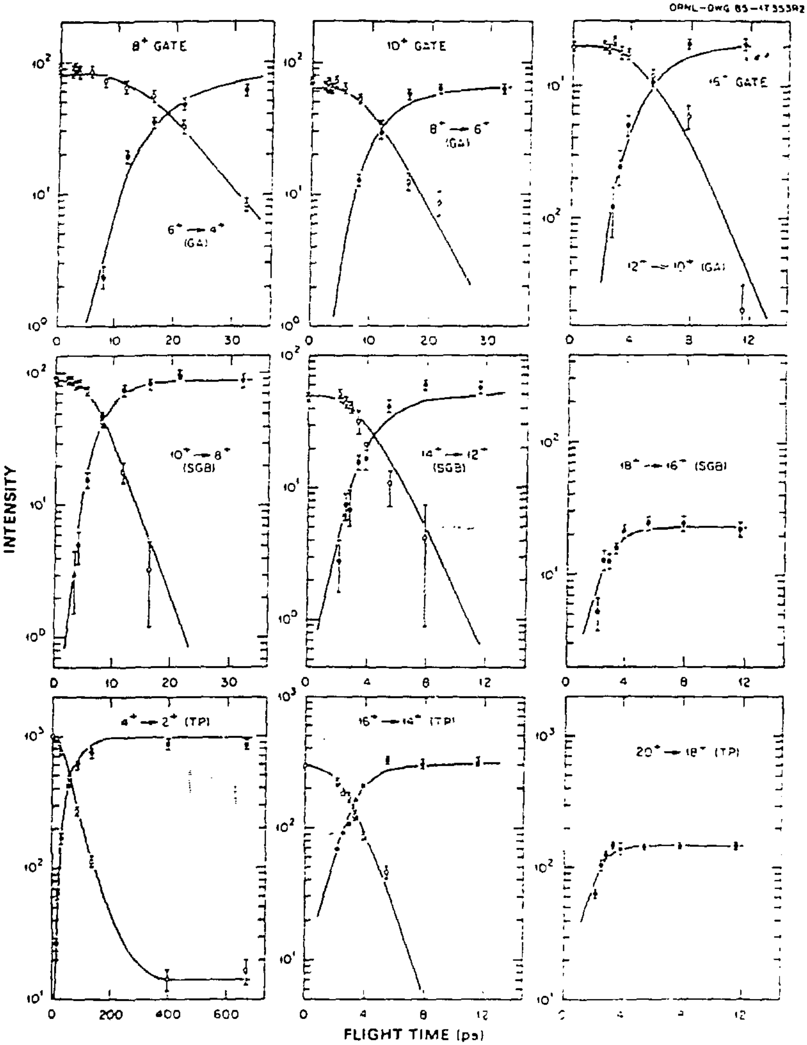

Fits to ^{172}W shifted and unshifted data.

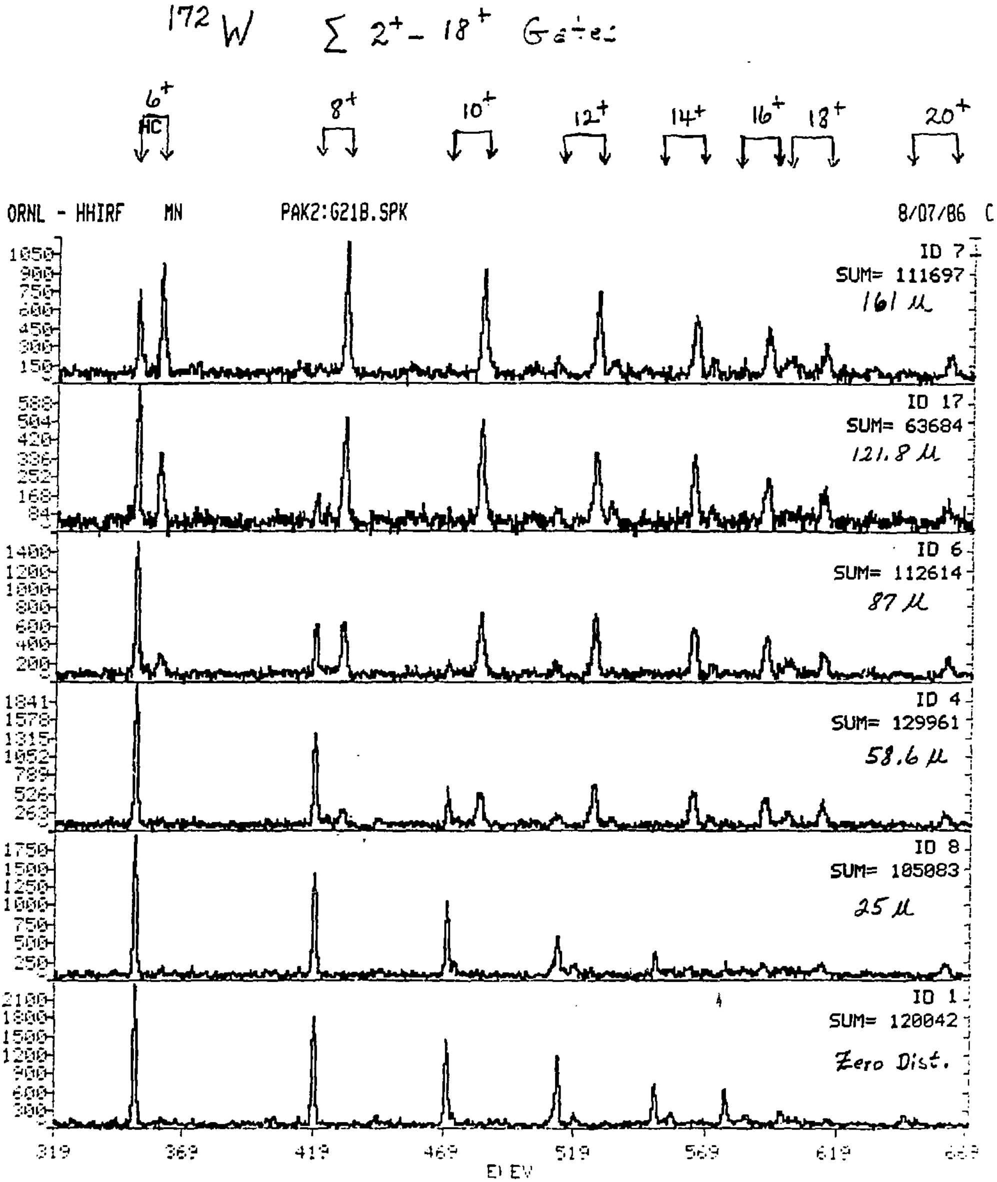

K+S Spectra of 172 W at some selected distances

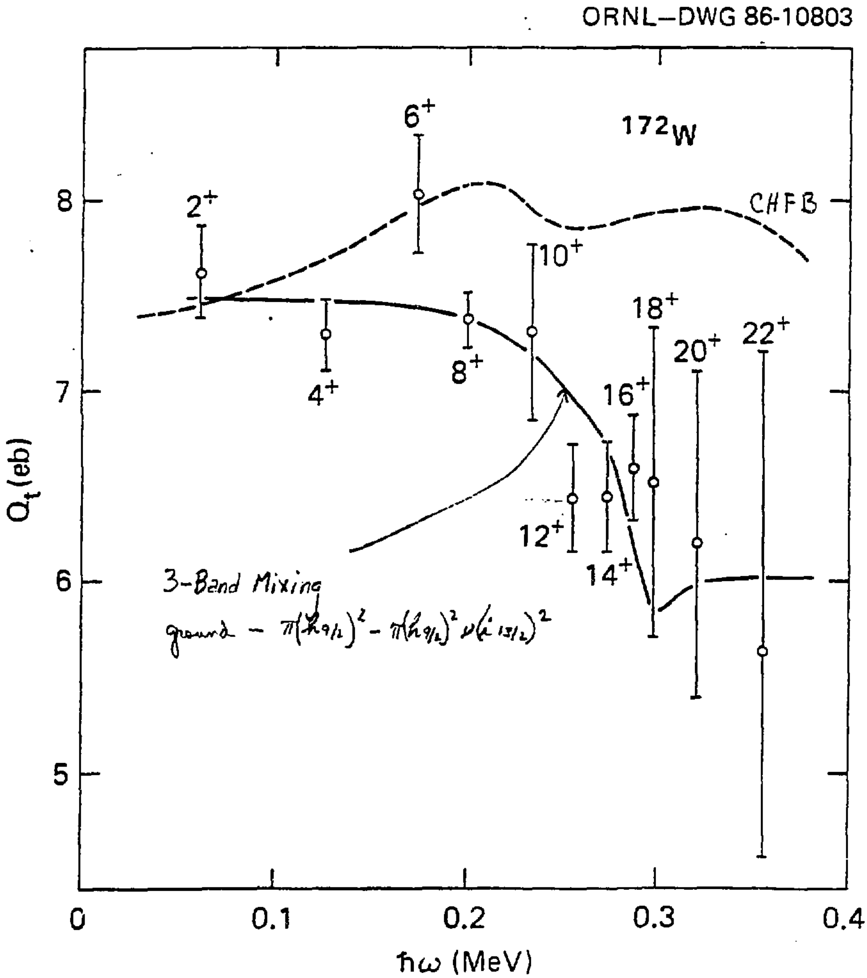
ORNL–DWG 86-10803
172W
CHFB
3-Band Mixing
ground – π(h9/2)² – π(h9/2)² ν(i13/2)²
2+
4+
6+
8+
10+
12+
14+
16+
18+
20+
22+
8
7
6
5
Qt (eb)
0
0.1
0.2
0.3
0.4
ħω (MeV)

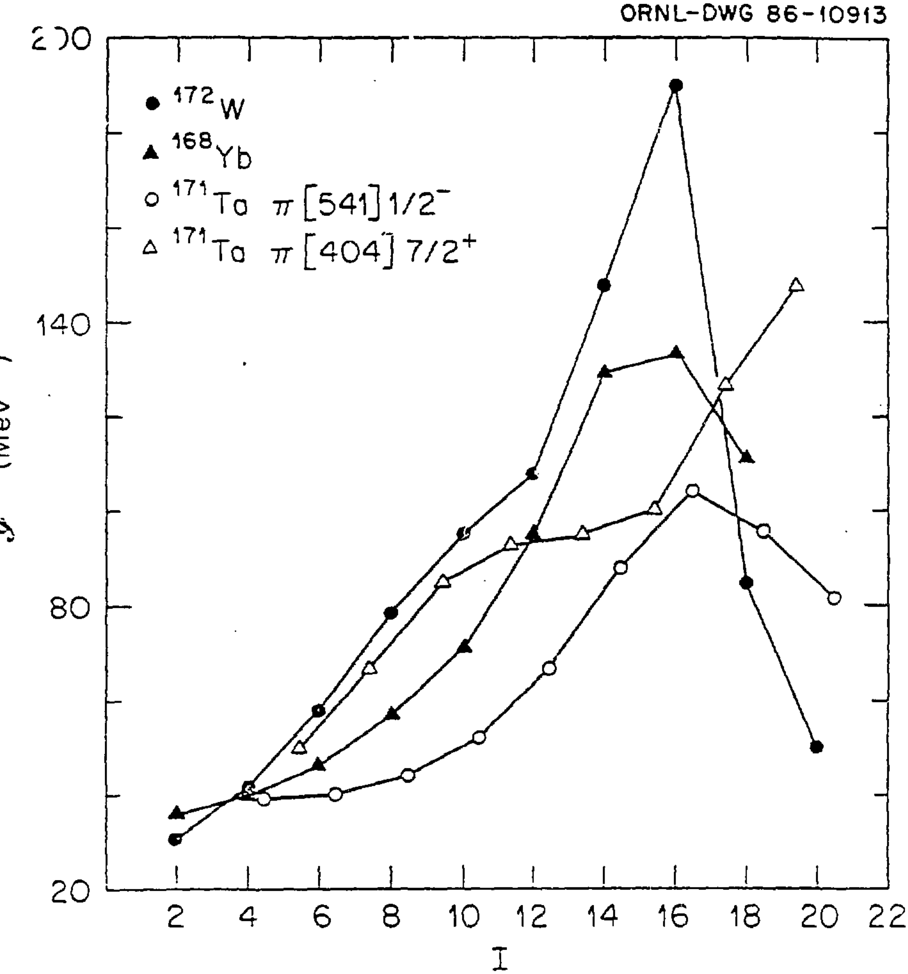

$\mathscr{J}^{(2)} = 4 / \{E_\gamma(I+2 \to I) - E_\gamma(I \to I-2)\}$

Comments on the bandmixing calculations for E2 properties of high spin states

Y. S. Chen, P. Semmes and G. A. Leander

Multybandmixing Model

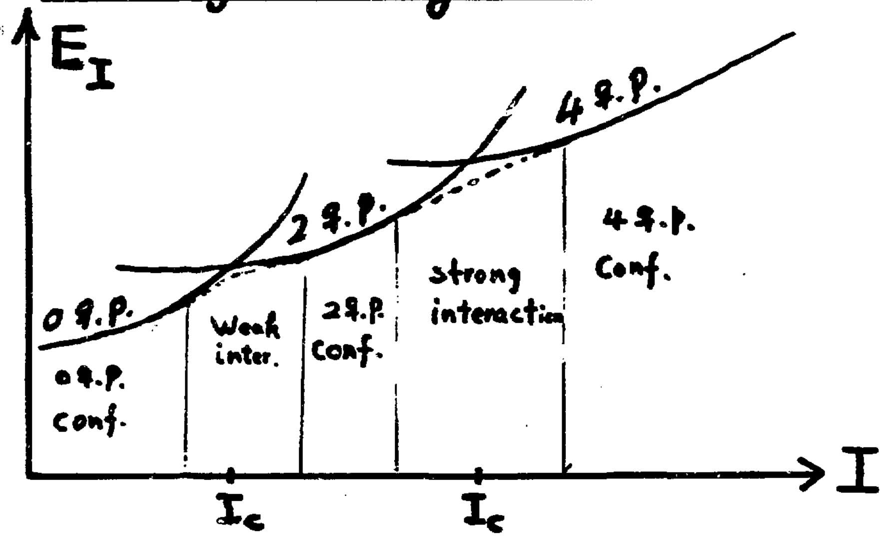

Combines bandmixing with intrinsic shapes to achieve an integrated description of E2 properties both within bands and in the interation regions.

$$Q_0^s = Q_0^g \frac{\bar{\beta}_s \cos(30^\circ + \bar{\gamma}_s)}{\bar{\beta}_g \cos(30^\circ + \bar{\gamma}_g)}$$

$$h' = \sum_{\nu} (\epsilon_\nu - \lambda) a_\nu^+ a_\nu + \frac{\Delta}{2} \sum_{\mu\nu} \delta(\bar{\nu},\mu)(a_\nu^+ a_\mu^+ + a_\mu a_\nu) - \omega \sum_{\nu\mu} \langle \nu | \hat{j}_x | \mu \rangle a_\nu^+ a_\mu$$

$$e'_\nu(\beta, \gamma; \omega)$$

$$E'_{conf.}(\beta, \gamma; \omega) = e'_{conf.}(\beta, \gamma; \omega) + E'_g(\beta, \gamma; \omega)$$

$$e'_{conf.}(\beta, \gamma; \omega) = \sum_{\nu \in conf.} e'_\nu(\beta, \gamma; \omega)$$

$$E'_g(\beta, \gamma; \omega) = \frac{1}{2} C_\beta (\beta - \bar{\beta})^2 + \frac{1}{2} C_\gamma \gamma^2 + E'_{rot}(\beta, \gamma; \omega)$$

$$E'_{rot}(\beta, \gamma; \omega) = E'_g(\beta, \gamma; \omega) - E'_g(\beta, \gamma; \omega = 0)$$

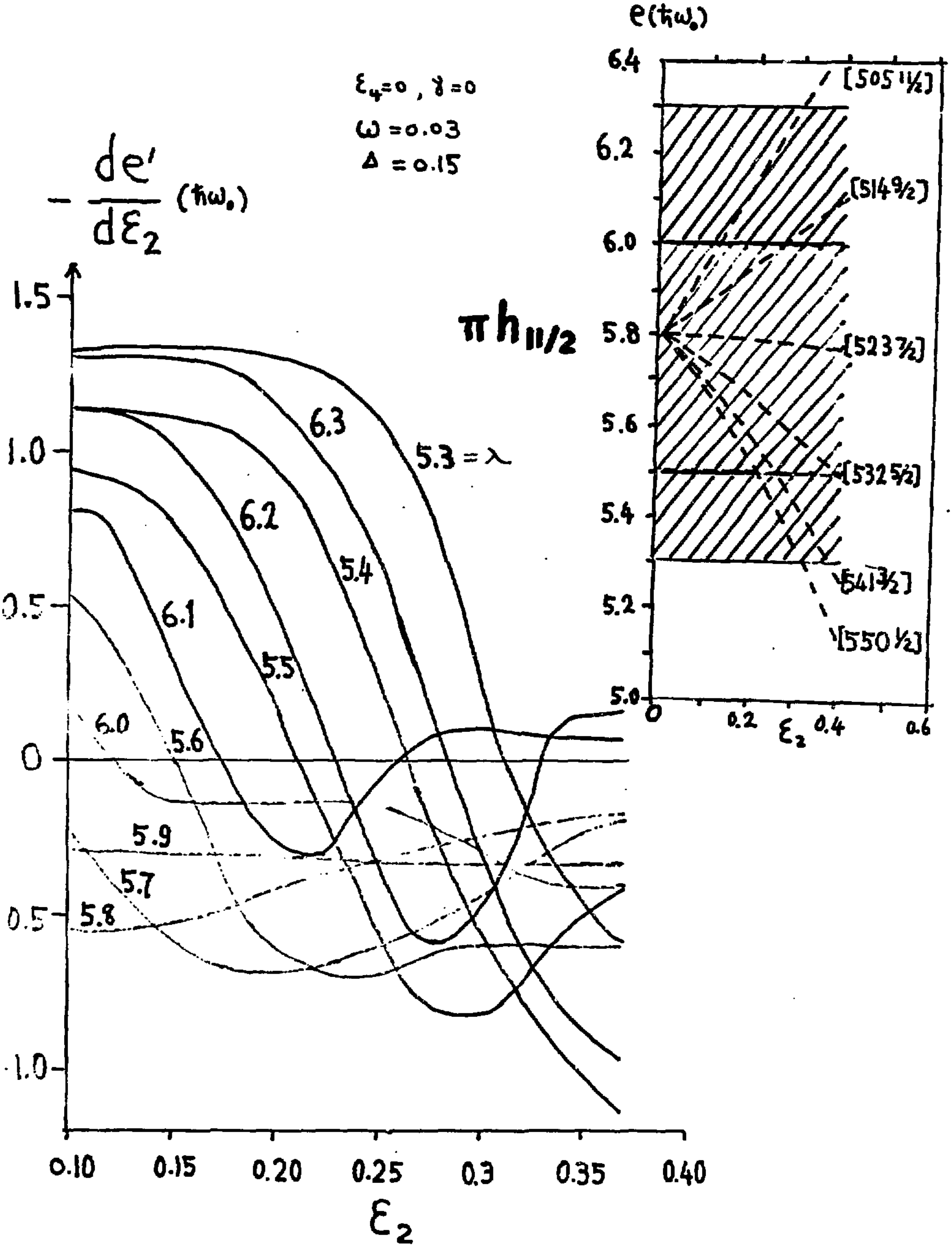
$\varepsilon_4=0$, $\gamma=0$
$\omega=0.03$
$\Delta=0.15$
$-\frac{de'}{d\varepsilon_2}(\hbar\omega_0)$
$\pi h_{11/2}$
1.5
1.0
0.5
0
-0.5
-1.0
6.3
5.3 = λ
6.2
5.4
6.1
5.5
6.0
5.6
5.9
5.7
5.8
0.10
0.15
0.20
0.25
0.3
0.35
0.40
ε_2
$e(\hbar\omega_0)$
6.4
6.2
6.0
5.8
5.6
5.4
5.2
5.0
[505 1/2]
[514 9/2]
[523 7/2]
[532 5/2]
[541 3/2]
[550 1/2]
0
0.2
0.4
0.6
ε_2

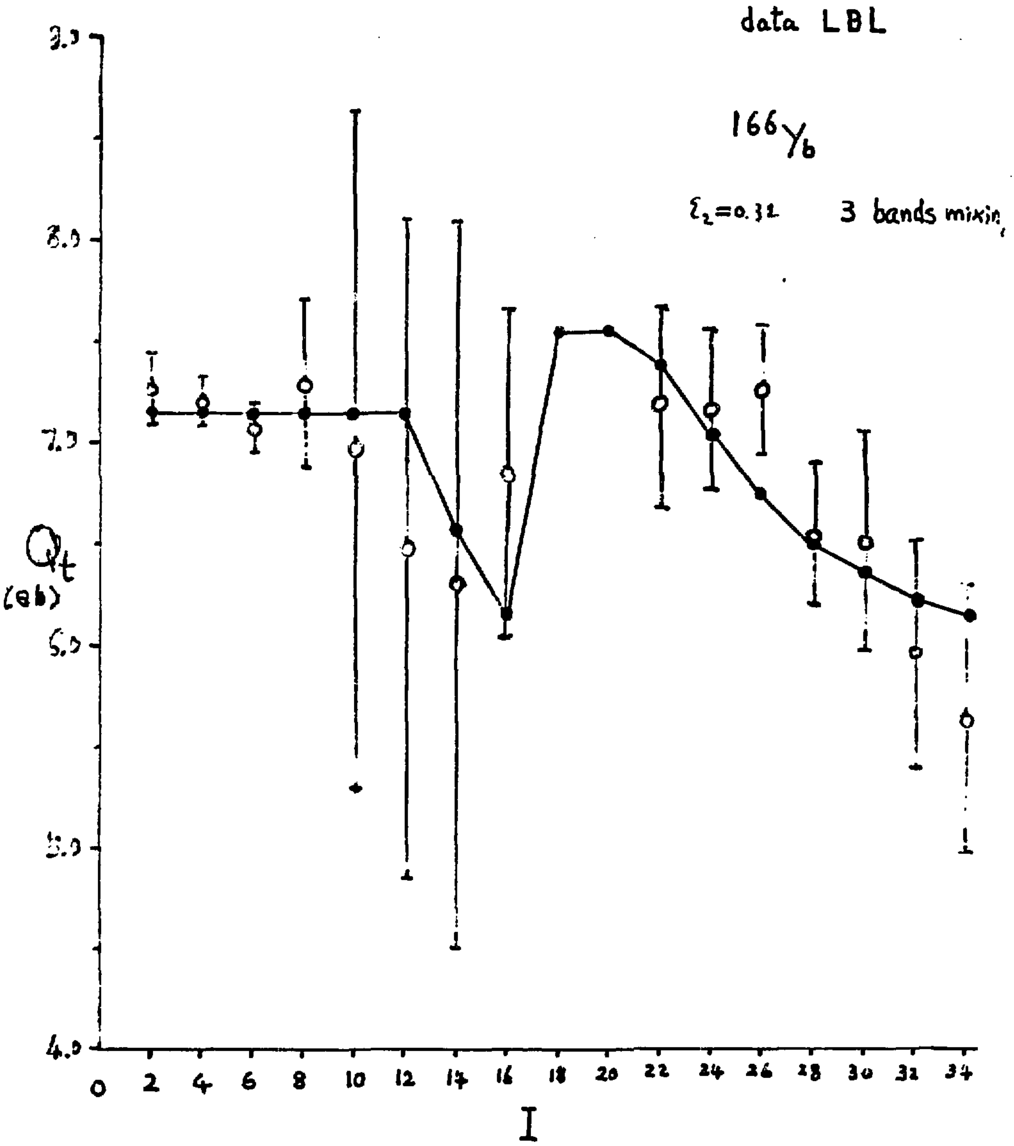
data LBL
166Yb
ε2=0.32
3 bands mixin
9.0
8.0
7.0
6.0
5.0
4.0
Qt
(eb)
0
2
4
6
8
10
12
14
16
18
20
22
24
26
28
30
32
34
I

ΔI = 1 Transition Rates

G.B. Hagemann
NBI

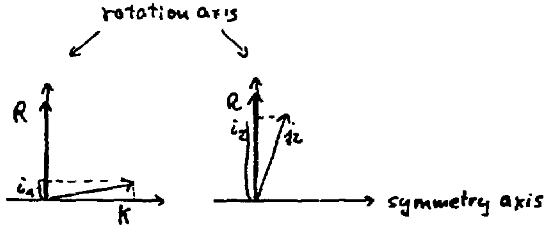

$$B(M1) \approx \frac{3}{8\pi} k^2 \left[(g_1 - g_R)\left(1 - \frac{i_1}{I}\right) - (g_2 - g_R)\frac{i_2}{I} \right]^2$$

$\pi h_{11/2} + 2\nu i_{13/2}$: $[+0.92(\quad) - (-0.6)(\quad)]^2$
1qp → 3qp

$\nu h_{11/2} + 2\nu i_{13/2}$: $[-0.64(\quad) - (-0.6)(\quad)]^2$
1qp → 3qp

$\nu(h_{11/2}\, i_{13/2}) + 2\nu i_{13/2}$: $[-0.64(\quad) - (-0.6)(\quad) - (-0.6)(\quad)]^2$
2qp → 4qp

$+ 2\pi h_{11/2}$ ⏟ $+0.92$

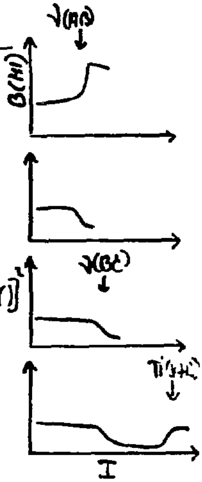

Fig 1

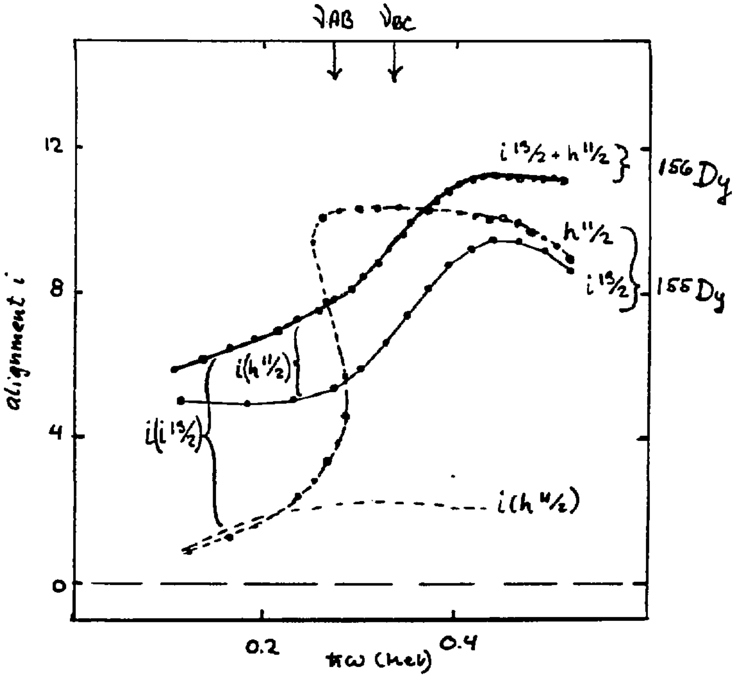

νAB
νBC
12
8
4
0
alignment i
0.2
0.4
ħω (MeV)
i 13/2 + h 11/2
156 Dy
h 11/2
i 13/2
155 Dy
i(h 11/2)
i(i 13/2)
i(h 11/2)

Fig 2

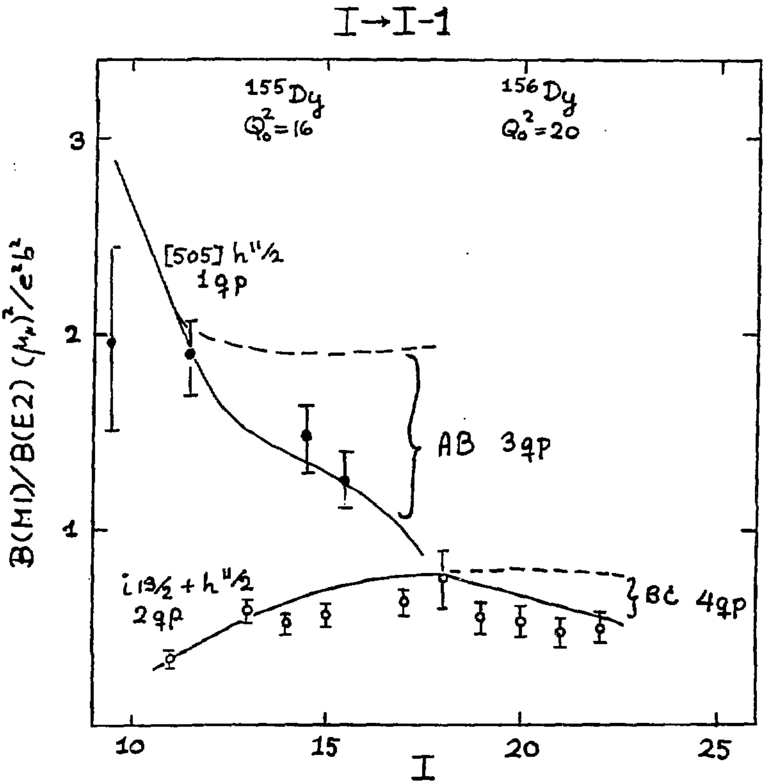
I→I-1
^{155}Dy
$Q_0^2=16$
^{156}Dy
$Q_0^2=20$
[505] h11/2
1qp
AB 3qp
i13/2 + h11/2
2qp
BC 4qp
B(M1)/B(E2) $(\mu_N)^2/e^2b^2$
I
3
2
1
10
15
20
25

Fig 3

Q Moments of isomeric states

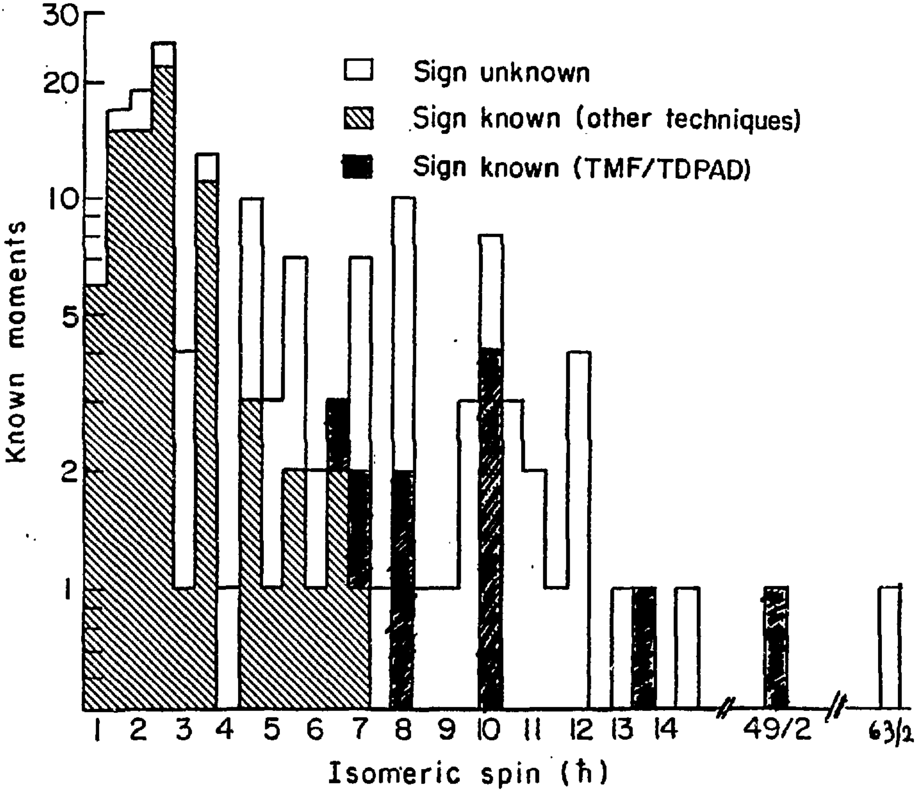

Levels of high spin are usually produced by fusion-evaporation reactions with unpolarized beams. Under these conditions no nuclear polarization is present and hence only |Q| could be measured hitherto. The atomic polarization in the multi-tilted foil interaction can be transferred to the nucleus and thus enable measurements of sign of Q as well.

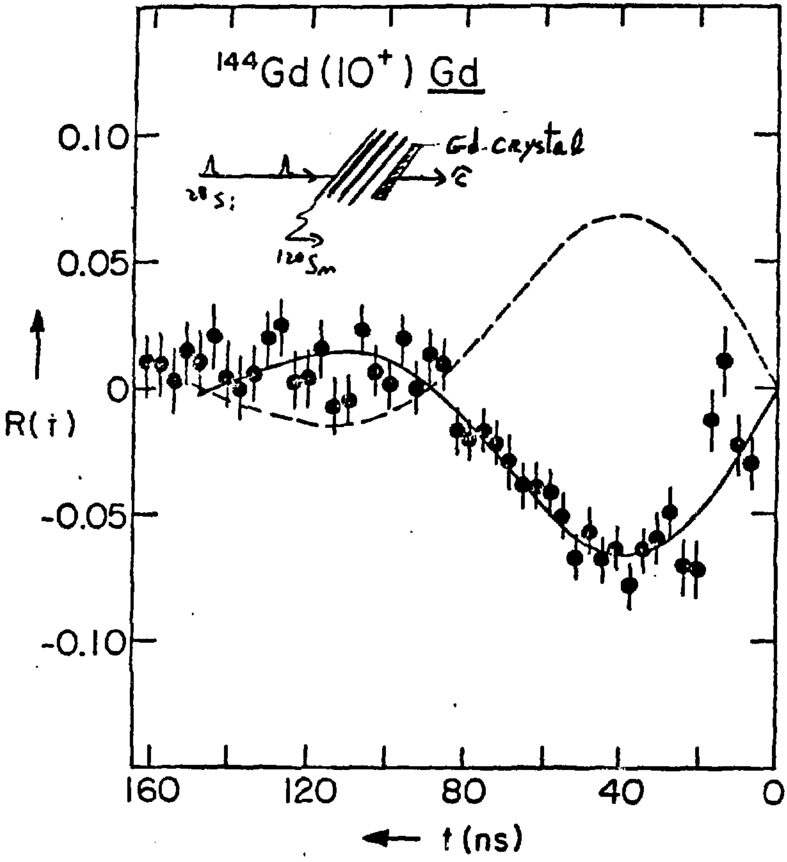

An example of a ratio function for the ^{144}Gd (10$^+$) level with the induced polarization by the tilted-foil interaction. The typical pattern for polarization can be seen. The dashed line represents R(t) for opposite sign of Q.

Table I

Summary of Q-moment measurements: the values of $T_{1/2}$, g and |Q| are from previous experiments (see text); sign of Q determinations and P_I values are from the measurements reviewed here.

	State	$T_{1/2}$[ns]	g	P_I	Q[e.fm^2]
①	^{54}Fe10$^+$)	357	+0.728	0.18(5)	+29.7(4)
①	^{88}Zr(8$^+$)	1700	-0.18	0.06(2)	+51(3)
①	^{90}Zr(8$^+$)	120	+1.36	0.05(1)	−51(3)
①	^{138}Ce(10$^+$)	82	-0.18	—	+ 77
③	^{134}Ce(10$^+$)	308	-0.187	0.12(3)	+132(12)
③	^{142}Sm(7$^-$)	170	-0.06	—	+112(27)
③	^{144}Gd(10$^+$)	130	+1.276	0.10(3)	−146(6)
③	^{147}Gd(13/2$^+$)	22.2	-0.037	-	−73(7)
②	^{147}Gd(27/2$^-$)	26.8	+0.840	0.11(2)	−126(8)
②	^{147}Gd(49/2$^+$)	510	+0.446	0.16(3)	−324(18)

Three classes of nuclei:

1.- Levels near closed shells
^{54}Fe(10$^+$), ^{88,90}Zr(8$^+$), ^{138}Ce(10$^+$).

2- Very high-spin levels in oblate nuclei:
^{147}Gd(49/2$^+$).

3- Transitional nuclei ("triaxiality")
^{134}Ce(10$^+$)?

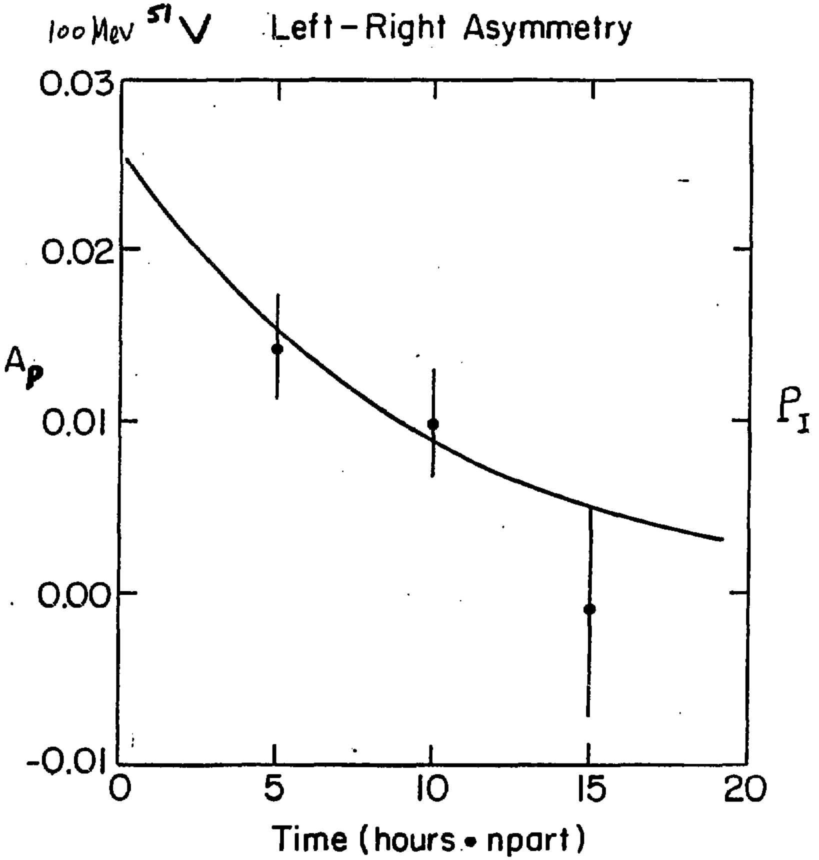

nuclear polarization of the $I=7/2$ ground state of ^{51}V detected by observing the left-right asymmetry in a coul. ex. experiment. The reduction of P_I is due to foil deterioration in beam and can be largely overcome by changes of foils.

Magnetic Moments and Lifetimes in ^{156}Dy

H. Emling

I. Lifetimes

Method : Doppler shift attenuation + $\gamma\gamma$-coincidence (HI, xn)
at Argonne - Notre Dame γ-ray facility

I. Ahmad, H. Emling, R. Holzmann, R.V.F Janssens
T. L. Khoo, W.C. Ma (Argonne Nat. Lab.)
P.J. Daly, Z. Grabowski, M. Piiparinen,
W.H. Trzaska, M A. Quader (Purdue University)
M W Drigert, U Garg (Notre Dame University)

II. Magnetic Moments

Method : Recoil Distance (HI, xn)
+ Transient Field

at Unilac / Darmstadt

R Kulessa*, E. Lubkiewicz*, H Emling, H Grein, E Grosse
R S Simon, H J Wollersheim (GSI Darmstadt; * on leave Univ Cracow)
J. Seiler-Clark, D. Schwalm (University Heidelberg)
V. H. Speidel (University Bonn) M Hass (Weizmann Inst Rehovot)

Analysis of Lineshapes

Input: slowing down in target + backing (Ziegler, Braune-Schulz)
angular straggling
finite detector size (EBS-code)
detector response
level scheme + feeder states (D. Twin et al., Daresbury)

Monte Carlo Integration ⟶ τ, τ_F, P_0

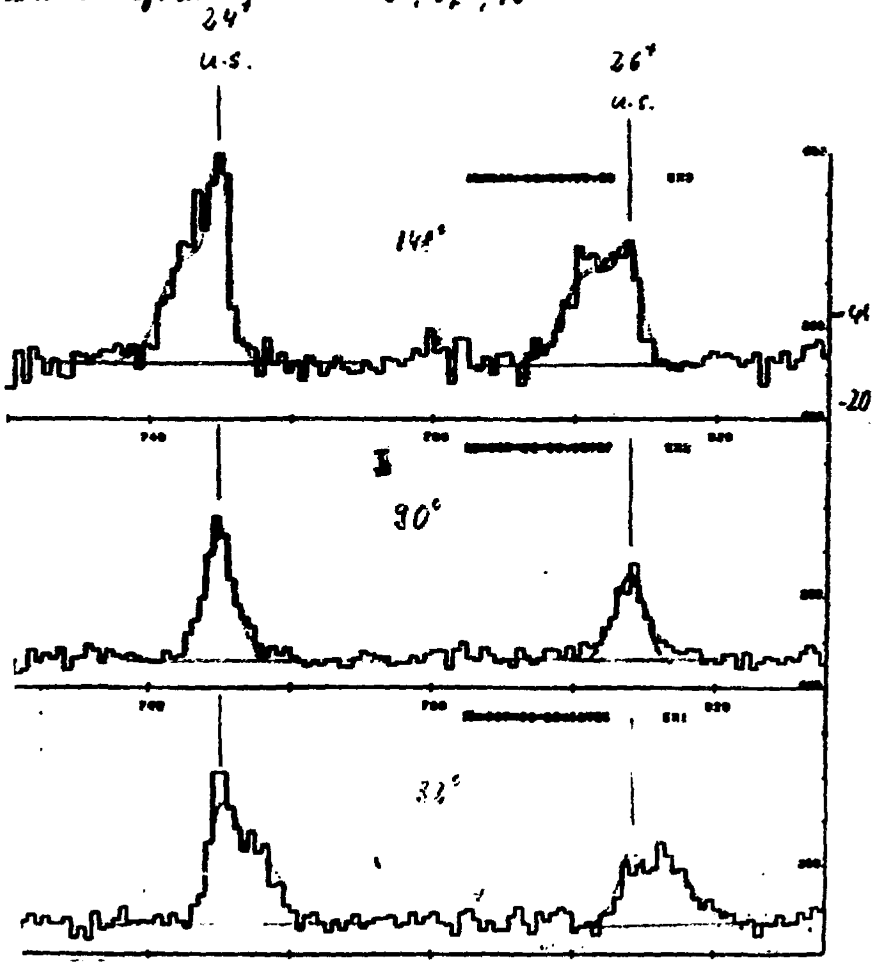

Comparison: Lifetimes obtained from DSAM (this exp.)
and RDM (H. Emling et al., NPA 419 (1984))

Spin	τ_{RDM} [ps]	τ_{DSAM} [ps]	$\frac{\tau_{RDM} - \tau_{DSA}}{\delta_{RDM} + \delta_{DSA}}$
24^+	0.45 (11)	0.22 (10)	1.1
26^+	0.35 (13)	0.25 (6)	0.5
28^+	0.21 (5)	0.17 (4)	0.3
30^+	0.16 (7)	0.12 (4)	0.4

Magnetic Moments

Problem in measuring g-factors of shortlived high spin states after HI, xn :

Complex history of the
excitation process,
no instantaneous population

⇙

apply Recoil · Distance Method

Experiment ${}^{156}Dy$

reaction: ${}^{136}Xe\,({}^{25}Mg, 5n)$; $E = 4.75$ MeV/u ; $v = 0.08c$

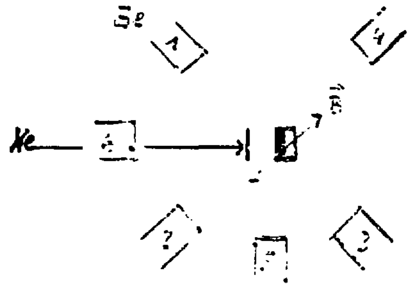

Target: 1mg Mg, 2mg Pb

Stopper: 5mg Fe, thick Cu

ext. $\vec{B}$ 400 Gauss

transient $\vec{B}$: up to 3.5 MGauss

4 Distances measured ≙ 3...11ps

$$R = \sqrt{\frac{Y_1^{\uparrow}\,Y_2^{\downarrow}}{Y_1^{\downarrow}\,Y_2^{\uparrow}}}$$

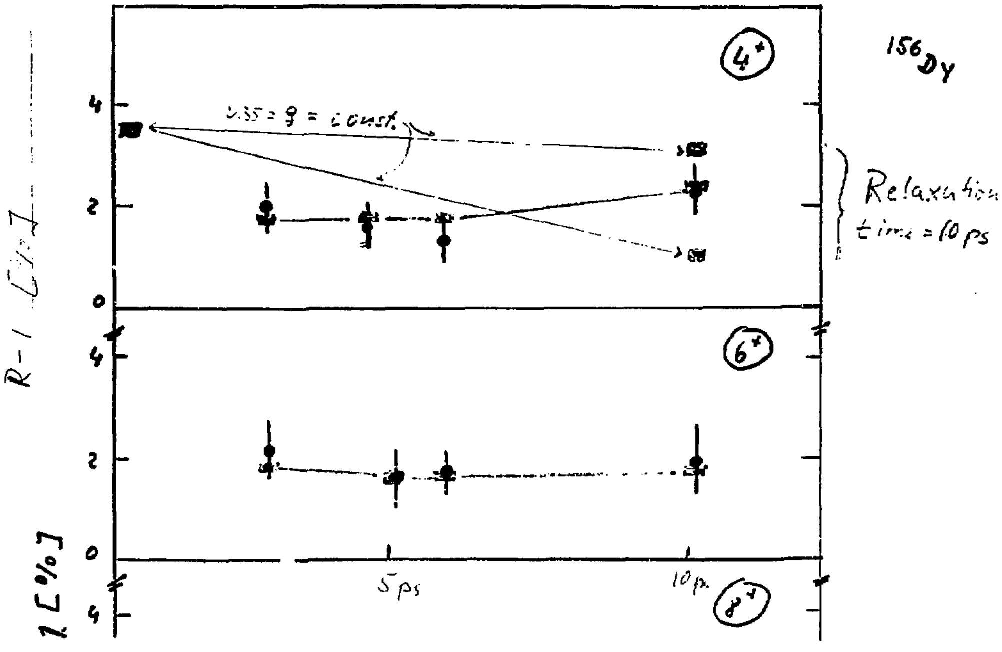

WORKSHOP ON NUCLEAR STRUCTURE AT MODERATE AND HIGH SPINS

Sven G. Aberg
Dept. of Mathematical Physics
Lund University
P.O. Box 118
S-221 00 Lund
Sweden

(+46) 46 10 96 33

Irshad Ahmad
Argonne National Lab
9700 So. Cass Ave.
Argonne, IL 60439

(312) 972-3612

H. Robert Andrews
Atomic Energy of Canada, Ltd.
Chalk River Nuclear Labs
Chalk River, ON, Canada K0J 1J0

(613) 584-3311, ext. 2891

A. Aprahamian
Lawrence Livermore National Lab
Livermore, CA 94550

Per O. Arve
Daresbury Nuclear Physics Lab
Daresbury, Warrington
Cheshire WA4 4AD, England

-44-925-603324

Rahmat Aryaeinejad
NSCL
Michigan State University
East Lansing, MI 48824

(517) 355-0088

Jose C. Bacelar
Lawrence Berkeley Laboratory
1 Cyclotron Road
Berkeley, CA 94720

(415) 486-5751

Cyrus Baktash
Oak Ridge National Lab
P. O. Box X
Oak Ridge, TN 37831

(615) 576-7949

Cornelius W. Beausang
State Univ. of New York
Physics Dept.
Stony Brook, NY 11794-3800

(516) 246-7110

Eva-Maria Beck
Lawrence Berkeley Laboratory
1 Cyclotron Road
Berkeley, CA 94720

(415) 486-5751

Carrol R. Bingham
Univ. of Tennessee
Physics Dept.
Knoxville, TN 37996-1200

(615) 974-7802

Jorrit de Boer
Universitat Munchen
Sektion Physik
Am Coulombwall 1
D-8046 Garching, West Germany

004989-3209-5082

Herbert H. Bolotin
Univ. of Melbourne
Parkville, Vict. 3052, Australia

(61-3) 344-5452

Thaddee Byrski
Strasbourg Univ.
Centre de Recherches Nucleaires
Div. de Physique Theorique, BP 20,
F-67037 Strasbourg CEDEX, France

88 28 63 01

Yong Shou Chen
Univ. of Tennessee
Physics Dept.
Knoxville, TN 37996-1200

(615) 974-7814

Douglas Cline
Nuclear Structure Research
Laboratory
University of Rochester
Rochester, NY 14627

(716) 275-4934

Tomasz Czosnyka
NSRL
University of Rochester
Rochester, NY 14627

(716) 275-4216

Patrick J. Daly
Chemistry Dept.
Purdue University
West Lafayette, IN 47907

(317) 494-5328

Haydeh Dejbakhsh
Texas A and M Univ.
Physics Dept.
College Station, TX 77843

(409) 845-1411

Richard M. Diamond
Lawrence Berkeley Laboratory
1 Cyclotron Road
Berkeley, CA 94720

(415) 486-5720

Thomas Dossing
Niels Bohr Institute
Blegdamsvej 17
DK-2100 Kobenhavn O
Denmark

George Dracoulis
Dept. Nuclear Physics
Australian National Univ.
Research School Phys. Sci.
Box 4, G.P.O.
Canberra, A.C.T., 2600, Australia

(062) 492095

James E. Draper
Univ. of California, Davis
Physics Dept.
Davis, CA 95616

(916) 752-1500

Mark W. Drigert
Univ. of Notre Dame
Physics Dept.
Notre Dame, IN 46556

(312) 972-4025, or -3663

Cemal Duyar
Univ. of California, Davis
Physics Dept.
Davis, CA 95616

(916) 752-1500

WORKSHOP ON NUCLEAR STRUCTURE AT MODERATE AND HIGH SPINS

Clive Ellegaard
Niels Bohr Insitute
Tandem Accelerator Laboratory
Riso, DK-4000 Roskilde, Denmark

(02) 37 1616, ex 6201

Yurdanur A. Ellis-Akovali
Oak Ridge National Lab
P. O. Box X
Oak Ridge, TN 37831

(615) 574-4695

Hans E. Emling
Gesellschaft fur Schwerionenforschung
Postfach 110 541
D-6100 Darmstadt 11, Germany

(6151) 359 669

Da Hsuan Feng
Drexel Univ.
Physics Dept.
Philadelphia, PA 19104

(215) 895-2719

David B. Fossan
State Univ. of New York
Physics Dept.
Stony Brook, NY 11794-3800

(516) 246-5041

Umesh Garg
University of Notre Dame
Notre Dame, IN 46556

Jules Gascon
Univ. de Montreal
Physics Dept.
C. P. 6128 A
Montreal, PQ, Canada H3C 3J7

(514) 343-6727

Jurgen Gerl
Physikalisches Institut
Universitat Heidelberg
Philosophenweg 19
D-69 Heidelberg, FRG

(06221) 516 516

Jean R. Gizon
Institut des Sciences Nucleaires,
Grenoble
53 Avenue des Martyrs
FR 38026 Grenoble Cedex, France

(76) 47.66.36

Gertrude Scharff Goldhaber
Brookhaven National Lab
Upton, NY 11973

(516) 282-3912

Alan L. Goodman
Tulane Univ.
Dept. of Physics
New Orleans, LA 70118

(504) 865-5520

Cynthia A. Gossett
Nuclear Physics Laboratory
Univ. of Washington
Physics Dept.
Seattle, WA 98195

(206) 543-4080

Henry C. Griffin
Department of Chemistry
University of Michigan
Ann Arbor, MI 48109

(313) 764-1438

M. W. Guidry
Univ. of Tennessee
Physics Dept.
Knoxville, TN 37996-1200

Gudrun Bertram Hagemann
Niels Bohr Insitute
Tandem Accelerator Laboratory
Riso, DK-4000 Roskilde, Denmark

(0) 2 371616

Michael Hass
Weizmann Inst. of Science
Dept. of Nuclear Physics
P. O. Box 26
76100 Rehovoth, Israel

(972)-(08) 482651

Jorma S. Hattula
Dept. of Physics
University of Jyvaskyla
Seminaarinkatu 15
FI 40100 Jyvaskyla 10, Finland

358 (211) 292528

David M. Headly
Chemistry Department
Florida State University
Tallahassee, FL 32306

(904) 644-6584

Romain Holzmann
Argonne National Lab
9700 So. Cass Ave.
Argonne, IL 60439

(312) 972-3896

Kari J. Honkanen
Department of Physics
University of Jyvaskyla
Seminaarinkatu 15
FI 40100 Jyvaskyla 10, Finland

(41) 292511

Deborah Howe
Univ. of Liverpool
Physics Dept.
Oliver Lodge Lab
P. O. Box 147
Liverpool L69 3BX, England

051 709 6022

Herbert C. Huebel
Institut Fuer Strahlen- u. Kernphysik
Nussallee 14-16
D-5300 Bonn 1, FRG

0228/733277

Robert V. F. Janssens
Argonne National Lab
9700 So. Cass Ave.
Argonne, IL 60439

(312) 972-8426, or -3063

WORKSHOP ON NUCLEAR STRUCTURE AT MODERATE AND HIGH SPINS

Victor P. Janzen
Univ. of Tennessee
Physics Dept.
Knoxville, TN 37996-1200

(615) 974-7812

Arne Johnson
Research Institute of Physics
Frescativaugen 24
SW S-10405 Stockholm
Sweden

46 (8) 150360

Noah R. Johnson
Oak Ridge National Lab
P. O. Box X
Oak Ridge, TN 37831

(615) 574-4739

Teng Lek Khoo
Argonne National Lab
9700 So. Cass Ave.
Argonne, IL 60439

(312) 972-4034, -3663

Noemie Koller
Rutgers Univ.
Physics Dept.
New Brunswick, NJ 08903

(201) 932-2525

Georg A. Leander
Oak Ridge Associated Universities
(ORAU/UNISOR)
P.O. Box X
Oak Ridge, TN 37830

(615) 576-0510

I-Yang Lee
Oak Ridge National Lab
P. O. Box X
Oak Ridge, TN 37831

(615) 574-4735

Rainer M. Lieder
IKP, Kernforschungsanlage Juelich
Postfach 1913
GR D-5170 Juelich
Federal Republic of Germany

(02461) 614114

Thomas Lindblad
Research Institute of Physics
Frescativaugen 24
SW S-10405 Stockholm
Sweden

46 (8) 150360

Wenchao Ma
Argonne National Lab
9700 So. Cass Ave.
Argonne, IL 60439

(312) 972-6545

K. Hugo Maier
Hahn Meitner Inst.
Glienicker Str. 100
D-1000 Berlin 39 FRG

(415) 422-8151

Eugene R. Marshalek
Univ. of Notre Dame
Physics Dept.
Notre Dame, IN 46556

(219) 234-0405

Richard J. McDonald
Lawrence Berkeley Laboratory
1 Cyclotron Road
Berkeley, CA 94720

(415) 486-6471

R. A. Meyer
Lawrence Livermore National Lab
Livermore, CA 94550

Paul J. Nolan
Univ. of Liverpool
Physics Dept.
Oliver Lodge Lab
P. O. Box 147
Liverpool L69 3BX, England

(051) 709-6022, ext. 2274

Edward Stephen Paul
State Univ. of New York
Physics Dept.
Stony Brook, NY 11794-3800

(516) 246-7110

Leon K. Peker
Brookhaven National Lab
Upton, NY 11973

(516) 282-5081

Matti J. Piiparinen
Purdue University
Dept. of Chemistry
Chemistry Bldg.
W. Lafayette, IN 47907

(317) 494-5498

Stephane Pilotte
Univ. de Montreal
Physics Dept.
C. P. 6128 A
Montreal, PQ, Canada H3C 3J7

Mubina A. Quader
Purdue University
Dept. of Chemistry
Chemistry Bldg.
W. Lafayette, IN 47907

(317) 494-5319

David C. Radford
Atomic Energy of Canada, Ltd.
Chalk River Nuclear Labs
Chalk River, ON, Canada K0J 1J0

(613) 584-3311, ext. 2891

Ingemar Ragnarsson
Dept. of Math. Physics
CERN
CH-1211 Geneva 23, Switzerland

(022) 832830

John O. Rasmussen
Lawrence Berkeley Laboratory
1 Cyclotron Road
Berkeley, CA 94720

(415) 486-6318

Lee L. Riedinger
Univ. of Tennessee
Physics Dept.
Knoxville, TN 37996-1200

(615) 974-6765

Peter Ring
Technische Universitat Munchen
D-8046 Garching
West Germany

(89) 3209 2353

Juerg X. Saladin
Univ. of Pittsburgh
Physics Dept.
Pittsburgh, PA 15260

(412) 524-2103

Claire Alice Schuck
C.N.R.S. (IN2P3)
Centre de Spectrometrie Nucleaire
Batiment 104
F-091406 Orsay, FRANCE

6941 5239

Gene D. Sprouse
State Univ. of New York
Physics Dept.
Stony Brook, NY 11794-3800

(516) 632-8118

Marie-Agnes D. Stephens-Deleplanque
Lawrence Berkeley Laboratory
1 Cyclotron Road
Berkeley, CA 94720

(415) 486-5384

Frank S. Stephens
Lawrence Berkeley Laboratory
1 Cyclotron Road
Berkeley, CA 94720

(415) 486-5724

Daniel Strottman
Los Alamos National Lab
P. O. Box 1663
Los Alamos, NM 87545

(505) 667-5608

W. J. Swiatecki
Lawrence Berkeley Laboratory
1 Cyclotron Road
Berkeley, CA 94720

(415) 486-5536

Paul Taras
Univ. de Montreal
Physics Dept.
C. P. 6128 A
Montreal, PQ, Canada H3C 3J7

(514) 343-7683

Peter John Twin
Science & Engineering Research
Council
Daresbury Nuclear Physics Lab
Daresbury, Warrington
Cheshire WA4 4AD, England

(0925) 603205

Martin J. A. De Voigt
University of Groningen/KVI
NL-9747 AA Groningen
The Netherlands

(415) 486-4243

Jim C. Waddington
McMaster University
Hamilton, Ontario
L8S4K1 Canada

(613) 584-3311 x2891

David Ward
Atomic Energy of Canada, Ltd.
Chalk River Nuclear Labs
Chalk River, ON, Canada K0J 1J0

(613) 584-3311, ext. 2891

John L. Wood
Georgia Inst. Tech.
School of Physics
Atlanta, GA 30332

(404) 894-5262

Cheng-Li Wu
Univ. of Tennessee
Physics Dept.
Knoxville, TN 37996-1200